Year : 2020

Functional Characterization and Therapeutic Implications of *SPOP* Mutations in Endometrial and Prostate Cancer

El Tekle Geniver

El Tekle Geniver, 2020, Functional Characterization and Therapeutic Implications of *SPOP* Mutations in Endometrial and Prostate Cancer

Originally published at : Thesis, University of Lausanne

Posted at the University of Lausanne Open Archive http://serval.unil.ch
Document URN : urn:nbn:ch:serval-BIB_AE23C83E419F5

UNIL | Université de Lausanne
Faculté de biologie
et de médecine

Département
Functional Cancer Genomics
Institute of Oncology Research

Functional Characterization and Therapeutic Implications of *SPOP* Mutations in Endometrial and Prostate Cancer

Thèse de doctorat ès sciences de la vie (PhD)

présentée à la

Faculté de biologie et de médecine
de l'Université de Lausanne

par

Geniver El Tekle

Master de l'Université Paris VII - Denis Diderot, Paris, France

Jury

Prof. Johanna A. Joyce, Présidente et Rapporteur
Prof. Jean-Philippe Theurillat, Directeur de thèse
Prof. Andrea Alimonti, Expert
Prof. Gian-Paolo Dotto, Expert

Lausanne 2020

UNIL | Université de Lausanne
Faculté de biologie
et de médecine

Département
Functional Cancer Genomics
Institute of Oncology Research

Functional Characterization and Therapeutic Implications of *SPOP* Mutations in Endometrial and Prostate Cancer

Thèse de doctorat ès sciences de la vie (PhD)

présentée à la

Faculté de biologie et de médecine
de l'Université de Lausanne

par

Geniver El Tekle

Master de l'Université Paris VII - Denis Diderot, Paris, France

Jury

Prof. Johanna A. Joyce, Présidente et Rapporteur
Prof. Jean-Philippe Theurillat, Directeur de thèse
Prof. Andrea Alimonti, Expert
Prof. Gian-Paolo Dotto, Expert

Lausanne 2020

UNIL | Université de Lausanne
Faculté de biologie et de médecine

Ecole Doctorale
Doctorat ès sciences de la vie

Imprimatur

Vu le rapport présenté par le jury d'examen, composé de

Président·e	Madame	Prof.	Johanna	**Joyce**
Directeur·trice de thèse	Monsieur	Prof.	Jean-Philippe	**Theurillat**
Expert·e·s	Monsieur	Prof.	Andrea	**Alimonti**
	Monsieur	Prof.	Gian-Paolo	**Dotto**

le Conseil de Faculté autorise l'impression de la thèse de

Madame Geniver El Tekle

Master en Biochimie, cellules, cibles thérapeutiques, Université Paris Diderot - Paris 7, France

intitulée

Functional characterization and therapeutic implications of *SPOP* mutations in endometrial and prostate cancer

Lausanne, le 20 avril 2020

pour le Doyen
de la Faculté de biologie et de médecine

Prof. Niko GELDNER
Directeur de l'Ecole Doctorale

Table of Contents

List of Figures and Tables

ACKNOWLEDGMENTS

This work was made possible through the support and guidance of Prof. Jean-Philippe Theurillat, who I would like to thank for giving me the opportunity to complete my Ph.D. and trusting me in being one of his first lab members (the crew of 3!). I would also like to thank all the members of the thesis committee, Prof. Johanna Joyce, Prof. Gian-Paolo Dotto and Prof. Andrea Alimonti, for accepting to be part of the jury, and for their suggestion and criticism that lead to a thoughtful discussion at both scientific and career-wise level.

I would also like to thank all the members of the JPT lab, from past and present, and all my colleagues from the IOR, for their support, advice and laugh during all these years. They always pushed me towards positivity when difficulties were becoming more apparent. Special thanks go to my boyfriend that always believed in me and contributed undeniably to the achievement of this journey.

I would finally like to thank my family and close friends for supporting me even from thousands of kilometers away (God Bless the internet); especially my parents, my sister and my adorable nephews for cheering me up while visiting and giving me the strength to pursue this work while being far away.

ABSTRACT (in English)

It is generally assumed that recurrent mutations within a given cancer driver gene elicit similar drug responses. Cancer genome studies have identified recurrent but divergent missense mutations affecting the substrate-recognition domain of the ubiquitin ligase adaptor SPOP in 5-10 % of endometrial and prostate cancer patients. Several studies have described prostate cancer-associated SPOP mutations and identified a subset of proteins implicated in tumorigenesis (e.g. TRIM24, DEK), while the endometrial cancer-associated mutations remain to date poorly characterized. More importantly, the therapeutic implications of both types of mutations remain incompletely understood. Here we analyzed changes in the ubiquitin landscape induced by endometrial cancer SPOP mutations and identified BRD2, BRD3 and BRD4 proteins (BETs) as SPOP–CUL3 substrates. We found that endometrial cancer–associated SPOP mutants preferentially degrade these proteins and the resulting reduction of their levels sensitized cancer cells to BET inhibitors *in vitro* and *in vivo* using xenograft tumor models. Conversely, prostate cancer–specific SPOP mutations resulted in impaired binding and degradation of BETs, promoting their resistance to pharmacologic inhibition. These results uncover an oncogenomics paradox, whereby mutations mapping to the same domain evoke opposing drug susceptibilities. Specifically, we provide a molecular rationale for the use of BET inhibitors to treat patients with endometrial but not prostate cancer who harbor SPOP mutations.

ABSTRACT (in French)

Les mutations récurrentes dans un même gène initiateur de cancer présentent généralement des similarités en terme de réponses thérapeutiques. Grâce aux récentes avancées technologiques, les bases de données génomiques ont permis d'identifier des mutations récurrentes dans le gène *SPOP* chez 5 à 10% des patients atteints du cancer de la prostate et de l'endomètre. Bien que ces mutations soient trouvées au sein du même domaine de liaison au substrat, chaque altération est spécifique à son type de cancer. La protéine SPOP est une enzyme appartenant à la famille des E3s ligases du système d'ubiquitination permettant le turn-over de certaines protéines. Ce mécanisme post-traductionnelle a pour principale fonction la reconnaissance - grâce aux enzymes E3s - et la dégradation de la protéine ainsi marquée via le complexe protéolytique du protéasome. Les mutations SPOP chez les patients atteints du cancer de la prostate ont largement été étudiées, et plusieurs protéines ayant un rôle dans la tumorigenèse ont été identifiées (e.g. TRIM24, DEK). Les mutations trouvées au sein du cancer de l'endomètre ont quant à elles été très peu caractérisées. Mais surtout, les implications thérapeutiques de ces différentes mutations demeurent encore assez méconnues. Nous avons donc analysé les changements dans le profil d'ubiquitination induits par les mutations spécifiques au cancer de l'endomètre et avons identifié les protéines BRD2, BRD3 et BRD4 (BETs) comme étant des substrats du complexe SPOP-E3 ligase. Ces protéines sont préférentiellement dégradées par les mutations endomètre-spécifiques et leur diminution permet par la suite une réponse thérapeutique plus élevés des cellules cancéreuses traitées avec des molécules inhibitrices des BETs (BET-i). A l'inverse, les mutations du gène SPOP spécifiques au cancer de la prostate altèrent leur liaison au BETs. Leur dégradation devient alors non fonctionnelle et amène à une augmentation des BETs, qui à long terme favorise leur résistance aux BET-i. Ces résultats mettent donc en lumière un paradoxe en oncogénomique, où des mutations se produisant au sein du même domaine, induisent une réponse opposée en terme de traitement thérapeutique. Plus précisément, notre étude fournit un rationnel moléculaire pour l'utilisation des BET-i, déjà présent dans plusieurs essais cliniques pour certains types de cancer. Les mutations du gène SPOP peuvent ainsi être utilisées comme biomarqueurs et donc permettre de traiter les patients arborant des mutations SPOP spécifiques au cancer de l'endomètre et non pas celles spécifiques au cancer de la prostate.

INTRODUCTION

A. The cancer genome

1. Principles of Cancer

Cancer is the second leading cause of mortality worldwide and the leading cause of death in wealthy countries according to the World Health Organization (WHO) with about 1 in 6 deaths being due to cancer (Figure 1). It includes more than 100 distinct diseases for which various risk factors and epidemiology have been described, and originates from almost all the cell types and organs of the human body.

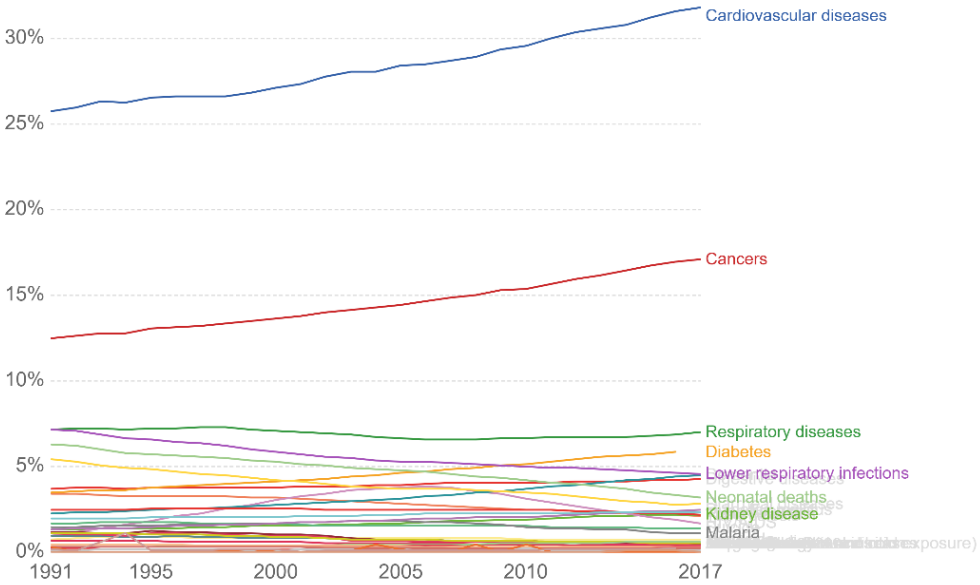

Figure 1. ***Cause of death in the World shown as the percentage of total death between 1991 and 2017****. Source: Our World Data, Global Burden of Disease Collaborative Network. Global Burden of Disease Study 2017 (GBD 2017) Results. Seattle, United States: Institute for Health Metrics and Evaluation (IHME), 2018.*

Cancer is a disease driven by epigenetic and genetic alterations that activate oncogenes and inactivate tumor suppressors. This process leads to the transformation of normal cells into malignant and unconstrained proliferative cells that escape the mechanisms of normal homeostasis in the organism.

In 2000, Douglas Hanahan and Robert Weinberg, conceptualized cancer under six hallmarks that contain the biological capabilities acquired during tumor growth and metastatic dissemination. They include sustaining proliferative signaling, evading growth suppressors, resisting cell death, enabling replicative immortality, inducing angiogenesis, and

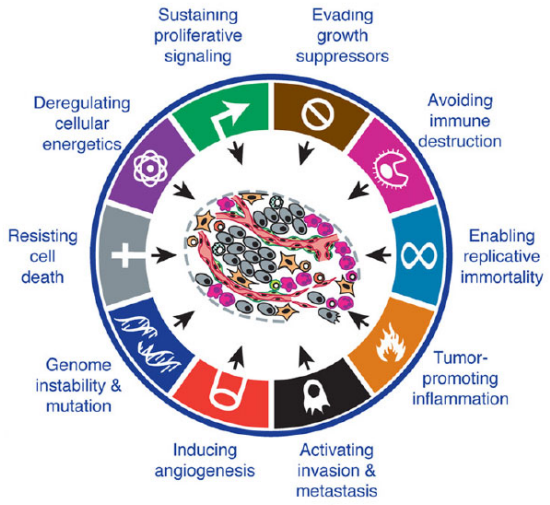

Figure 2. ***Representation of the cancer hallmarks concept. Adapted from D. Hanahan and R. Weinberg***

activating invasion and metastasis [1]. Significant research progress and technologies' breakthroughs have led them to update their perspective in 2011, leading to the addition of more sophisticated mechanisms such as avoiding immune destruction, tumor-promoting inflammation and deregulating cellular energetics (**Figure 2**). Many known cancer genes encode proteins that directly regulate these processes whereas many of the recently discovered ones remain without precise connection to cancer and affect more global processes. Indeed, though disruption of gene expression, they can affect one or several targets involved in cancer progression, for example by activating or repressing specific genes, deregulating the transcription machinery or disturbing the steady-state levels of specific proteins.

2. Somatic mutations

The first insights about the crucial role of the genome in cancer development were described by David von Hansemann and Theodor Bovery in 1890 and 1940 respectively [2, 3]. They noted atypical chromosomal aberrations while observing dividing cancer cells under the microscope, which led them to the hypothesis that cancer arises from abnormal clones due to abnormalities in the material inherited. The identification of the molecular structure of the DNA in 1953 and that agents damaging DNA and generating mutations are as well able to cause cancer, later on supported this theory [4-6].

In the process of tumorigenesis, cancer cells acquire specific mutations that accumulate in the genome over the lifetime of an individual. These alterations are known as somatic mutations, to differentiate them from germline mutations that are inherited and transmitted from parents. They can be acquired at an early stage in embryonic cell division, which leads to their presence in almost all of the somatic cells (**Figure 3**). Some of the well-established genomic changes are common to many tumor types, whereas others are restricted to a particular kind of cancer [7].

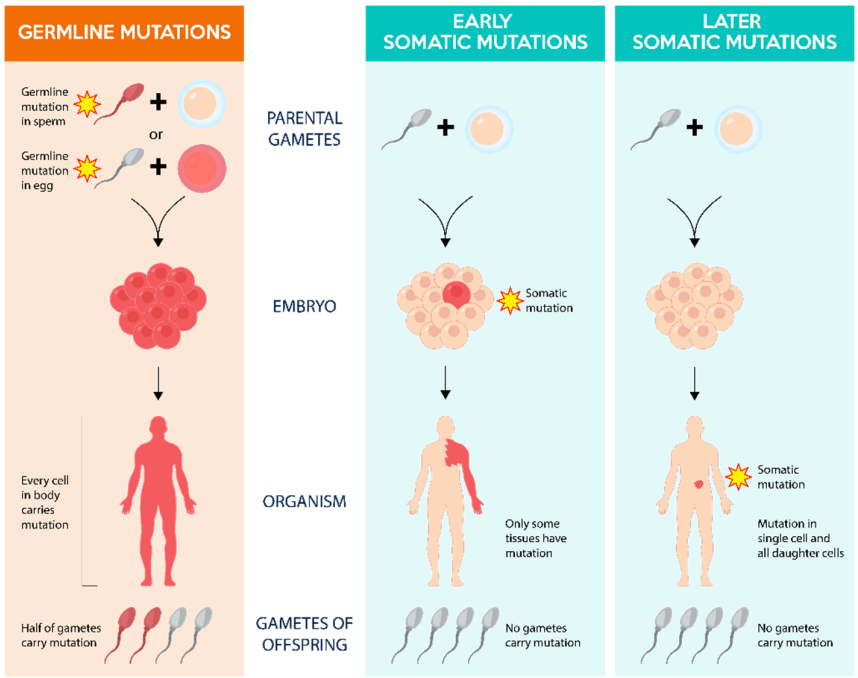

Figure 3. ***Germline and somatic mutations.*** *Source https://kintalk.org/genetics-101*

3. Driver and passenger mutations

Not all somatic mutations present in a cancer genome have been involved in the development of the cancer. Indeed, depending on its consequence on tumor progression, a somatic mutation can be categorized into two subgroups, namely drivers or passengers' mutations (**Figure 4**) [8]. A "driver" mutation confers growth advantage to the cell and has been positively selected in the microenvironment of the specific tissue during cancer evolution. In contrast, a "passenger" mutation does not confer any growth advantage, and therefore has not contributed to tumorigenesis but has been present in an ancestor of the cancer cell once it has acquired one of its drivers, and it is thus found within the cancer genome.

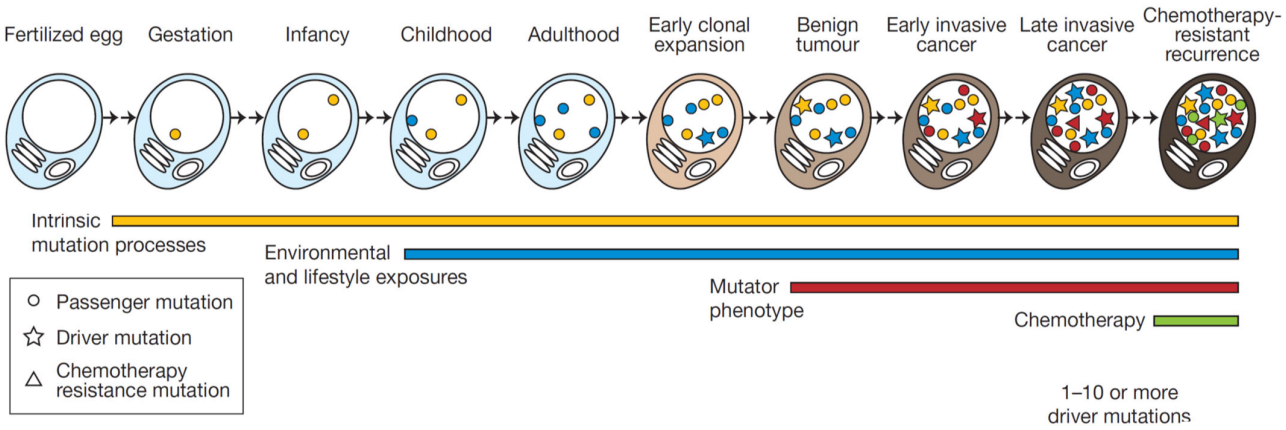

*Figure 4. **Somatic mutations are acquired by cancer cells during time**. Adapted from Stratton MR, Campbell PJ and Futreal PA, Nature, 2009 [8].*

Driver mutations are not only essential to initiate tumorigenesis, but also required for tumor growth and survival [9].

B. Genetics and Biology of Prostate Cancer

1. Epidemiology

Prostate cancer (PCa) is the second most frequent cancer in men worldwide and the fourth most commonly occurring cancer according to the WHO. In 2018, prostate cancer represented about 7% of all cancers (**Figure 5**) [10]. Indeed, more than a million new cases were reported, with higher prevalence in developed countries. There is a chance of 1 in 10,000 men under 40 years to develop prostate cancer, with an increase to 1 in 7 by the age of 60.

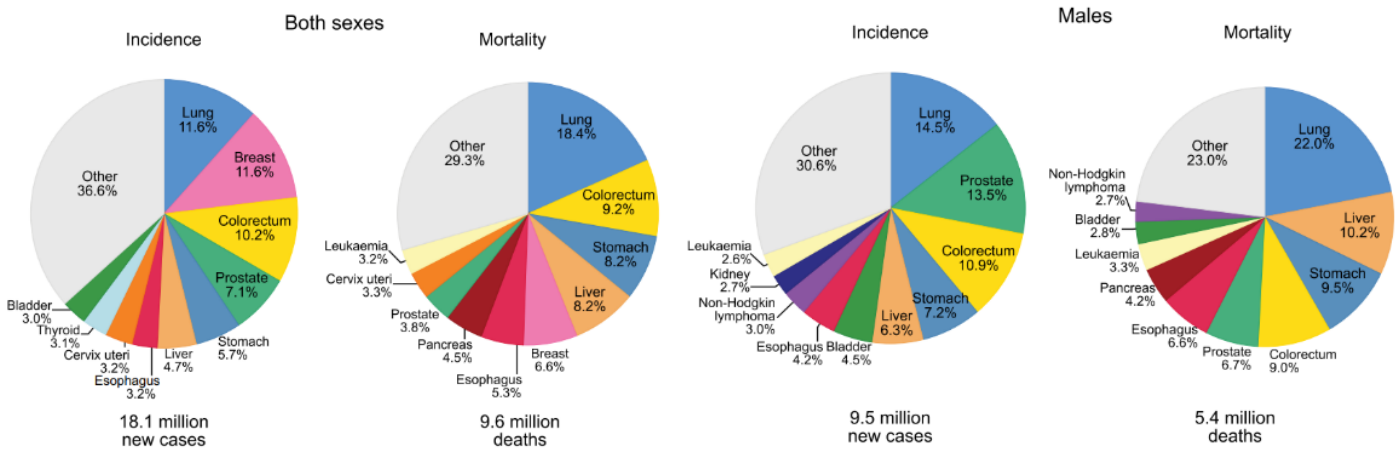

*Figure 5**. Incidence and mortality distribution for 36 cancers in 185 countries in 2018**. Left: both sexes. Right: only males. The pie chart area reflects the proportion of the total number of cases or deaths; nonmelanoma skin cancers are included in the "other" category. Source: GLOBOCAN 2018[10].*

Prostate cancer incidence rate varies greatly across regions and populations (**Figure 6)** [10]. The strongest established risk factors for prostate cancer are the age, ethnic group, and family history [11]. However, differences in social, environmental and genetic have also been established as possible reasons for the disparity. Importantly, diet and physical activity seem to play a role in prostate cancer development and progression, and are mainly associated with the ethnic differences in the incidence rates [12].

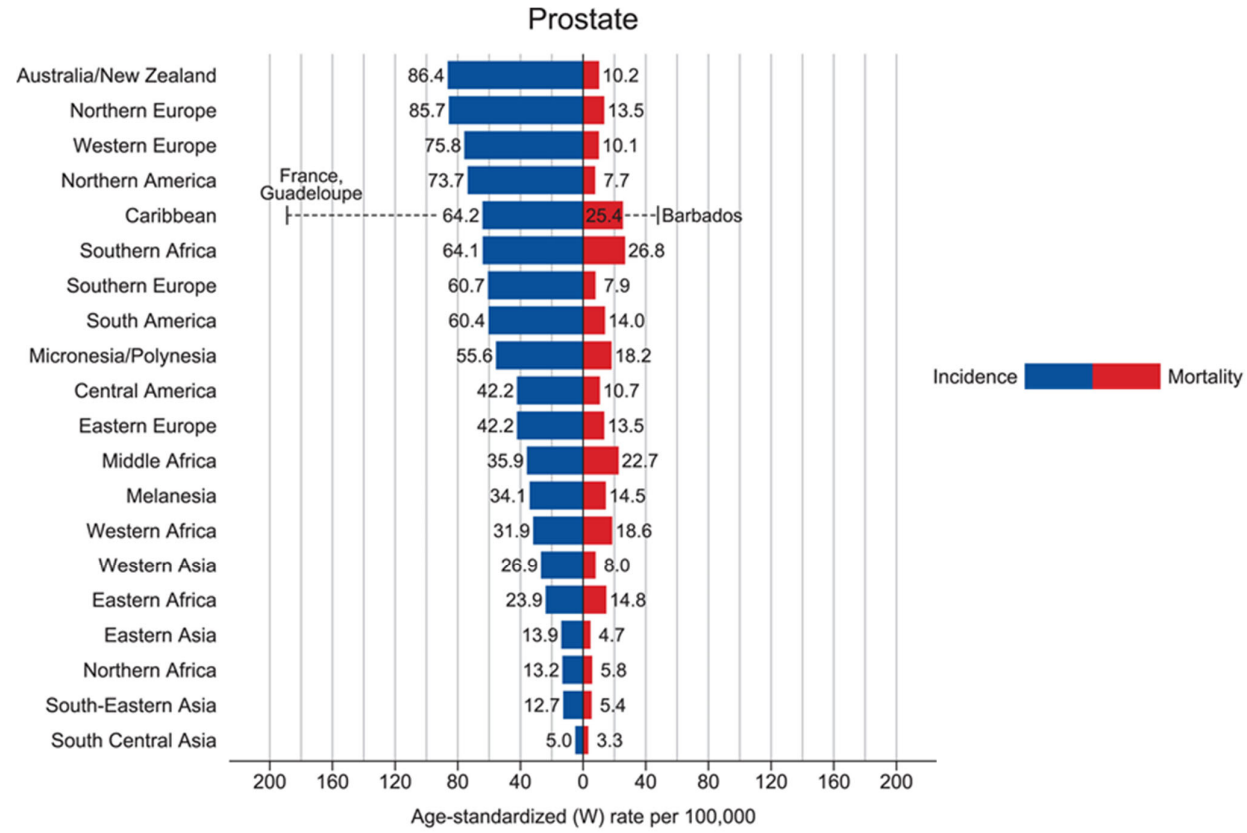

*Figure 6. **Region-Specific Incidence and Mortality Age-Standardized Rates for Prostate Cancer in 2018**. Adapted from Globocan 2018 [10].*

The highest rates were measured in Australia/New Zealand and Europe, followed by North America. On the other hand, Africa and Asia display lower incidence rates than those from developed countries. The worldwide variations in PCa incidence might be attributed to differences in health care access and to prostate-specific antigen (PSA) testing, a glycoprotein normally expressed by prostate tissue. Most of prostate cancers are detected through its elevated plasmatic levels (values higher than 4ng/mL). About 30% of the prostate cancer cases in the USA and Europe are supposedly due to over-diagnosis from extensive PSA screening according to latest research [13-15]. Mortality rates for prostate cancer differ as well significantly worldwide (**Figure 6).** Interestingly, men of African–American descent have the highest incidence rates and mortality rates compared to other ethnic groups [16]. Their incidence rate was reported to be about 40 times higher than in Africa or than Asian-American. These data suggest first an important role for environmental factors, and second the existence of PCa-associated genetic risk factors that are concomitant with a more aggressive phenotype [17-20].

Although in the last decades, scientific research has made significant progress to understand the molecular mechanisms and risk factors involved, prostate cancer remains a considerable medical problem as mortality rate is estimated to double in the next 20 years.

2. Anatomy and cell of origins

The prostate is a secretory gland located in the pelvis of men. In 1981, McNeil described the different areas from which cancer cells can arise as follow : the central zone (cz), the peripheral zone (pz) the transitional zone (tz) and finally the anterior zone (az) (**Figure 7**) [21].

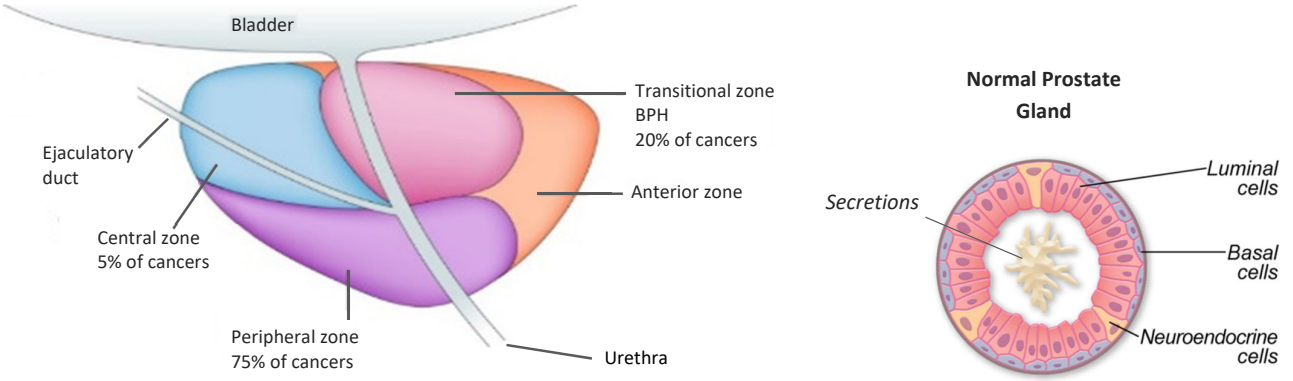

Figure 7. ***Schematic Representation of the prostate****. Left: The Prostate gland. Adapted from Sathianathen, N.J., Konety, B.R., Crook, J. et al. Landmarks in prostate cancer. Nat Rev Urol 15, 627–642 (2018) [22]. Right: Cross-sectional diagram of a prostate gland duct with the different cells types. Adapted from Wang G. et al, Gens Dev., 2018 [23].*

Most of the carcinomas (about 70%) typically develop in the peripheral zone, whereas benign prostatic hyperplasia (BPH) occurs in the transitional zone [24]. Prostate cancer can arise from both luminal and basal cells. It remains unclear whether neuroendocrine cells can be transformed to generate prostate cancer. The luminal cells produce secretory proteins such as PSA and express the androgen receptor (AR), a transcription

factor representing a key player in prostate tumorigenesis [25]. The basal cells are located between the basal lamina and luminal cells and express very low levels of AR. Neuroendocrine cells are a small population of endocrine–paracrine cells situated on the basal cell layer that express neuroendocrine markers (e.g. synaptophysin and chromogranin A) and do not express AR (**Figure 7**).

3. Diagnosis

Prostate cancer can be identified relatively early using PSA blood screening test and digital rectal exam (DRE). Patients with abnormal PSA levels will usually undergo biopsies to detect possible prostatic tumor lesions. The Gleason grading and scoring system, originally defined by Donald Gleason in 1966, is based on histological appearance of prostate adenocarcinoma, scaled from very well differentiated (grade 1) to very poorly differentiated (grade 5) (**Figure 8**) [26, 27]. The Gleason score is then determined by a combination of the two most predominant architectural patterns, as prostate cancer is a highly heterogeneous disease. Prostate tumors with a Gleason score ranging from 2 to 4 are considered to be less aggressive, whereas the ones ranging from 7 to 10 are considered as the most aggressive [28]. This classification has been refined over the years, and the latest in 2016, is the most commonly used and accepted by the WHO [29, 30]. In addition to PSA screening and its benefits of getting an early diagnosis, prostate biopsies and their histological analysis, remain the main evaluation tool to define the tumor grading.

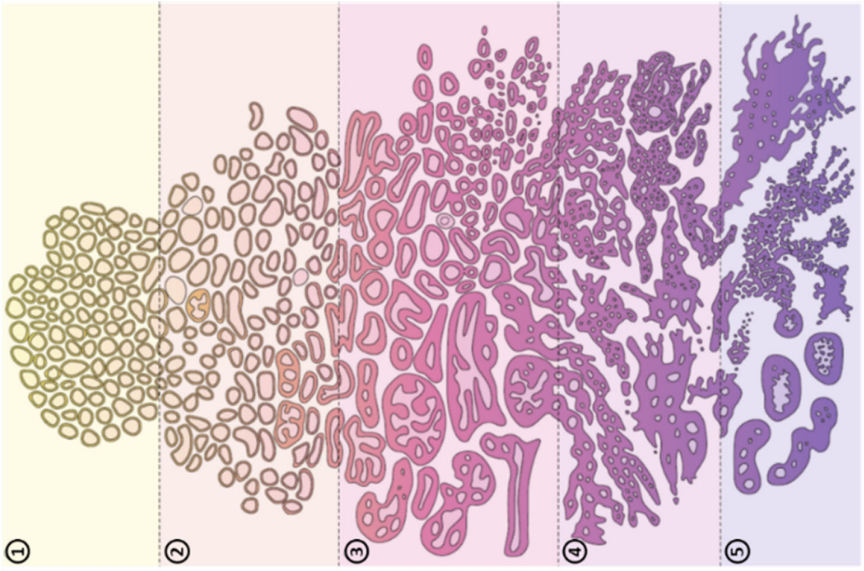

Figure 8. ***The grading and scoring system developed by Gleason [****25]. This system is based on the histological appearance of prostate cancer cells, specifically, the extent of glandular differentiation and the pattern of growth in the stroma. Adapted from Ref [21].*

At the histological level, prostatic intraepithelial neoplasia (PIN) is characterized by the manifestation of atypical cytological features of the epithelial cells in prostatic glands or ducts and is widely accepted as the precursor of prostate tumorigenesis [31]. High-grade PIN (HG-PIN) has been suggested to be the transition phase between benign prostate epithelium and invasive cancer as it shares several morphological and

genomic features with PCa. Upon this transition phase, the disease reaches its first stage commonly identified as Localized PCa.

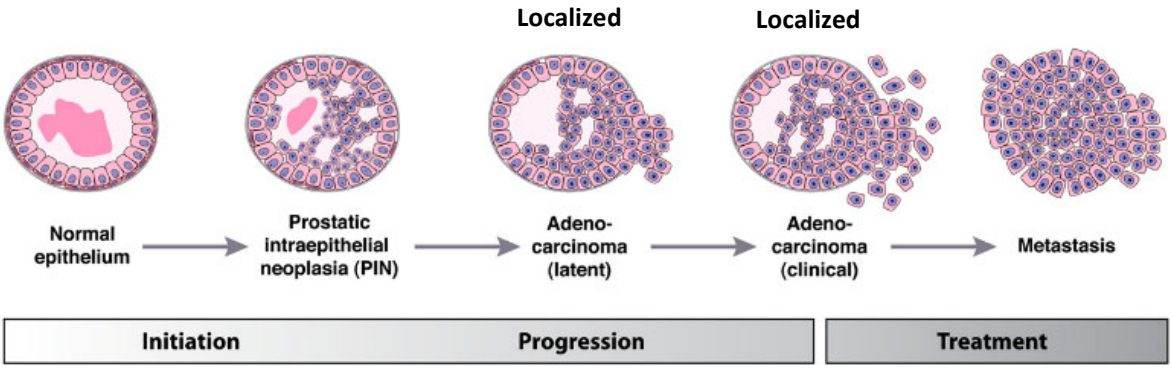

Figure 9. ***Human prostate cancer progression.*** *Adapted from Shen and Abate-Shen (2010)[32].*

4. Evolution and therapeutic options

a) Localized Prostate cancer

Localized PCa is thus an early stage of malignancy that is restrained to the prostate itself and is considered as either indolent or aggressive depending on the clinical and pathological features (Gleason score, PSA levels). At this stage, treatments possibilities include surgery (prostatectomy) and radiation therapy. About one third of the patients however develop recurrent disease, and are then treated with androgen deprivation therapy (ADT) that delays cancer progression [33].

b) The androgen receptor signaling

ADT is commonly used as a treatment for PCa because of its dependency towards the androgen receptor (AR) signaling, dependency that was established by the Nobel prize winner Huggins in 1941 [34].

AR is a nuclear hormone-regulated receptor that functions as a transcription factor [35]. When bound by its ligand (testosterone and other androgens), AR undergoes conformational changes by displacing heat-shock proteins (HSP), allowing its nuclear translocation and homodimer formation (**Figure 10**). Inside the nucleus and along with other co-activators, it binds to DNA at promoter and enhancer region (androgen response elements, ARE), and regulates the transcription of its target genes and (e.g. *PSA* and *TMPRSS2*) and various biological processes such as growth and survival [36-39]. AR function is required for the normal development and regulation of the prostate, but undergoes abnormal activation in an autonomous manner in the case of prostate cancer progression.

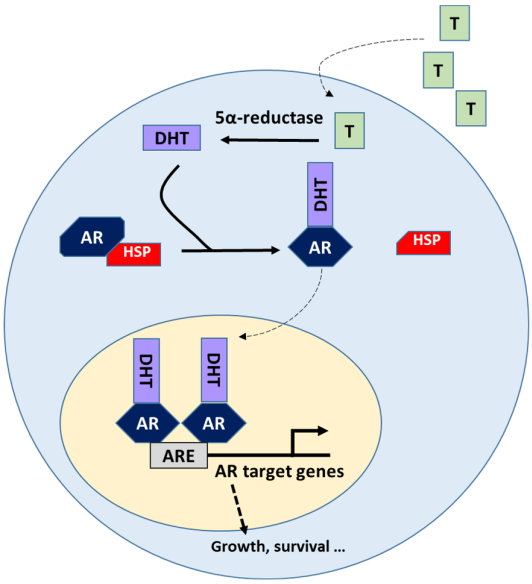

Figure 10. ***Simplified mechanism of the androgen receptor signaling in the prostate cells****. Inspired by Punit Saraon et al, Clinical Chemistry, 2011 [40]. Testosterone in the most secreted androgen of the male circulation, and is mainly produced by the Leydig cells of the testes through the hypothalamus axis. Free circulating testosterone can enter prostate cells and be converted to a more potent metabolite, namely dihydrotestosterone (DHT) through the 5a reductase enzyme.*

c) Castration Resistant Prostate Cancer (CRPC)

Although ADT remains universally accepted as the first-line standard of care of PCa with initial response reaching about 80% of the patients, many patients develop disease relapse and progress to androgen-independent prostate cancer, identified as castration resistant prostate cancer (CRPC) (**Figure 11**) [41]. Indeed, in about 20-40% of the patients, prostate cancer re-occur and metastasis to the bones, lymph nodes and bladder [42-45]. Patients with metastatic CRPC (mCRPC) are often treated with chemotherapy (docetaxel), or later on with abiraterone (inhibition of androgen production), enzalutamide (antagonist of AR) or a second-line chemotherapeutic agent (cabazitaxel). The discrimination between tumors that will evolve in a more or less aggressive cancer remains not fully characterized. There is thus an essential need to understand and correlate the molecular markers that can predict a specific outcome and lead to a more effective management of the disease.

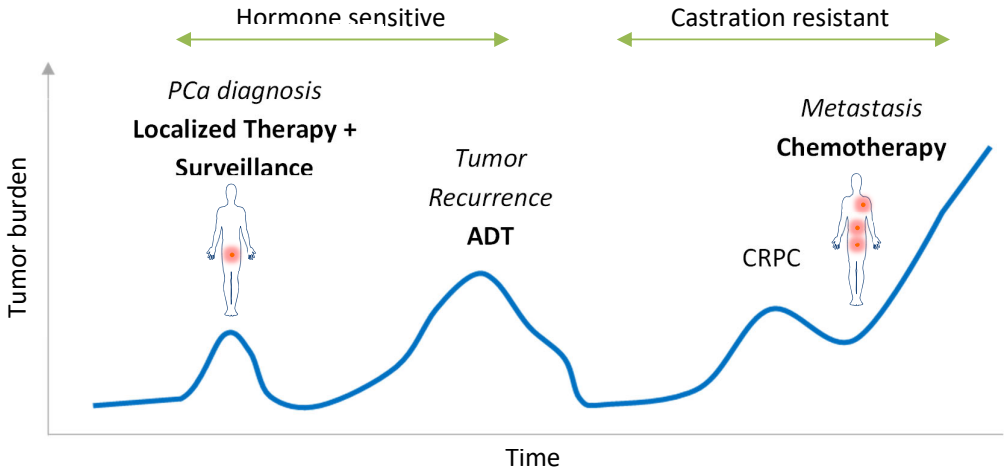

Figure 11. ***Evolution of Prostate Cancer and associated therapeutic interventions****.*

5. Molecular subtypes of Prostate Cancer

Large-scale genomic sequencing projects in PCa have identified several recurrent DNA alterations implicated in various biological processes, at both primary and late stage of prostate tumorigenesis [46-50]. Globally, PCa has a relatively low mutational burden of about 1 mutation per megabase (approximatively 10 times lower than melanomas') whereas chromosomal gains and losses are quite commonly found in PCa genomes [46, 51-53].

a) Primary prostate cancer

Inactivation of tumor suppressor genes such as *NKX3.1* and *RB1* are commonly observed as important events in oncogenesis [54]. Chromosomal alterations resulting in somatic copy number alteration (SCNA) involving *PTEN*, *TP53* and *CDKN1B* for example, are also a characteristic of PCa progression [53].

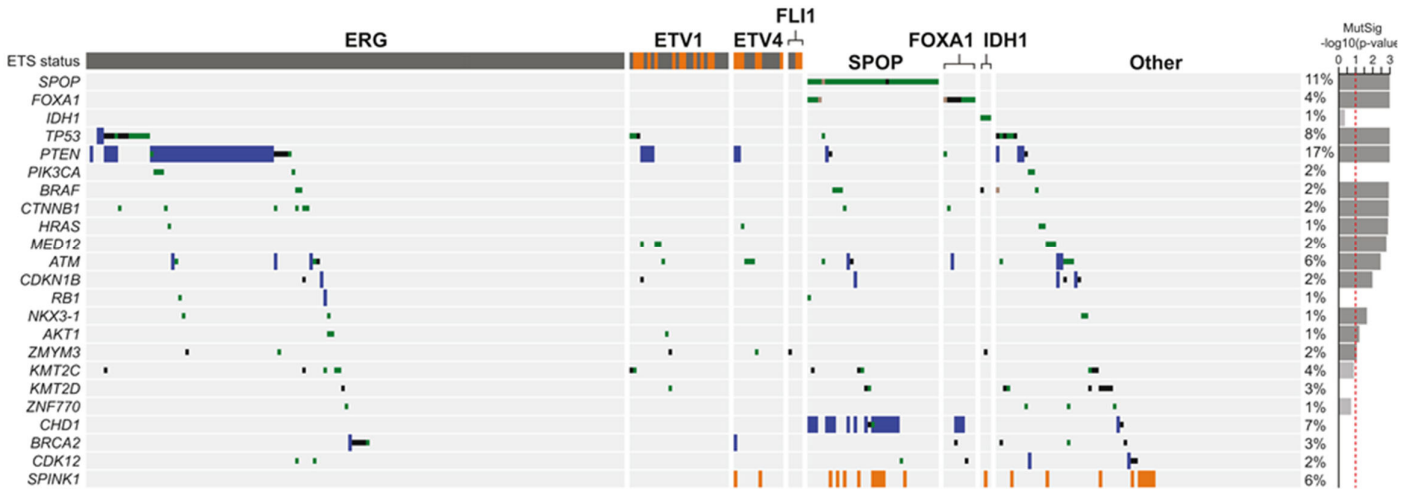

Figure 12. ***Genomic alterations in primary PCa****. Adapted from The Molecular taxonomy of Primary Prostate Cancer [51].*

The most frequent genomic gains arise from chromosome 7 and 8q, where *c-MYC* oncogene is situated. High-throughput sequencing efforts of SCNA have exposed their relevance as prognostic markers of recurrence and metastatic PCa, with CNA burden positively correlating with disease progression [53]. Many other genomic alterations have been also uncovered by the The Cancer genome Atlas project (TCGA) in 333 primary PCa samples (**Figure 12**). The study distinguished seven main subtypes with more than half of the tumors harbor fusions that involve the E-twenty-six (ETS) transcription factor family with *ERG (*46%), *ETV1* (8%), *ETV4* (4%), *FLI1* (1%). Other 15% of primary tumors carried mutations in *SPOP* (11%), *FOXA1* (3%) and *IDH1* (1%). In these tumors, ETS fusion status is a key determinant in shaping primary PCa transcriptome as measured by mRNA expression analysis. Among all the subtypes, *FOXA1* and *SPOP*-mutant tumors displayed the highest AR transcriptional activity. Interestingly, several of these alterations have been found to be mutually exclusive from each other's. On the other hand, about one third of the tumors remained however unclassified (unknown specific molecular events). In a larger sequencing effort of about 1013 local PCa tumors, nearly 100 additional putative drivers have been reported to be mutated at a frequency below 3%, indicating the need to further investigate their functional role and relevance in PCa [55].

b) mCRPC

Several studies have as well described the genomic landscape of mCRPC, revealing distinct genomic subtypes than from the primary localized disease. In a cohort of 429 patients, integrative genomic analysis of single-nucleotide variants (SNVs), CNV and gene fusions revealed genomic alterations in *AR*, *ETS* family members, *TP53*, *PTEN*, and *RB1* as the most frequently found (**Figure 13**) [56]. High fraction of oncogenic mutations emerged also in *PIK3CA, BRCA2, APC*, and CDK12. Mutual-exclusive patterns present at the primary stage of the disease, were also kept in mCRPC such as alterations in genes of the ETS family (e.g. *ERG* and *ETV1*), and between alterations in *ERG* and *SPOP* or *FOXA1* [47]. *ERG* and *PTEN* were co-occurring, in line with previous studies showing a synergistic role in promoting oncogenesis in mouse models of prostate cancer [57]. In addition, alterations in *TP53* and *RB1* were also co-occurring, confirming as well previous studies showing their occurrence at high frequency in neuroendocrine cancers and the aggressive phenotype of this association found in several prostate cancer models [58-61]. Interestingly, *CHD1* alterations also seemed to co-occur with *SPOP* mutations as already seen in primary PCa.

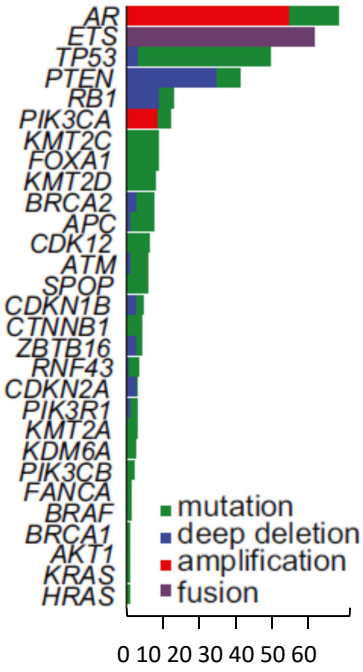

Figure 13. ***Genomic alterations in mCRPC****. Potential biologic relevant altered genes by frequency found in 444 tumors of 429 patients with mCRPC. Adapted from Abida et al, PNAS, 2019 [56]. Frequency of ETS gene alterations applies to the subset of 323 patients who underwent tumor RNA sequencing, where fusion status could be determined.*

C. Genetics and Biology of Endometrial Cancer

1. Epidemiology

Endometrial cancer (ECa) is the most common gynecologic malignancy and the sixth most common cancer in women worldwide [10, 62]. ECa represents more than 94% of uterine cancer. The number of new cases is increasing over time and is in part attributed to increasing rates of obesity and aging, two risk factors of endometrial cancer [63].

The highest incidence rate is found in Central and Eastern Europe and North America; and the lowest rate in low-middle income countries (Middle and Western Africa) (**Table 1**). Exposition to estrogens (endogenous and exogenous) associated with obesity, diabetes and late-onset menopause and older age (>55 years) are some of the main risk factors of ECa [64-66].

Rank	Country	Age-standardised rate per 100,000
1	Belarus	24.9
2	Samoa	24.8
3	Macedonia	24.3
4	Lithuania	24.0
5	Canada	23.6
6	Greece	21.5
7	Ukraine	21.4
8	US	20.1
9	Slovakia	19.7
10	Croatia	19.6

A meta-analysis has shown a significant association between ECa and body mass index (BMI) [67]. Indeed, many studies have reported an increased risk of mortality in patients with high BMI as well as a reduced risk by weight loss (diet and physical activity) [68-70]. Ethnical disparities are also present with a 5–year survival rate of 84% for white women and 62% for black women according to the American Cancer Society.

Table 1. ***Top 10 ECa incidence rates in 2018****. Source Globocan 2018 [10].*

2. Anatomy and cell of origins

ECa arises from the endometrium, which is the linen part of the uterus (**Figure 14**).

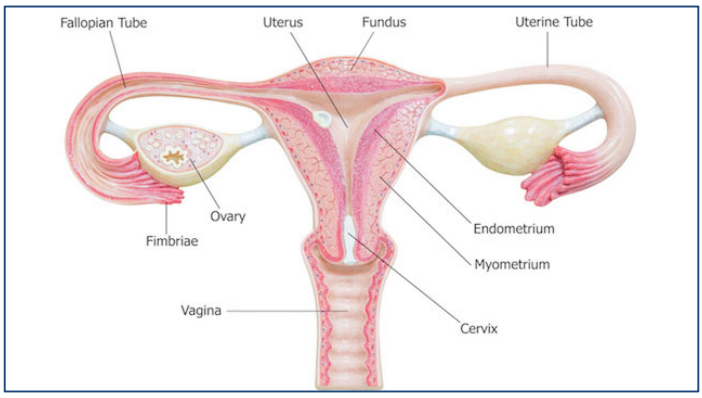

Figure 14. ***Schematic representation of the female reproductive system.***

This layer experiences morphologic and functional changes closely associated with the cyclic release of sexual hormones. Before puberty or following menopause, this tissue has a constant morphology and thickness.

3. Diagnosis

ECa is generally diagnosed rather soon as the disease often produces symptoms at relatively early stages. Unusual vaginal bleeding is a common sign of endometrial cancer that may lead to biopsy. Complex hyperplasia with atypia is often a precursor of type 1 endometrial cancer. Almost all ECa start in the glandular cells of the endometrium and are defined under the endometrioid adenocarcinomas subtype.

4. Classification of ECa: pathogenesis and histological/molecular features

Endometrial tumors can be classified using three categories: histopathology, pathogenetic and molecular alterations. At the histopathology level, and according to the WHO, endometrial carcinoma can be classified as endometrioid and its variants, mucinous, serous, clear cell, neuroendocrine, mixed, undifferentiated, or

dedifferentiated. Among newly diagnosed cases, approximately 85% or more are endometrioid carcinoma, 3–10% are serous carcinoma, 2–3% are clear cell carcinoma, and fewer than 2% are carcinosarcoma [66].

The Bockman classification from the 1980s, categorizes endometrial cancer into two subtypes that are based on histological characteristics, hormone receptor expression, and grade (**Table 2**) [71]. Low-grade or type 1 is the most common subtype encountering for approximately 70–80% of the new cases, and under the endometrioid histological subtype.

	Type I	Type II
Associated clinical features	Metabolic syndrome: obesity, hyperlipidaemia, hyperglycaemia, and increased oestrogen concentrations	None
Grade	Low	High
Hormone receptor expression	Positive	Negative
Histology	Endometrioid	Non-endometrioid (serous, clear-cell carcinoma)
Genomic stability	Diploid, frequent microsatellite instability (40%)	Aneuploid
TP53 mutation	No	Yes
Prognosis	Good (overall survival 85% at 5 years)	Poor (overall survival 55% at 5 years)

Table 2. ***Dual classification of ECa according to Bockman subtypes****. Adapted from Ref [66]*

They are estrogen mediated (hormone receptor positive) with high rates of *PTEN* and *KRAS* loss/mutation. Defects in mismatch repair (*MMR*) genes have also been identified [72-75]. Women with type 1 ECa are often obese and show evidence of endogenous estrogen excess. Type 2 ECa occurs in older women thought to be leaner initially, but show as well increasing BMI. Cancers of this type exhibit TP53 mutations, aneuploidy, and overexpression *HER-2/neu*. They are considered as higher-grade adenocarcinomas and under the non-endometrioid subtype.

Finally, integrated genomic analysis of endometrioid and serous carcinomas by TCGA in 2013, led to the classification of ECa into 4 subgroups: *POLE*-mutated (ultramutated), microsatellite instable (MSI, hypermutated), copy number low (endometrioid), and copy number high (serous-like) [76]. Tumors from the *POLE*-mutated subtype are characterized by high mutations rates (232 x 10^{-6} mutation/Mb) and hotspots mutations in the catalytic subunit of the replicative DNA polymerase epsilon (ε), encoded by *POLE [77].* They also exhibit few CNA, higher frequency of C→ T transversions, mutations in *PTEN, PIK3R1, PIK3CA, FBXW7*, and *KRAS*, and a more favorable outcome. MSI tumors are characterized by microsatellite instability and high mutation rate (18 x 10^{-6} mutations/Mb), as well as frequent MLH1 promoter hypermethylation, indicating a defective MMR. They also show few CNA, recurrent *RPL22* frameshift deletions, and *KRAS* and *PTEN* mutations. Copy-number low subtype consists of grade 1 and 2 endometrioid tumors with stable MSI and low mutation rates (2.9 x 10^{-6} mutations/Mb). Copy-number high are serous-like tumors characterized by extensive CNA, stable MSI, low mutation rates (2.3×10^{-6} mutations/Mb), recurrent somatic mutations in *TP53* (92%), and poor outcome[76]. In terms of clinical outcome in the TCGA cohort, the *POLE* subgroup had the most favorable prognosis, and the copy-number-high subgroup the poorest. An outline of all three classifications is presented in **Table 3**.

	Bockman	WHO*	TCGA
Basis / Features	Clinical and Epidemiological	Histological	Genomic characterization
Categories	Type I Type II	Endometrioid Serous Clear Cell	POLE (ultramutated) MSI (hypermutated Copy-number low (endometrioid) Copy-number high (serous-like)
*WHO remaining subtypes were not considered in Bockman's classification			

Table 3. ***Classification systems of endometrial cancer.*** *Adapted from Murali et al [78].*

a) Endometrioid Carcinoma

As mentioned above, endometrioid carcinoma is the most common type of endometrial carcinoma and account for approximately 85% of cases. Based on the presence of specific types of cellular differentiation it is usually divided into usual and variant types. The usual types are composed of large glands with complex architectural growth patter and extensive glandular branching that are not usually found in the normal proliferative endometrium (**Figure 15**). The variant types depend on the presence of squamous, occurring in about 10-25% of endometrioid carcinomas, mucinous and villoglandular differentiation.

At least 216 protein-coding genes as either bona fide or putative pathogenic driver genes were identified by TCGA in this subgroup. Overall, it is characterized by frequent perturbations of the PI3K–PTEN–AKT–mTOR, RAS–MEK–ERK, and canonical WNT–β catenin pathways; a high rate of MSI and a high incidence of *POLE* mutations. The tumor suppressor *ARID1A* has also been found to be frequently dysregulated [79].

b) Serous Carcinoma

The serous type represents about 3-10% of ECa and exhibit the most aggressive phenotype with a rather high number of deaths. One of its main distinguished feature is a marked nuclear atypia when compared to low-grade nuclei from grade 1 and 2 of endometrioid carcinomas (**Figure 15**). All serous carcinomas are considered as high-grade tumors. In terms of mutational load, serous carcinomas are considered as relatively quiet in comparison to most endometrioid carcinomas but higher rates of CNA and other clear distinctions [76]. The most frequent alterations occur in *TP53* in about 85% of all serous carcinomas and is considered as an early event in the pathogenesis [76, 80-82]. Perturbations in *p53* and its relevance in the initiation of serous carcinoma, have been further underscored by a mouse model in which deletion of *TP53* in the endometrium led to the development of type II endometrial carcinomas [83]. Additional molecular alterations include somatic mutation in *PPP2R1A* (17-43%), *FBXW7* (17-32%), *SPOP* (7-8%), *CHD4* (10-19%), and *TAF1* (5-13%); amplification and/or overexpression of *ERBB2* (17-57%), *MYC*, and *CCNE1* (cyclin-E), and alterations of the PI3K pathway (17–43%) [84-87].

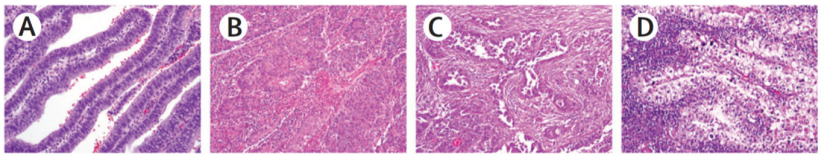

Histological type	Endometrioid	Endometrioid	Serous	Clear cell
Histological grade	Low	High	High	High
Metastasis	Uncommon	Lymph nodes Distant organs	Lymph nodes Peritoneal Distant organs	Lymph nodes Peritoneal –/+
Prognosis	Favourable	Poor	Poor*	Poor*†

Figure 15. ***Characteristics of the common types of epithelial endometrial carcinoma.*** *Adapted from [78]*

c) Clear Cell

Clear cell carcinoma is a rare subtype, accounting for less than 5% of endometrial carcinomas, in which almost all tumors are classified as grade 3. Morphologically, these tumors are composed of cells with high-grade nuclei and clear cytoplasm that grow in architectural patterns (tubulocystic, papillary, or solid) (**Figure 15**). Of note, not all clear cell carcinomas have clear cells and not all carcinomas with clear cells are clear cell carcinomas. Indeed, clear cell differentiation can also be seen in both endometrioid and serous carcinoma and even pure clear cell carcinoma consists of a heterogeneous group of tumors. In most of the cases, tumors are negative for estrogen receptor and progesterone receptor, and about 46% show focal and strong p53 staining supporting the presence of subclonal *TP53* mutations [88-90]. Clear cell carcinoma is usually found in older women. The 5-year survival rate is approximately of 50%, however women with stage I disease have a more favorable prognosis. TCGA did not analyze clear cell carcinomas subtype, thus its molecular features remain yet not fully characterized in comparison to endometrioid or serous carcinomas even though a small number of exomes have been sequenced [91]. The most frequent genomic alteration is in *TP53* that undergoes somatic mutations in 31–50% of cases and exhibits aberrant protein expression in about 34% of cases [90, 92-94]. Other mutations have been found *in PP2R1A* (16–32%), *PIK3CA* (14–37%), *FBXW7* (7–27%), *PTEN (*0–25%), *KRAS* (0–13%), *ARID1A* (14–22%), *SPOP* (14–29%), and *POLE* (0–6%). Genomic gains have been described for *CCNE1* (18%), *ERBB2* (11%), and *CEBP1* (11%), and genomic deletions for *DAXX* (11%). MSI have been identified in 0–19% of cases. Importantly, clear cell carcinoma tumors seem to share molecular features with both endometrioid and serous carcinomas that could be attributed to misclassifications from the histopathologic diagnosis. Further analysis and its genomic features is required to correctly outline the proper genomic landscape of this subtype.

d) Carcinosarcomas

Uterine carcinosarcoma is uncommon and very aggressive, accounting for less than 2% of all uterine cancer diagnoses. Tumors of this subtype show both carcinomatous and sarcomatous components. They

metastasize in a similarly to endometrial carcinomas, with the majority of the metastases being of the carcinomatous component. Integrated genomic analysis by TCGA show that most of carcinosarcomas are aneuploid, and that about 90% have undergone at least one whole genome-doubling event [95]. TP53 is as well the most commonly mutated gene (64 to 91%) in this subtype [85, 95-99]. Frequent mutations are also found in *FBXW7* (11–38%), *PTEN* (18–47%), *PIK3CA* (15–41%), *CHD4* (16–17%), *ARID1A* (10–24%), *KRAS* (9–29%), *PPP2R1A* (13–27%), and *FOXA2* (5–15%) [85, 95-99]. Interestingly about 67 to 78% of uterine carcinosarcoma bear molecularly resemblance to serous carcinomas, and 22–33% to endometrioid carcinomas. Other putative driver genes are RB1 (4–11%), *U2AF1* (4%), ZBTB7B (11%), *ARHGAP35* (11%), *SPOP* (7–18%), *HIST1H2BJ* (7%), and *HIST1H2BG* (7%). *POLE* mutations and *MMR* defects are rather uncommon, with about 2 to 4% of uterine carcinosarcomas, whereas alterations involving the P13K pathway is quite frequent with 62-67% of all tumors [85, 95-99].

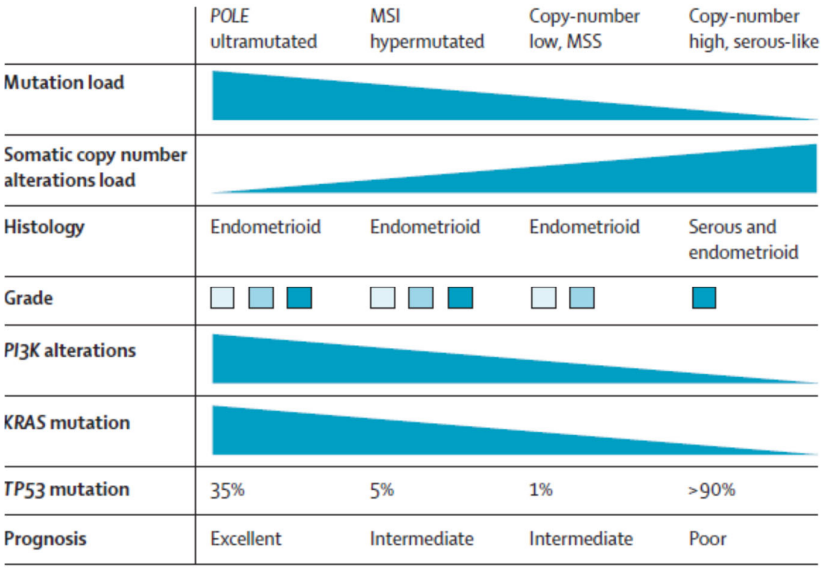

Figure 16. ***Molecular and genomic heterogeneity of ECa.*** *Adapated from Ref [100].*

5. Therapeutic options

Surgery (total hysterectomy) is the gold standard of care for early stage endometrial cancer and is effective in most of the cases. As lymph node metastases are quite noticeable in grade 2 and 3 of the disease, pelvic and para-aortic lymphadenectomy can be added to the procedure, though this process has emerged as quite controversial in the last decade [101, 102]. Type II ECa needs a different type of management. Indeed, as it accounts for less than 15% of all ECa but causes 40% of deaths due to the high incidence of associated extra uterine disease and lymph node metastasis, surgery includes hysterectomy with removal of both tubes and ovaries, pelvic and para-aortic lymphadenectomy, omentectomy, and peritoneal biopsies [103, 104].

Adjuvant radiation and vaginal brachytherapy are usually indicated to improve pelvic control and to prevent local relapse in patients with intermediate/high-risk recurrence [105]. Chemotherapy can also be used for adjuvant treatment of high-risk recurrence, advanced disease or for treatment of recurrent disease, or a combination with radiotherapy [105, 106]. Hormonal treatment with progesterone has also emerged for the treatment of metastatic disease, but the response rates (15-20%) are tightly related to the presence of steroid-hormone receptors [107, 108]. So far, only few drugs have been approved for the treatment of ECa and several trials are emerging for advanced, recurrent and metastatic disease. Characterization of genetic aberrations and their specific molecular processes in tumorigenesis are thus important to implement new-targeted therapies.

D. Role of Speckle-type POZ protein (SPOP)

SPOP is located on chromosome 17 and was first identified in 1997 [109]. The product protein is an E3 ubiquitin ligase substrate adaptor-protein of the cullin3-RING ubiquitin ligase (CRL3) that recruit targeted substrates proteins and lead to their ubiquitination and proteasomal degradation. SPOP is thus part of the so-called ubiquitin-proteasome system (UPS) [110-112].

1. Brief overview of the ubiquitination machinery

Ubiquitination is the second most abundant post-translational modification. It is involved in many biological processes and consists on molecular binding of an ubiquitin molecule to distinct substrate proteins [113-117]. The ubiquitin transfer is mediated by substrate adaptor proteins, which bind and therefore recruit the substrate to the ubiquitin ligase complex [118]. Ubiquitination requires the sequential chemical activation of ubiquitin-activating enzymes (E1s), ubiquitin-conjugating enzymes (E2s) and ubiquitin ligases (E3s).

E1 enzymes (encoded by only two genes in the genome) use ATP to generate a high-energy thioester bond between the carboxyl terminus of ubiquitin (Ub) and an active site cysteine residue (Cys) (**Figure 17**). Charged E1s then transfer ubiquitin to one of, more or less, 40 E2s present in the human body. It then complexes with one of the 600 E3s to produce an ubiquitylated substrate. E3 ligases that directly transfer ubiquitin from E2s, are part of the RING family (really interesting new gene). If they undergo charging of their active Cys residues from which ubiquitin is then transferred to the substrate, they are part of either the HECT (homologous to E6AP carboxyl terminus) or the RBR (RING-between-RING) family. About 100 human deubiquitinases (DUBs) can then cleave ubiquitin off its targeted protein and terminate its signaling event.

Proteins are marked either for selective proteasome or for lysosomal degradation, whereas organelles are marked for autophagic clearance [119, 120]. Ubiquitination has also multiple non-degradative functions, such

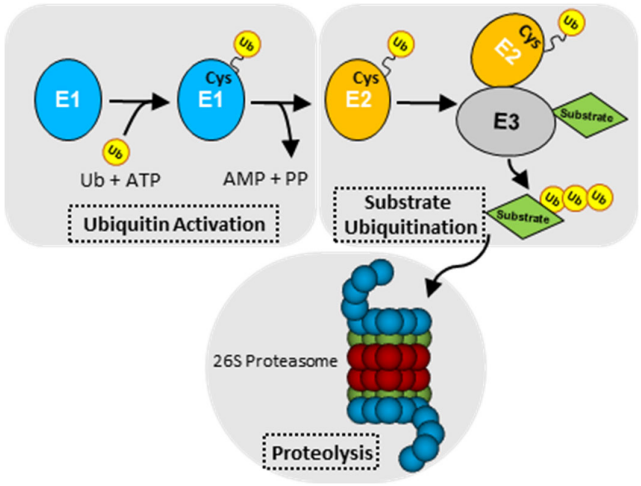

as the regulation of protein activity and their localization and is thus is associated with practically all cellular process (e.g. transcriptional regulation and metabolism) [115-117]. Ubiquitylation has a central role in maintaining body homeostasis. Its deregulation is thus associated with several diseases, including cancer [121]. Indeed, many E3s are deregulated in cancer through epigenetic and genetic mechanisms [122].

Figure 17. ***The enzymatic cascade of ubiquitin transfer.*** *Inspired by Albekairy et al, Int. J. Med. Med. Sci., 2013.*

2. SPOP Structure

Human SPOP is a protein of 374 amino acid residues, divided into three main domains and a nuclear localization signal (NLS) (**Figure 18**):

1) The meprin and TRAF homology (MATH) domain serves as a binding surface that recruits protein substrates to the ubiquitin ligase complex [112].

2) The central Bric-a-brac/Tramtrack/Broad (BTB) domain mediates homo-oligomerization of SPOP molecules and its interaction with the cullin3-RING E3 ubiqutin ligase complex (CRL3). The human genome contains more or less 205 genes that encode BTB domains.

3) The Kelch (BACK) domain is also important for dimerization as highly ordered SPOP molecules are required for the ubiquitin ligase activity and SPOP proper localization [112, 123-125].

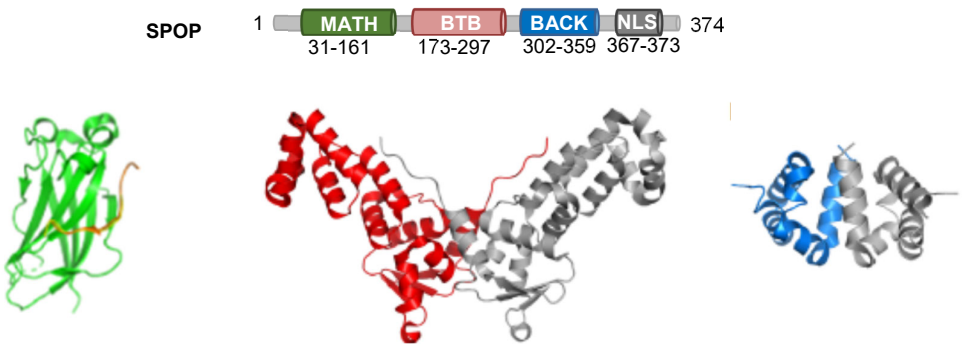

Figure 18. ***Schematic representation of SPOP and its main domains and corresponding 3D structure.*** *(Top) SPOP domains with MATH (green), BTB (red), BACK (blue). (Bottom) Domains' structure with MATH (green), BTTB (red) and BACK (blue). Adapted from Ref. [126].*

The cullin-RING E3 ligase (CRL) complex family is the largest one and comprises 8 members (CRL1, CRL2, CRL3, CRL4A, CRL4B, CRL5, CRL7, CRL9). Cullin3 substrates adaptors count many proteins; however, SPOP is the only one to form oligomers and self-associate that way, affecting dramatically its function.

The substrate recognition site is present within the MATH domain, where most of the cancer-associated mutations are found [47]. It is composed of a sandwich of two anti-parallel β-sheets forming a groove in which the substrate can bind. Structural studies have described that SPOP selectively binds with its substrates by recognizing their SPOP binding consensus motif (SBC) , a five-residues motif described as follow : φ - π – S – S/T – S/T , where **φ** represents a nonpolar residue, and **π** a polar one (**Figure 19**) [112] . In addition, SPOP is largely conserved across species: chimpanzee, Rhesus monkey, dog, cow, mouse, rat, chicken, zebrafish, fruit fly, mosquito, C.elegans, A.thaliana, rice, and frog.

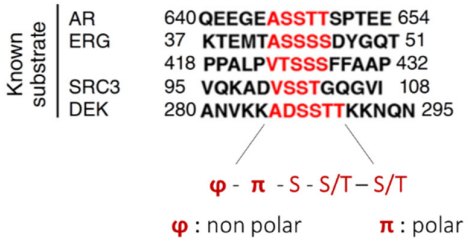

*Figure 19. **SPOP binding consensus sequence (SBC) highlighted in known SPOP substrates**. Adapted from Dai et al [127]*

3. SPOP in cancer

Accumulating evidence suggests multiple roles for the ubiquitin ligase substrate adaptor protein SPOP in cancer. Indeed, SPOP is classified as an important cancer gene across 21 different types of cancers (**Figure 20**) [128]. However, SPOP exhibits opposing function towards oncogenicity in a context-dependent manner. In several studies SPOP has been shown to suppress tumorigenesis in multiple types of cancer such as prostate, lung, gastric, liver, colon and endometrial , through mainly its ability to bind and target an important emerging number of substrates for proteasomal degradation. In lung cancer (LC), SPOP has been observed to be downregulated at mRNA and protein levels in non-small cell LC (NSCLC) [129]. Moreover, its low level was considered as a predictor of poor prognosis. In colorectal cancer (CRC), SPOP has also been shown to be downregulated, and linked to clinicopathologic features such as distant metastasis [130]. Interestingly, recurrent somatic mutations have been found in 4-14% of prostate and endometrial cancer patients [47, 48, 86, 98, 131-133].

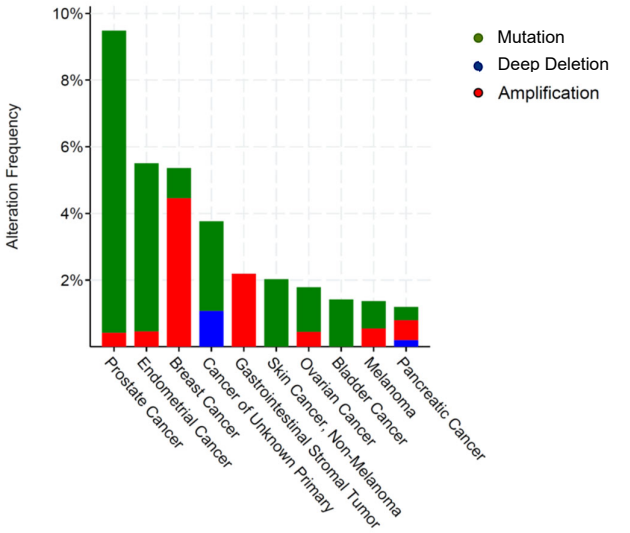

*Figure 20. **Genetic aberrations in SPOP across depicted cancer type.** Threshold of 100 minimum cases and altered in minimum 1% of all the cases. PanCancer study MSK-IMPACT clinical sequencing Cohort [134].*

a) Prostate cancer associated SPOP mutations

In prostate cancer, the heterozygous point mutations cluster in amino acid residues of the substrate-binding cleft (**Figure 21**) [47]. This specific region within the MATH domain is crucial for substrate binding and implies that the various mutations might alter interaction and ubiquitination of certain substrates in order to promote tumorigenesis [48, 112]. They have been identified as early events in genomic instability and prostate tumorigenesis [135, 136]. Most of these hot-spot mutations, such as SPOP-Y83, -Y87, -F102, - F125, -K129, -D130, -W131, -F133, have showed to impair ubiquitination of specific proteins in a dominant-negative manner, as one mutant allele is sufficient to disrupt the binding [137]. At the molecular level, SPOP mutants form with the wild type protein, heteromeric complexes that lose the ability to bind oncogenic substrates[137].

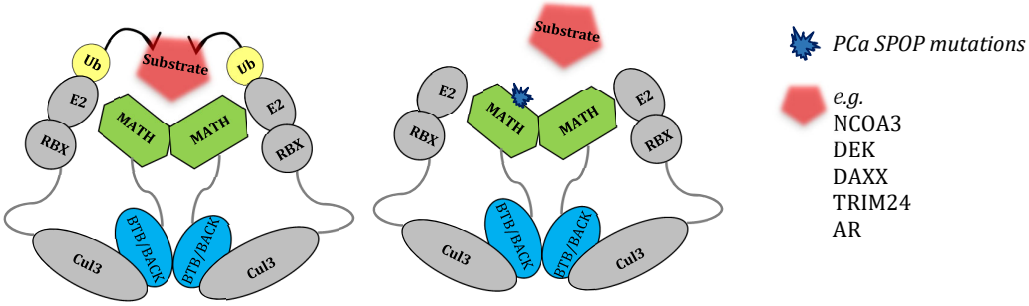

*Figure 21. **Schematic representation of SPOP in complex with E3 ligase CUL3.RBX and E2.** Wild-type SPOP (left) and SPOP PCa-associated point mutations (right) are illustrated.*

Several animal models have been generated to understand the physiological role of SPOP in PCa. In zebrafish, homozygous deletion of *SPOP* led to impairment of the brain, eye and body development that could be rescued through injection of *SPOP* mRNA. In mice, *SPOP* $^{-/-}$, resulted in non-viable pups with death occurring between embryonic day 18.5 and postnatal day 1 [138]. Recently, a transgenic prostate-specific mouse model (*SPOP* ^{F133V}) has also been developed. Functional studies revealed the implication of *PTEN* loss and both P13K/mTOR and AR signaling pathway in prostate tumorigenesis in the context of mutant *SPOP [139]*.

Importantly, several molecular and biochemical studies further highlighted the tumor suppressive role of SPOP in PCa though its ability to degrade specific substrate-oncogenes such as SRC3, AR, TRIM24, c-Myc, DEK, SENP7, EglN2, ATF2, cdc20, ERG, PD-L1 and cyclin E1 [131, 137, 140-149].

b) Endometrial cancer associated SPOP mutations

In endometrial cancer, the recurrent clonal mutations are all missense mutations in seven hotspots (SPOP-E47K, -E50K, -E78K, -E80R, -M117V, -R121Q and D140N) and localized in a yet uncharacterized territory of the MATH domain (**Figure 22**) [86, 133]. SPOP-E47K, -E50K, -E78K and E80R cluster within a small acidic region that is composed of four glutamic acid residues. Interestingly, mutations within this region, except for one, change all to lysine residues, which reverts the charge from acidic to basic. These various types of mutations

lead to a nonrandom distribution, which match the signature of cancer driver events (**Figure 22**). Consequently, *SPOP* is a significantly mutated gene in endometrial cancer [128].

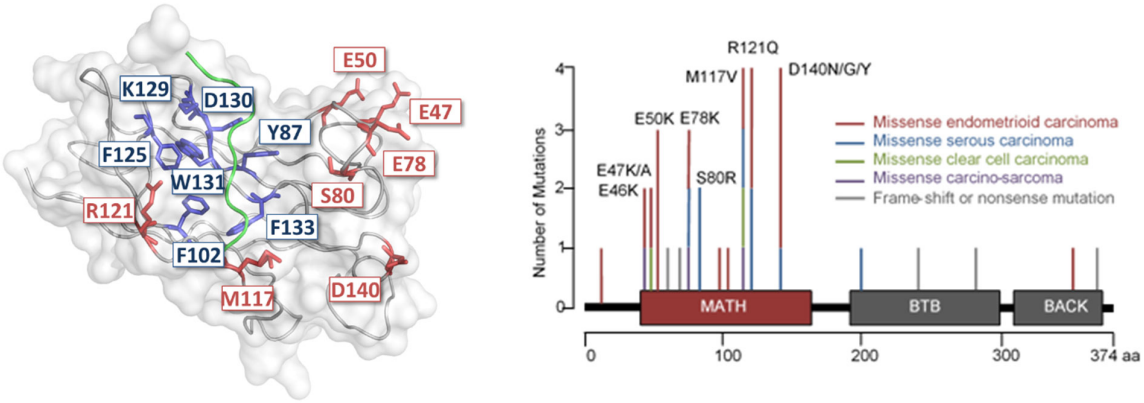

*Figure 22. **Recurrent SPOP mutations in endometrial and prostate cancer. Left:** Outer surface of the SPOP substrate recognition domain with recurrently mutated amino acid residues highlighted in blue for prostate cancer and red for endometrial cancer, respectively [112]. Substrate in green in the substrate binding cleft. **Right:** Histogram of SPOP mutations as detected in three genomic studies of endometrial cancer and carcinosarcoma, mutation depicted with an allelic fraction of 0.1 or higher [86, 98, 133].*

In contrast to prostate cancer, where *SPOP* mutant tumors retain one wild type SPOP allele, 20-30% of endometrial tumors lack SPOP wild type DNA [133]. Besides, an endometrial cell line with a recurrent SPOP mutation (EN cancer cell line, SPOP-R121Q) harbors only mutant SPOP DNA. The loss of the wild type allele may have functional implications in tumorigenesis. Indeed, since mutant and wild type SPOP are likely to form oligomers, they may have different specificity to certain substrates when compared to mutant oligomers only. The recurrent mutations of *SPOP* across endometrial cancer patients indicate that these alterations have been selected during tumor growth. However, it is unclear how they contribute to tumorigenesis and to patient survival. Characterization of *SPOP* mutations may thus open new therapeutic opportunities for both endometrial and prostate cancer patients with advanced or recurrent disease.

c) Oncogenic or undetermined function of SPOP

In contrast to its tumor suppressive functions in many of the above described cancer types, SPOP has also been shown to act as an oncogene. Indeed, in clear cell renal cell carcinoma (ccRCC, kidney cancer), SPOP is over expressed and mislocated to the cytoplasm and is a direct transcriptional target of hypoxia-inducible factors (HIFs) [150]. This mislocation leads SPOP to target proteins containing an SBC motif that are not usually substrates such as PTEN and other dual-specificity phosphatases (DUSPs) for degradation through the proteasome [150]. Silencing of SPOP mediated by RNAi resulted in apoptosis and anti-proliferative activity in renal cell cancer cells [151]. In addition, germline polymorphisms and mutations in SPOP correlate with an increased predisposition to glioma [152]. SPOP is also amplified in about 5% of breast cancer and seems to exhibit both tumorigenic and suppressive role, through degradation of various substrates (e.g. SRC3, BRSM1

4. SPOP substrates

SPOP has thus been shown to exhibit both tumor suppressor and tumorigenic functions through its specific substrates and their role towards cancer progression. To date, more than 30 targeted proteins have been found to be specifically regulated by SPOP (**Table 4**). Overall, SPOP targets a wide range of biological processes, including hormone signaling effectors (e.g. androgen, estrogen, progesterone receptors) and transcriptional regulator steroid receptor coactivator (SRC3). SPOP also targets several transcription factors such as Gli2 (affecting cell fate determination and tissue patterning) as well as epigenetic writing through SETD2 [163].

Cancer type	Substrates	Function/Implicated in	Ref
Breast	c-Myc SRC3 PR : Progesterone Receptor	Cell cycle Nuclear hormone receptor Nuclear hormone receptor	[153] [154] [155]
Colorectal	Gli2 HDAC6	Transcription factor Epigenetic/chromatin remodelling	[130] [156]
Endometrial	ERα : Estrogen Receptor	Nuclear hormone receptor	[157]
Gastric	Gli2	Transcription factor	[158]
Hepatocellular carcinoma	SENP7	SUMO-specific protease	[143, 159]
Kidney	Daxx DUSP7 Gli2 PTEN	Cell cycle Protein-tyrosine phosphatase Transcription factor Tumor suppressor	[150, 160]
Lung	SIRT2 FADD	NAD-dependent deacetylase Apoptosis	[161] [162]
Prostate	AR: Androgen Receptor ATF2 cdc20 c-Myc, Cyclin E1 DEK EgiN2 ERG PD-L1 SENP7 SRC-3 TRIM24 NANOG	Nuclear hormone receptor Transcription factor Cell cycle Cell cycle Nucleic acid transactions Hypoxia inducible factor Transcription factor Adaptive immunity SUMO-specific protease Nuclear hormone receptor Transcription factor / AR co-activator Embryonic stem cell	[131, 137, 139-144, 147-149]

*Table 4. **SPOP substrates to date and corresponding cancer type**. Inspired from [126]*

E. Bromodomain and Extra-Terminal domain (BET) proteins: epigenetic readers in cancer

1. Epigenetics

In 1942, Waddington first used the word "epigenetic", in trying to describe the changes in phenotype without changes in genotype [164, 165]. In other term, the interactions between the environment and the genome itself that would lead to a different phenotype. Epigenetic is thus the mechanism through which heritable changes in gene function occur that are not attributed to DNA sequence variations but by adapting the chromatin. Regulation of particular genes occurs in the nucleosome, a very well-organized structure (**Figure 23**). It contains the DNA packaged within eight histone proteins of two H2A, H2B, H3 and H4 [166].

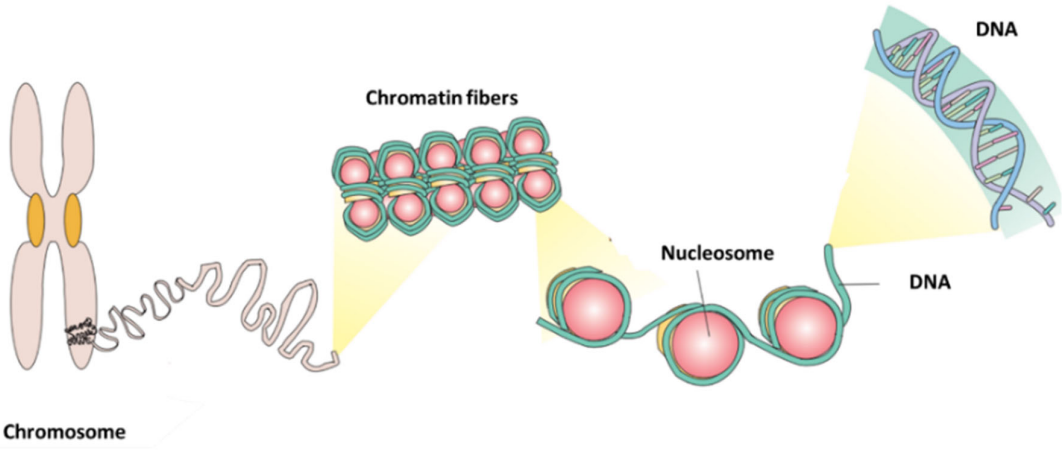

*Figure 23. **Schematic representation of the chromatin and histones**. Nucleosome is the fundamental structural unit of chromatin. It consists of DNAwound around an octameric histone core composed of two molecules of H2A, H2B, H3 and H4 subunits. Each nucleosome unit is connected to each other's through a DNA linked with histone H1 subunit. Adapted from Medical and Biological Laboratories CO, LTD.*

These histone proteins have long N-terminal tails protruding from the nucleosome that can undergo several post-translational modifications (PTMs) such as acetylation, methylation, and phosphorylation with several implications for normal and disease development [167, 168]. Acetylation of histone's lysines is in principle the most dynamic of these alterations. This reversible, and thus targetable, process leads to structural changes in chromatin and plays a key role in the regulation of several cellular processes, such as protein conformations, interactions and transcription activation [169-171].

The key players that contribute to these modifications are being characterized progressively with the latest research studies and acquired knowledge in epigenetics. They are divided into 3 subgroups based on their function (**Figure 24**): (1) Epigenetic **writers** are a group of enzymes that can modify nucleotide base and specific amino acid residues present on the histones. This family contains histone acetyltransferases (HAT), histone methyltransferases (HMT), and kinases. (2) Epigenetic **erasers** are a class of enzymes that can

removing these marks. It comprises histone deacetylases (HDAC), demethylases, and phosphatases. (3) Epigenetic **readers** are a class of proteins scaffolds that are specialized in recognizing the specific covalent modifications of histone proteins or DNA in a locus. These proteins contain specific domains such as bromodomains, chromodomains, PHD fingers, PWWP domains.

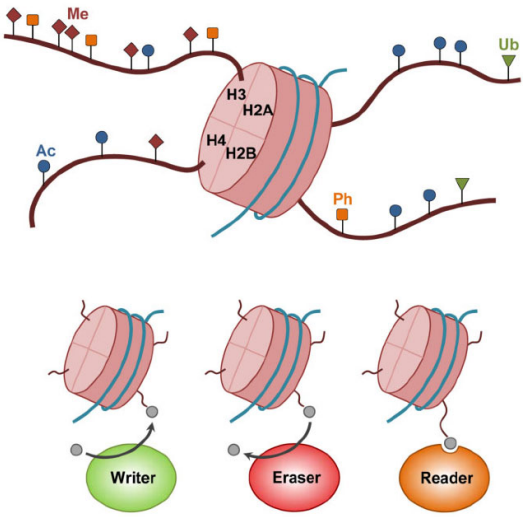

Figure 24. ***Epigenetic tools and PTMs****. Core histone tails are protrude from nucleosomes and can undergo PTMs, including methylation (Me), acetylation (Ac), phosphorylation (Ph) and ubiquitination (Ub). Epigenetic writers add chemical modifications, erasers remove the covalent modifications and readers recognize and bind to these modifications. Adapted from Ref. [170].*

2. Biology of BET family proteins

The bromodomain and extra-terminal (BET) family is composed of BRD2, BRD3, BRD4 and BRDT, and are known as epigenetic readers of the chromatin. These highly-conserved proteins share a common domain architecture of two N-terminal bromodomains (BD1 and BD2), an extraterminal domain (ET) and a C-terminal recruitment domain (CTD) [172] (**Figure 25**). The bromodomain (BRD) is a 110 amino acid motif consisting of four anti-parallel α-helices (αZ, αA, αB, αC) and two connecting loops that form a binding pocket and interact with acetylated lysine residues of histone tails [173, 174]. The Human genome encodes about 61 BRDs that can be found in 46 diverse proteins, which sequence variations occur in the binding-loops [175, 176]. BET proteins are part of larger nuclear complexes implicated in transcriptional regulations and chromatin remodeling. Some studies also show a contribution to several biological processes such as proliferation, inflammation, adipogenesis, post-mitotic memory, and virus latency and memory [177-180].

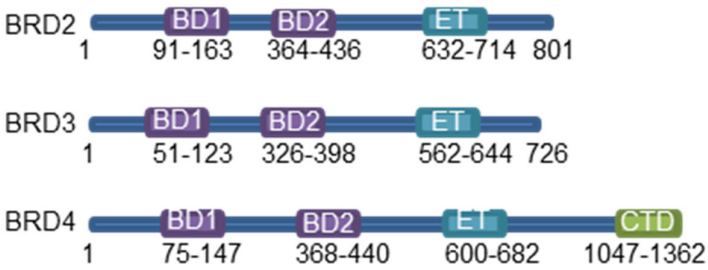

Figure 25. ***Schematic representation of BRD2, BRD3 and BRD4 domains.***

BRDT

BRDT is primarily expressed in germ cells of the testis and plays a role in spermatogenesis through gene regulation during meiosis whereas BRD2, 3 and 4 are ubiquitously expressed [181].

BRD4

BRD4 is the most studied and characterized member of the BET family. It recruits the active form of the positive transcription elongation factor b (P-TEFb) to promoters of cell-proliferation genes with active transcription load (**Figure 26**) [182]. P-TEFb is a multiprotein complex that contains a catalytic subunit CDK9, and a regulatory subunit cyclin T1. It is the BD2 domain of BRD4 that interact with the acetylated lysines of cyclin T1 [183]. During elongation, active P-TEFb phosphorylates RNA Polymerase II (POL II) at Ser2 residue, important for the activation of its CDK9 kinase unit [184][156]. BRD4 is thus essential for the expression of several genes through its ability to drive active elongation and transcription. Through its ET domain, BRD4 is also able to recruit JMJD6 (a histone arginine demethylase), NSD3 (a histone lysine methyltransferase) and CHD4 (the catalytic component of the NuRD nucleosome remodeler) [185, 186]. BRD4 promotes as well the transcription of several *M/G1* genes, serves as a bookmark of active genes during mitosis, and the progression of the cell cycle (G1 to S and G2 to M) [187, 188].

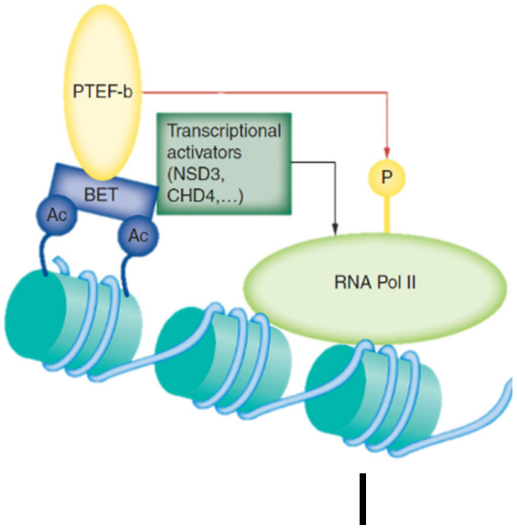

*Figure 26. **BET proteins' mechanism of function**. Adapted from Ref. [206]*

BRD3

BRD3 plays a role in the regulation of the E2F-Rb pathway, interacts with acetylated GATA1 (essential of erythropoiesis) to promote its chromatin occupancy at targeted genes [189, 190].

BRD2

BRD2 serves as a scaffold that mediates the recruitment of HATs, HDACs and E2 promoter binding factors (E2Fs) and is therefore regulating transcription in a P-TEFb independent manner [182, 191]. Indeed, E2F1 and E2F2, key transcriptional regulator of the S phase, are associated with BRD2.

3. BET proteins in cancer

Several molecular alterations found in cancer, occur in chromatin related encoding genes. Indeed, altered histone acetylation is often associated with aberrant transcription of cancer-related genes. More specifically,

genetic screening efforts have consistently identified BET proteins as essential for neoplastic cells survival in several cancer types [192-195]. Their implication was first identified in NUT midline carcinoma (NMC), a very rare and aggressive form of squamous cell carcinoma. This disease generally exhibits chromosomal rearrangements involving the *NUT* gene on chromosome 15q14 that fuses to *BRD4* on chromosome 19p13.1, or less frequently to other genes, such as g *BRD3* and *NSD3BRD* [196, 197]. This translocation generates BRD–NUT in-frame oncogene protein that drives tumorigenesis through a BRD-dependent cellular transformation, with MYC present as a downstream effector [198]. Importantly, silencing of the *BRD4–NUT* fusion gene leads to growth arrest of NUT carcinoma cells.

Several studies reported that BET proteins promote disease progression through in part the aberrant expression of *MYC* in various hematologic malignancies (mixed-lineage leukemia, acute myeloid leukemia AML, Burkitt's lymphoma and Burkitt-like lymphoma) but also in solid tumors (lung, ovary, and breast cancer) [194, 199-203]. BET proteins are also overexpressed in glioblastoma and in primary and metastatic melanoma [204, 205].

Lastly, BRD4 forms as well "super-enhancer" complexes (SEs) together with the Mediator, a multiprotein transcriptional regulator that contains the CDK8/CDK19/MED12/MED13 kinase module, and regulates the expression of several oncogenic drivers. SEs, present in a broad range of human cell types, consist of large clusters of regulatory elements with exceptionally high levels of transcription co-activators binding [207]. Cancer cells have been shown to acquire SEs at oncogenes promoters and to become later on dependent/addicted to these dysregulated transcriptional programs [208].
Consequently, targeting epigenetic proteins using small-molecule inhibitors is thus a relevant path for drug development in a wide range of cancer types.

4. BET inhibitors

In 2010, the study led by Filippakopoulos et al. [209] was the first to characterize the ability of a small molecule (a thienotriazolodiazepine, JQ1), to competitively inhibit the binding of acetylated histones (**Figure 27**). By displacing the bromodomains from the chromatin, JQ1 altered the transcriptional activity of target genes and lead in term to anti-tumor activity in NUT carcinoma cells *in vitro* but also in patient-derived xenografts models. This high affinity and specific binding towards BD1 and BD2 bromodomains opened the way to many others studies to develop novel BET inhibitors, confirming that pharmacologic inhibition of BET proteins has relevant preclinical antitumor activity in a variety of solid tumors and hematologic cancers [210-212]. BET inhibitors target the bromodomains and are thus considered as pan-BET inhibitors [213].

Many small-molecule compounds have entered clinical trials and are currently in phase I or II for hematologic malignancies and solid tumors. The safety, tolerability, pharmacokinetics, pharmacodynamics and clinical activity of BET inhibitors is thus being monitored, for example for hematological malignancies with OTX15

and GSK525762/I-BET762 in NMC (NCT02259114, OncoEthix ; NCT01587703, GlaxoSmithKline) ; CPI-0610 in refractory AML, elastodynamics syndrome (NCT02308761, NCT01949883,Constellation Pharmaceuticals) and in multiple myeloma (MM, NCT02157636).

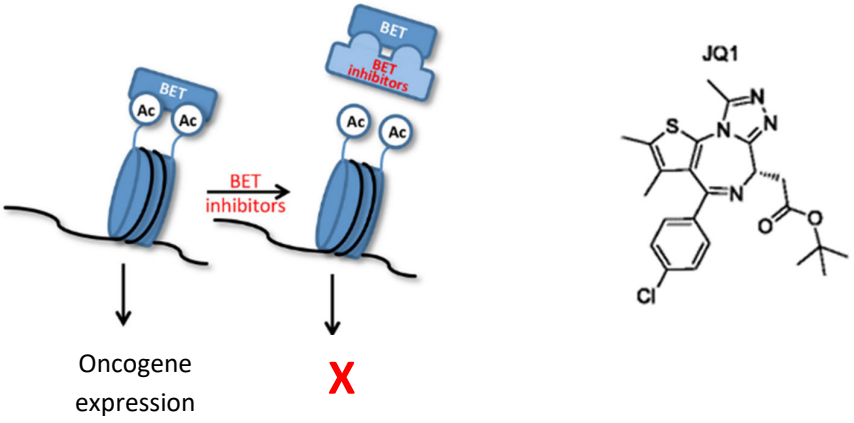

Figure 27. ***BET inhibitors mechanism of action****. Left: BET-I bind competitively to the bromodomain of BET proteins and displace them from acetylated histone tails. Transcription of targeted genes is thus shut down. (Adapted from Sahai V et al, Oncotarget, 2016) [214]. Right: JQ1 chemical structure.*

Other single and combination agent trials are also ongoing in solid tumors, in triple negative and ER+ breast cancer, small-cell and non-small-cell lung cancers (SCLC, NSCLC), CRPC, pancreatic ductal adenocarcinoma (PDAC), colorectal cancer (CC), neuroblastoma and MYCN-driven solid tumors. To date, trials have revealed mixed results with in some cases efficient clinical activity, but also the emergence of adverse events. A Phase Ib trial of OTX015 in 47 patients with advanced solid tumors showed four partial responses (PRs) and seven cases of stable disease (SD) for 4–8 months. Toxicities included thrombocytopenia, anemia and fatigue [215]. In an additional study, BAY1238097 treatment in eight patients with advanced solid tumors or NHL was stopped because of development of grade 3 headache, vomiting and low-back pain [216]. Finally, in an OTX015 trial for NMC on four patients, two achieved CT confirmed PRs, one of whom showed SUV normalization on PET scan and a third SD all with longer than expected survivals [217].

RESULTS

Article 1:

Opposing effects of cancer-type specific SPOP mutations on BET protein degradation and sensitivity to BET inhibitors

My first work focused on the functional characterization of *SPOP* mutations in prostate and endometrial cancer. As mentioned in the introduction, genomic studies have revealed recurrent point mutations within the substrate recognition domain (MATH domain) of SPOP in 4-14% of prostate and endometrial cancers. In prostate cancer, SPOP mutations are confined to amino acid residues of the substrate-binding cleft (essential for substrate interaction and ubiquitin transfer). Previous studies have shown that these mutations act in a dominant-negative fashion to repress ubiquitination and degradation of oncogenic substrate proteins. In endometrial cancer, recurrent SPOP mutations occur in an uncharacterized territory of the MATH domain. Since the mutation pattern is different in these tumor types, we hypothesized that in endometrial cancer, SPOP mutations might differently affect protein ubiquitination, which could result in distinct therapeutic opportunities.

Cancer-type-specific *SPOP* mutations have opposing effects on BET protein levels

In collaboration with the proteomics platform at the Broad Institute, the lab had previously determined the changes in the ubiquitin landscape that was induced by the seven recurrent endometrial SPOP mutants , SPOP-E47K, -E5OK; -E78K; -S80R; -M117V; -R121Q; -D140N (**Figures 1b, Supplementary Fig.1 and Fig. 2** work performed by Namrata Udeshi and Jean-Philippe Theurillat). SPOP mutants decreased the expression and impaired the ubiquitination of a subset of relevant proteins implicated in tumorigenesis (TRIM24, AGR2). We also identified a subset of proteins with enhanced ubiquitination and decreased expression and as top candidates BRD2, BRD3 and BRD4, members of the BET protein family. I generated stable cell lines over expressing each endometrial SPOP point mutations in Ishikawa (endometrial cancer cell line) and confirmed that BET proteins were downregulated at the protein levels, using western blotting and qRT-PCR (**Fig. 1c, Supplementary Fig. 3b,** performed by myself) . I also found that prostate cancer-associated SPOP mutants increased BET protein expression in a dominant-negative fashion, when I overexpressed different prostate SPOP mutants (SPOP-Y87C; -F102C; -W131G) in 22RV1 (prostate cancer cell line) , (**Fig. 1d** , performed by myself). Different prostate and endometrial cell lines were also used to show that these differential effects were determined by the specific mutations and not by the cell lineage specificities (**Supplementary Fig. 3c, d** performed by Hana Janouskova and **Supplementary Fig. 3e, f** performed by myself). Importantly, through immunohistochemistry analysis, we found that the nuclear levels of BET proteins correlated inversely with recurrent SPOP mutations in human primary endometrial cancer tissues, whereas a positive correlation was

noted in primary human prostate cancer tissues (**Fig. 1f, g and Supplementary Fig. 4**, performed by Marco Losa and Jean-Philippe Theurillat).

BET proteins are bona fide SPOP substrates

To determine whether SPOP directly interacts with BET proteins to promote ubiquitination, I first searched for the presence of the conserved SPOP-binding motif consensus sequence and found it in the primary amino acid sequences of all three BET proteins (**Fig. 2a,** generated by myself). I focused on BRD3 for experimental follow-up and generated a degron mutant variant by substitution of three threonine residues into alanine residues (degron-MT, **Supplementary Fig. 5a**). Using knockdown, co-immunoprecipitation, time course experiments, proteasome inhibition, and ubiquitination assays we showed that the SPOP-CUL3 ubiquitin ligase complex degrades BET proteins through the specific conserved binding motif present in all BET proteins (**Fig.2b-e** performed by myself**, Supplementary Fig. 5d** performed by Anna Ulbricht, and **Supplementary 5a-c , 5e-f** performed by Hana Janouskova).

Cancer-type-specific SPOP mutants induce differential ubiquitination of BET proteins

Through comparison of different endometrial cancer cell lines, the EN cell line was found to harbor a recurrent SPOP mutation (SPOP-R121Q) at the endogenous locus and expressed the lowest levels of BET proteins (**Supplementary Fig 6a and Fig. 3a** performed by Hana Janouskova). I found a more significant increase in BET protein levels upon SPOP depletion or short-term proteasome inhibition in EN cells than in Ishikawa cells (**Fig. 3b and Supplementary Fig. 6c–e**, performed by myself). In addition, we found that endogenous SPOP-R121Q bound more efficiently to BET proteins in EN cells, with a more pronounced degradation of BET proteins after inhibition of protein synthesis with cycloheximide **(Fig. 3c and Supplementary Fig. 6f** performed by Hana Janouskova and **Supplementary Fig.6g** by myself).

Next, I analyzed the activity of different SPOP species side by side in 293T cells in order to test whether the different BET protein binding and degradation kinetics in EN and Ishikawa cells were a result of the specific SPOP mutation. We found that endometrial cancer–associated SPOP mutants (E50K and R121Q) bound more strongly to HA-BRD3 than SPOP-WT *in vivo* and *in vitro*, whereas the interaction with the prostate cancer–specific SPOP mutants W131G and F133L was reduced (**Fig. 3d**, performed by myself and **Supplementary Fig. 6h,** performed by Anna Ulbricht). Ubiquitination of HA-BRD3 was increased with the endometrial cancer–specific SPOP mutants and decreased with the prostate cancer–specific mutants (**Fig. 3e** performed by myself, and **Supplementary Fig. 6i** performed by Anna Ulbricht). Moreover, SPOP-E50K failed to ubiquitinate the degron variant of BRD3 and to reduce its protein levels (**Fig. 3f and Supplementary Fig. 6j**, performed by myself).

Sensitivity to BET inhibitors is altered by cancer-type-specific *SPOP* mutations

We wanted to investigate if our data could have specific clinical implications, as small molecules targeting BET proteins (BET inhibitors, BET-i) are currently under clinical investigation for several cancer types [218-221]. We sought to determine if the differences in BET proteins levels upon expression of SPOP mutations could influence the susceptibility of cancer cells to BET-i. Indeed, endometrial cancer–specific SPOP mutants, exhibiting lower BET protein levels, sensitized Ishikawa cells to both BET inhibitors, JQ1 and OTX015, by promoting apoptosis and reducing cellular proliferation (**Fig. 4a and Supplementary Fig. 7b–d** , performed by myself, **Supplementary Fig. 7e** performed by Hana Janouskova). We found similar results in HEC-151 and RL95-2 endometrial cancer cells (**Supplementary Fig. 7f**, performed by Hana Janouskova). I found that the levels of each BET proteins in response to endometrial-SPOP mutants in Ishikawa cells correlated with a decrease of the half-maximal inhibitory concentration (IC50) upon JQ1 treatment (**Fig. 4b**, performed by myself). Additionally, overexpression of the BRD2, BRD3 and BRD4 degron variants in the sensitive cell line SPOP-E50K Ishikawa cells lead to increased resistance to JQ1 (**Fig. 4c and Supplementary Fig. 7g**, performed by Hana Janouskova). On the contrary, Ishikawa and 22Rv1 cell lines overexpressing prostate cancer–associated SPOP mutants were more resistant to JQ1 in comparison to SPOP-WT (**Fig. 4a and Supplementary Fig. 7h, i**, performed by myself). Importantly, the individual or combined knockdown of BET proteins in the context of mutated SPOP-Y87C rescued this phenotype (**Fig. 4d and Supplementary Fig. 7j-l**, performed by myself).

We then wanted to determine if the recurrent SPOP mutations or BET protein levels in general would predict sensitivity to BET inhibition across a wide-range of endometrial cancer cell lines. I assessed the JQ1 sensitivity in 3D culture conditions across 12 different human cell lines, and correlated it with their respective BET protein levels. Lower levels of BRD2, BRD3 and BRD4 (when compared to Ishikawa cells) were associated with sensitivity to JQ1 in many cases (**Supplementary Fig. 8a–c,** performed by myself). I also found a couple of cell lines that did not correlate and that could be explained by other previously established molecular mechanisms regulating the response to BET inhibitors [214, 222]. Importantly, the EN cells (SPOP-R121Q) were highly sensitive to JQ1 inhibition (**Supplementary Fig. 8b,** performed by myself). We looked for additional cell lines with recurrent endometrial cancer–associated *SPOP* mutations at the endogenous locus and identified a colorectal (NCI-H508) and a urothelial (VM-CUB1) cancer cell lines in the Catalogue of Somatic Mutations in Cancer (COSMIC) Cell Lines Project that harbored *SPOP* mutations (E47K and E50K , respectively). Both cell lines were particularly sensitive to JQ1, exhibited lower BET protein levels in respect to Ishikawa cells and were responsive to proteasome inhibition (**Fig. 4e** and **Supplementary Fig. 8d,** performed by myself). Taken together, the data show that endometrial cancer–associated *SPOP* mutations may be more broadly associated with sensitivity to BET-i. To understand whether established SPOP substrates could influence responses to JQ1 through changes in BET protein levels, we performed knockdown and overexpression of DEK, TRIM24, NCOA3 or ERG and did not found significant changes in BET protein

levels or JQ1 response. The data show that SPOP mutants affect sensitivity to JQ1 directly through regulation of BET protein degradation (**Supplementary Fig. 9,** performed by myself).

Transcriptome analysis identifies *FOSL1* as a determinant of JQ1 response

BET inhibitors bind competitively to the bromodomains of BET proteins to displace them from the acetylated histone tails of transcriptionally active sites. We thus decided to investigate the transcriptional profile of Ishikawa cells overexpressing SPOP-WT and two endometrial cancer and prostate cancer–associated SPOP mutants (**Supplementary Table 2,** performed by Anna Rinaldi and Luciano Cascione) and found mainly opposing transcriptional changes with SPOP-WT positioned in between the two types of SPOP mutants (**Supplementary Fig. 10a**, **b** performed by Anna Rinaldi and Luciano Cascione). Interestingly, the multidimensional scaling (MDS) analysis revealed a second feature that discriminated both types of mutants from SPOP-WT, which could be the reflection of shared SPOP substrates dysregulation such as TRIM24 or NCOA3. Moreover, we found a significant overlap between the differentially expressed genes in the untreated conditions and upon JQ1 treatment (**Fig. 5a**, **b** and **Supplementary Fig. 10a**–**c,** treatment performed by Hana Janouskova, transcriptome analysis performed by Anna Rinaldi and Luciano Cascione).

We identified 16 genes with altered expression across all conditions (untreated, 500 nM or 2 µM JQ1), including *FOSL1*, a previously reported target gene for BET proteins and implicated in sensitivity to BET inhibitors. Both FOSL1 mRNA and protein levels were reduced in cells that overexpressed endometrial cancer–specific, as compared to prostate cancer–specific, SPOP mutants (**Fig. 5c,** performed by myself). Our *in vitro* data correlated as well with human tumor tissues as FOSL1 mRNA and protein levels were decreased in individuals with endometrial cancer harboring mutated *SPOP* (**Fig. 5d**, **e** and **Supplementary Fig. 7c,** performed by Marco Losa and Jean-Philippe Theurillat).

As BRD2, BRD3 and BRD4 have been reported at the *FOSL1* promoter, we investigated if changes in BET protein levels in response to SPOP mutants and JQ1 treatment would affect *FOSL1* transcription levels, (**Supplementary Fig. 10d,** generated by Luciano Cascione)[221]. We found that JQ1 treatment decreased FOSL1 expression levels in each cell type, maintaining the relative differences between both subtypes (endometrial versus prostate SPOP mutants, Fig**. 5f,** performed by Hana Janouskova**)**. Importantly, knockdown of each BET proteins decreased *FOSL1* mRNA levels in JQ1-resistant Ishikawa cells (SPOP-Y87C) (**Supplementary Fig. 10e,** performed by Hana Janouskova) and *FOSL1* knockdown itself directly rescued partially the phenotype by lowering the resistance to JQ1 treatment in this setting (**Fig. 5g,** performed by Hana Janouskova). Taken together, our data suggest that BET protein level changes in response to SPOP mutants affect the sensitivity to JQ1 treatment in part through regulation of the downstream target FOSL1.

JQ1 treatment blocks tumor growth in xenografts expressing endometrial cancer–specific SPOP mutants *in vivo*

Finally, we investigated whether our *in vitro* results showing altered sensitivity to JQ1 in response to SPOP mutants could be validated in an *in vivo* setting. We generated xenograft tumor models established from EN endometrial cancer cells (SPOP-R121Q), Ishikawa parental cells (SPOP-WT) and from Ishikawa cells overexpressing two SPOP mutants (SPOP-E50K; -S80R) and found that endometrial-associated SPOP mutations tumor growth was blocked very efficiently upon JQ1 treatment (**Fig. 6a**–**c ,** performed by Hana Janouskova, **Fig. 6d**,**e** performed by myself).

Article 2:

De novo variants in *SPOP* causes two clinically distinct Neurodevelopmental Disorders

Using clinical exome sequencing, our collaborators identified six de novo pathogenic missense variants in *SPOP* in seven individuals with developmental delay/intellectual disability, facial dysmorphisms and congenital anomalies. All mutations were missense mutations and were located in Exon 5, exon 6, exon 7 and 8: SPOP-T25A, - Y83C, -R121Q, - G132V, -R138C, -D144N (**Figure 1, Table 1-2, and Table S2**). We first mapped the different variants and all mutations were located within the MATH domain except for SPOP-T25A (Figure 2A). Through reverse deep phenotyping of the seven individuals, our collaborators found that all individuals had intellectual disability, motor and speech delay, facial dysmorphisms, and congenital anomalies (**Table 2; Table S3; Figure 1; Figure S3**).

All *in vitro* experiments were performed in our laboratory. First, we generated and cloned the construct into our vector of usage (performed by Tiziano Bernasocchi and myself). I later on amplified the different plasmids and generated lentiviral particles in HEK293 cells system. I infected Ishikawa endometrial cancer cells with the different overexpression constructs, selected them and thus generated stable cell lines of each SPOP variants. I further on harvested pellets at different passaging times and performed several immunoblots in order to measure the levels of different proteins, of which SPOP itself and the BET proteins (BRD2, BRD3, and BRD4). I repeated this experiment four times in order to have biological replicates. I also performed qRT-PCR in order to verify that the transcription levels of these proteins were not affected and thus confirm a dysregulation at the protein level (**Figures 2B, C**). I found that SPOP-T25A, - Y83C, -G132V, -R138C lead to an upregulation of BET protein levels, whereas SPOP-R121Q and SPOP-D144N lead to a downregulation of BET protein levels. We also received patient-derived cell lines (Epstein-Barr Virus Growth-Transformed Lymphoblastoid Cell Lines, EBV) for which I performed the same experiments described previously for Ishikawa cells and we could confirm a similar result than the one in the isogenic system.

To functionally analyze the effects of SPOP on BET degradations, I then decided to focus on two SPOP variants (SPOP-R138C and SPOP-D144N) showing opposing effects towards the BETs. I performed time course experiments by blocking the protein synthesis using cycloheximide and by blocking the protein degradation by proteasome inhibition (MG132). The effects of SPOP variants on BET levels, in human Ishikawa endometrial cancer cells were then assessed by immunoblotting. I could confirm that SPOP-R138C, was acting in a dominant-negative manner towards the BET proteins by showing no effect in protein degradation (constant upregulation of the protein on the immunoblot at all time points) and no effect of the proteasome inhibition, leading to protein stability. I could also confirm that SPOP-D144N was a gain-of-function mutation towards BET proteins, by showing an increase in protein turn-over when compared to SPOP-WT and a

detectable rescue of protein levels when blocking the proteasome with MG132 (**Figure S6**). As we were collaborating in a double-blind way, we did not know any of the individuals' phenotype while providing the functional results to our collaborators. Strikingly, we could establish a molecular basis for the contrasting phenotype. Indeed, the individuals harboring the two gain of function mutations (SPOP-T25A and SPOP-D144N) share craniofacial dysmorphisms including microcephaly. On the contrary, the five individuals harboring the dominant-negative mutations towards BET proteins, had macrocephaly and hypertelorism.

These findings suggest that the opposite functional effects caused by SPOP mutations result in two distinct and clinically recognizable syndromic forms of intellectual disability with contrasting craniofacial dysmorphisms.

Article 3:

Dual Functions of SPOP and ERG dictate Differential Therapy Response in Prostate Cancer (manuscript under review)

For this project, initially started by Tiziano Bernasocchi (PhD student), we focused on the two main subtypes of prostate cancer, defined on one side by *SPOP* mutations, occurring in about to 11 % of prostate cancer patients, and on the other side by the genetic rearrangements of the ERG transcription factor (*TMPRSS2-ERG)*, occurring in almost half of the primary prostate tumors [47, 223]. These two subtypes are mutually exclusively distributed across tumor genomes, and thus never co-occur together at the primary but also at the metastatic stage of the disease [48, 50, 224]. Our project aimed at identifying why this biology occurs and how it could lead to a better-personalized therapy.

Activation of the ERG oncogene and missense mutation in SPOP are synthetic sick

First, we generated stable cell lines over expressing each prostate cancer-specific *SPOP* mutations (-Y87C, -F102C, -W131G, -F133S) in VCaP human prostate cancer cells that harbor at the endogenous level, the *TMPRSS2-ERG* fusion, and performed several phenotypic assays (**Extended Fig. 1f,g** performed by Tiziano Bernasocchi) . We found that the over expression of the mutants but not the wild type SPOP decreased ERG positive cancer cells growth. We found similar results in *Pten-wt* mouse prostate epithelial cells (organoids system). Indeed, SPOP mutant organoids displayed a round shape, and the over-expression of ΔERG gave rise to characteristic finger-like protrusions while expression of both driver alterations diminished cell growth and reduced finger-like protrusion (**Fig. 1b, Extended Data Fig. 1b, c** performed by Tiziano Bernasocchi). We also assessed if the synthetic sick relationship could be translated also in an *in vivo* setting and performed xenografts in immune-compromised mice (**Fig. 1c, d** performed by Tiziano Bernasocchi). We performed similar experiments taking advantage of the LuCaP147 PDX model harboring a recurrent SPOP mutation (SPOP Y83C) and found that overexpression of ΔERG significantly reduced the growth of the cancer cells *in vitro* and *in vivo* (**Fig. 1e, Extended Fig. 2a,b** performed by Tiziano Bernasocchi). The growth advantage conferred by the overexpression of the oncogene MYC in both VCaP and LuCaP-147 , confirmed the specificity of the synthetic sick relationship between the two driver genes, and excluded the notion that our overexpression system is the underlying cause of the observed phenotype (**Extended Data Fig. 2c, d**, performed by myself). The inhibition of ERG through small molecule inhibitor (YK-4279) reverted the synthetic lethal phenotype of SPOP mutants in VCaP ERG positive cells, illustrating the specific dependency of the phenotype on the interaction of both driver genes (**Fig. 1f** performed by myself).

Mutant SPOP induced androgen receptor signaling antagonizes ERG activity.

To understand the underlying molecular alterations of the synthetic-lethal relationship of the two driver genes, we then assessed the transcriptional changes occurring in the VCaP cells in response to SPOP mutations. We analyzed the effect of mutant SPOP (SPOP-Y87C, -F102C, -F133S) on AR- and ERG-related transcription in VCaP cells, and generated custom signatures using ChIP-seq data and matched RNA seq samples (**Fig 2a,b,c and Extended Fig 3a-e**, wet-lab experiments performed by Tiziano Bernasocchi, corresponding computational analysis by Marco Bolis) . We found that the androgen receptor (AR) signaling pathway was significantly upregulated, while specific ERG target genes were repressed. Indeed, SPOP-MTs increased the transcription of genes bound by AR and induced by its ligand dihydrotestosterone (DHT) whereas the opposite effect was observed on genes bound only by ERG. Indeed, mutant SPOP downregulated ERG-induced genes such as MYC and upregulated ERG-repressed genes. The most striking transcriptional changes were found in co-bound genes linked to cellular differentiation and cell cycle arrest that are directly induced by DHT and repressed by ERG (e.g. HOXA genes, CDKN1A/p21, Fig. 1d, Fig. 2b, Extended Data Fig. 3b, c). The striking downregulation of cell cycle genes (E2F, MY targets) implies a direct link between the induction of AR/ERG co bound genes, the repression of ERG targets, cell differentiation and the synthetic sick relationship observed in the VCaP ERG-positive cells overexpressing mutant SPOP.

Importantly, we could found similar corresponding transcriptional changes in human clinical tissue highlighting the validity of our custom gene set signatures (**Fig. 2d, Extended Data Fig. 4a** performed by Marco Bolis).

ZMYND11 is a SPOP substrate that induces AR and represses ERG transcription

In collaboration with the Broad Institute, we performed mass spectrometry-based proteomics experiment in SPOP mutants VCaP cells and found a possible *de novo* SPOP substrate namely ZMYND11 that was the most upregulated protein, without changes at the mRNA level out of 9000 proteins (**Fig. 3a and Extended Data Fig. 4c, d**, performed by Tiziano Bernasocchi, corresponding proteomics and computational analysis performed by Namrata Udeshi and Tanya Svinkina). We analyzed the primary protein sequence and found two putative degron binding sites for which we generated mutant-variants (**Extended Data Fig. 5c**, performed by myself, **Extended Data Fig. 5d** performed by Tiziano Bernasocchi). I show through several *in vitro* assays (co-immunoprecipitation, proteasome inhibition, time-course protein turn over and ubiquitination assays) that the SPOP-CUL3 ubiquitin ligase complex degrades ZMYND11 through a conserved binding motif (**Extended Data Fig. 5a-i**, performed by myself). Prostate cancer SPOP mutants lose the ability to bind ZMYND11 and are thus loss-of-function mutations. Taken together, our data indicate that ZMYND11 is a *bona fide* SPOP substrate.

Several experiments (rescue by knockdown in the context of SPOP-Y87C VCaP cells , overexpression of the different degron mutated variants in VCaP cells) show that ZMYND11 is implicated in the synthetic lethality of mutant SPOP and ERG in VCaP cells (**Fig. 3b, Extended Data Fig. 6a,b** performed by Tiziano Bernasocchi,

Fig. 3c performed by myself) . The transcriptome profile was significantly overlapping with the changes observed in VCaP cells overexpressing SPOP mutant species **(Fig. 3d, Extended Data Fig. 6c**, experiments performed respectively by Tiziano Bernasocchi and myself, and corresponding computational analysis by Marco Bolis).

Wild type SPOP is required for ERG oncogenic function

We then hypothesized that ERG positive tumors might require SPOP-WT in order to degrade ZMYND11 and keep AR and ERG signaling pathways at specific levels. Indeed, while analyzing previously published ChIP seq data we found that ERG itself was recruited to the promoter region of SPOP (**Extended Data Fig. 7c**). We took advantage of another prostate cancer model, the PC3 AR-independent cancer cell line where ΔERG overexpression promotes cell invasion. We found that downregulation of *SPOP* by two short hairpins RNA reduced the capability of PC3 cells overexpressing ΔERG to invade matrigel (**Fig. 4c**, performed by Tiziano Bernasocchi).

Moreover, knockdown of *SPOP* by two short hairpins RNA in VCaP cells lead to significant decrease of colony formation capacity in 3D methylcellulose assay, and recapitulated the transcriptome changes induced by SPOP mutants exhibiting upregulation of AR signaling pathway and repression of ERG target genes (**Extended data 7e,f**, performed by myself and corresponding computational analysis performed by Marco Bolis). Importantly, overexpression of SPOP mutants (SPOP-Y87C, -F102C, -W131G, -F133S) and HA-ZMYND11-DMT2 also decreased the invasion ability of PC3 cells overexpressing ΔERG **(Extended Data Fig. 7g,h and Fig. 4d,e** performed by Tiziano Bernasocchi). Taken together, our data point out towards an important role of SPOP WT , required for ERG's oncogenic function by, in part, dampening the AR signaling pathway and promoting ERG signaling pathway.

ERG and mutant SPOP trigger different responses to therapeutic interventions

To further understand if our results could be translated into clinical implications, we tested a previously generated SPOP inhibitor, SPOP-i (compound 6b) in order to recapitulate the requirement of SPOP wild type in ERG-positive cells [225]. Indeed, the VCaP cells were the most sensitive cell line compared to several others prostate cancer cells that do not harbor the TMPRSS2-ERG translocation (PC3, LNCAP, 22RV1), *in vitro* in 3D culture conditions, whereas the inactive analogue SPOP 6c did not exert any activity (**Extended Data Fig. 8e** performed by Azzura Mutti and myself, **Extended Data Fig. 8d** performed by myself). Importantly, SPOP inhibitor increased the protein but not the mRNA levels of established SPOP substrates and ZMNYD11 while the related inactive analog compound 6c did not (**Extended Data Fig. 8a,b** performed by Azzura Muti, **Extended Data Fig. 8c** performed by myself). We then assessed the validity of our findings *in vivo* taking advantage of previously characterized PDX models, namely LuCaP-35 (ERG positive) and LuCaP-78 (SPOP-W131G). In agreement with our previous data, ERG-positive xenograft tumor models (VCaP, LuCaP-23.1, -35)

were sensitive to SPOP-i whereas SPOP mutant cells (LuCaP-78, -147) did not show any response to the drug (**Extended Data Fig. 8f,h** performed by myself, **Extended Data Fig. 8g,i,j** performed by Tiziano Benasocchi). This result was further validated in an isogenic system, where mouse prostate epithelial organoids show increased sensitivity of ΔERG-expressing cells to SPOP inhibition (**Fig. 5c**, performed by Tiziano Bernasocchi).

We then tested if by increasing the levels of dihydrotestosterone (DHT) - AR ligand - , we could recapitulate the synthetic lethality observed in VCaP cells overexpressing mutant SPOP, through the upregulation of the AR signaling pathway. We found that the VCaP cells were indeed highly sensitive to even small amount of DHT (0.01 nM) when compared to the PDX LuCaP-147 cell line harboring the point mutation SPOP-Y83C (**Extended Data Fig. 9c**, performed by myself). Moreover, exposure to high-dose of testosterone *in vivo* or DHT *in vitro* under starved condition significantly suppressed the growth of ERG-fusion positive cells but not of SPOP mutant cells (**Fig. 5a,d and Extended Data Fig. 9d,e,f,g** performed by Tiziano Bernasocchi, **Extended Data Fig. 9h,i** performed by myself). Interestingly, the transcriptome profile show induction of similar molecular changes as for the over-expression of mutant SPOP (**Extended Data Fig. 9a, b** performed by Tiziano Bernasochi, corresponding computational analysis performed by Marco Bolis). Importantly, we found a striking correlation between ERG levels and sensitivity to SPOP-i and testosterone *in vivo* (**Fig. 5a**, performed by Tiziano Bernasocchi, **Fig. 5b** performed by myself). Taken together, out data suggest a therapeutic opportunity for SPOP inhibition or high-dose androgen therapy for prostate cancer patients which cancer cells express high levels of ERG.

On the other hand, through reanalysis of published clinical data, we found that the prevalence of SPOP mutations in primary tumors and tumors that had progressed after initial surgery or radiotherapy, was strikingly higher when compared to tumors that had become resistant to subsequent androgen deprivation therapy (ADT) (**Extended Data Fig. 9j**, performed by Marco Bolis). Moreover, we could also appreciate a trend towards better overall survival despite progressing faster after initial therapy for tumors harboring a SPOP mutation (**Extended Data Fig. 9k, l**, performed by Marco Bolis and Arianna Vallerga). To functionally analyze the response of androgen deprivation or the anti-androgen enzalutamide, we overexpressed different SPOP variants and ΔERG in the androgen-dependent human LAPC4 prostate cancer cells (WT for both genes). We found that LAPC4-mutant SPOP (SPOP-Y87C, SPOP-W131G) cells were sensitive to either ADT or enzalutamide in comparison to cells expressing control vector (**Fig. 5e, Extended Data Fig. 9m**, performed by Tiziano Bernasocchi). Conversely, LAPC4-ΔERG cells were more resistant to enzalutamide. In line with our previous findings, ΔERG expression rendered LAPC4 cells susceptible to high levels of DHT, while mutant SPOP had the opposite effect (**Extended Data Fig. 9m**, performed by Tiziano Bernasocchi).

Taken together, the different therapeutic responses exhibited by mutant SPOP and ERG cells lines and PDX, highlight again the divergent AR molecular pathway implicated in both tumor type tumorigenesis.

DISCUSSION

Cancer-associated *SPOP* mutations

Comprehensive genome sequencing studies have revealed recurrent missense mutations in SPOP—encoding a substrate receptor of a cullin–RING ubiquitin ligase—in 5–10% of prostate and endometrial cancers (PCa and ECa respectively). Even though they occur in the same substrate-recognition domain, each genetic alteration is specific to its tumor type. In other term, none of them show overlap between both cancer types. Several studies have shown that PCa *SPOP* mutations stabilize targeted proteins that are important to prostate tumorigenesis (e.g. TRIM24, DEK). Regarding ECa SPOP mutations, very few studies have focused on their functional aspects. In a study from 2015, Zhang et al. showed that estrogen receptor-α (ERα) is a targeted substrate of SPOP that facilitates tumorigenesis of endometrial cancer cells [13]. However, we had difficulties to recapitulate those data in our *in vitro* cell culture models. More recently, a *SPOP−/−* mouse model was generated that displayed an infertility phenotype with lower levels of progesterone receptors (PRs) in the uterus [14]. Other *in vivo* studies show that SPOP was required for embryonic implantation and for endometrial decidualization [15].

Although an increasing number of research studies have emerged to understand the functional role of SPOP in these tumor types, their therapeutic implications remain largely uncharacterized.

Our study, together with two other groups, identifies the BET proteins (BRD2, BRD3 and BRD4) as *bona fide* SPOP substrates [16, 17]. Small-molecule inhibitors against this group of proteins (BET-i) are under clinical investigation in hematological and solid tumors. They are indeed critical in driving lineage-specific oncogenic transcriptional programs. In line with the loss-of-function properties of PCa SPOP mutations reported previously, we found that these mutations impair degradation of BET proteins. Conversely, ECa SPOP mutations enhance BET protein degradation through a gain-of-function mechanism. The specific structural basis through which ECa SPOP mutations enhance binding and ubiquitination of BET proteins and other substrates (for example, DEK) remains unclear.

Indeed, a couple of years after our publication (May 2019), a study by Ostertag et al., provided preliminary insights through the first co-crystal structure of SPOP and BRD3 [18]. Their structural and biophysical data confirmed the loss-of-function in PCa SPOP mutants and provided a mechanistic explanation. However, their data failed to show that ECa SPOP mutants altered the binding behavior compared to SPOP-WT. Only the point mutation SPOP-M117V seemed to show increased affinity in their isothermal titration calorimetry (ITC) experiments. While looking at their data in more details, we can still observe a tendency for an increased binding affinity of ECa SPOP mutants compared to WT (**Table A**). For example, by looking only at the mean K_D, we can notice an important decrease with all ECa mutations. For instance, SPOP WT exhibits a KD of 61 µM, while SPOP-E47K, -E50K, -E78K, -R121Q, and -D140N have a K_D between 41 and 48 µM. Still, the statistics relevance for these other point mutations was not reached and could be due to standard deviation and/or reproducibility of the replicates.

SPOP protein	BRD3 construct	K_D (μM)	ΔH (kJ/mol)	ΔG (kJ/mol)	-TΔS (kJ/mol)	n
WT	24-416	61 ± 11	-95 ± 13	-24.1 ± 0.4	70 ± 13	3
E47K	24-416	48 ± 11	-85 ± 14	-24.7 ± 0.6	61 ± 15	3
E50K	24-416	47 ± 2	-86 ± 2	-24.7 ± 0.1	61 ± 2	3
E78K	24-416	47 ± 3	-92 ± 1	-24.8 ± 0.1	67 ± 1	3
S80R	-	-	-	-	-	-
M117V	24-416	13 ± 3	-83 ± 2	-27.9 ± 0.5	55 ± 2	6
R121Q	24-416	41 ± 3	-80 ± 1	-25.0 ± 0.2	55 ± 1	3
D140N	24-416	55 ± 8	-102 ± 8	-24.4 ± 0.3	78 ± 8	3

Table 5. ***ITC for titrations of different SPOP constructs to BRD3 protein****. K_D represents the affinity (dissociation constant), ΔH the enthalpy, ΔG the Gibbs free energy, −TΔS indicates entropy. (n= number of independent experiments) Values are depicted as mean ± s.d. Because of sample instability, no data could be obtained for SPOP S80R. Ref. [19].*

As for explanation, the authors indicate that, likely, a more complex regulatory mechanism is involved, that is most probably related to physiological conditions. Some of these processes that cannot be unraveled in an *in vitro* setting could be linked to protein localization, liquid-liquid phase separation (a process that has recently emerged to be caused by SPOP mutations in cancer cells) or additional binding partners [20]. Moreover, as described in the introduction, SPOP forms higher-order oligomers through self-association by its BTB/BACK domain. These complexes have been demonstrated to increase ubiquitination efficiency, and emphasize the functional importance of oligomerization [21, 22]. The increased binding affinity towards BET proteins could be then dependent on that specific status that does not seem to be achieved in their structural experiments.

In addition to the discovery of BET proteins as SPOP substrates, we found that BET proteins altered levels influence the transcription of previously established target genes such as *FOSL1*, which in term alter the sensitivity of cancer cells to BET-i. *FOSL1* increased transcriptional activity has also been linked to mechanism of resistance in ovarian cancer cells [23]. Our model extends thus the list of previously reporter mechanisms that could influence BET-i sensitivity [5, 24, 25].

In line with our data on BETi sensitivity by PCa SPOP mutants, Zhang et al, demonstrated that the expression of AR, ERG and their downstream genes were inhibited by JQ1 in both SPOP-WT and PCa SPOP mutant-expressing cells, suggesting that intrinsic BET-i resistance was independent of the elevated AR and ERG signaling in SPOP-mutated prostate cancer cells. Importantly, both AR and ERG are direct binding-partners of BRD4 bromodomain. They also show that expression of PCa associated SPOP mutant increases the basal levels of phosphorylation of AKT-mTORC1 proteins, and inhibit JQ1-induced inhibition of their phosphorylation. They found that the levels of *RAC1* and cholesterol biosynthesis genes, that are required for the AKT-mTORC1 pathway activation, are upregulated in SPOP-mutated prostate tumors in patients. In addition, they provide evidence that targeting the AKT pathway can be a possible treatment option to overcome BET-i resistance in SPOP-mutated prostate cancer. In support, Blattner et al. generated a transgenic mouse model harboring a prostate-specific SPOP-F133V mutation and found that prostate cancer was developed in part through the activation of the PI3K/mTOR and AR signaling pathways as well as the loss of *PTEN* [26].

As described in the introduction, BET-i are currently under clinical development, and there is a critical need to identify patients who may respond to this treatment. Our preclinical study identifies *SPOP* mutations as a clinically detectable biomarker of BET-i response. Thus, the detection of specific SPOP mutations may be used to select patients who may (endometrial cancer–associated SPOP mutations) or may not (prostate cancer–associated SPOP mutations) benefit from treatment with BET inhibitors.

More broadly, our data suggest a paradigm whereby mutations within the same domain of a particular protein induce opposing drug responses. Given the increasing use of cancer genome information in the clinical setting, it would be important to analyze functionally the mutations involved prior to extrapolating therapeutic responses based on similar alterations.

Germline de novo SPOP mutations and neurodeveloppemental disorders

A year after the publication of our study focusing on the dysregulation of the BET proteins by mutant SPOP, the De Vries lab from the Radboud University in Nijmegen (Netherlands) identified seven individuals with neurodevelopment disorders and de novo missense variants in SPOP. As part of a collaboration, we performed several in vitro assays, and we have been able to demonstrate that these mutations induced opposite effects on BET protein activity, as supported by elevated or reduced BET protein expression levels. Interestingly, the individuals harboring the point mutations showed growth abnormalities, including a head size spectrum ranging from microcephaly to macrocephaly with distinct recognizable facial dysmorphisms. While individuals with gain-of-function mutations exhibited microcephaly, individuals with mutations leading to BETs functional loss, had absolute macrocephaly or a head circumference (HC) in the normal centile range, though exceeding the centile for height (relative macrocephaly). So far, no true congenital macrocephaly was observed, though birth HC measurements of three of the individuals were unknown. Additional investigation is required to understand the mechanisms involved in head growth in individuals with pathogenic SPOP variants, which could be determined by specific signaling pathways that govern cell proliferation. Interestingly, BET proteins have been shown to be involved in cell cycle progression [234]. In mice, BRD2, BRD3, and BRD4 levels were found to be downregulated in differentiating neural progenitor cells, but remained unaltered in proliferating neural progenitor cells [235]. In Brd2-deficient neuroepithelial cells, cell cycle progression was accelerated and neuronal differentiation as well as cell cycle exit were impaired [236]. These data tend to correlate with the phenotype (congenital microcephaly) of the two patients harboring a gain-of-function SPOP mutation that resulted in less BET protein levels leading to theoretically less neuronal differentiation. On the contrary, increased levels of BET proteins would stimulate the latter process, resulting in the same way in macrocephaly. Interestingly, a heterozygous missense mutation in BRD4 has been described resulting in macrocephaly and short stature, resembling the individuals with dominant-negative variants in SPOP [237]. The missense mutation (BRD4-H304) in the reported BRD4 variant, is in close

proximity to the described SPOP degron (AA: 292-299), which could thus lead to an increased protein stabilization.

In summary, SPOP variants have been identified in individuals with intellectual disability and in tumor samples. The data suggest that mutations in SPOP can occur at different times of development, specifically germline versus somatic tissue, and result in different consequences, i.e. neurodevelopmental delay or cancer respectively. Importantly, the individuals with NDD and de novo SPOP variants could be differentiated based on their distinct craniofacial dysmorphisms and congenital anomalies, indicating the presence of diverse clinically recognizable intellectual disability syndromes. The opposing effects of the mutations impairing SPOP function provide a molecular basis for the contrasting phenotypic differences.

Further research needs to be done in order to assess the real incidence of these mutations in NDD patients. Additionally, the evaluation of other proteins or related SPOP substrates' implication need to be identified. For example, in the 3rd article present in my thesis, we found that ZMYND11 is a de novo SPOP substrate that is implicated in the synthetic lethality between mutant SPOP and ERG, two main driver genes of prostate tumorigenesis. In the literature, ZMYND11 has also been described as being implicated in developmental delay [238, 239]. Indeed, mutations in *ZMYND11* have been identified in patients with autism spectrum disorders and intelectual disability, which support the notion that the gene is implicated in chromosome 10p15.3 microdeletion syndrome. The deletions in this region are characterized by several specificities such as development delay, speech disorders and brain abnormalities. Two genes within this area are frequently deleted, namely *DIP2C* and *ZMYND11* and are thought to contribute to the disease. Several studies implicating different patients with characteristic dysmorphic features now exhibit clear implication of *ZMYND11* [240]. Likewise, other already known or unknown SPOP substrates might as well play a role in the resulted growth abnormalities. A possible way to address this aspect would be to differentiate the patient derive cell lines (Epstein-Barr virus lymphoblastoid cell lines, EBV LCLs) into neuronal cells and assess whether specific alterations of these substrates would lead to any changes in their phenotype. Indeed, reprogramming EBV LCLs cells have recently emerged as a successful method to gather more relevant *in vitro* models [27, 28]. Generating patient LCL-derived iPCSCs (LiPCSCs , iPCSCs for patient-specific induced pluripotent stem cells) would thus function as an important tool in disease modeling. A study from the Okano lab in 2016 has actually refined the established protocol and developed a method (direct neurosphere conversion method , dNS method) in which LiPSCs could be differentiated into functional neurons in order to study effectively Parkinson's disease [29].

It would also be interesting to understand why these specific point mutations, found in cancer-related diseases, are also found at the germline level. The emergence of de novo mutations has been described to be from a paternal-age-related origin in about 80% of the cases, as a major risk factor is the advanced paternal age at the time of conception [241-243]. Indeed spermatogonial cells divide continuously during

male lifetime, allowing the the accumulation of random DNA mutations and failure of the DNA repair machinery [244]. *De novo* mutations could also contribute in giving a growth advantage to spermatogonial stem cells, which in term would lead to the clonal expansion of mutant cells in the testis [245]. Mutations in genes involved in the RAS–MAPK pathway have indeed been shown to cause clonal expansion through proliferative selective advantage, of spermatogonial stem cells [246]. It remains to be elucidated if SPOP mutations found in endometrial and prostate cancer patients would confer as well a selective advantage to primordial germ cells.

The development of conditioned engineered mouse models could for example be an approach to understand the mechanisms through which SPOP contributes to tumorigenesis and intellectual disabilities. Genome-wide screening of SPOP mutations in human cancer but also in other diseases, together with a combined proteomics approach, could be of interest to unravel the remaining SPOP functions in disease. At the era of big data, and with the recent technology improvements, these studies could be done in a rather near future. Finally, it is important to establish the rational of SPOP-targeting therapeutic capability while designing specific strategies, pre-clinical and clinical studies. It is tempting to consider whether the SPOP inhibitor, developed initially for kidney cancer and tested in our *in vitro* and *in vivo* PCa models, could be of use in a tissue-specific manner in other SPOP-dependent disease [225].

REFERENCES

1. Hanahan D, Weinberg RA: **The hallmarks of cancer**. *Cell* 2000, **100**(1):57-70.
2. Hansemann D: **Ueber asymmetrische Zelltheilung in Epithelkrebsen und deren biologische Bedeutung**. *Archiv für pathologische Anatomie und Physiologie und für klinische Medicin* 1890, **119**(2):299-326.
3. Boveri T: **Zur Frage der Entstehung maligner Tumoren**. Jena: Gustav Fischer; 1914.
4. Avery OT, Macleod CM, McCarty M: **STUDIES ON THE CHEMICAL NATURE OF THE SUBSTANCE INDUCING TRANSFORMATION OF PNEUMOCOCCAL TYPES : INDUCTION OF TRANSFORMATION BY A DESOXYRIBONUCLEIC ACID FRACTION ISOLATED FROM PNEUMOCOCCUS TYPE III**. *The Journal of experimental medicine* 1944, **79**(2):137-158.
5. Watson JD, Crick FH: **Molecular structure of nucleic acids; a structure for deoxyribose nucleic acid**. *Nature* 1953, **171**(4356):737-738.
6. Loeb LA, Harris CC: **Advances in chemical carcinogenesis: a historical review and prospective**. *Cancer research* 2008, **68**(17):6863-6872.
7. Garraway LA, Lander ES: **Lessons from the cancer genome**. *Cell* 2013, **153**(1):17-37.
8. Stratton MR, Campbell PJ, Futreal PA: **The cancer genome**. *Nature* 2009, **458**(7239):719-724.
9. Torti D, Trusolino L: **Oncogene addiction as a foundational rationale for targeted anti-cancer therapy: promises and perils**. *EMBO molecular medicine* 2011, **3**(11):623-636.
10. Bray F, Ferlay J, Soerjomataram I, Siegel RL, Torre LA, Jemal A: **Global cancer statistics 2018: GLOBOCAN estimates of incidence and mortality worldwide for 36 cancers in 185 countries**. *CA: a cancer journal for clinicians* 2018, **68**(6):394-424.
11. Patel AR, Klein EA: **Risk factors for prostate cancer**. *Nature clinical practice Urology* 2009, **6**(2):87-95.
12. Chan JM, Gann PH, Giovannucci EL: **Role of diet in prostate cancer development and progression**. *Journal of clinical oncology : official journal of the American Society of Clinical Oncology* 2005, **23**(32):8152-8160.
13. Quinn M, Babb P: **Patterns and trends in prostate cancer incidence, survival, prevalence and mortality. Part I: international comparisons**. *BJU international* 2002, **90**(2):162-173.
14. Draisma G, Etzioni R, Tsodikov A, Mariotto A, Wever E, Gulati R, Feuer E, de Koning H: **Lead time and overdiagnosis in prostate-specific antigen screening: importance of methods and context**. *Journal of the National Cancer Institute* 2009, **101**(6):374-383.
15. Etzioni R, Penson DF, Legler JM, di Tommaso D, Boer R, Gann PH, Feuer EJ: **Overdiagnosis due to prostate-specific antigen screening: lessons from U.S. prostate cancer incidence trends**. *Journal of the National Cancer Institute* 2002, **94**(13):981-990.
16. Kheirandish P, Chinegwundoh F: **Ethnic differences in prostate cancer**. *British journal of cancer* 2011, **105**(4):481-485.
17. Haiman CA, Chen GK, Blot WJ, Strom SS, Berndt SI, Kittles RA, Rybicki BA, Isaacs WB, Ingles SA, Stanford JL *et al*: **Characterizing genetic risk at known prostate cancer susceptibility loci in African Americans**. *PLoS genetics* 2011, **7**(5):e1001387.
18. Odedina FT, Akinremi TO, Chinegwundoh F, Roberts R, Yu D, Reams RR, Freedman ML, Rivers B, Green BL, Kumar N: **Prostate cancer disparities in Black men of African descent: a comparative literature review of prostate cancer burden among Black men in the United States, Caribbean, United Kingdom, and West Africa**. *Infectious agents and cancer* 2009, **4 Suppl 1**:S2.
19. Zeigler-Johnson CM, Rennert H, Mittal RD, Jalloh M, Sachdeva R, Malkowicz SB, Mandhani A, Mittal B, Gueye SM, Rebbeck TR: **Evaluation of prostate cancer characteristics in four populations worldwide**. *The Canadian journal of urology* 2008, **15**(3):4056-4064.
20. Chu LW, Ritchey J, Devesa SS, Quraishi SM, Zhang H, Hsing AW: **Prostate cancer incidence rates in Africa**. *Prostate cancer* 2011, **2011**:947870.
21. McNeal JE: **The zonal anatomy of the prostate**. *The Prostate* 1981, **2**(1):35-49.

22. Sathianathen NJ, Konety BR, Crook J, Saad F, Lawrentschuk N: **Landmarks in prostate cancer**. *Nature Reviews Urology* 2018, **15**(10):627-642.
23. Wang G, Zhao D, Spring DJ, DePinho RA: **Genetics and biology of prostate cancer**. *Genes & development* 2018, **32**(17-18):1105-1140.
24. McNeal JE, Redwine EA, Freiha FS, Stamey TA: **Zonal distribution of prostatic adenocarcinoma. Correlation with histologic pattern and direction of spread**. *The American journal of surgical pathology* 1988, **12**(12):897-906.
25. Heinlein CA, Chang C: **Androgen Receptor in Prostate Cancer**. *Endocrine Reviews* 2004, **25**(2):276-308.
26. Gleason DF: **Classification of prostatic carcinomas**. *Cancer chemotherapy reports* 1966, **50**(3):125-128.
27. Humphrey PA: **Gleason grading and prognostic factors in carcinoma of the prostate**. *Modern pathology : an official journal of the United States and Canadian Academy of Pathology, Inc* 2004, **17**(3):292-306.
28. True L, Coleman I, Hawley S, Huang CY, Gifford D, Coleman R, Beer TM, Gelmann E, Datta M, Mostaghel E *et al*: **A molecular correlate to the Gleason grading system for prostate adenocarcinoma**. *Proceedings of the National Academy of Sciences of the United States of America* 2006, **103**(29):10991-10996.
29. Epstein JI, Zelefsky MJ, Sjoberg DD, Nelson JB, Egevad L, Magi-Galluzzi C, Vickers AJ, Parwani AV, Reuter VE, Fine SW *et al*: **A Contemporary Prostate Cancer Grading System: A Validated Alternative to the Gleason Score**. *Eur Urol* 2016, **69**(3):428-435.
30. Delahunt B, Miller RJ, Srigley JR, Evans AJ, Samaratunga H: **Gleason grading: past, present and future**. *Histopathology* 2012, **60**(1):75-86.
31. Brawer MK: **Prostatic intraepithelial neoplasia: an overview**. *Reviews in urology* 2005, **7 Suppl 3**:S11-18.
32. Shen MM, Abate-Shen C: **Molecular genetics of prostate cancer: new prospects for old challenges**. *Genes & development* 2010, **24**(18):1967-2000.
33. Fakhrejahani F, Madan RA, Dahut WL: **Management Options for Biochemically Recurrent Prostate Cancer**. *Current treatment options in oncology* 2017, **18**(5):26.
34. HUGGINS C, STEVENS RE, Jr., HODGES CV: **STUDIES ON PROSTATIC CANCER: II. THE EFFECTS OF CASTRATION ON ADVANCED CARCINOMA OF THE PROSTATE GLAND**. *Archives of Surgery* 1941, **43**(2):209-223.
35. Mangelsdorf DJ, Thummel C, Beato M, Herrlich P, Schutz G, Umesono K, Blumberg B, Kastner P, Mark M, Chambon P *et al*: **The nuclear receptor superfamily: the second decade**. *Cell* 1995, **83**(6):835-839.
36. Shang Y, Myers M, Brown M: **Formation of the androgen receptor transcription complex**. *Molecular cell* 2002, **9**(3):601-610.
37. Dehm SM, Tindall DJ: **Molecular regulation of androgen action in prostate cancer**. *Journal of cellular biochemistry* 2006, **99**(2):333-344.
38. Wang Q, Carroll JS, Brown M: **Spatial and temporal recruitment of androgen receptor and its coactivators involves chromosomal looping and polymerase tracking**. *Molecular cell* 2005, **19**(5):631-642.
39. Beato M, Herrlich P, Schutz G: **Steroid hormone receptors: many actors in search of a plot**. *Cell* 1995, **83**(6):851-857.
40. Saraon P, Jarvi K, Diamandis EP: **Molecular alterations during progression of prostate cancer to androgen independence**. *Clinical chemistry* 2011, **57**(10):1366-1375.
41. Ritch CR, Cookson MS: **Advances in the management of castration resistant prostate cancer**. *BMJ (Clinical research ed)* 2016, **355**:i4405.
42. Kupelian P, Katcher J, Levin H, Zippe C, Klein E: **Correlation of clinical and pathologic factors with rising prostate-specific antigen profiles after radical prostatectomy alone for clinically localized prostate cancer**. *Urology* 1996, **48**(2):249-260.

43. Hull GW, Rabbani F, Abbas F, Wheeler TM, Kattan MW, Scardino PT: **Cancer control with radical prostatectomy alone in 1,000 consecutive patients**. *The Journal of urology* 2002, **167**(2 Pt 1):528-534.
44. Stephenson AJ, Scardino PT, Eastham JA, Bianco FJ, Jr., Dotan ZA, Fearn PA, Kattan MW: **Preoperative nomogram predicting the 10-year probability of prostate cancer recurrence after radical prostatectomy**. *Journal of the National Cancer Institute* 2006, **98**(10):715-717.
45. Damber JE, Aus G: **Prostate cancer**. *Lancet (London, England)* 2008, **371**(9625):1710-1721.
46. Fraser M, Sabelnykova VY, Yamaguchi TN, Heisler LE, Livingstone J, Huang V, Shiah YJ, Yousif F, Lin X, Masella AP *et al*: **Genomic hallmarks of localized, non-indolent prostate cancer**. *Nature* 2017, **541**(7637):359-364.
47. Barbieri CE, Baca SC, Lawrence MS, Demichelis F, Blattner M, Theurillat JP, White TA, Stojanov P, Van Allen E, Stransky N *et al*: **Exome sequencing identifies recurrent SPOP, FOXA1 and MED12 mutations in prostate cancer**. *Nature genetics* 2012, **44**(6):685-689.
48. Baca SC, Prandi D, Lawrence MS, Mosquera JM, Romanel A, Drier Y, Park K, Kitabayashi N, MacDonald TY, Ghandi M *et al*: **Punctuated evolution of prostate cancer genomes**. *Cell* 2013, **153**(3):666-677.
49. Robinson D, Van Allen EM, Wu YM, Schultz N, Lonigro RJ, Mosquera JM, Montgomery B, Taplin ME, Pritchard CC, Attard G *et al*: **Integrative clinical genomics of advanced prostate cancer**. *Cell* 2015, **161**(5):1215-1228.
50. Grasso CS, Wu YM, Robinson DR, Cao X, Dhanasekaran SM, Khan AP, Quist MJ, Jing X, Lonigro RJ, Brenner JC *et al*: **The mutational landscape of lethal castration-resistant prostate cancer**. *Nature* 2012, **487**(7406):239-243.
51. TCGA: **The Molecular Taxonomy of Primary Prostate Cancer**. *Cell* 2015, **163**(4):1011-1025.
52. Berger MF, Lawrence MS, Demichelis F, Drier Y, Cibulskis K, Sivachenko AY, Sboner A, Esgueva R, Pflueger D, Sougnez C *et al*: **The genomic complexity of primary human prostate cancer**. *Nature* 2011, **470**(7333):214-220.
53. Hieronymus H, Schultz N, Gopalan A, Carver BS, Chang MT, Xiao Y, Heguy A, Huberman K, Bernstein M, Assel M *et al*: **Copy number alteration burden predicts prostate cancer relapse**. *Proceedings of the National Academy of Sciences of the United States of America* 2014, **111**(30):11139-11144.
54. Rubin MA, Demichelis F: **The Genomics of Prostate Cancer: emerging understanding with technologic advances**. *Modern pathology : an official journal of the United States and Canadian Academy of Pathology, Inc* 2018, **31**(S1):S1-11.
55. Armenia J, Wankowicz SAM, Liu D, Gao J, Kundra R, Reznik E, Chatila WK, Chakravarty D, Han GC, Coleman I *et al*: **The long tail of oncogenic drivers in prostate cancer**. *Nature genetics* 2018, **50**(5):645-651.
56. Abida W, Cyrta J, Heller G, Prandi D, Armenia J, Coleman I, Cieslik M, Benelli M, Robinson D, Van Allen EM *et al*: **Genomic correlates of clinical outcome in advanced prostate cancer**. *Proceedings of the National Academy of Sciences of the United States of America* 2019, **116**(23):11428-11436.
57. Carver BS, Tran J, Gopalan A, Chen Z, Shaikh S, Carracedo A, Alimonti A, Nardella C, Varmeh S, Scardino PT *et al*: **Aberrant ERG expression cooperates with loss of PTEN to promote cancer progression in the prostate**. *Nature genetics* 2009, **41**(5):619-624.
58. Beltran H, Prandi D, Mosquera JM, Benelli M, Puca L, Cyrta J, Marotz C, Giannopoulou E, Chakravarthi BV, Varambally S *et al*: **Divergent clonal evolution of castration-resistant neuroendocrine prostate cancer**. *Nature medicine* 2016, **22**(3):298-305.
59. Aparicio AM, Shen L, Tapia EL, Lu JF, Chen HC, Zhang J, Wu G, Wang X, Troncoso P, Corn P *et al*: **Combined Tumor Suppressor Defects Characterize Clinically Defined Aggressive Variant Prostate Cancers**. *Clinical cancer research : an official journal of the American Association for Cancer Research* 2016, **22**(6):1520-1530.
60. Ku SY, Rosario S, Wang Y, Mu P, Seshadri M, Goodrich ZW, Goodrich MM, Labbe DP, Gomez EC, Wang J *et al*: **Rb1 and Trp53 cooperate to suppress prostate cancer lineage plasticity, metastasis, and antiandrogen resistance**. *Science (New York, NY)* 2017, **355**(6320):78-83.
61. Mu P, Zhang Z, Benelli M, Karthaus WR, Hoover E, Chen CC, Wongvipat J, Ku SY, Gao D, Cao Z *et al*: **SOX2 promotes lineage plasticity and antiandrogen resistance in TP53- and RB1-deficient prostate cancer**. *Science (New York, NY)* 2017, **355**(6320):84-88.

62. Siegel RL, Miller KD, Jemal A: **Cancer statistics, 2019**. *CA: a cancer journal for clinicians* 2019, **69**(1):7-34.
63. Gaber C, Meza R, Ruterbusch JJ, Cote ML: **Endometrial Cancer Trends by Race and Histology in the USA: Projecting the Number of New Cases from 2015 to 2040**. *Journal of racial and ethnic health disparities* 2016.
64. Key TJ, Pike MC: **The dose-effect relationship between 'unopposed' oestrogens and endometrial mitotic rate: its central role in explaining and predicting endometrial cancer risk**. *British journal of cancer* 1988, **57**(2):205-212.
65. Kaaks R, Lukanova A, Kurzer MS: **Obesity, endogenous hormones, and endometrial cancer risk: a synthetic review**. *Cancer epidemiology, biomarkers & prevention : a publication of the American Association for Cancer Research, cosponsored by the American Society of Preventive Oncology* 2002, **11**(12):1531-1543.
66. Purdie DM, Green AC: **Epidemiology of endometrial cancer**. *Best practice & research Clinical obstetrics & gynaecology* 2001, **15**(3):341-354.
67. Renehan AG, Tyson M, Egger M, Heller RF, Zwahlen M: **Body-mass index and incidence of cancer: a systematic review and meta-analysis of prospective observational studies**. *Lancet (London, England)* 2008, **371**(9612):569-578.
68. Arem H, Chlebowski R, Stefanick ML, Anderson G, Wactawski-Wende J, Sims S, Gunter MJ, Irwin ML: **Body mass index, physical activity, and survival after endometrial cancer diagnosis: results from the Women's Health Initiative**. *Gynecologic oncology* 2013, **128**(2):181-186.
69. Arem H, Park Y, Pelser C, Ballard-Barbash R, Irwin ML, Hollenbeck A, Gierach GL, Brinton LA, Pfeiffer RM, Matthews CE: **Prediagnosis body mass index, physical activity, and mortality in endometrial cancer patients**. *Journal of the National Cancer Institute* 2013, **105**(5):342-349.
70. McCarroll ML, Armbruster S, Frasure HE, Gothard MD, Gil KM, Kavanagh MB, Waggoner S, von Gruenigen VE: **Self-efficacy, quality of life, and weight loss in overweight/obese endometrial cancer survivors (SUCCEED): a randomized controlled trial**. *Gynecologic oncology* 2014, **132**(2):397-402.
71. Bokhman JV: **Two pathogenetic types of endometrial carcinoma**. *Gynecologic oncology* 1983, **15**(1):10-17.
72. Maxwell GL, Risinger JI, Gumbs C, Shaw H, Bentley RC, Barrett JC, Berchuck A, Futreal PA: **Mutation of the PTEN tumor suppressor gene in endometrial hyperplasias**. *Cancer research* 1998, **58**(12):2500-2503.
73. Basil JB, Goodfellow PJ, Rader JS, Mutch DG, Herzog TJ: **Clinical significance of microsatellite instability in endometrial carcinoma**. *Cancer* 2000, **89**(8):1758-1764.
74. Mutter GL, Lin MC, Fitzgerald JT, Kum JB, Baak JP, Lees JA, Weng LP, Eng C: **Altered PTEN expression as a diagnostic marker for the earliest endometrial precancers**. *Journal of the National Cancer Institute* 2000, **92**(11):924-930.
75. Hecht JL, Mutter GL: **Molecular and pathologic aspects of endometrial carcinogenesis**. *Journal of clinical oncology : official journal of the American Society of Clinical Oncology* 2006, **24**(29):4783-4791.
76. Kandoth C, Schultz N, Cherniack AD, Akbani R, Liu Y, Shen H, Robertson AG, Pashtan I, Shen R, Benz CC *et al*: **Integrated genomic characterization of endometrial carcinoma**. *Nature* 2013, **497**(7447):67-73.
77. Church DN, Briggs SE, Palles C, Domingo E, Kearsey SJ, Grimes JM, Gorman M, Martin L, Howarth KM, Hodgson SV *et al*: **DNA polymerase epsilon and delta exonuclease domain mutations in endometrial cancer**. *Human molecular genetics* 2013, **22**(14):2820-2828.
78. Murali R, Soslow RA, Weigelt B: **Classification of endometrial carcinoma: more than two types**. *The Lancet Oncology* 2014, **15**(7):e268-278.
79. Wiegand KC, Lee AF, Al-Agha OM, Chow C, Kalloger SE, Scott DW, Steidl C, Wiseman SM, Gascoyne RD, Gilks B *et al*: **Loss of BAF250a (ARID1A) is frequent in high-grade endometrial carcinomas**. *The Journal of pathology* 2011, **224**(3):328-333.
80. Lax SF, Kendall B, Tashiro H, Slebos RJ, Hedrick L: **The frequency of p53, K-ras mutations, and microsatellite instability differs in uterine endometrioid and serous carcinoma: evidence of distinct molecular genetic pathways**. *Cancer* 2000, **88**(4):814-824.

81. Tashiro H, Isacson C, Levine R, Kurman RJ, Cho KR, Hedrick L: **p53 gene mutations are common in uterine serous carcinoma and occur early in their pathogenesis**. *The American journal of pathology* 1997, **150**(1):177-185.
82. Sherman ME, Bur ME, Kurman RJ: **p53 in endometrial cancer and its putative precursors: evidence for diverse pathways of tumorigenesis**. *Human pathology* 1995, **26**(11):1268-1274.
83. Wild PJ, Ikenberg K, Fuchs TJ, Rechsteiner M, Georgiev S, Fankhauser N, Noske A, Roessle M, Caduff R, Dellas A *et al*: **p53 suppresses type II endometrial carcinomas in mice and governs endometrial tumour aggressiveness in humans**. *EMBO molecular medicine* 2012, **4**(8):808-824.
84. Kuhn E, Wu RC, Guan B, Wu G, Zhang J, Wang Y, Song L, Yuan X, Wei L, Roden RB *et al*: **Identification of molecular pathway aberrations in uterine serous carcinoma by genome-wide analyses**. *Journal of the National Cancer Institute* 2012, **104**(19):1503-1513.
85. Zhao S, Choi M, Overton JD, Bellone S, Roque DM, Cocco E, Guzzo F, English DP, Varughese J, Gasparrini S *et al*: **Landscape of somatic single-nucleotide and copy-number mutations in uterine serous carcinoma**. *Proceedings of the National Academy of Sciences of the United States of America* 2013, **110**(8):2916-2921.
86. Le Gallo M, O'Hara AJ, Rudd ML, Urick ME, Hansen NF, O'Neil NJ, Price JC, Zhang S, England BM, Godwin AK *et al*: **Exome sequencing of serous endometrial tumors identifies recurrent somatic mutations in chromatin-remodeling and ubiquitin ligase complex genes**. *Nature genetics* 2012, **44**(12):1310-1315.
87. Buza N, Roque DM, Santin AD: **HER2/neu in Endometrial Cancer: A Promising Therapeutic Target With Diagnostic Challenges**. *Archives of pathology & laboratory medicine* 2014, **138**(3):343-350.
88. Lax SF, Pizer ES, Ronnett BM, Kurman RJ: **Clear cell carcinoma of the endometrium is characterized by a distinctive profile of p53, Ki-67, estrogen, and progesterone receptor expression**. *Human pathology* 1998, **29**(6):551-558.
89. Fadare O, Zhao C, Khabele D, Parkash V, Quick CM, Gwin K, Desouki MM: **Comparative analysis of Napsin A, alpha-methylacyl-coenzyme A racemase (AMACR, P504S), and hepatocyte nuclear factor 1 beta as diagnostic markers of ovarian clear cell carcinoma: an immunohistochemical study of 279 ovarian tumours**. *Pathology* 2015, **47**(2):105-111.
90. DeLair DF, Burke KA, Selenica P, Lim RS, Scott SN, Middha S, Mohanty AS, Cheng DT, Berger MF, Soslow RA *et al*: **The genetic landscape of endometrial clear cell carcinomas**. *The Journal of pathology* 2017, **243**(2):230-241.
91. Le Gallo M, Rudd ML, Urick ME, Hansen NF, Zhang S, Lozy F, Sgroi DC, Vidal Bel A, Matias-Guiu X, Broaddus RR *et al*: **Somatic mutation profiles of clear cell endometrial tumors revealed by whole exome and targeted gene sequencing**. *Cancer* 2017, **123**(17):3261-3268.
92. An HJ, Logani S, Isacson C, Ellenson LH: **Molecular characterization of uterine clear cell carcinoma**. *Modern pathology : an official journal of the United States and Canadian Academy of Pathology, Inc* 2004, **17**(5):530-537.
93. Hoang LN, McConechy MK, Meng B, McIntyre JB, Ewanowich C, Gilks CB, Huntsman DG, Kobel M, Lee CH: **Targeted mutation analysis of endometrial clear cell carcinoma**. *Histopathology* 2015, **66**(5):664-674.
94. Stelloo E, Bosse T, Nout RA, MacKay HJ, Church DN, Nijman HW, Leary A, Edmondson RJ, Powell ME, Crosbie EJ *et al*: **Refining prognosis and identifying targetable pathways for high-risk endometrial cancer; a TransPORTEC initiative**. *Modern pathology : an official journal of the United States and Canadian Academy of Pathology, Inc* 2015, **28**(6):836-844.
95. Cherniack AD, Shen H, Walter V, Stewart C, Murray BA, Bowlby R, Hu X, Ling S, Soslow RA, Broaddus RR *et al*: **Integrated Molecular Characterization of Uterine Carcinosarcoma**. *Cancer cell* 2017, **31**(3):411-423.
96. McConechy MK, Hoang LN, Chui MH, Senz J, Yang W, Rozenberg N, Mackenzie R, McAlpine JN, Huntsman DG, Clarke BA *et al*: **In-depth molecular profiling of the biphasic components of uterine carcinosarcomas**. *The journal of pathology Clinical research* 2015, **1**(3):173-185.
97. McConechy MK, Ding J, Cheang MC, Wiegand K, Senz J, Tone A, Yang W, Prentice L, Tse K, Zeng T *et al*: **Use of mutation profiles to refine the classification of endometrial carcinomas**. *The Journal of pathology* 2012, **228**(1):20-30.

98. Jones S, Stransky N, McCord CL, Cerami E, Lagowski J, Kelly D, Angiuoli SV, Sausen M, Kann L, Shukla M *et al*: **Genomic analyses of gynaecologic carcinosarcomas reveal frequent mutations in chromatin remodelling genes**. *Nat Commun* 2014, **5**:5006.
99. Le Gallo M, Rudd ML, Urick ME, Hansen NF, Merino MJ, Mutch DG, Goodfellow PJ, Mullikin JC, Bell DW: **The FOXA2 transcription factor is frequently somatically mutated in uterine carcinosarcomas and carcinomas**. *Cancer* 2018, **124**(1):65-73.
100. Morice P, Leary A, Creutzberg C, Abu-Rustum N, Darai E: **Endometrial cancer**. *Lancet (London, England)* 2015.
101. Bogani G, Dowdy SC, Cliby WA, Ghezzi F, Rossetti D, Mariani A: **Role of pelvic and para-aortic lymphadenectomy in endometrial cancer: current evidence**. *The journal of obstetrics and gynaecology research* 2014, **40**(2):301-311.
102. Abida W, Armenia J, Gopalan A, Brennan R, Walsh M, Barron D, Danila D, Rathkopf D, Morris M, Slovin S *et al*: **Prospective Genomic Profiling of Prostate Cancer Across Disease States Reveals Germline and Somatic Alterations That May Affect Clinical Decision Making**. *JCO Precis Oncol* 2017, **2017**.
103. Boruta DM, 2nd, Gehrig PA, Fader AN, Olawaiye AB: **Management of women with uterine papillary serous cancer: a Society of Gynecologic Oncology (SGO) review**. *Gynecologic oncology* 2009, **115**(1):142-153.
104. Setiawan VW, Yang HP, Pike MC, McCann SE, Yu H, Xiang YB, Wolk A, Wentzensen N, Weiss NS, Webb PM *et al*: **Type I and II endometrial cancers: have they different risk factors?** *Journal of clinical oncology : official journal of the American Society of Clinical Oncology* 2013, **31**(20):2607-2618.
105. Colombo N, Creutzberg C, Amant F, Bosse T, Gonzalez-Martin A, Ledermann J, Marth C, Nout R, Querleu D, Mirza MR *et al*: **ESMO-ESGO-ESTRO Consensus Conference on Endometrial Cancer: Diagnosis, Treatment and Follow-up**. *International journal of gynecological cancer : official journal of the International Gynecological Cancer Society* 2016, **26**(1):2-30.
106. Moher D, Liberati A, Tetzlaff J, Altman DG: **Preferred reporting items for systematic reviews and meta-analyses: the PRISMA statement**. *Journal of clinical epidemiology* 2009, **62**(10):1006-1012.
107. Whitney CW, Brunetto VL, Zaino RJ, Lentz SS, Sorosky J, Armstrong DK, Lee RB: **Phase II study of medroxyprogesterone acetate plus tamoxifen in advanced endometrial carcinoma: a Gynecologic Oncology Group study**. *Gynecologic oncology* 2004, **92**(1):4-9.
108. Singh M, Zaino RJ, Filiaci VJ, Leslie KK: **Relationship of estrogen and progesterone receptors to clinical outcome in metastatic endometrial carcinoma: a Gynecologic Oncology Group Study**. *Gynecologic oncology* 2007, **106**(2):325-333.
109. Nagai Y, Kojima T, Muro Y, Hachiya T, Nishizawa Y, Wakabayashi T, Hagiwara M: **Identification of a novel nuclear speckle-type protein, SPOP**. *FEBS Lett* 1997, **418**(1-2):23-26.
110. Kwon JE, La M, Oh KH, Oh YM, Kim GR, Seol JH, Baek SH, Chiba T, Tanaka K, Bang OS *et al*: **BTB domain-containing speckle-type POZ protein (SPOP) serves as an adaptor of Daxx for ubiquitination by Cul3-based ubiquitin ligase**. *The Journal of biological chemistry* 2006, **281**(18):12664-12672.
111. Kent D, Bush EW, Hooper JE: **Roadkill attenuates Hedgehog responses through degradation of Cubitus interruptus**. *Development* 2006, **133**(10):2001-2010.
112. Zhuang M, Calabrese MF, Liu J, Waddell MB, Nourse A, Hammel M, Miller DJ, Walden H, Duda DM, Seyedin SN *et al*: **Structures of SPOP-substrate complexes: insights into molecular architectures of BTB-Cul3 ubiquitin ligases**. *Molecular cell* 2009, **36**(1):39-50.
113. Hershko A, Heller H, Elias S, Ciechanover A: **Components of ubiquitin-protein ligase system. Resolution, affinity purification, and role in protein breakdown**. *The Journal of biological chemistry* 1983, **258**(13):8206-8214.
114. Hershko A, Ciechanover A: **The ubiquitin system**. *Annu Rev Biochem* 1998, **67**:425-479.
115. Popovic D, Vucic D, Dikic I: **Ubiquitination in disease pathogenesis and treatment**. *Nature medicine* 2014, **20**(11):1242-1253.
116. Husnjak K, Dikic I: **Ubiquitin-binding proteins: decoders of ubiquitin-mediated cellular functions**. *Annu Rev Biochem* 2012, **81**:291-322.

117. Yau R, Rape M: **The increasing complexity of the ubiquitin code**. *Nature cell biology* 2016, **18**(6):579-586.
118. Ardley HC, Robinson PA: **E3 ubiquitin ligases**. *Essays Biochem* 2005, **41**:15-30.
119. Ciechanover A: **The unravelling of the ubiquitin system**. *Nature reviews Molecular cell biology* 2015, **16**(5):322-324.
120. Khaminets A, Behl C, Dikic I: **Ubiquitin-Dependent And Independent Signals In Selective Autophagy**. *Trends in cell biology* 2016, **26**(1):6-16.
121. Senft D, Qi J, Ronai ZA: **Ubiquitin ligases in oncogenic transformation and cancer therapy**. *Nature reviews Cancer* 2018, **18**(2):69-88.
122. Qi J, Ronai ZA: **Dysregulation of ubiquitin ligases in cancer**. *Drug resistance updates : reviews and commentaries in antimicrobial and anticancer chemotherapy* 2015, **23**:1-11.
123. Errington WJ, Khan MQ, Bueler SA, Rubinstein JL, Chakrabartty A, Prive GG: **Adaptor protein self-assembly drives the control of a cullin-RING ubiquitin ligase**. *Structure* 2012, **20**(7):1141-1153.
124. van Geersdaele LK, Stead MA, Harrison CM, Carr SB, Close HJ, Rosbrook GO, Connell SD, Wright SC: **Structural basis of high-order oligomerization of the cullin-3 adaptor SPOP**. *Acta Crystallogr D Biol Crystallogr* 2013, **69**(Pt 9):1677-1684.
125. Marzahn MR, Marada S, Lee J, Nourse A, Kenrick S, Zhao H, Ben-Nissan G, Kolaitis RM, Peters JL, Pounds S *et al*: **Higher-order oligomerization promotes localization of SPOP to liquid nuclear speckles**. *The EMBO journal* 2016, **35**(12):1254-1275.
126. Cuneo MJ, Mittag T: **The ubiquitin ligase adaptor SPOP in cancer**. *The FEBS Journal* 2019, **286**(20):3946-3958.
127. Dai X, Gan W, Li X, Wang S, Zhang W, Huang L, Liu S, Zhong Q, Guo J, Zhang J *et al*: **Prostate cancer-associated SPOP mutations confer resistance to BET inhibitors through stabilization of BRD4**. *Nature medicine* 2017, **23**(9):1063-1071.
128. Lawrence MS, Stojanov P, Mermel CH, Robinson JT, Garraway LA, Golub TR, Meyerson M, Gabriel SB, Lander ES, Getz G: **Discovery and saturation analysis of cancer genes across 21 tumour types**. *Nature* 2014, **505**(7484):495-501.
129. Li JJ, Zhang JF, Yao SM, Huang H, Zhang S, Zhao M, Huang JA: **Decreased expression of speckle-type POZ protein for the prediction of poor prognosis in patients with non-small cell lung cancer**. *Oncology letters* 2017, **14**(3):2743-2748.
130. Xu J, Wang F, Jiang H, Jiang Y, Chen J, Qin J: **Properties and Clinical Relevance of Speckle-Type POZ Protein in Human Colorectal Cancer**. *Journal of gastrointestinal surgery : official journal of the Society for Surgery of the Alimentary Tract* 2015, **19**(8):1484-1496.
131. Geng C, He B, Xu L, Barbieri CE, Eedunuri VK, Chew SA, Zimmermann M, Bond R, Shou J, Li C *et al*: **Prostate cancer-associated mutations in speckle-type POZ protein (SPOP) regulate steroid receptor coactivator 3 protein turnover**. *Proceedings of the National Academy of Sciences of the United States of America* 2013, **110**(17):6997-7002.
132. Blattner M, Lee DJ, O'Reilly C, Park K, MacDonald TY, Khani F, Turner KR, Chiu YL, Wild PJ, Dolgalev I *et al*: **SPOP mutations in prostate cancer across demographically diverse patient cohorts**. *Neoplasia (New York, NY)* 2014, **16**(1):14-20.
133. Cancer Genome Atlas Research N, Kandoth C, Schultz N, Cherniack AD, Akbani R, Liu Y, Shen H, Robertson AG, Pashtan I, Shen R *et al*: **Integrated genomic characterization of endometrial carcinoma**. *Nature* 2013, **497**(7447):67-73.
134. Zehir A, Benayed R, Shah RH, Syed A, Middha S, Kim HR, Srinivasan P, Gao J, Chakravarty D, Devlin SM *et al*: **Mutational landscape of metastatic cancer revealed from prospective clinical sequencing of 10,000 patients**. *Nature medicine* 2017, **23**(6):703-713.
135. Jung SH, Shin S, Kim MS, Baek IP, Lee JY, Lee SH, Kim TM, Lee SH, Chung YJ: **Genetic Progression of High Grade Prostatic Intraepithelial Neoplasia to Prostate Cancer**. *Eur Urol* 2016, **69**(5):823-830.
136. Boysen G, Barbieri CE, Prandi D, Blattner M, Chae SS, Dahija A, Nataraj S, Huang D, Marotz C, Xu L *et al*: **SPOP mutation leads to genomic instability in prostate cancer**. *eLife* 2015, **4**.
137. Theurillat JP, Udeshi ND, Errington WJ, Baca SC, Wild PJ, Blattner M, Rubin MA, Moch H, Prive GG, Carr SA *et al*: **Ubiquitylome analysis identifies dominant-negative deregulation of candidate effector substrates in SPOP-mutant prostate cancer.** *Science (New York, NY)* 2014.

138. Claiborn KC, Sachdeva MM, Cannon CE, Groff DN, Singer JD, Stoffers DA: **Pcif1 modulates Pdx1 protein stability and pancreatic β cell function and survival in mice**. *The Journal of clinical investigation* 2010, **120**(10):3713-3721.
139. Blattner M, Liu D, Robinson BD, Huang D, Poliakov A, Gao D, Nataraj S, Deonarine LD, Augello MA, Sailer V *et al*: **SPOP Mutation Drives Prostate Tumorigenesis In Vivo through Coordinate Regulation of PI3K/mTOR and AR Signaling**. *Cancer cell* 2017, **31**(3):436-451.
140. Geng C, Rajapakshe K, Shah SS, Shou J, Eedunuri VK, Foley C, Fiskus W, Rajendran M, Chew SA, Zimmermann M *et al*: **Androgen receptor is the key transcriptional mediator of the tumor suppressor SPOP in prostate cancer**. *Cancer research* 2014, **74**(19):5631-5643.
141. Groner AC, Cato L, de Tribolet-Hardy J, Bernasocchi T, Janouskova H, Melchers D, Houtman R, Cato AC, Tschopp P, Gu L *et al*: **TRIM24 Is an Oncogenic Transcriptional Activator in Prostate Cancer**. *Cancer cell* 2016.
142. Geng C, Kaochar S, Li M, Rajapakshe K, Fiskus W, Dong J, Foley C, Dong B, Zhang L, Kwon OJ *et al*: **SPOP regulates prostate epithelial cell proliferation and promotes ubiquitination and turnover of c-MYC oncoprotein**. *Oncogene* 2017, **36**(33):4767-4777.
143. Zhu H, Ren S, Bitler BG, Aird KM, Tu Z, Skordalakes E, Zhu Y, Yan J, Sun Y, Zhang R: **SPOP E3 Ubiquitin Ligase Adaptor Promotes Cellular Senescence by Degrading the SENP7 deSUMOylase**. *Cell reports* 2015, **13**(6):1183-1193.
144. Zhang L, Peng S, Dai X, Gan W, Nie X, Wei W, Hu G, Guo J: **Tumor suppressor SPOP ubiquitinates and degrades EglN2 to compromise growth of prostate cancer cells**. *Cancer letters* 2017, **390**:11-20.
145. Zhang J, Bu X, Wang H, Zhu Y, Geng Y, Nihira NT, Tan Y, Ci Y, Wu F, Dai X *et al*: **Cyclin D-CDK4 kinase destabilizes PD-L1 via cullin 3-SPOP to control cancer immune surveillance**. *Nature* 2018, **553**(7686):91-95.
146. Ju LG, Zhu Y, Long QY, Li XJ, Lin X, Tang SB, Yin L, Xiao Y, Wang XH, Li L *et al*: **SPOP suppresses prostate cancer through regulation of CYCLIN E1 stability**. *Cell death and differentiation* 2019, **26**(6):1156-1168.
147. Gan W, Dai X, Lunardi A, Li Z, Inuzuka H, Liu P, Varmeh S, Zhang J, Cheng L, Sun Y *et al*: **SPOP Promotes Ubiquitination and Degradation of the ERG Oncoprotein to Suppress Prostate Cancer Progression**. *Molecular cell* 2015, **59**(6):917-930.
148. Wu F, Dai X, Gan W, Wan L, Li M, Mitsiades N, Wei W, Ding Q, Zhang J: **Prostate cancer-associated mutation in SPOP impairs its ability to target Cdc20 for poly-ubiquitination and degradation**. *Cancer letters* 2017, **385**:207-214.
149. Ma J, Chang K, Peng J, Shi Q, Gan H, Gao K, Feng K, Xu F, Zhang H, Dai B *et al*: **SPOP promotes ATF2 ubiquitination and degradation to suppress prostate cancer progression**. *Journal of experimental & clinical cancer research : CR* 2018, **37**(1):145.
150. Li G, Ci W, Karmakar S, Chen K, Dhar R, Fan Z, Guo Z, Zhang J, Ke Y, Wang L *et al*: **SPOP promotes tumorigenesis by acting as a key regulatory hub in kidney cancer**. *Cancer cell* 2014, **25**(4):455-468.
151. Liu X, Sun G, Sun X: **RNA interference-mediated silencing of speckle-type POZ protein promotes apoptosis of renal cell cancer cells**. *OncoTargets and therapy* 2016, **9**:2393-2402.
152. Frattini V, Trifonov V, Chan JM, Castano A, Lia M, Abate F, Keir ST, Ji AX, Zoppoli P, Niola F *et al*: **The integrated landscape of driver genomic alterations in glioblastoma**. *Nature genetics* 2013, **45**(10):1141-1149.
153. Luo L, Tang H, Ling L, Li N, Jia X, Zhang Z, Wang X, Shi L, Yin J, Qiu N *et al*: **LINC01638 lncRNA activates MTDH-Twist1 signaling by preventing SPOP-mediated c-Myc degradation in triple-negative breast cancer**. *Oncogene* 2018, **37**(47):6166-6179.
154. Li C, Ao J, Fu J, Lee DF, Xu J, Lonard D, O'Malley BW: **Tumor-suppressor role for the SPOP ubiquitin ligase in signal-dependent proteolysis of the oncogenic co-activator SRC-3/AIB1**. *Oncogene* 2011, **30**(42):4350-4364.
155. Gao K, Jin X, Tang Y, Ma J, Peng J, Yu L, Zhang P, Wang C: **Tumor suppressor SPOP mediates the proteasomal degradation of progesterone receptors (PRs) in breast cancer cells**. *American journal of cancer research* 2015, **5**(10):3210-3220.
156. Tan Y, Ci Y, Dai X, Wu F, Guo J, Liu D, North BJ, Huo J, Zhang J: **Cullin 3SPOP ubiquitin E3 ligase promotes the poly-ubiquitination and degradation of HDAC6**. *Oncotarget* 2017, **8**(29):47890-47901.

157. Zhang P, Gao K, Jin X, Ma J, Peng J, Wumaier R, Tang Y, Zhang Y, An J, Yan Q *et al*: **Endometrial cancer-associated mutants of SPOP are defective in regulating estrogen receptor-alpha protein turnover**. *Cell death & disease* 2015, **6**:e1687.
158. Zeng C, Wang Y, Lu Q, Chen J, Zhang J, Liu T, Lv N, Luo S: **SPOP suppresses tumorigenesis by regulating Hedgehog/Gli2 signaling pathway in gastric cancer**. *Journal of experimental & clinical cancer research : CR* 2014, **33**:75.
159. Ji P, Liang S, Li P, Xie C, Li J, Zhang K, Zheng X, Feng M, Li Q, Jiao H *et al*: **Speckle-type POZ protein suppresses hepatocellular carcinoma cell migration and invasion via ubiquitin-dependent proteolysis of SUMO1/sentrin specific peptidase 7**. *Biochemical and biophysical research communications* 2018, **502**(1):30-42.
160. Zhao W, Zhou J, Deng Z, Gao Y, Cheng Y: **SPOP promotes tumor progression via activation of beta-catenin/TCF4 complex in clear cell renal cell carcinoma**. *International journal of oncology* 2016, **49**(3):1001-1008.
161. Luo J, Bao YC, Ji XX, Chen B, Deng QF, Zhou SW: **SPOP promotes SIRT2 degradation and suppresses non-small cell lung cancer cell growth**. *Biochemical and biophysical research communications* 2017, **483**(2):880-884.
162. Luo J, Chen B, Gao CX, Xie HK, Han CN, Zhou CC: **SPOP promotes FADD degradation and inhibits NF-kappaB activity in non-small cell lung cancer**. *Biochemical and biophysical research communications* 2018, **504**(1):289-294.
163. Zhu K, Lei PJ, Ju LG, Wang X, Huang K, Yang B, Shao C, Zhu Y, Wei G, Fu XD *et al*: **SPOP-containing complex regulates SETD2 stability and H3K36me3-coupled alternative splicing**. *Nucleic acids research* 2017, **45**(1):92-105.
164. Waddington CH: **The epigenotype. 1942**. *International journal of epidemiology* 2012, **41**(1):10-13.
165. Waddington CH: **Canalization of development and the inheritance of acquired characters.** *Nature* 1942, **150**(3811):563-565.
166. Kornberg RD: **Chromatin structure: a repeating unit of histones and DNA**. *Science (New York, NY)* 1974, **184**(4139):868-871.
167. Zhao Y, Garcia BA: **Comprehensive Catalog of Currently Documented Histone Modifications**. *Cold Spring Harbor perspectives in biology* 2015, **7**(9):a025064.
168. Kouzarides T: **Chromatin modifications and their function**. *Cell* 2007, **128**(4):693-705.
169. Jones RS: **Epigenetics: reversing the 'irreversible'**. *Nature* 2007, **450**(7168):357-359.
170. Simo-Riudalbas L, Esteller M: **Targeting the histone orthography of cancer: drugs for writers, erasers and readers**. *British journal of pharmacology* 2015, **172**(11):2716-2732.
171. Choudhary C, Kumar C, Gnad F, Nielsen ML, Rehman M, Walther TC, Olsen JV, Mann M: **Lysine acetylation targets protein complexes and co-regulates major cellular functions**. *Science (New York, NY)* 2009, **325**(5942):834-840.
172. Belkina AC, Denis GV: **BET domain co-regulators in obesity, inflammation and cancer**. *Nature reviews Cancer* 2012, **12**(7):465-477.
173. Dhalluin C, Carlson JE, Zeng L, He C, Aggarwal AK, Zhou MM: **Structure and ligand of a histone acetyltransferase bromodomain**. *Nature* 1999, **399**(6735):491-496.
174. Dawson MA, Kouzarides T, Huntly BJ: **Targeting epigenetic readers in cancer**. *The New England journal of medicine* 2012, **367**(7):647-657.
175. Filippakopoulos P, Picaud S, Mangos M, Keates T, Lambert JP, Barsyte-Lovejoy D, Felletar I, Volkmer R, Muller S, Pawson T *et al*: **Histone recognition and large-scale structural analysis of the human bromodomain family**. *Cell* 2012, **149**(1):214-231.
176. Fu LL, Tian M, Li X, Li JJ, Huang J, Ouyang L, Zhang Y, Liu B: **Inhibition of BET bromodomains as a therapeutic strategy for cancer drug discovery**. *Oncotarget* 2015, **6**(8):5501-5516.
177. Xiao Y, Liang L, Huang M, Qiu Q, Zeng S, Shi M, Zou Y, Ye Y, Yang X, Xu H: **Bromodomain and extra-terminal domain bromodomain inhibition prevents synovial inflammation via blocking IkappaB kinase-dependent NF-kappaB activation in rheumatoid fibroblast-like synoviocytes**. *Rheumatology (Oxford, England)* 2016, **55**(1):173-184.
178. Voigt P, Reinberg D: **BRD4 jump-starts transcription after mitotic silencing**. *Genome biology* 2011, **12**(11):133.

179. You J, Srinivasan V, Denis GV, Harrington WJ, Jr., Ballestas ME, Kaye KM, Howley PM: **Kaposi's sarcoma-associated herpesvirus latency-associated nuclear antigen interacts with bromodomain protein Brd4 on host mitotic chromosomes**. *Journal of virology* 2006, **80**(18):8909-8919.
180. Korb E, Herre M, Zucker-Scharff I, Darnell RB, Allis CD: **BET protein Brd4 activates transcription in neurons and BET inhibitor Jq1 blocks memory in mice**. *Nature neuroscience* 2015, **18**(10):1464-1473.
181. Shang E, Nickerson HD, Wen D, Wang X, Wolgemuth DJ: **The first bromodomain of Brdt, a testis-specific member of the BET sub-family of double-bromodomain-containing proteins, is essential for male germ cell differentiation**. *Development* 2007, **134**(19):3507-3515.
182. Houzelstein D, Bullock SL, Lynch DE, Grigorieva EF, Wilson VA, Beddington RS: **Growth and early postimplantation defects in mice deficient for the bromodomain-containing protein Brd4**. *Molecular and cellular biology* 2002, **22**(11):3794-3802.
183. Yang Z, He N, Zhou Q: **Brd4 recruits P-TEFb to chromosomes at late mitosis to promote G1 gene expression and cell cycle progression**. *Molecular and cellular biology* 2008, **28**(3):967-976.
184. Devaiah BN, Singer DS: **Cross-talk among RNA polymerase II kinases modulates C-terminal domain phosphorylation**. *The Journal of biological chemistry* 2012, **287**(46):38755-38766.
185. Rahman S, Sowa ME, Ottinger M, Smith JA, Shi Y, Harper JW, Howley PM: **The Brd4 extraterminal domain confers transcription activation independent of pTEFb by recruiting multiple proteins, including NSD3**. *Molecular and cellular biology* 2011, **31**(13):2641-2652.
186. Liu W, Ma Q, Wong K, Li W, Ohgi K, Zhang J, Aggarwal A, Rosenfeld MG: **Brd4 and JMJD6-associated anti-pause enhancers in regulation of transcriptional pause release**. *Cell* 2013, **155**(7):1581-1595.
187. Devaiah BN, Singer DS: **Two faces of brd4: mitotic bookmark and transcriptional lynchpin**. *Transcription* 2013, **4**(1):13-17.
188. Zhao R, Nakamura T, Fu Y, Lazar Z, Spector DL: **Gene bookmarking accelerates the kinetics of post-mitotic transcriptional re-activation**. *Nature cell biology* 2011, **13**(11):1295-1304.
189. Lamonica JM, Deng W, Kadauke S, Campbell AE, Gamsjaeger R, Wang H, Cheng Y, Billin AN, Hardison RC, Mackay JP *et al*: **Bromodomain protein Brd3 associates with acetylated GATA1 to promote its chromatin occupancy at erythroid target genes**. *Proceedings of the National Academy of Sciences of the United States of America* 2011, **108**(22):E159-168.
190. Gamsjaeger R, Webb SR, Lamonica JM, Billin A, Blobel GA, Mackay JP: **Structural basis and specificity of acetylated transcription factor GATA1 recognition by BET family bromodomain protein Brd3**. *Molecular and cellular biology* 2011, **31**(13):2632-2640.
191. LeRoy G, Rickards B, Flint SJ: **The double bromodomain proteins Brd2 and Brd3 couple histone acetylation to transcription**. *Molecular cell* 2008, **30**(1):51-60.
192. Baratta MG, Schinzel AC, Zwang Y, Bandopadhayay P, Bowman-Colin C, Kutt J, Curtis J, Piao H, Wong LC, Kung AL *et al*: **An in-tumor genetic screen reveals that the BET bromodomain protein, BRD4, is a potential therapeutic target in ovarian carcinoma**. *Proceedings of the National Academy of Sciences of the United States of America* 2015, **112**(1):232-237.
193. Toyoshima M, Howie HL, Imakura M, Walsh RM, Annis JE, Chang AN, Frazier J, Chau BN, Loboda A, Linsley PS *et al*: **Functional genomics identifies therapeutic targets for MYC-driven cancer**. *Proceedings of the National Academy of Sciences of the United States of America* 2012, **109**(24):9545-9550.
194. Zuber J, Shi J, Wang E, Rappaport AR, Herrmann H, Sison EA, Magoon D, Qi J, Blatt K, Wunderlich M *et al*: **RNAi screen identifies Brd4 as a therapeutic target in acute myeloid leukaemia**. *Nature* 2011, **478**(7370):524-528.
195. Marcotte R, Sayad A, Brown KR, Sanchez-Garcia F, Reimand J, Haider M, Virtanen C, Bradner JE, Bader GD, Mills GB *et al*: **Functional Genomic Landscape of Human Breast Cancer Drivers, Vulnerabilities, and Resistance**. *Cell* 2016, **164**(1-2):293-309.
196. French CA, Rahman S, Walsh EM, Kuhnle S, Grayson AR, Lemieux ME, Grunfeld N, Rubin BP, Antonescu CR, Zhang S *et al*: **NSD3-NUT fusion oncoprotein in NUT midline carcinoma: implications for a novel oncogenic mechanism**. *Cancer discovery* 2014, **4**(8):928-941.
197. French CA, Ramirez CL, Kolmakova J, Hickman TT, Cameron MJ, Thyne ME, Kutok JL, Toretsky JA, Tadavarthy AK, Kees UR *et al*: **BRD-NUT oncoproteins: a family of closely related nuclear proteins**

that block epithelial differentiation and maintain the growth of carcinoma cells. *Oncogene* 2008, **27**(15):2237-2242.
198. Grayson AR, Walsh EM, Cameron MJ, Godec J, Ashworth T, Ambrose JM, Aserlind AB, Wang H, Evan G, Kluk MJ *et al*: **MYC, a downstream target of BRD-NUT, is necessary and sufficient for the blockade of differentiation in NUT midline carcinoma**. *Oncogene* 2014, **33**(13):1736-1742.
199. Stewart HJ, Horne GA, Bastow S, Chevassut TJ: **BRD4 associates with p53 in DNMT3A-mutated leukemia cells and is implicated in apoptosis by the bromodomain inhibitor JQ1**. *Cancer medicine* 2013, **2**(6):826-835.
200. Ott CJ, Kopp N, Bird L, Paranal RM, Qi J, Bowman T, Rodig SJ, Kung AL, Bradner JE, Weinstock DM: **BET bromodomain inhibition targets both c-Myc and IL7R in high-risk acute lymphoblastic leukemia**. *Blood* 2012, **120**(14):2843-2852.
201. Dawson MA, Prinjha RK, Dittmann A, Giotopoulos G, Bantscheff M, Chan WI, Robson SC, Chung CW, Hopf C, Savitski MM *et al*: **Inhibition of BET recruitment to chromatin as an effective treatment for MLL-fusion leukaemia**. *Nature* 2011, **478**(7370):529-533.
202. Mertz JA, Conery AR, Bryant BM, Sandy P, Balasubramanian S, Mele DA, Bergeron L, Sims RJ, 3rd: **Targeting MYC dependence in cancer by inhibiting BET bromodomains**. *Proceedings of the National Academy of Sciences of the United States of America* 2011, **108**(40):16669-16674.
203. Vita M, Henriksson M: **The Myc oncoprotein as a therapeutic target for human cancer**. *Seminars in cancer biology* 2006, **16**(4):318-330.
204. Pastori C, Daniel M, Penas C, Volmar CH, Johnstone AL, Brothers SP, Graham RM, Allen B, Sarkaria JN, Komotar RJ *et al*: **BET bromodomain proteins are required for glioblastoma cell proliferation**. *Epigenetics* 2014, **9**(4):611-620.
205. Segura MF, Fontanals-Cirera B, Gaziel-Sovran A, Guijarro MV, Hanniford D, Zhang G, Gonzalez-Gomez P, Morante M, Jubierre L, Zhang W *et al*: **BRD4 sustains melanoma proliferation and represents a new target for epigenetic therapy**. *Cancer research* 2013, **73**(20):6264-6276.
206. Alqahtani A, Choucair K, Ashraf M, Hammouda DM, Alloghbi A, Khan T, Senzer N, Nemunaitis J: **Bromodomain and extra-terminal motif inhibitors: a review of preclinical and clinical advances in cancer therapy**. *Future Science OA* 2019, **5**(3):FSO372.
207. Niederriter AR, Varshney A, Parker SC, Martin DM: **Super Enhancers in Cancers, Complex Disease, and Developmental Disorders**. *Genes* 2015, **6**(4):1183-1200.
208. Bradner JE, Hnisz D, Young RA: **Transcriptional Addiction in Cancer**. *Cell* 2017, **168**(4):629-643.
209. Filippakopoulos P, Qi J, Picaud S, Shen Y, Smith WB, Fedorov O, Morse EM, Keates T, Hickman TT, Felletar I *et al*: **Selective inhibition of BET bromodomains**. *Nature* 2010, **468**(7327):1067-1073.
210. Ceribelli M, Kelly PN, Shaffer AL, Wright GW, Xiao W, Yang Y, Mathews Griner LA, Guha R, Shinn P, Keller JM *et al*: **Blockade of oncogenic IkappaB kinase activity in diffuse large B-cell lymphoma by bromodomain and extraterminal domain protein inhibitors**. *Proceedings of the National Academy of Sciences of the United States of America* 2014, **111**(31):11365-11370.
211. Picaud S, Da Costa D, Thanasopoulou A, Filippakopoulos P, Fish PV, Philpott M, Fedorov O, Brennan P, Bunnage ME, Owen DR *et al*: **PFI-1, a highly selective protein interaction inhibitor, targeting BET Bromodomains**. *Cancer research* 2013, **73**(11):3336-3346.
212. Liu Z, Wang P, Chen H, Wold EA, Tian B, Brasier AR, Zhou J: **Drug Discovery Targeting Bromodomain-Containing Protein 4**. *Journal of medicinal chemistry* 2017, **60**(11):4533-4558.
213. Zhang G, Plotnikov AN, Rusinova E, Shen T, Morohashi K, Joshua J, Zeng L, Mujtaba S, Ohlmeyer M, Zhou MM: **Structure-guided design of potent diazobenzene inhibitors for the BET bromodomains**. *Journal of medicinal chemistry* 2013, **56**(22):9251-9264.
214. Sahai V, Redig AJ, Collier KA, Eckerdt FD, Munshi HG: **Targeting BET bromodomain proteins in solid tumors**. *Oncotarget* 2016, **7**(33):53997-54009.
215. Massard C, Soria JC, Stathis A, Delord JP, Awada A, Peters S, Lewin J, Bekradda M, Rezai K, Zeng Z *et al*: **A phase Ib trial with MK-8628/OTX015, a small molecule inhibitor of bromodomain (BRD) and extra-terminal (BET) proteins, in patients with selected advanced solid tumors**. *European Journal of Cancer* 2016, **69**:S2-S3.
216. Postel-Vinay S, Herbschleb K, Massard C, Woodcock V, Soria JC, Walter AO, Ewerton F, Poelman M, Benson N, Ocker M *et al*: **First-in-human phase I study of the bromodomain and extraterminal motif**

inhibitor BAY 1238097: emerging pharmacokinetic/pharmacodynamic relationship and early termination due to unexpected toxicity. *European journal of cancer (Oxford, England : 1990)* 2019, **109**:103-110.

217. Stathis A, Zucca E, Bekradda M, Gomez-Roca C, Delord JP, de La Motte Rouge T, Uro-Coste E, de Braud F, Pelosi G, French CA: **Clinical Response of Carcinomas Harboring the BRD4-NUT Oncoprotein to the Targeted Bromodomain Inhibitor OTX015/MK-8628**. *Cancer discovery* 2016, **6**(5):492-500.
218. Jung M, Gelato KA, Fernandez-Montalvan A, Siegel S, Haendler B: **Targeting BET bromodomains for cancer treatment**. *Epigenomics* 2015, **7**(3):487-501.
219. Shi J, Vakoc CR: **The mechanisms behind the therapeutic activity of BET bromodomain inhibition**. *Molecular cell* 2014, **54**(5):728-736.
220. Wang CY, Filippakopoulos P: **Beating the odds: BETs in disease**. *Trends Biochem Sci* 2015, **40**(8):468-479.
221. Asangani IA, Dommeti VL, Wang X, Malik R, Cieslik M, Yang R, Escara-Wilke J, Wilder-Romans K, Dhanireddy S, Engelke C *et al*: **Therapeutic targeting of BET bromodomain proteins in castration-resistant prostate cancer**. *Nature* 2014, **510**(7504):278-282.
222. Shu S, Lin CY, He HH, Witwicki RM, Tabassum DP, Roberts JM, Janiszewska M, Huh SJ, Liang Y, Ryan J *et al*: **Response and resistance to BET bromodomain inhibitors in triple-negative breast cancer**. *Nature* 2016, **529**(7586):413-417.
223. Cancer Genome Atlas Research N: **The Molecular Taxonomy of Primary Prostate Cancer**. *Cell* 2015, **163**(4):1011-1025.
224. Robinson D, Van Allen EM, Wu YM, Schultz N, Lonigro RJ, Mosquera JM, Montgomery B, Taplin ME, Pritchard CC, Attard G *et al*: **Integrative clinical genomics of advanced prostate cancer**. *Cell* 2015, **161**(5):1215-1228.
225. Guo ZQ, Zheng T, Chen B, Luo C, Ouyang S, Gong S, Li J, Mao LL, Lian F, Yang Y *et al*: **Small-Molecule Targeting of E3 Ligase Adaptor SPOP in Kidney Cancer**. *Cancer cell* 2016, **30**(3):474-484.
226. Hai L, Szwarc MM, He B, Lonard DM, Kommagani R, DeMayo FJ, Lydon JP: **Uterine function in the mouse requires speckle-type poz protein**. *Biology of reproduction* 2018, **98**(6):856-869.
227. Liu N, Liu X, Yu Q, Chen X, Ding Y, He J, Gao R, Wang Y, Liu X: **SPOP Regulates Endometrial Stromal Cell Decidualization in Mice**. *Reproductive sciences (Thousand Oaks, Calif)* 2016, **23**(11):1565-1574.
228. Zhang P, Wang D, Zhao Y, Ren S, Gao K, Ye Z, Wang S, Pan CW, Zhu Y, Yan Y *et al*: **Intrinsic BET inhibitor resistance in SPOP-mutated prostate cancer is mediated by BET protein stabilization and AKT-mTORC1 activation**. *Nature medicine* 2017, **23**(9):1055-1062.
229. !!! INVALID CITATION !!! {Ostertag, 2019 #716}.
230. Ostertag MS, Hutwelker W, Plettenburg O, Sattler M, Popowicz GM: **Structural Insights into BET Client Recognition of Endometrial and Prostate Cancer-Associated SPOP Mutants**. *Journal of molecular biology* 2019, **431**(11):2213-2221.
231. Bouchard JJ, Otero JH, Scott DC, Szulc E, Martin EW, Sabri N, Granata D, Marzahn MR, Lindorff-Larsen K, Salvatella X *et al*: **Cancer Mutations of the Tumor Suppressor SPOP Disrupt the Formation of Active, Phase-Separated Compartments**. *Molecular cell* 2018, **72**(1):19-36.e18.
232. Kurimchak AM, Shelton C, Duncan KE, Johnson KJ, Brown J, O'Brien S, Gabbasov R, Fink LS, Li Y, Lounsbury N *et al*: **Resistance to BET Bromodomain Inhibitors Is Mediated by Kinome Reprogramming in Ovarian Cancer**. *Cell reports* 2016, **16**(5):1273-1286.
233. Shi X, Mihaylova VT, Kuruvilla L, Chen F, Viviano S, Baldassarre M, Sperandio D, Martinez R, Yue P, Bates JG *et al*: **Loss of TRIM33 causes resistance to BET bromodomain inhibitors through MYC- and TGF-beta-dependent mechanisms**. *Proceedings of the National Academy of Sciences of the United States of America* 2016, **113**(31):E4558-4566.
234. Doroshow DB, Eder JP, LoRusso PM: **BET inhibitors: a novel epigenetic approach**. *Annals of oncology : official journal of the European Society for Medical Oncology* 2017, **28**(8):1776-1787.
235. Li J, Ma J, Meng G, Lin H, Wu S, Wang J, Luo J, Xu X, Tough D, Lindon M *et al*: **BET bromodomain inhibition promotes neurogenesis while inhibiting gliogenesis in neural progenitor cells**. *Stem cell research* 2016, **17**(2):212-221.

236. Tsume M, Kimura-Yoshida C, Mochida K, Shibukawa Y, Amazaki S, Wada Y, Hiramatsu R, Shimokawa K, Matsuo I: **Brd2 is required for cell cycle exit and neuronal differentiation through the E2F1 pathway in mouse neuroepithelial cells**. *Biochemical and biophysical research communications* 2012, **425**(4):762-768.
237. Jin HS, Kim J, Kwak W, Jeong H, Lim GB, Lee CG: **Identification of a Novel Mutation in BRD4 that Causes Autosomal Dominant Syndromic Congenital Cataracts Associated with Other Neuro-Skeletal Anomalies**. *PloS one* 2017, **12**(1):e0169226.
238. Moskowitz AM, Belnap N, Siniard AL, Szelinger S, Claasen AM, Richholt RF, De Both M, Corneveaux JJ, Balak C, Piras IS *et al*: **A de novo missense mutation in ZMYND11 is associated with global developmental delay, seizures, and hypotonia**. *Cold Spring Harbor molecular case studies* 2016, **2**(5):a000851.
239. Tumiene B, Čiuladaitė Ž, Preikšaitienė E, Mameniškienė R, Utkus A, Kučinskas V: **Phenotype comparison confirms ZMYND11 as a critical gene for 10p15.3 microdeletion syndrome**. *Journal of applied genetics* 2017, **58**(4):467-474.
240. Poluha A, Bernaciak J, Jaszczuk I, Kędzior M, Nowakowska BA: **Molecular and clinical characterization of new patient with 1,08 Mb deletion in 10p15.3 region**. *Molecular Cytogenetics* 2017, **10**(1):34.
241. Goldmann JM, Wong WS, Pinelli M, Farrah T, Bodian D, Stittrich AB, Glusman G, Vissers LE, Hoischen A, Roach JC *et al*: **Parent-of-origin-specific signatures of de novo mutations**. *Nature genetics* 2016, **48**(8):935-939.
242. Rahbari R, Wuster A, Lindsay SJ, Hardwick RJ, Alexandrov LB, Turki SA, Dominiczak A, Morris A, Porteous D, Smith B *et al*: **Timing, rates and spectra of human germline mutation**. *Nature genetics* 2016, **48**(2):126-133.
243. Kong A, Frigge ML, Masson G, Besenbacher S, Sulem P, Magnusson G, Gudjonsson SA, Sigurdsson A, Jonasdottir A, Jonasdottir A *et al*: **Rate of de novo mutations and the importance of father's age to disease risk**. *Nature* 2012, **488**(7412):471-475.
244. Gao Z, Wyman MJ, Sella G, Przeworski M: **Interpreting the Dependence of Mutation Rates on Age and Time**. *PLoS biology* 2016, **14**(1):e1002355.
245. Goriely A, Wilkie AO: **Missing heritability: paternal age effect mutations and selfish spermatogonia**. *Nature reviews Genetics* 2010, **11**(8):589.
246. Yoon SR, Choi SK, Eboreime J, Gelb BD, Calabrese P, Arnheim N: **Age-dependent germline mosaicism of the most common noonan syndrome mutation shows the signature of germline selection**. *American journal of human genetics* 2013, **92**(6):917-926.
247. Mina M, Raynaud F, Tavernari D, Battistello E, Sungalee S, Saghafinia S, Laessle T, Sanchez-Vega F, Schultz N, Oricchio E *et al*: **Conditional Selection of Genomic Alterations Dictates Cancer Evolution and Oncogenic Dependencies**. *Cancer cell* 2017, **32**(2):155-168.e156.
248. Davies H, Bignell GR, Cox C, Stephens P, Edkins S, Clegg S, Teague J, Woffendin H, Garnett MJ, Bottomley W *et al*: **Mutations of the BRAF gene in human cancer**. *Nature* 2002, **417**(6892):949-954.
249. An J, Ren S, Murphy SJ, Dalangood S, Chang C, Pang X, Cui Y, Wang L, Pan Y, Zhang X *et al*: **Truncated ERG Oncoproteins from TMPRSS2-ERG Fusions Are Resistant to SPOP-Mediated Proteasome Degradation**. *Molecular cell* 2015, **59**(6):904-916.
250. Shoag J, Liu D, Blattner M, Sboner A, Park K, Deonarine L, Robinson BD, Mosquera JM, Chen Y, Rubin MA *et al*: **SPOP mutation drives prostate neoplasia without stabilizing oncogenic transcription factor ERG**. *The Journal of clinical investigation* 2017.
251. King JC, Xu J, Wongvipat J, Hieronymus H, Carver BS, Leung DH, Taylor BS, Sander C, Cardiff RD, Couto SS *et al*: **Cooperativity of TMPRSS2-ERG with PI3-kinase pathway activation in prostate oncogenesis**. *Nature genetics* 2009, **41**(5):524-526.
252. Bose R, Karthaus WR, Armenia J, Abida W, Iaquinta PJ, Zhang Z, Wongvipat J, Wasmuth EV, Shah N, Sullivan PS *et al*: **ERF mutations reveal a balance of ETS factors controlling prostate oncogenesis**. *Nature* 2017, **546**(7660):671-675.
253. Saar M, Zhao H, Nolley R, Young SR, Coleman I, Nelson PS, Vessella RL, Peehl DM: **Spheroid culture of LuCaP 147 as an authentic preclinical model of prostate cancer subtype with SPOP mutation and hypermutator phenotype**. *Cancer letters* 2014, **351**(2):272-280.

254. An J, Wang C, Deng Y, Yu L, Huang H: **Destruction of full-length androgen receptor by wild-type SPOP, but not prostate-cancer-associated mutants**. *Cell reports* 2014, **6**(4):657-669.
255. Theurillat JP, Udeshi ND, Errington WJ, Svinkina T, Baca SC, Pop M, Wild PJ, Blattner M, Groner AC, Rubin MA *et al*: **Prostate cancer. Ubiquitylome analysis identifies dysregulation of effector substrates in SPOP-mutant prostate cancer**. *Science (New York, NY)* 2014, **346**(6205):85-89.
256. Janouskova H, El Tekle G, Bellini E, Udeshi ND, Rinaldi A, Ulbricht A, Bernasocchi T, Civenni G, Losa M, Svinkina T *et al*: **Opposing effects of cancer-type-specific SPOP mutants on BET protein degradation and sensitivity to BET inhibitors**. *Nature medicine* 2017, **23**(9):1046-1054.
257. Stelloo S, Nevedomskaya E, Kim Y, Schuurman K, Valle-Encinas E, Lobo J, Krijgsman O, Peeper DS, Chang SL, Feng FY-C *et al*: **Integrative epigenetic taxonomy of primary prostate cancer**. *Nature Communications* 2018, **9**(1):4900.
258. Chng KR, Chang CW, Tan SK, Yang C, Hong SZ, Sng NY, Cheung E: **A transcriptional repressor co-regulatory network governing androgen response in prostate cancers**. *The EMBO journal* 2012, **31**(12):2810-2823.
259. Wen H, Li Y, Xi Y, Jiang S, Stratton S, Peng D, Tanaka K, Ren Y, Xia Z, Wu J *et al*: **ZMYND11 links histone H3.3K36me3 to transcription elongation and tumour suppression**. *Nature* 2014, **508**(7495):263-268.
260. Mani RS, Iyer MK, Cao Q, Brenner JC, Wang L, Ghosh A, Cao X, Lonigro RJ, Tomlins SA, Varambally S *et al*: **TMPRSS2-ERG-mediated feed-forward regulation of wild-type ERG in human prostate cancers**. *Cancer research* 2011, **71**(16):5387-5392.
261. Yu J, Yu J, Mani RS, Cao Q, Brenner CJ, Cao X, Wang X, Wu L, Li J, Hu M *et al*: **An integrated network of androgen receptor, polycomb, and TMPRSS2-ERG gene fusions in prostate cancer progression**. *Cancer cell* 2010, **17**(5):443-454.
262. Mounir Z, Korn JM, Westerling T, Lin F, Kirby CA, Schirle M, McAllister G, Hoffman G, Ramadan N, Hartung A *et al*: **ERG signaling in prostate cancer is driven through PRMT5-dependent methylation of the Androgen Receptor**. *eLife* 2016, **5**.
263. Boysen G, Rodrigues DN, Rescigno P, Seed G, Dolling D, Riisnaes R, Crespo M, Zafeiriou Z, Sumanasuriya S, Bianchini D *et al*: **SPOP-Mutated/CHD1-Deleted Lethal Prostate Cancer and Abiraterone Sensitivity**. *Clinical cancer research : an official journal of the American Association for Cancer Research* 2018.
264. Teply BA, Wang H, Luber B, Sullivan R, Rifkind I, Bruns A, Spitz A, DeCarli M, Sinibaldi V, Pratz CF *et al*: **Bipolar androgen therapy in men with metastatic castration-resistant prostate cancer after progression on enzalutamide: an open-label, phase 2, multicohort study**. *The Lancet Oncology* 2018, **19**(1):76-86.
265. Zhao D, Lu X, Wang G, Lan Z, Liao W, Li J, Liang X, Chen JR, Shah S, Shang X *et al*: **Synthetic essentiality of chromatin remodelling factor CHD1 in PTEN-deficient cancer**. *Nature* 2017, **542**(7642):484-488.
266. Lee SC, North K, Kim E, Jang E, Obeng E, Lu SX, Liu B, Inoue D, Yoshimi A, Ki M *et al*: **Synthetic Lethal and Convergent Biological Effects of Cancer-Associated Spliceosomal Gene Mutations**. *Cancer cell* 2018, **34**(2):225-241.e228.
267. Zeineldin M, Federico S, Chen X, Fan Y, Xu B, Stewart E, Zhou X, Jeon J, Griffiths L, Nguyen R *et al*: **MYCN amplification and ATRX mutations are incompatible in neuroblastoma**. *Nat Commun* 2020, **11**(1):913.
268. Cole CB, Verdoni AM, Ketkar S, Leight ER, Russler-Germain DA, Lamprecht TL, Demeter RT, Magrini V, Ley TJ: **PML-RARA requires DNA methyltransferase 3A to initiate acute promyelocytic leukemia**. *The Journal of clinical investigation* 2016, **126**(1):85-98.
269. Ley TJ, Miller C, Ding L, Raphael BJ, Mungall AJ, Robertson A, Hoadley K, Triche TJ, Jr., Laird PW, Baty JD *et al*: **Genomic and epigenomic landscapes of adult de novo acute myeloid leukemia**. *The New England journal of medicine* 2013, **368**(22):2059-2074.
270. Beshiri ML, Tice CM, Tran C, Nguyen HM, Sowalsky AG, Agarwal S, Jansson KH, Yang Q, McGowen KM, Yin J *et al*: **A PDX/Organoid Biobank of Advanced Prostate Cancers Captures Genomic and Phenotypic Heterogeneity for Disease Modeling and Therapeutic Screening**. *Clin Cancer Res* 2018, **24**(17):4332-4345.

271. Tomlins SA, Laxman B, Dhanasekaran SM, Helgeson BE, Cao X, Morris DS, Menon A, Jing X, Cao Q, Han B *et al*: **Distinct classes of chromosomal rearrangements create oncogenic ETS gene fusions in prostate cancer**. *Nature* 2007, **448**(7153):595-599.
272. Drost J, Karthaus WR, Gao D, Driehuis E, Sawyers CL, Chen Y, Clevers H: **Organoid culture systems for prostate epithelial and cancer tissue**. *Nature protocols* 2016, **11**(2):347-358.
273. Corey E, Quinn JE, Buhler KR, Nelson PS, Macoska JA, True LD, Vessella RL: **LuCaP 35: a new model of prostate cancer progression to androgen independence**. *Prostate* 2003, **55**(4):239-246.
274. Wang L, Wang S, Li W: **RSeQC: quality control of RNA-seq experiments**. *Bioinformatics (Oxford, England)* 2012, **28**(16):2184-2185.
275. Chen S, Huang T, Zhou Y, Han Y, Xu M, Gu J: **AfterQC: automatic filtering, trimming, error removing and quality control for fastq data**. *BMC Bioinformatics* 2017, **18**(Suppl 3):80.
276. Garcia-Alcalde F, Okonechnikov K, Carbonell J, Cruz LM, Gotz S, Tarazona S, Dopazo J, Meyer TF, Conesa A: **Qualimap: evaluating next-generation sequencing alignment data**. *Bioinformatics (Oxford, England)* 2012, **28**(20):2678-2679.
277. Dobin A, Davis CA, Schlesinger F, Drenkow J, Zaleski C, Jha S, Batut P, Chaisson M, Gingeras TR: **STAR: ultrafast universal RNA-seq aligner**. *Bioinformatics (Oxford, England)* 2013, **29**(1):15-21.
278. Harrow J, Frankish A, Gonzalez JM, Tapanari E, Diekhans M, Kokocinski F, Aken BL, Barrell D, Zadissa A, Searle S *et al*: **GENCODE: the reference human genome annotation for The ENCODE Project**. *Genome research* 2012, **22**(9):1760-1774.
279. Love MI, Huber W, Anders S: **Moderated estimation of fold change and dispersion for RNA-seq data with DESeq2**. *Genome biology* 2014, **15**(12):550.
280. Wu D, Smyth GK: **Camera: a competitive gene set test accounting for inter-gene correlation**. *Nucleic acids research* 2012, **40**(17):e133.
281. Liberzon A, Birger C, Thorvaldsdottir H, Ghandi M, Mesirov JP, Tamayo P: **The Molecular Signatures Database (MSigDB) hallmark gene set collection**. *Cell Syst* 2015, **1**(6):417-425.
282. Liberzon A, Subramanian A, Pinchback R, Thorvaldsdottir H, Tamayo P, Mesirov JP: **Molecular signatures database (MSigDB) 3.0**. *Bioinformatics (Oxford, England)* 2011, **27**(12):1739-1740.
283. Li H, Durbin R: **Fast and accurate long-read alignment with Burrows-Wheeler transform**. *Bioinformatics (Oxford, England)* 2010, **26**(5):589-595.
284. Zhang Y, Liu T, Meyer CA, Eeckhoute J, Johnson DS, Bernstein BE, Nusbaum C, Myers RM, Brown M, Li W *et al*: **Model-based analysis of ChIP-Seq (MACS)**. *Genome biology* 2008, **9**(9):R137.
285. Quinlan AR, Hall IM: **BEDTools: a flexible suite of utilities for comparing genomic features**. *Bioinformatics (Oxford, England)* 2010, **26**(6):841-842.
286. Shannon P, Markiel A, Ozier O, Baliga NS, Wang JT, Ramage D, Amin N, Schwikowski B, Ideker T: **Cytoscape: a software environment for integrated models of biomolecular interaction networks**. *Genome research* 2003, **13**(11):2498-2504.
287. Colaprico A, Silva TC, Olsen C, Garofano L, Cava C, Garolini D, Sabedot TS, Malta TM, Pagnotta SM, Castiglioni I *et al*: **TCGAbiolinks: an R/Bioconductor package for integrative analysis of TCGA data**. *Nucleic acids research* 2016, **44**(8):e71.
288. Hanzelmann S, Castelo R, Guinney J: **GSVA: gene set variation analysis for microarray and RNA-seq data**. *BMC Bioinformatics* 2013, **14**:7.
289. Gu Z, Gu L, Eils R, Schlesner M, Brors B: **circlize Implements and enhances circular visualization in R**. *Bioinformatics (Oxford, England)* 2014, **30**(19):2811-2812.
290. Yokoyama Y, Zhu H, Lee JH, Kossenkov AV, Wu SY, Wickramasinghe JM, Yin X, Palozola KC, Gardini A, Showe LC *et al*: **BET Inhibitors Suppress ALDH Activity by Targeting ALDH1A1 Super-Enhancer in Ovarian Cancer**. *Cancer Res* 2016, **76**(21):6320-6330.
291. Yu G, Wang LG, He QY: **ChIPseeker: an R/Bioconductor package for ChIP peak annotation, comparison and visualization**. *Bioinformatics (Oxford, England)* 2015, **31**(14):2382-2383.
292. Welch RP, Lee C, Imbriano PM, Patil S, Weymouth TE, Smith RA, Scott LJ, Sartor MA: **ChIP-Enrich: gene set enrichment testing for ChIP-seq data**. *Nucleic acids research* 2014, **42**(13):e105.
293. Hieronymus H, Lamb J, Ross KN, Peng XP, Clement C, Rodina A, Nieto M, Du J, Stegmaier K, Raj SM *et al*: **Gene expression signature-based chemical genomic prediction identifies a novel class of HSP90 pathway modulators**. *Cancer cell* 2006, **10**(4):321-330.

ARTICLES

ARTICLE 1

nature medicine

Opposing effects of cancer-type-specific SPOP mutants on BET protein degradation and sensitivity to BET inhibitors

Hana Janouskova[1,2,15], Geniver El Tekle[1–3,15], Elisa Bellini[4], Namrata D Udeshi[5], Anna inaldi[1,2], Anna Ulbricht[6], Tiziano Bernasocchi[1–3], Gianluca Civenni[1,2], Marco Losa[1,2], Tanya Svinkina[5], Craig M Bielski[5,14], Gregory V Kryukov[5], Luciano Cascione[1,2], Sara Napoli[1,2], Radoslav I Enchev[6], David G Mutch[7], Michael E Carney[8], Andrew Berchuck[9], Boris J N Winterhoff[10], Russell R Broaddus[11], Peter Schraml[4], Holger Moch[4], Francesco Bertoni[1,2], Carlo V Catapano[1–3], Matthias Peter[6], Steven A Carr[5], Levi A Garraway[5,12,13], Peter J Wild[4] & Jean-Philippe P Theurillat[1–3]

It is generally assumed that recurrent mutations within a given cancer driver gene elicit similar drug responses. Cancer genome studies have identified recurrent but divergent missense mutations affecting the substrate-recognition domain of the ubiquitin ligase adaptor SPOP in endometrial and prostate cancers. The therapeutic implications of these mutations remain incompletely understood. Here we analyzed changes in the ubiquitin landscape induced by endometrial cancer-associated *SPOP* mutations and identified BRD2, BRD3 and BRD4 proteins (BETs) as SPOP-CUL3 substrates that are preferentially degraded by endometrial cancer-associated SPOP mutants. The resulting reduction of BET protein levels sensitized cancer cells to BET inhibitors.Conversely, prostate cancer-specific *SPOP* mutations resulted in impaired degradation of BETs, promoting their resistance to pharmacologic inhibition. These results uncover an oncogenomics paradox, whereby mutations mapping to the same domain evoke opposing drug susceptibilities. Specifically, we provide a molecular rationale for the use of BET inhibitors to

Specific mutations in cancer-related genes can indicate whether a patient with cancer may or may not respond to a given drug[1]. Generally, it is assumed that recurrent mutations within a specific gene have similar therapeutic implications, especially if the resulting amino acid changes occur within the same protein-coding domain. Genome studies have revealed recurrent point mutations mapping to the substrate-recognition domain of the ubiquitin ligase adaptor speckle-type POZ protein (SPOP) in 4–14% of prostate and endome- trial cancers (**Fig. 1a**)[2–6]. In prostate cancer, *SPOP* mutations are con- fined to the amino acid residues of the substrate-binding cleft—a specific region within the substrate-recognition domain that is essential for substrate interaction and ubiquitin transfer[7]. We and others have subsequently shown that these mutations act in a domi- nant-negative fashion to repress ubiquitination and degradation of oncogenic substrate proteins[8–12]. In contrast, recurrent amino acid substitutions in endometrial cancer and carcinosarcoma occur in an uncharacterized portion of the substrate-recognition domain (**Fig. 1a** and **Supplementary Fig. 1a**)[4–6]. Given the divergent mutation patterns in these tumor types, we speculated that *SPOP* mutations associated with endometrial cancer might differentially affect protein ubiquitination in comparison to prostate cancer–specific *SPOP* muta- tions, possibly resulting in distinct therapeutic opportunities.

RESULTS

Cancer-type-specific *SPOP* mutations have opposing effects on BET protein levels

To explore this hypothesis, we characterized changes in the ubiquitination landscape specific to endometrial cancer–associated SPOP mutants by mass spectrometry–based proteomics. To ensure that dis- ease-relevant proteins were being expressed in our experimental set- ting, we chose human Ishikawa endometrial cancer cells, derived from a well-differentiated endometrioid cancer, for experimentation because their robustly expressed genes substantially overlapped with those found in *SPOP*-mutant tumor tissues (**Supplementary Fig. 1b**)[6,13]. Subsequently, we generated cells that stably overexpressed control vector, wild-type SPOP (SPOP-WT) or one of seven endometrial

[1]Institute of Oncology Research, Oncology Institute of Southern Switzerland, Bellinzona, Switzerland. [2]Faculty of Biomedical Science, Università della Svizzera Italiana, Lugano, Switzerland. [3]Centre Hospitalier Universitaire Vaudois, University of Lausanne, Lausanne, Switzerland. [4]Institute of Surgical Pathology, University Hospital Zurich, Zurich, Switzerland. [5]Broad Institute of Harvard and MIT, Cambridge, Massachusetts, USA. [6]Department of Biochemistry, Eidgenössische Technische Hochschule, Zurich, Switzerland. [7]Division of Gynecologic Oncology, Washington University, St. Louis, Missouri, USA. [8]Department of Obstetrics, Gynecology and Women's Health, John A. Burns School of Medicine, University of Hawaii at Manoa, Honolulu, Hawaii, USA. [9]Division of Gynecologic Oncology, Duke Cancer Center, Durham, North Carolina, USA. [10]Division of Gynecologic Oncology, University of Minnesota, Minneapolis, Minnesota, USA. [11]Department of Pathology, University of Texas MD Anderson Cancer Center, Houston, Texas, USA. [12]Department of Medical Oncology, Dana-Farber Cancer Institute, Boston, Massachusetts, USA. [13]Center for Cancer Genome Discovery, Dana-Farber Cancer Institute, Boston, Massachusetts, USA. [14]Present address: Molecular Oncology, Memorial Sloan Kettering Cancer Center, New York, New York, USA. [15]These authors contributed equally to this work. Correspondence should be addressed to J.P.T. (jeanp_theurillat@ior.iosi.ch).

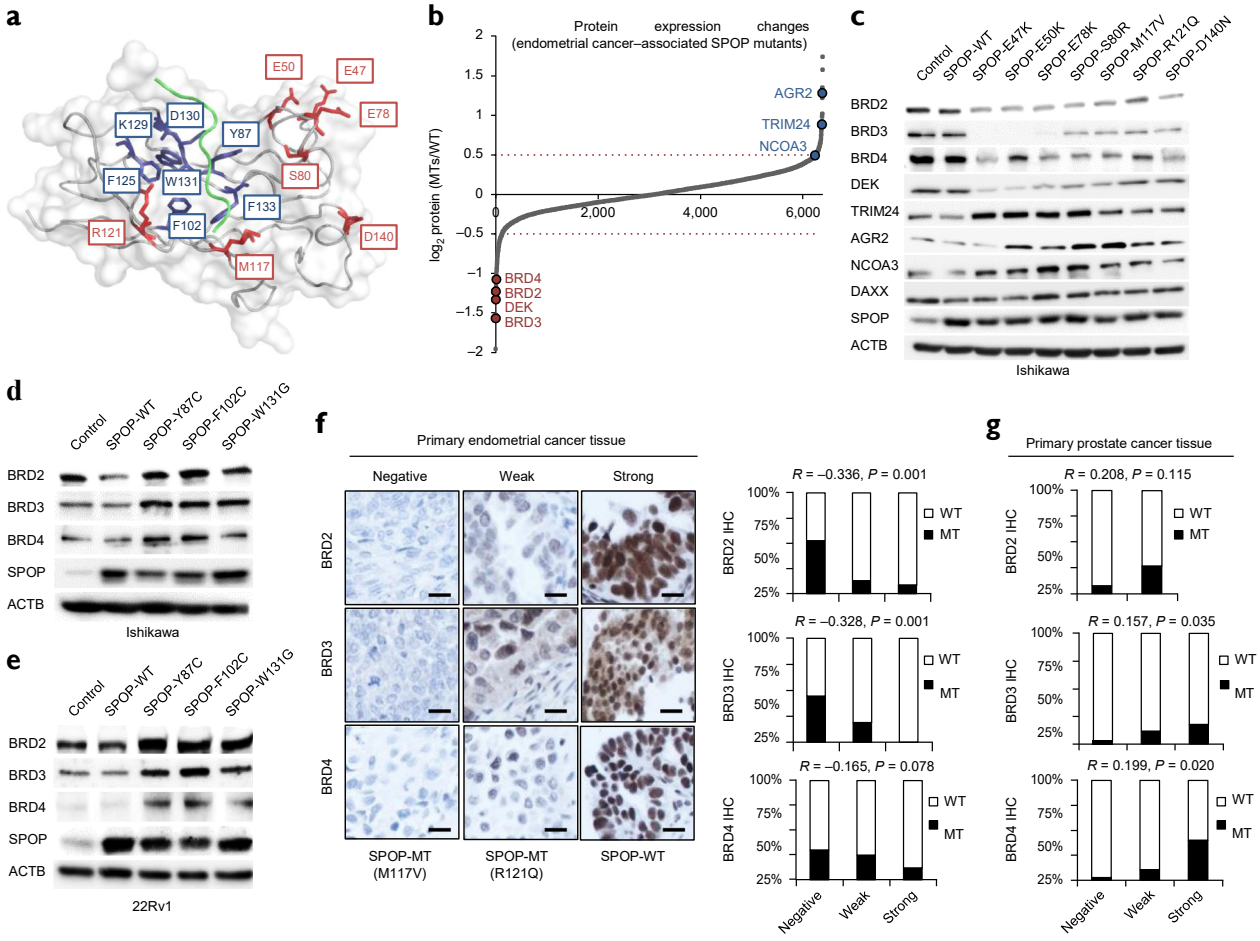

Figure 1 Endometrial cancer– and prostate cancer–associated SPOP mutants induce opposing effects on BET protein levels. (**a**) Outer surface of the SPOP substrate-recognition domain. Recurrently mutated amino acid residues in prostate cancer are highlighted in blue and those in endometrial cancer are in red[7]. The substrate-binding cleft is shown in green. (**b**) Scatterplot showing expression differences for the indicated proteins in Ishikawa endometrial cancer cells expressing SPOP mutants (SPOP-MTs) versus wild-type SPOP (SPOP-WT). Dashed red lines, ±2 s.d. (**c**) Representative western blot validation for the indicated proteins in Ishikawa cells stably expressing vector control, SPOP-WT or an endometrial cancer–specific SPOP mutant (n = 5). (**d**) Representative western blot for the indicated proteins in Ishikawa endometrial cancer cells expressing prostate cancer–specific SPOP mutants (n = 3). (**e**) Representative western blot for the indicated proteins in 22Rv1 prostate cancer cells stably expressing prostate cancer–associated SPOP mutants (n = 3). In **b–d**, β-actin (ACTB) is used as a loading control. (**f**) Left, representative images of primary human endometrial cancer tissues stained for BRD2, BRD3 and BRD4 by immunohistochemistry (IHC) (**Supplementary Fig. 4c,d**); right, corresponding quantification of protein expression levels in primary tumors stratified according to *SPOP* mutation status. Scale bars, 20 μm. (**g**) Analysis of BRD2, BRD3 and BRD4 expression in primary human prostate cancer tissues stratified according to *SPOP* mutation status (**Supplementary Fig. 4g**). R correlation coefficients and P values were derived from Kendall's tau-b. In each panel, n indicates the number of independent experiments performed.

cancer–specific mutated SPOP variants (E47K, E50K, E78K, S80R, M117V, R121Q and D140N; SPOP-MTs) (**Supplementary Fig. 1c**). In each case, we measured glycine-glycine remnants of ubiquitinated lysines (K-ε-GG) after trypsin digestion and stable isotope labeling of amino acids in cell culture (SILAC)-based mass spectrometry (**Supplementary Fig. 1d**)[14]. All K-ε-GG values (n = 17,239), defined as ratios of mutant to SPOP-WT, were normalized to the corresponding protein ratios to account for ubiquitination-related changes in protein levels (**Supplementary Table 1**). K-ε-GG peptide values for cells expressing individual SPOP-MTs were compared to those from cells overexpressing SPOP-WT within experiments (**Supplementary Fig. 2a,c,e,g**).

Because protein ubiquitination is often linked to proteasomal degradation, we asked which differentially expressed K-ε-GG peptides showed an inverse correlation with protein abundance (**Supplementary Table 1** and **Supplementary Fig. 2b,d,f,h**). We identified two patterns of ubiquitination and protein dysregula- tion in known and putative SPOP substrates pointing to possi- ble private contact points between individual substrates and the mutant meprin and TRAF homology (MATH) domain (**Fig. 1b,c** and **Supplementary Figs. 2** and **3a**). Peptides corresponding to tri- partite-motif-containing 24 (TRIM24), anterior gradient protein 2 homolog (AGR-2) and nuclear receptor coactivator 3 (NCOA3)—all proteins with reported oncogenic properties—showed a decrease in K-ε-GG peptide abundance in cells expressing SPOP-MTs, followed by an increase in levels of the corresponding protein[9,15,16]. Similar dominant-negative patterns of substrate dysregulation by prostate cancer–specific SPOP mutants have been reported for TRIM24 and NCOA3 (refs. 8,9,17).

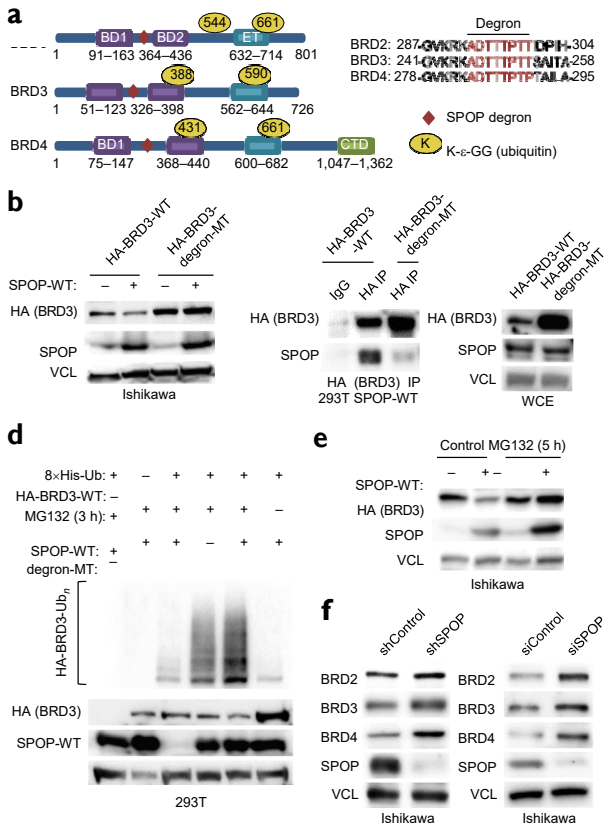

Figure 2 BET proteins are bona fide substrates of wild-type SPOP.

(**a**) Schema of the BET proteins with the positions of bromodomains 1 and 2 (BD1 and BD2), the extraterminal (ET) domain, the C-terminal domain (CTD) and the ubiquitinated lysines (K-ε-GG) detected by mass pectrometry indicated; the SPOP degron motif is depicted in red. Effect of transient SPOP-WT overexpression on the levels of HA-tagged wild-type BRD3 (HA-BRD3-WT) and HA-tagged BRD3 with the mutated degron (HA-BRD3-degron-MT) assessed by western blot in Ishikawa cells (n = 3). (**c**) Interaction between SPOP-WT and BRD3-WT or HA-BRD3-degron-MT. HA immunoprecipitation (IP) (top) and whole-cell extract (WCE) (bottom) are shown from transiently transfected 293T cells (n = 3). (**d**) *In vivo* ubiquitination of HA-BRD3-WT and HA-BRD3- degron-MT by SPOP-WT. 293T cells were transfected to express 8× histidine (8×His)-tagged ubiquitin (Ub) and the indicated constructs followed by 3 h of MG132 treatment. 8×His-Ub pulldown from lysed cells was performed using nickel beads (n = 3). (**e**) HA-BRD3 protein level determined by western blot in Ishikawa cells transiently expressing SPOP-WT and HA-BRD3 with or without 5 h of MG132 treatment (n = 3). (**f**) Representative western blot of the indicated proteins upon knockdown of *SPOP* with shRNA (left) or siRNA (right) in Ishikawa cells (n = 3). The western blots shown in **b** and **d**–**f** are representative. Vinculin (VCL) was used as a loading control. In **b**–**f**, n indicates the number of independent experiments performed.

The most striking changes were found in proteins that exhibited robust upregulation of K-ε-GG peptides coupled with downregulation of the corresponding protein (**Fig. 1b**,**c** and **Supplementary Figs. 2** and **3a**), including DEK, another characterized SPOP substrate[8]. Yet, the most profound changes at the protein level without concurrent changes at the mRNA level were found in BRD3, BRD2 and BRD4 (**Fig. 1b**,**c** and **Supplementary Fig. 3b**). These bromodomain and extraterminal (BET)-motif-containing proteins, which serve as prom- ising targets for cancer therapy[18], may be increasingly ubiquitinated and degraded by endometrial cancer–specific SPOP mutants. Notably, similar changes were also found in human HEC-151 and RL95-2 endometrial cancer cells and in human 22Rv1 prostate cancer cells (**Supplementary Fig. 3c–e**).

Because prostate cancer–specific SPOP mutants have been found to impair ubiquitination of substrates in a dominant-negative man- ner, we speculated that these mutants might have the opposite effect on BET protein levels of those identified in endometrial cancer[8–11]. Indeed, overexpression of recurrent prostate cancer–specific mutants increased BET protein levels in human Ishikawa endometrial cancer cells, human 22Rv1 prostate cancer cells, human LHMAR prostate epithelial cells[8] (**Fig. 1d**,**e** and **Supplementary Fig. 3f–h**) and in mouse prostate epithelial cells[19]. In aggregate, our findings suggest that BET proteins might represent SPOP substrates that are differen- tially ubiquitinated and degraded by endometrial cancer– and prostate cancer–specific mutants irrespective of cellular lineage. In support of these findings, nuclear levels of BET proteins correlated inversely with recurrent *SPOP* mutations in human primary endometrial cancer tis- sues analyzed by immunohistochemistry, whereas a positive correla- tion was noted in primary human prostate cancer tissues (**Fig. 1f**,**g** and **Supplementary Fig. 4**).

BET proteins are bona fide SPOP substrates

We sought to determine whether SPOP directly interacts with BET proteins to promote ubiquitination. In agreement with this hypoth- esis, the primary amino acid sequences of the BET proteins con- tain a conserved consensus sequence that is a SPOP-binding motif (**Fig. 2a**)[7]. We focused on BRD3 for experimental follow-up because it was the most differentially regulated BET family member (**Fig. 1b**). First, we overexpressed HA-tagged BRD3 (HA-BRD3) harboring three threonine-to-alanine substitutions at the binding motif (degron-MT) in Ishikawa cells (**Supplementary Fig. 5a**) and assessed the ability of SPOP-WT to mediate BRD3 degradation. The substitutions in the degron variant abolished the repressive effect of SPOP and resulted in elevated levels of BRD3 protein relative to those of controls, in agree- ment with the notion that endogenous SPOP was not able to degrade the degron variant (**Fig. 2b** and **Supplementary Fig. 5b**). To deter- mine whether the motif mediated direct binding of SPOP to BRD3, we performed immunoprecipitation experiments in cells express- ing either wild-type HA-BRD3 or the degron variant. SPOP protein was detectable after immunoprecipitation of wild-type HA-BRD3, whereas the substitutions in the BRD3 degron variant disrupted the BRD3–SPOP interaction (**Fig. 2c**). Thus, the SPOP-binding motif within BRD3 appears to be necessary for SPOP binding.

Next, we tested whether SPOP could ubiquitinate BRD3 as part of a cullin-3 (CUL3)–RING-box protein 1 (RBX1) ubiquitin E3 ligase complex[20]. Knockdown of *CUL3* increased HA-BRD3 levels and decreased BRD3 ubiquitination relative to control in 293T cells (**Supplementary Fig. 5c**). Furthermore, SPOP-WT, along with RBX1 and CUL3, directly ubiquitinated wild-type HA-BRD3 *in vivo* and *in vitro*, whereas the degron variant of HA-BRD3 remained unaffected (**Fig. 2d** and **Supplementary Fig. 5d**). Additional CUL3-dependent substrate adaptors (kelch-like family member 9 (KLHL9), KLHL13, KLHL21) failed to ubiquitinate BRD3 *in vitro*, verifying the specificity of SPOP toward BRD3 (**Supplementary Fig. 5d**).

To determine whether BRD3 ubiquitination induces its proteaso- mal degradation, we cultured SPOP- and BRD3-expressing 293T cells in the presence or absence of the proteasome inhibitor MG132. Short- term MG132 treatment increased levels of ubiquitinated HA-BRD3 (**Fig. 2d**). Prolonged proteasomal inhibition increased HA-BRD3

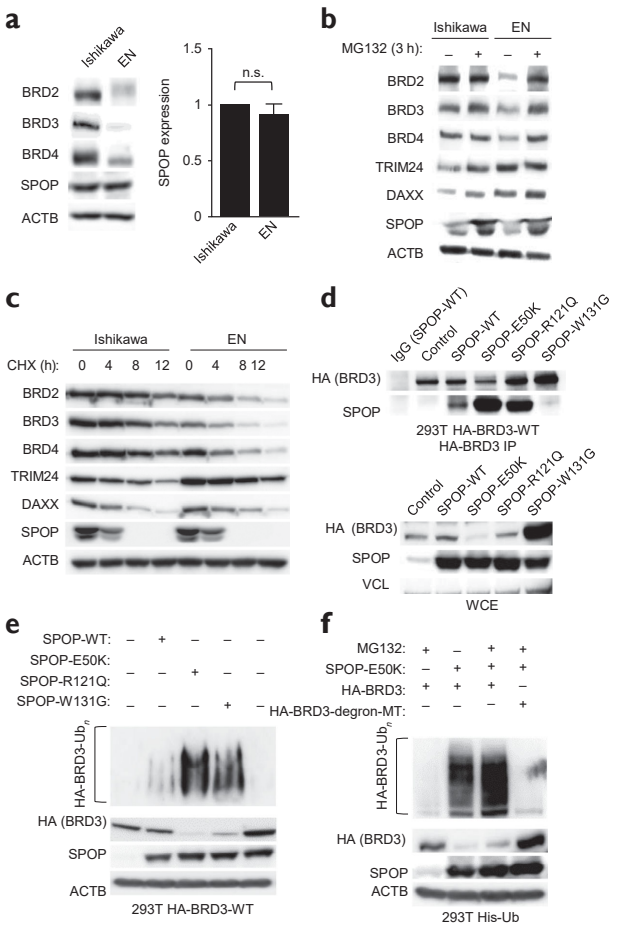

Figure 3 BET proteins are differentially ubiquitinated and degraded by endometrial cancer– and prostate cancer–specific SPOP mutants. (**a**) Representative western blot (n = 4) of BET proteins and SPOP in Ishikawa and EN human endometrial cell lines. Statistical significance was determined by unpaired, two-tailed Student's t-test (n.s., not significant). Error bars, s.e.m. (**b**) Representative western blot of the indicated proteins in Ishikawa and EN cells with or without 3 h of MG132 treatment (n = 3). (**c**) Representative western blot of the indicated proteins after the specified duration of cycloheximide (CHX) treatment in Ishikawa and EN cells (n = 3). (**d**) Interaction of HA-BRD3 with SPOP-WT, endometrial cancer–associated SPOP mutants (E50K, R121Q) and one prostate cancer–associated SPOP mutant (W131G). HA immunoprecipitation (top) and WCE (bottom) are shown from transiently transfected 293T cells overexpressing HA-BRD3 and the indicated SPOP constructs (n = 3). (**e**) Effects of SPOP-WT and SPOP mutants on *in vivo* ubiquitination of HA-BRD3 (n = 3). (**f**) *In vivo* ubiquitination of HA-BRD3- WT or HA-BRD3-degron-MT by SPOP-E50K (n = 3). Western blots shown in **a**–**f** are representative. ACTB were used as loading control. In each legend, n indicates the number of independent experiments performed.

and endogenous BET protein levels in the presence of SPOP-WT overexpression (**Fig. 2e** and **Supplementary Fig. 5e**). SPOP was also detectable after immunoprecipitation of endogenous BET proteins (**Supplementary Fig. 5f**). Moreover, *SPOP* knockdown increased BET protein levels without concomitant changes in mRNA levels and impaired protein degradation after inhibition of protein synthesis with cycloheximide (**Fig. 2f** and **Supplementary Fig. 5g,h**). In aggre- gate, these data are consistent with a model in which ubiquitination of BET proteins promotes their proteasomal degradation.

Cancer-type-specific SPOP mutants induce differential ubiquitination of BET proteins

To test whether the functional properties of endometrial cancer–specific SPOP mutants may translate into reduced BET protein levels in comparison to SPOP-WT when these mutants are expressed at endog- enous levels, we identified the human EN endometrial cancer cell line that harbors a recurrent *SPOP* mutation (p.R121Q) in the Cancer Cell Line Encyclopedia (CCLE) (**Supplementary Fig. 6a**). We compared BET protein levels in EN cells to those in Ishikawa cells expressing equivalent levels of SPOP-WT (**Fig. 3a**). We found that EN cancer cells exhibited lower levels of BET proteins despite having higher levels of the corresponding mRNAs (**Fig. 3a** and **Supplementary Fig. 6b**). In line with the notion that enhanced protein degradation by SPOP-R121Q leads to reduced BET protein levels in EN cells, we found more significant increases in BET protein levels upon *SPOP* depletion or short-term proteasome inhibition in EN cells than in Ishikawa cells (**Fig. 3b** and **Supplementary Fig. 6c–e**). In addition to and in accordance with our observations above, endogenous SPOP-R121Q bound more efficiently to BET proteins in EN cells, in which we noted more pronounced degradation of BET proteins after inhibition of protein synthesis with cycloheximide (**Fig. 3c** and **Supplementary Fig. 6f,g**). Of note, endogenous SPOP levels were also increased after prolonged proteasome inhibition and reduced after inhibition of protein synthesis, indicating proteasomal turnover of SPOP itself (**Figs. 2e** and **3b,c**).

To test whether the different BET protein binding and degradation kinetics in human EN and Ishikawa cells were a result of the specific amino acid substitutions within SPOP, we analyzed the activity of different SPOP species side by side in 293T cells. Endometrial cancer–associated SPOP mutants (E50K and R121Q) bound more strongly to HA-BRD3 than SPOP-WT did *in vivo* and *in vitro*, whereas the interaction of the prostate cancer–specific SPOP mutants W131G and F133L was reduced (**Fig. 3d** and **Supplementary Fig. 6h**). In line with this observation, ubiquitination of HA-BRD3 was increased with the endometrial cancer–specific SPOP mutants and decreased with the prostate cancer–specific mutants (**Fig. 3e** and **Supplementary Fig. 6i**). We next investigated whether the increase in ubiquitination mediated by the endometrial cancer– specific SPOP mutants was dependent on an intact degron on BRD3. Indeed, SPOP-E50K failed to ubiquitinate the degron variant of BRD3 (**Fig. 3f**) and to reduce BRD3 protein levels (**Supplementary Fig. 6j**). These results suggest that BET protein levels are at least in part affected by differential interactions between SPOP mutants and the BET degron.

Sensitivity to BET inhibitors is altered by cancer-type-specific *SPOP* mutations

Some cancer cells depend on the presence of BET proteins for tumor growth and survival[18,21]. Therefore, we sought to determine whether enhanced degradation of BET proteins in the context of endometrial cancer–specific SPOP mutants might create specific vulnerabilities; we speculated that endometrial cancer cells with low BET protein levels might become particularly susceptible to further reduction of BET protein levels. Indeed, EN cells were susceptible to individual knockdown of the BET proteins, which resulted in decreased growth (**Supplementary Fig. 7a**). In contrast, to achieve a similar effect on growth in Ishikawa cells, individual BET proteins had to be knocked down in the context of the SPOP-R121Q mutant. These data sug- gest that endometrial cancer cells with low levels of BET proteins in the context of endometrial cancer–specific SPOP mutants are

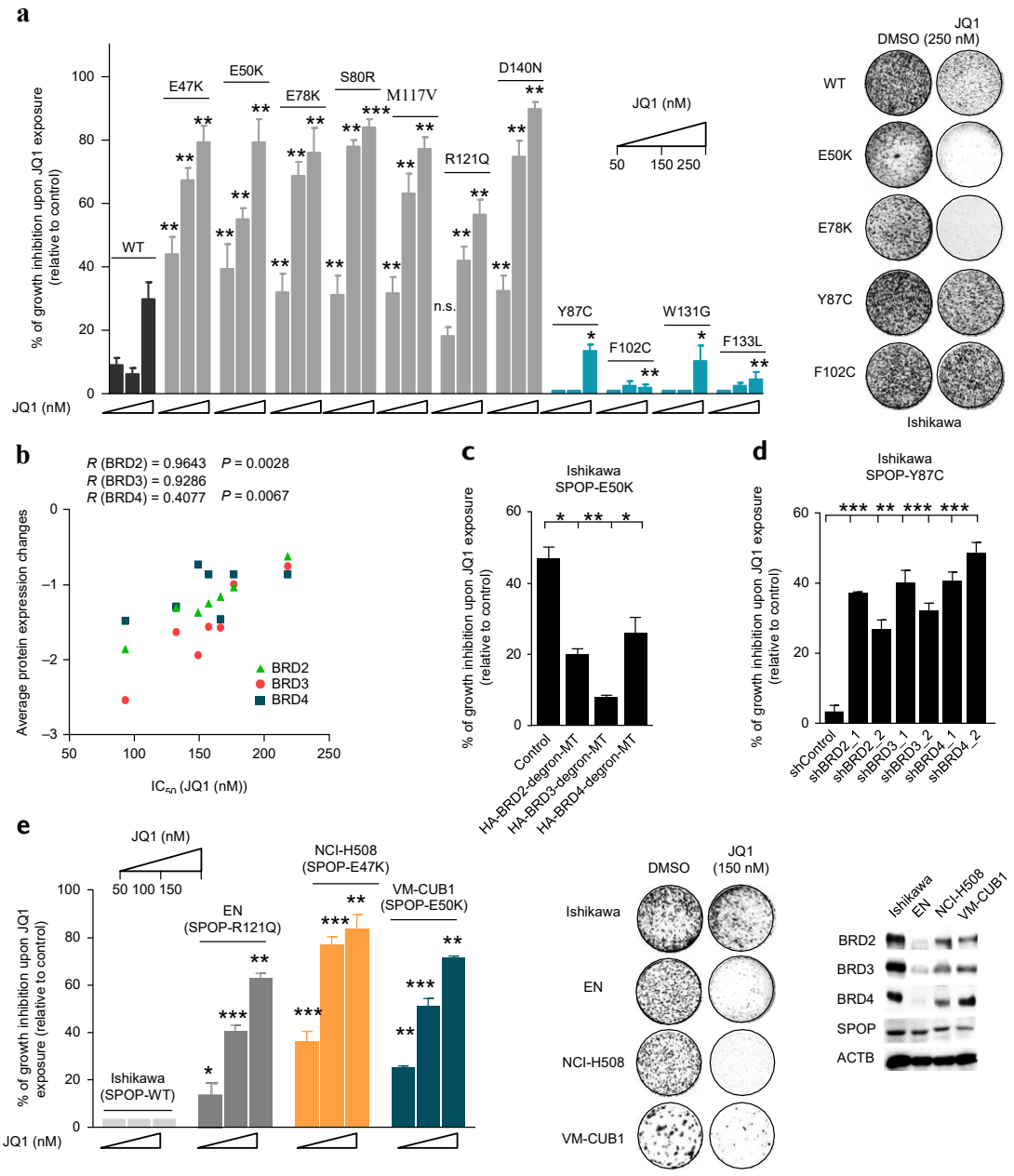

Figure 4 Cancer-type-specific SPOP mutants alter BET inhibitor sensitivity in an opposing manner. (**a**) Response to JQ1 treatment by Ishikawa cells stably overexpressing SPOP mutants specific to endometrial cancer (E47K, E50K, E78K, S80R, M117V, R121Q, D140N; in grey) or prostate cancer (Y87C, F102C, W131G, F133L; in blue) in 3D semisolid cell culture (n = 3). Statistical analysis was performed using two-way ANOVA with Dunnett's post test, 112 degrees of freedom (d.f.). (**b**) Correlation of IC_{50} (JQ1), shown in **Supplementary Figure 7c**, with BET protein levels, as quantified by mass spectrometry, in Ishikawa cells stably expressing recurrent endometrial cancer–specific SPOP mutants (R and P values were calculated using Spearman rank correlation). Each point represents the change in protein expression of individual SPOP mutants relative to that of SPOP-WT. (**c**) Response to JQ1 treatment (250 nM) by Ishikawa cells stably overexpressing SPOP-E50K and different degron-mutant constructs of the BET proteins (n = 3). (**d**) Effect of shRNA-mediated depletion of *BRD2*, *BRD3* and *BRD4* individually on JQ1 (200 nM) sensitivity in Ishikawa cells expressing SPOP-Y87C (n = 3). (**e**) JQ1 sensitivity of: Ishikawa cells expressing SPOP-WT, EN human endometrial cancer cells expressing SPOP-R121Q, NCI-H508 human large intestine cancer cells expressing SPOP-E47K and mutant VM-CUB1 human urothelial cancer cells expressing SPOP-E50K in 3D semisolid culture (n = 4). A representative immunoblot for the indicated proteins and cell lines is shown. ACTB was used as a loading control. P values in **e** are indicated above the compared bars (two-way ANOVA with Dunnett's post test, 30 d.f.). Data represent mean ± s.e.m. Statistical significance was determined by unpaired, two-tailed Student's t-test unless otherwise specified. *P < 0.05, **P < 0.01, ***P < 0.001. In each legend, n indicates the number of independent experiments performed.

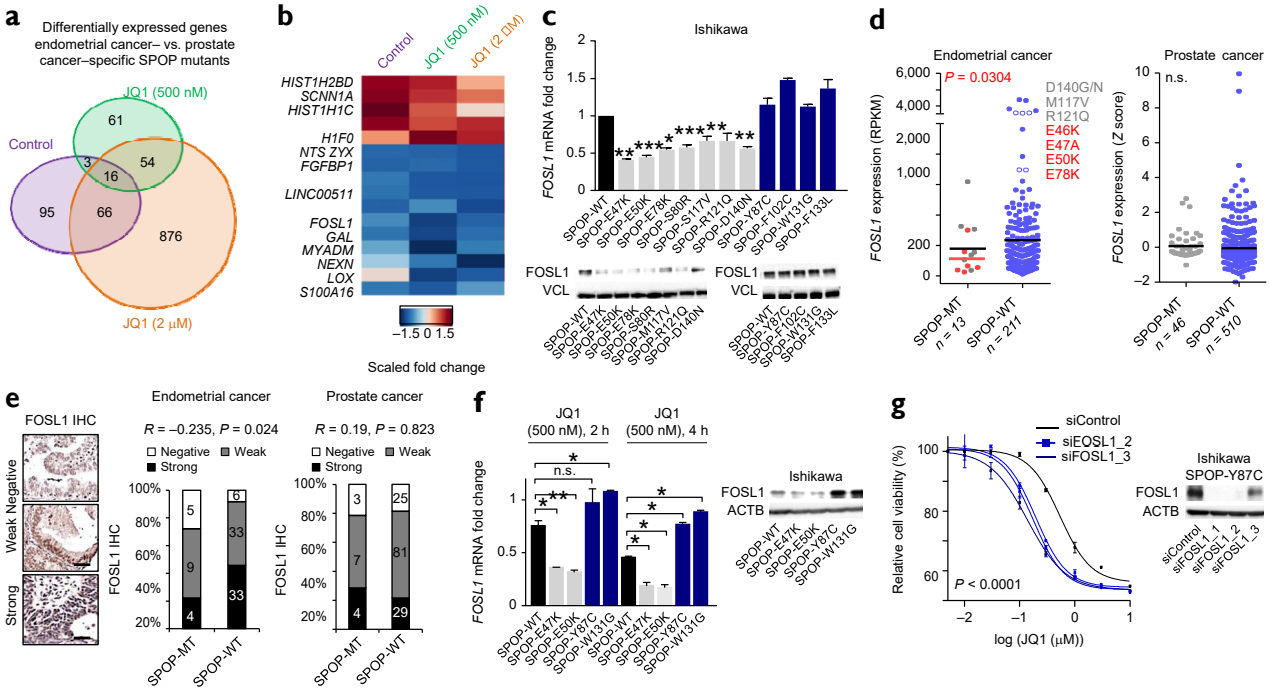

Figure 5 Downregulation of *FOSL1* sensitizes Ishikawa cells to JQ1 treatment. (**a**) Venn diagram depicting the overlap of significantly differentially expressed genes in Ishikawa cells stably expressing SPOP mutants specific to endometrial cancer (E47K, E50K) versus prostate cancer (Y87C, W131G) with or without JQ1 treatment. Overlap corresponds to the number of genes with a significant *P* value of <0.05 (Benjamini–Hochberg test). (**b**) Heat map showing fold change in expression for the 16 genes in the overlap area of **a**. (**c**) *FOSL1* mRNA (normalized to cyclophilin expression) (top) and FOSL1 protein (bottom) levels of Ishikawa cells stably expressing SPOP-WT or either endometrial cancer– or prostate cancer–specific SPOP mutants (shown in gray and blue, respectively; $n = 4$). VCL was used as a loading control. (**d**) *FOSL1* mRNA expression in data sets of individuals with endometrial[30] and prostate[31–33] cancer stratified according to *SPOP* mutation status. *P* values were derived from unpaired *t*-tests with Welch's correction. RPKM, reads per kilobase of transcript per million mapped reads. Red, SPOP mutants with a strong effect on degradation of BETs; gray, SPOP mutants with a less pronounced effect on degradation of BETs as compared to SPOP-WT. Midlines correspond to means. (**e**) Left, representative images of human primary endometrial cancer tissues ($n = 239$) stained for FOSL1; right, corresponding expression analysis on human primary tumors stratified by *SPOP* mutation status. *P* values were determined by Kendall's tau-b. Scale bars, 80 μm. (**f**) *FOSL1* mRNA (left) and FOSL1 protein (right) expression levels after JQ1 (500 nM) treatment in Ishikawa cells stably expressing SPOP-WT or SPOP mutants specific to endometrial cancer (E47K, E50K) or prostate cancer (Y87C, W131G) ($n = 3$). (**g**) Left, JQ1 dose-response curves for Ishikawa cells expressing SPOP-Y87C upon *FOSL1* knockdown ($n = 3$). *P* values are indicated below the dose-response curves, as calculated by extra sum-of-squares *F* test. Right, corresponding western blot validation of *FOSL1* knockdown. In **f** and **g**, ACTB was used as a loading control. In each legend, *n* indicates the number of independent experiments performed. In **c**, **f** and **g**, data are represented as mean ± s.e.m. Statistical significance was determined by unpaired, two-tailed Student's *t*-test unless otherwise specified. $*P < 0.05$, $**P < 0.01$, $***P < 0.001$.

particularly susceptible to further suppression of BET protein function. In support of this view, a functional overlap among BET proteins has been reported[22].

BET inhibitors are under clinical investigation as anticancer therapeutics, including for solid tumors[18,21,23,24]. We anticipated that the susceptibility of cancer cells to these inhibitors might be influenced by differences in BET protein levels corresponding to SPOP mutants. Indeed, forced expression of endometrial cancer–specific SPOP mutants (shown to lower BET protein levels) sensitized Ishikawa cells to both BET inhibitors, JQ1 and OTX015, by promoting apoptosis and reduc- ing cellular proliferation (**Fig. 4a** and **Supplementary Fig. 7b–e**)[25,26]. Similar results were found in HEC-151 and RL95-2 endometrial can- cer cells (**Supplementary Fig. 7f**). We aimed to discover whether changes in BET protein levels contribute to sensitivity to JQ1. To this end, we found that reduced levels of individual BET proteins in response to expression of SPOP mutants in Ishikawa cells cor- related with a decrease in the half-maximal inhibitory concentration (IC_{50}) during JQ1 treatment (**Fig. 4b**). Functionally, overexpression of the BRD2, BRD3 and BRD4 degron variants reduced SPOP-E50K-mediated sensitization to JQ1 (**Fig. 4c** and **Supplementary Fig. 7g**). We then investigated whether increased BET protein levels in the context of prostate cancer might, on the contrary, induce resistance to BET inhibitors. Overexpression of prostate cancer–specific SPOP mutants in comparison to SPOP-WT rendered Ishikawa and 22Rv1 cells more resistant to JQ1 (**Fig. 4a** and **Supplementary Fig. 7h,i**), whereas individual (**Fig. 4d** and **Supplementary Fig. 7j,l**) or com- bined (**Supplementary Fig. 7k**) knockdown of BET proteins in the context of mutated SPOP-Y87C dampened this phenotype.

Next, we sought to determine whether recurrent *SPOP* mutations or decreased BET protein levels in general might predict sensitivity to pharmacologic BET inhibition across cell line models of human endometrial cancer. For this purpose, we assessed JQ1 sensitivity in 3D semisolid culture conditions across 12 different human cell lines, for which we determined BET protein levels in parallel. Decreased expression levels of BRD2, BRD3 and BRD4 were associated with sensitivity to JQ1 in many cases (**Supplementary Fig. 8a–c**); however,

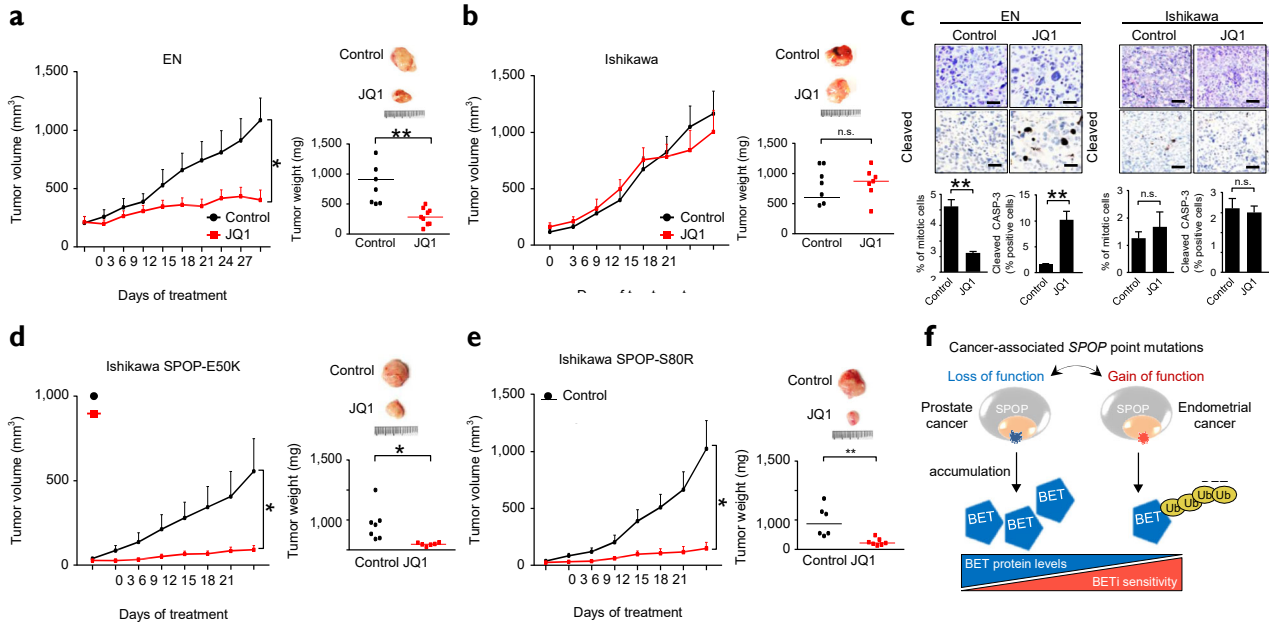

Figure 6 Endometrial cancer–associated SPOP mutants sensitize cells to JQ1 treatment *in vivo*. (**a**) Tumor growth kinetics (left) and individual tumor weight (right) with (n = 9) or without (control; n = 7) JQ1 treatment in xenografts established from EN cells. (**b**) Tumor growth kinetics (left) and individual tumor weight (right) with (n = 7) or without (control; n = 7) JQ1 treatment in xenografts established from Ishikawa cells. (**c**) Representative histology (n = 7) (top) and quantification (bottom) of mitotic and apoptotic cells in EN and Ishikawa xenografts treated with vehicle (control) or JQ1. Scale bar, 50 μm. (**d**) Tumor growth kinetics (left) and individual tumor weight (right) with (n = 7) or without (n = 6) JQ1 treatment in xenografts established from Ishikawa cells stably overexpressing SPOP-E50K. (**e**) Tumor growth kinetics (left) and individual tumor weight (right) with (n = 6) or without (n = 7) JQ1 treatment in xenografts established from Ishikawa cells stably overexpressing SPOP-S80R. (**f**) Model showing the differential effects of cancer-specific *SPOP* mutations on both BET protein levels and sensitivity to BET inhibitors (BETi). Representative images of the indicated number of tumors (n) for each xenograft group are shown in **a**, **b**, **d** and **e**. Data in **a**, **b**, **d** and **e** shown as mean tumor volume + s.e.m.; midlines represent means. Statistical significance was determined by unpaired, two-tailed Student's t-test. $^*P < 0.05$, $^{**}P < 0.01$, $^{***}P < 0.001$.

we also found some notable exceptions to this rule, in agreement with the existence of other molecular mechanisms that regulate suscep- tibility to BET inhibitors[27,28]. Nevertheless, EN cells expressing the SPOP-R121Q mutant were sensitive to JQ1 inhibition, in line with our data generated in isogenic cell lines (**Fig. 4a,e** and **Supplementary Figs. 7f** and **8b**). This finding led us to search for additional cell lines with recurrent endometrial cancer–associated *SPOP* mutations at the endogenous locus. We identified colorectal (NCI-H508) and urothelial (VM-CUB1) cancer cell lines in the Catalogue of Somatic Mutations in Cancer (COSMIC) Cell Lines Project that harbored *SPOP* mutations encoding p.E47K and p.E50K, respectively. Both cell lines were partic- ularly sensitive to JQ1 and displayed low BET protein levels that were responsive to proteasomal inhibition (**Fig. 4e** and **Supplementary Fig. 8d**). Thus, endometrial cancer–associated *SPOP* mutations may be more broadly associated with sensitivity to BET inhibitors.

Moreover, we tested whether established SPOP substrates might either directly or indirectly influence responses to JQ1 through changes in BET protein levels. Neither knockdown nor overexpression of DEK, TRIM24, NCOA3 or ERG led to substantial changes in BET protein levels or the JQ1 response, further supporting the notion that SPOP mutants affect sensitivity to JQ1 directly through regulation of BET protein degradation (**Supplementary Fig. 9**).

Transcriptome analysis identifies *FOSL1* as a determinant of JQ1 response

BET inhibitors bind to the bromodomains of BET proteins to displace them from the acetylated histone tails of transcriptionally active sites. Considering this function, we investigated transcriptional changes in response to overexpression of SPOP-WT or two recurrent endometrial cancer– and prostate cancer–associated SPOP mutants in Ishikawa cells (**Supplementary Table 2**). Unsupervised clustering and mul- tidimensional scaling (MDS) analyses of gene expression revealed mainly opposing transcriptional changes in response to expression of the endometrial cancer– and prostate cancer–associated SPOP mutants, with SPOP-WT positioned in between the different types of SPOP mutants (**Supplementary Fig. 10a,b**). This result aligns well with the different BET protein levels observed across the cell lines (**Supplementary Fig. 3f**). Interestingly, the MDS analysis revealed a second feature that discriminated both types of mutants from SPOP- WT, possibly reflecting shared dysregulation of SPOP substrates such as TRIM24 or NCOA3 (**Fig. 1c** and **Supplementary Fig. 10b**)[8].

Next, we interrogated transcriptional changes under JQ1 treat- ment in cells overexpressing endometrial cancer– versus prostate cancer–associated SPOP mutants and found a significant overlap between the differentially expressed genes and those with altered expression in the untreated conditions (**Fig. 5a,b** and **Supplementary Fig. 10a–c**). We identified 16 genes with altered expression across all conditions (untreated, 500 nM or 2 μM JQ1), including *FOSL1*, a reported target gene for BET proteins implicated in sensitivity to BET inhibitors[29]. *FOSL1* mRNA and FOSLI protein levels were reduced in cells that overexpressed endometrial cancer–specific, as compared to prostate cancer–specific, SPOP mutants, in accordance with the observed changes in BET protein levels and the transcriptome analy- sis (**Fig. 5c**). Notably, in human tumor tissues, *FOSL1* mRNA and FOSLI protein levels were also decreased in individuals with endome- trial cancer harboring mutated *SPOP*, with the lowest mRNA levels

observed in individuals who harbored the SPOP mutants shown to have the strongest effects on BET protein levels and sensitivity to JQ1 in our study (**Fig. 5d,e** and **Supplementary Fig. 7c**)[30–33].

Next, we investigated whether changes in BET protein levels in response to SPOP mutants and JQ1 treatment might decrease *FOSL1* transcription, as triple occupancy of BRD2, BRD3 and BRD4 has been reported at the *FOSL1* promoter (**Supplementary Fig. 10d**)[24]. JQ1 treatment reduced FOSL1 expression levels in all conditions, whereas the relative expression levels remained the same between the differ- ent types of SPOP mutants (**Fig. 5f**). Knockdown of individual BET proteins decreased *FOSL1* mRNA levels in JQ1-resistant Ishikawa cells overexpressing the prostate cancer–specific SPOP-Y87C variant (**Fig. 4a** and **Supplementary Fig. 10e**). Moreover, *FOSL1* depletion itself directly lowered resistance to JQ1 in this setting, indicating func- tional involvement of this gene downstream of changes in BET pro- tein levels and SPOP mutants (**Fig. 5g**). Taken together, these results suggest that BET protein level changes in response to SPOP mutants alter susceptibility to JQ1, at least in part, through transcriptional regulation of *FOSL1*.

JQ1 treatment blocks tumor growth in xenografts expressing endometrial cancer-specific SPOP mutants *in vivo*

Finally, we investigated whether our results showing altered sensitivity to JQ1 in response to SPOP mutants could be validated in an *in vivo* setting. For this purpose, we focused on expression of endometrial cancer–associated SPOP mutants because patients receiving a ben- eficial response from BET inhibitors may be identified in this setting. Indeed, JQ1 efficiently blocked the growth of tumor xenograft models established from *SPOP*-mutant EN cells by reducing cell proliferation and inducing apoptosis, whereas Ishikawa-cell-derived tumors were largely resistant to JQ1 treatment (**Fig. 6a–c**). In accordance with the *in vitro* data, forced expression of SPOP-E50K or SPOP-S80R sensi- tized Ishikawa cells to JQ1 *in vivo* (**Fig. 6d,e**).

DISCUSSION

Recurrent missense mutations in *SPOP*—encoding a substrate recep- tor of a cullin–RING ubiquitin ligase—have been found in 5–10% of prostate and endometrial cancers in comprehensive genome sequenc- ing studies[2–6]. Surprisingly, the specific genetic alterations show no overlap between these tumor types, even though they are confined to the same substrate-recognition domain. Although the prostate cancer– associated mutations have been shown more recently to stabilize pro- tein substrates relevant to prostate tumorigenesis[8–12], the therapeutic implications of both mutation types remain largely elusive.

Our study identifies the BET proteins (BRD2, BRD3 and BRD4) as bona fide SPOP substrates. Small-molecule inhibitors against this group of proteins are under clinical investigation in hematological and solid tumors because of the critical importance of these proteins in driving lineage-specific oncogenic transcriptional programs[18,21,23,24]. We found that prostate cancer–associated *SPOP* mutations impair degradation of BET proteins, in line with the loss-of-function proper- ties of these mutations reported previously[8,9], whereas endometrial cancer–associated *SPOP* mutations enhance BET protein degrada- tion through a gain-of-function mechanism (**Fig. 6f**). The precise structural basis through which endometrial cancer–associated *SPOP* mutations enhance binding and ubiquitination of BET proteins and other substrates (for example, DEK) remains to be further elucidated. The altered BET protein levels in the *SPOP*-mutant setting influence the transcription of established target genes, such as *FOSL1* (ref. 29), and thereby alter the susceptibility of cancer cells to BET inhibitors.

Of note in this regard, a recent report implicates enhanced FOSL1 activity as a mechanism of acquired resistance in ovarian cancer cells aswell[34]. Overall, our established model extends the list of previously reported mechanisms that influence BET inhibitor sensitivity[27,35,36].

BET inhibitors are currently under clinical development, and there is a critical need to identify patients who may respond to this treat- ment. Our preclinical study identifies *SPOP* mutations as a clinically detectable biomarker of BET inhibitor response. Thus, the detec- tion of specific *SPOP* mutations may be used to select patients who may (endometrial cancer–associated *SPOP* mutations) or may not (prostate cancer–associated *SPOP* mutations) benefit from treatment with BET inhibitors.

More broadly, our results suggest a paradigm whereby mutations mapping to the same domain of a particular protein evoke opposing drug responses. Given the increasing use of cancer genome informa- tion in the clinical setting, caution may be needed when extrapolating therapeutic responses on the basis of similar mutations.

METHODS

Methods, including statements of data availability and any associated accession codes and references, are available in the online version of the paper.

Note: Any Supplementary Information and Source Data files are available in the online version of the paper.

ACKNoWLEDGMENTS

We thank M. Losa, M. Storz, P. Schraml, S. Dettwiler and F. Prutek for help with tissue handling and histology assistance. We thank Q. Zhong for his help with the next-generation sequencing bioinformatics pipeline. We thank all members of the IRB animal core facility for technical assistance and the animal work.

We thank E. Samartzis and K. Dedes (University Hospital Zurich) for providing AN3CA, HEC1A, HEC1B, HEC116, SNG-II, EFE184 and KLE cell lines.

We thank the Oregon Health & Science University (OHSU) and the Cooperative Human Tissue Network (CHTN) for the tissue repository. We also thank all members of the laboratory for scientific discussions. J.-P.P.T. is funded by a Swiss National Science Foundation Professorship (PP00P3_150645) grant, a Swiss Cancer League (KSL-3654-02-2015) grant, a grant by the Jubiläumsstiftung Swiss Life AG and a grant by the Vontobel Stiftung. The Swiss National Science Foundation (310030B_160312/1), the European Research Council (268930), SystemsX IPhD (2013/128), Krebsforschungs Schweiz (KFS-3498-08-2014) and a GRL grant from the Korean government fund M.P. This work was also funded in part by a grant to P.J.W. provided by Oncosuisse (KLS-3384-02-2014-R) and the Foundation for Research in Science and the Humanities at the University of Zurich (SWF).

AUTHoR CoNTRIBUTIoNS

J.-P.P.T. originally developed the concept, further elaborated on it and designed the experiments together with H.J., G.E.T. and N.D.U. H.J., G.E.T., A.R., J.-P.P.T., N.D.U., T.S., S.N., A.U. and R.I.E. performed experiments and analyzed the data. H.J., G.C., G.E.T. and T.B. performed tumor xenograft experiments in immune-deficient mice. M.L., H.J. and J.-P.P.T. performed immunohistochemical experiments and analysis. P.J.W., P.S., H.M. and E.B. provided endometrial and prostate cancer samples with annotation for *SPOP* mutation status. D.G.M., M.E.C., A.B., B.J.N.W. and R.R.B. provided SPOP-mutant endometrial cancer samples. C.M.B., G.V.K., A.R. and L.C. analyzed genomic and RNA-seq data. J.-P.P.T., L.A.G., S.A.C., M.P., C.V.C., F.B. and P.J.W. provided funding and resources. J.-P.P.T., H.J. and G.E.T. interpreted the data and wrote the paper. H.J. and G.E.T. contributed equally to this work.

CoMPETING FINANCIAL INTERESTS

The authors declare competing financial interests: details are available in the online version of the paper.

1. Roychowdhury, S. & Chinnaiyan, A.M. Translating genomics for precision cancer medicine. *Annu. Rev. Genomics Hum. Genet.* **15**, 395–415 (2014).

2. Barbieri, C.E. *et al*. Exome sequencing identifies recurrent *SPOP*, *FOXA1* and
3. *MED12* mutations in prostate cancer. *Nat. Genet*. **44**, 685–689 (2012). Blattner, M. *et al*. *SPOP* mutations in prostate cancer across demographically diverse patient
4. cohorts. *Neoplasia* **16**, 14–20 (2014).

Le Gallo, M. *et al*. Exome sequencing of serous endometrial tumors identifies
5. recurrent somatic mutations in chromatin-remodeling and ubiquitin ligase complex genes. *Nat. Genet*. **44**, 1310–1315 (2012).

6. Jones, S. *et al*. Genomic analyses of gynaecologic carcinosarcomas reveal frequent mutations in chromatin remodelling genes. *Nat. Commun*. **5**, 5006 (2014).
7. Kandoth, C. *et al*. Integrated genomic characterization of endometrial carcinoma.
8. *Nature* **497**, 67–73 (2013).
9. Zhuang, M. *et al*. Structures of SPOP–substrate complexes: insights into molecular architectures of BTB–Cul3 ubiquitin ligases. *Mol. Cell* **36**, 39–50 (2009).
Sci. USA **110**, 6997–7002 (2013).
10. Gan, W. *et al*. SPOP promotes ubiquitination and degradation of the ERG oncoprotein to suppress prostate cancer progression. *Mol. Cell* **59**, 917–930 (2015).
11. An, J. *et al*. Truncated ERG oncoproteins from TMPRSS2-ERG fusions are resistant to SPOP-mediated proteasome degradation. *Mol. Cell* **59**, 904–916 (2015).
12. Geng, C. *et al*. Androgen receptor is the key transcriptional mediator of the tumor suppressor SPOP in prostate cancer. *Cancer Res.* **74**, 5631–5643 (2014).
13. Nishida, M., Kasahara, K., Kaneko, M., Iwasaki, H. & Hayashi, K. Establishment of a new human endometrial adenocarcinoma cell line, Ishikawa cells, containing estrogen and progesterone receptors. *Nihon Sanka Fujinka Gakkai Zasshi* **37**, 1103–1111 (1985).
14. Udeshi, N.D., Mertins, P., Svinkina, T. & Carr, S.A. Large-scale identification of ubiquitination sites by mass spectrometry. *Nat. Protoc.* **8**, 1950–1960 (2013).
15. Tsai, W.W. *et al*. TRIM24 links a non-canonical histone signature to breast cancer. *Nature* **468**, 927–932 (2010).
16. Salmans, M.L., Zhao, F. & Andersen, B. The estrogen-regulated anterior gradient 2 (AGR2) protein in breast cancer: a potential drug target and biomarker. *Breast Cancer Res.* **15**, 204 (2013).
17. Groner, A.C. *et al*. TRIM24 is an oncogenic transcriptional activator in prostate cancer. *Cancer Cell* **29**, 846–858 (2016).
18. Jung, M., Gelato, K.A., Fernández-Montalván, A., Siegel, S. & Haendler, B. Targeting
19. Blattner, M. *et al*. *SPOP* mutation drives prostate tumorigenesis *in vivo* through coordinate regulation of PI3K/mTOR and AR signaling. *Cancer Cell* **31**, 436–451 (2017).
20. Kwon, J.E. *et al*. BTB domain–containing speckle-type POZ protein (SPOP) serves as an adaptor of Daxx for ubiquitination by Cul3-based ubiquitin ligase. *J. Biol. Chem.* **281**, 12664–12672 (2006).
21. Shi, J. & Vakoc, C.R. The mechanisms behind the therapeutic activity of BET bromodomain inhibition. *Mol. Cell* **54**, 728–736 (2014).
22. Stonestrom, A.J. *et al*. Functions of BET proteins in erythroid gene expression. *Blood* **125**, 2825–2834 (2015).
23. Wang, C.Y. & Filippakopoulos, P. Beating the odds: BETs in disease. *Trends Biochem. Sci.* **40**, 468–479 (2015).
24. Asangani, I.A. *et al*. Therapeutic targeting of BET bromodomain proteins in castration-resistant prostate cancer. *Nature* **510**, 278–282 (2014).
25. Filippakopoulos, P. *et al*. Selective inhibition of BET bromodomains. *Nature* **468**, 1067–1073 (2010).
26. Boi, M. *et al*. The BET bromodomain inhibitor OTX015 affects pathogenetic pathways in preclinical B-cell tumor models and synergizes with targeted drugs. *Clin. Cancer Res.* **21**, 1628–1638 (2015).
27. Shu, S. *et al*. Response and resistance to BET bromodomain inhibitors in triple-negative breast cancer. *Nature* **529**, 413–417 (2016).
28. Sahai, V., Redig, A.J., Collier, K.A., Eckerdt, F.D. & Munshi, H.G. Targeting BET bromodomain proteins in solid tumors. *Oncotarget* **7**, 53997–54009 (2016).
29. Lockwood, W.W., Zejnullahu, K., Bradner, J.E. & Varmus, H. Sensitivity of human lung adenocarcinoma cell lines to targeted inhibition of BET epigenetic signaling proteins. *Proc. Natl. Acad. Sci. USA* **109**, 19408–19413 (2012).
30. Gibson, W.J. *et al*. The genomic landscape and evolution of endometrial carcinoma progression and abdominopelvic metastasis. *Nat. Genet*. **48**, 848–855 (2016).
31. Cancer Genome Atlas Research Network. The molecular taxonomy of primary prostate cancer. *Cell* **163**, 1011–1025 (2015).
32. Kumar, A. *et al*. Substantial interindividual and limited intraindividual genomic diversity among tumors from men with metastatic prostate cancer. *Nat. Med*. **22**, 369–378 (2016).
33. Robinson, D. *et al*. Integrative clinical genomics of advanced prostate cancer. *Cell* **161**, 1215–1228 (2015).
34. Kurimchak, A.M. *et al*. Resistance to BET bromodomain inhibitors is mediated by kinome reprogramming in ovarian cancer. *Cell Rep.* **16**, 1273–1286 (2016).
35. Marcotte, R. *et al*. Functional genomic landscape of human breast cancer drivers, vulnerabilities, and resistance. *Cell* **164**, 293–309 (2016).
36. Shi, X. *et al*. Loss of TRIM33 causes resistance to BET bromodomain inhibitors through MYC- and TGF-β-dependent mechanisms. *Proc. Natl. Acad. Sci. USA* **113**,

ONLINE METHODS

SILAC labeling and cell culture. For SILAC experiments, human Ishikawa endometrial cancer cells were cultured in DMEM/F12 medium defi- cient in l-arginine and l-lysine and supplemented with 10% dialyzed FBS (Sigma-Aldrich), penicillin, streptomycin and l-glutamine (Invitrogen), and l-arginine (Arg-0) and l-lysine (Lys-0), l-arginine [$^{13}C_6$]HCl (Arg-6) and **1**-lysine-4,4,5,5-d_4 (Lys-4), or [$^{13}C_6$,$^{15}N_4$]HCl (Arg-10) and **1**-lysine [$^{13}C_6$,$^{15}N_2$]HCl (Lys-8) (Sigma-Aldrich) for 14 d (10 doublings). All media were supplemented with l-proline to prevent the conversion of arginine to proline[37]. Specifically, isogenic cell lines expressing vector control (C), wild- type SPOP (SPOP-WT) or mutants (MTs) were isotopically labeled with SILAC media and grouped into four experiments (**Supplementary Fig. 1d**). Each experiment included a cell line with overexpression of SPOP-WT for cell line comparison within and across experiments. The labeling for this cell line was switched to rule out labeling artifacts in the first three experiments. Approximately 100 million cells per condition were washed twice with PBS, harvested and snap frozen.

K-ε-GG profiling and proteome analysis by liquid chromatography mass spectrometry. Preparation of proteins for mass spectrometry analysis was com- pleted as previously described[14]. Briefly, cell pellets were lysed in an ice-cold urea lysis buffer containing 8 M urea; 50 mM Tris-HCl, pH 8; 150 mM NaCl; 1 mM EDTA; 2 μg/ml aprotinin (Sigma-Aldrich); 10 mg/ml leupeptin (Roche Applied Science); 1 mM phenylmethylsulfonyl fluoride (PMSF); 50 μM PR-619; and 1 mM chloroacetamide. The lysate was cleared by centrifugation at 20,000*g* for 10 min. A bicinchoninic acid (BCA) protein assay (Thermo Fisher Scientific) was used to determine the protein concentration of each sample. Respective SILAC mixes were created by combining equal amount of protein per SILAC state. Proteins were reduced with 5 mM dithiothreitol (DTT) at room tempera- ture (RT) and subsequently alkylated with 10 mM iodoacetamide at RT in the dark. Lysates were diluted 1:4 with 50 mM Tris-HCl, pH 8, and proteins were digested with sequencing-grade trypsin using an enzyme-to-substrate ratio of 1:50, overnight at 25 °C. Digestion reactions were quenched with trifluoroacetic acid (TFA), and the peptide solutions were cleared by centrifugation before desalting. Peptides were desalted using tC18 SepPak SPE cartridges (Waters) exactly as previously described[14]. Peptides were fractionated offline by basic pH reverse-phase (bRP) chro- matography, as previously described[14,38]. Input for each bRP separation was equivalent to 30 mg of starting protein material (10 mg protein per SILAC state) for replicate. Briefly, dried peptides were reconstituted in bRP buffer A (5 mM ammonium formate (pH 10.0)/2% acetonitrile). A Zorbax 300 Extend-C18 col- umn (9.4 × 250 mm, 300 Å, 5 μm; Agilent) was used for separation. Using the gradient and flow-rate settings previously described[14], a total of 96 2-ml fractions were collected across the entirety of the bRP separation. For proteome analysis, 5% of each fraction was taken and combined in a noncontiguous manner such that every 24th fraction was combined to create 24 final fractions. For K-ε-GG analysis, the remainder of each fraction was combined in a noncontiguous man- ner such that every eighth fraction was combined to create eight final fractions. Pooled fractions were dried completely using vacuum centrifugation. For enrichment of K-ε-GG peptides, anti-K-ε-GG antibody from the PTMScan Ubiquitin Remnant Motif (K-ε-GG) kit was used (Cell Signaling Technology, cat. no. 5562). Prior to enrichment, the antibody was cross-linked to protein A beads using dimethyl pimelimidate (DMP)[14]. Peptides were recon- stituted in immunoaffinity purification (IAP) buffer, and enrichment was com- pleted exactly as previously described[14]. Briefly, peptides were incubated with approximately 31 μg of anti-K-ε-GG antibody beads and incubated for 1 h at 4 °C with rotation. Beads were washed twice with 1.5 ml of ice-cold IAP buffer followed by three washes with ice-cold PBS. K-ε-GG peptides were eluted from the antibody with 2 × 50 μl of 0.15% trifluoroacetic acid (TFA). Peptides were desalted using StageTips. StageTips were conditioned by washing with 50 μl of 50% acetonitrile (MeCN) /0.1% formic acid (FA) followed by 2 × 50 μl of 0.1% FA. Peptides were then loaded on StageTips, washed twice with 50 μl of 0.1% FA and eluted with 50 μl of 50% MeCN/0.1% FA. Eluted peptides were dried completely using vacuum centrifugation. Samples were reconstituted in 3% MeCN/0.1% FA. All samples were analyzed by nanoflow-ultra-performance liquid chromatography (UPLC)–higher-energy collisional dissociation (HCD)–MS/MS using a Q Exactive mass spectrometer (Thermo Fisher Scientific) coupled online to an Easy-nLC 1000 system (Proxeon). For K-ε-GG and proteome samples, 4/8 μl and 1/20 μl, respectively, were injected into the mass spectrometer. Samples were injected at a flow rate of 500 nl/min onto a PicoFrit column (360 μm (OD) × 75 μm (ID), 10-μm ID tip, 50-cm length (New Objective) self-packed with 24 cm of ReproSil-Pur 120-Å, 1.9-μm C18-AQ beads). The nanoflow column was heated to 50 °C using a column heater (Pheonix S&T). For liquid chromatography mass spectrometry (LC–MS/MS) analyses, the gradient and flow-rate settings were used as previously described[14] and the MS acquisition time used for each K-ε-GG and proteome sample was 120 min. The Q Exactive was operated by acquiring an MS1 scan (R = 70,000) followed by MS/MS scans (R = 17,500) on the 12 most abundant ions. An MS1 and MS2 ion target of 3×10^6 and 5×10^4 ions, respectively, was used for acquisition. A maximum ion time of 10 ms and 120 ms was used for the MS1 and MS2 scans, respectively. The isolation width was set to 2.5 m/z, the HCD collision energy was set to 25, the dynamic exclusion time was set to 20 s, and the peptide-match and isotope-exclusion functions were enabled. A second round of bRP fractionation, K-ε-GG and MS analysis was completed for experiments 3 and 4 (6 mg per SILAC state for experiment 3 and 10 mg per SILAC state for experiment 4).

Mass spectrometry data analysis. Data were processed using the MaxQuant (version 1.2.2.5) software package. The human UniProt database including 248 common laboratory contaminants was used for searching. The enzyme specifi- city was set to trypsin, the maximum number of missed cleavages was set to 2 for proteome data and 4 for K-ε-GG data, the precursor mass tolerance was set to 20 ppm for the first search, and the tolerance was set to 6 ppm for the main search. Carbamidomethylation of cysteines was searched as a fixed modifica- tion, and oxidation of methionines and N-terminal acetylation of proteins were searched as variable modifications.

For K-ε-GG data, addition of glycine-glycine to lysine was also searched as a variable modification. For identification, the minimum peptide length was set to 7, and the false discovery rate for peptide, protein and side identification was set to 1%. The filter-labeled amino acid and peptide quantification functions were enabled. For proteome data, normalized ratios were obtained from the "proteinGroups" table. For K-ε-GG data, normalized SILAC ratios were obtained from the "GlyGly(K)Sites" table. For K-ε-GG and proteome data sets, reverse and contaminant hits were removed from the analysis. Proteins were included in the data set if they were identified and quantified by two or more razor peptides per unique peptide in each SILAC triple-labeled experiment. K-ε-GG peptides were included in the final data set if the corresponding protein was quantified in the proteome data. To capture the ubiquitination changes associated with protein degradation, we normalized the K-ε-GG changes to their measured protein levels. The leading accession number was used to match the protein and K-ε-GG data. Quantitative, protein-normalized measurements were available for 17,239 K-ε-GG peptides. To assess and highlight which of the significantly deregulated K-ε-GG pep- tides were paralleled with opposing effects on total protein expression in the case of SPOP-MT versus SPOP-WT, protein-normalized SILAC ratios for K-ε-GG were multiplied by their corresponding protein-level ratio and also by −1 (**Supplementary Fig. 2** and **Supplementary Table 1**).

Cell culture, transfection and infection. Ishikawa cells were purchased from Sigma; RL95-2, 22Rv1, MEF-962, VM-CUB1 and NCI-H508 cells were purchased from ATCC; EN cells were purchased from DSMZ; and HEC-151 cells were purchased from JCRB. AN3CA, HEC1A, HEC 1B, HEC116, SNG-II, EFE184 and KLE cells were kindly provided by E. Samartzis and K. Dedes (University Hospital Zurich). Ishikawa, RL95-2 and KLE cells were grown in F12/DMEM (Gibco); MEF-962, HEC-151, EN, HEC1A, HEC1B, AN3CA, HEC116 and SNG-II cells were grown in DMEM (Gibco); and 22Rv1 and EFE184 cells were grown in RPMI medium (Gibco); all were supplemented with 10% FBS (Gibco), 1% penicillin-streptomycin and l-glutamate. All cells were incubated at 37 °C and 5% CO_2. Cells were routinely tested for mycoplasma contamination.

For transient transfection, cells were transfected with 50 nM *siSPOP* (Hs_SPOP_7, Qiagen), 50 nM *siFOSL1* (Hs_FOSL1_1, Hs_FOSL1_2 and Hs_FOSL1_3, Qiagen) or *siControl* (Qiagen) using Fugene (Promega).

For stable knockdown experiments, cells were infected with pLKO-1 vectors (Sigma) and the following clones were used: *SPOP*: TRCN0000140431 (*shSPOP*); *BRD2*: TRCN00000315433 (*shBRD2_1*), TRCN0000350530 (*shBRD2_2*); *BRD3*: TRCN0000021376 (*shBRD3_1*), TRCN0000021377 (*shBRD3_2*); *BRD4*: TRCN0000021426 (*shBRD4_1*), TRCN0000021427 (*shBRD4_2*) and *shBET* (5μ-TCCAACTGCTATAAGTACAAT-3μ); *CUL-3*: TRCN0000073343 (*shCUL- 3_1*) and TRCN0000073344 (*shCUL-3_2*); *DEK*: TRCN0000013104 (*shDEK_1*) and TRCN0000013105 (*shDEK_2*); *TRIM24*: TRCN0000021259 (*shTRIM24_#*) and TRCN0000194983 (*shTRIM24_2*); *NCOA3*: TRCN0000370320 (*shNCOA3_1*) and TRCN0000365253 (*shNCOA3_2*). After infection, cells were selected in the presence of puromycin (2 μg/ml). For overexpression, a derivate of the pLX304 vector was used throughout, in which the CMV pro- moter had been exchanged with a PGK promoter and the blastocidin cassette exchanged with mOrange or a puromycin-resistance cassette (pLX_TRC_307, available at Addgene as plasmid 41392, pCW107). All open reading frames (ORFs) were cloned into pLX_TRC_307–mOrange using Nhe1 and Mlu1 (Thermo Fisher Scientific).

Dose-response curves and cell-growth assays. Cells were seeded (between 1×10^3 and 1×10^4 cells/well) in a 96-well plate. Cells were subsequently treated with serial dilutions of JQ1 or OTX-015 in media to determine dose-response curves or were left untreated for cell-growth assays. After 96 h of treatment in the case of dose-response curves and 6 d for cell-growth assays cells were washed with PBS and stained with 0.5% crystal violet solution in 25% methanol. Crystal violet was then solubilized with 10% acetic acid and absorbance (OD, 590 nm) was measured in a microplate reader.

Clonogenic assay in methylcellulose. Cells were seeded (between 5×10^3 and 1×10^4 cells) in methylcellulose (Methocult H4100, StemCell Technologies) in duplicate and treated with vehicle (0.1% DMSO) or drug (JQ1). Cells were incubated at 37 °C and 5% CO_2 for 7–14 d, colonies were stained with MTT solution at 37 °C overnight and absorbance (OD, 590 nm) was measured in a microplate reader.

Xenograft model. All animal experiments were carried out in female athymic nude mice (BALB/c nu/nu, aged 4–6 weeks) according to a protocol approved by the Swiss Veterinary Authority (no. TI-14-2014). 2×10^6 Ishikawa and EN cells each were resuspended in 200 μl of PBS and subcutaneously injected into both of the dorsal flanks of nude mice. Once tumors reached approximately 100 mm^3, mice were randomized and were intraperitoneally administrated either vehicle or JQ1 at 50 mg/kg bodyweight (twice per day) for the indicated duration. Tumor growth was recorded using digital calipers, and tumor volumes were calculated using the formula $(L \times W^2)/2$, where L is the length and W is the width of the tumor. At the end of the experiment, mice were euthanized and tumors were extracted, weighed and histologically analyzed by a board-certified pathologist (J.P.T.) by H&E staining and immunohistochemistry for cleaved caspase-3 (Cell Signaling protocol).

Antibodies, immunoblotting and immunoprecipitation. Antibodies used in immunoblotting and immunoprecipitation assays were as follows: anti- BRD2 (A302-583A, Bethyl Labs), anti-BRD3 (sc-81202, Santa Cruz), anti- BRD4 (sc-48772, Santa Cruz), anti-SPOP (ab81163, Abcam), anti-TRIM24 (sc-271266, Santa Cruz), anti-NCOA3 (2126, Cell Signaling), anti-DEK (610948, BD Bioscience), anti-ERG (sc-271048, Santa Cruz), anti-FOSL1 (5281, Cell Signaling), anti-VCL (4650, Cell Signaling), anti-μ-actin (4967, Cell Signaling), anti-HA (9658, Sigma) and anti-cleaved caspase-3 (Asp175) (9661, Cell Signaling). All antibodies were employed at dilutions suggested by the manufacturers.

For immunoblotting, cells were washed with PBS and subsequently lysed in RIPA buffer (Sigma) and sonicated. Protein concentration was determined using BCA reagent (Thermo Fisher); proteins were separated by SDS–PAGE (Bio-Rad) and transferred onto a polyvinyl difluoride (PVDF) membrane (Thermo Scientific). The membrane was incubated for 1 h in 5% nonfat dry milk/TBS-T blocking buffer followed by incubation with the primary antibody overnight at 4 °C. The membrane was washed with TBS-T, followed by incubation with horseradish peroxidase–conjugated secondary antibody (Promega).

To detect interactions of SPOP and HA-BRD3, cells were lysed in 1% NP-40 buffer (50 mM Tris-HCl, pH 7.4; 150 mM NaCl; 1% NP-40) with 2× protease inhibitor cocktail (Complete, Roche) and sonicated; 3 mg of lysate was incubated overnight with 2 μg of anti-HA-tag antibody (9658, Sigma) or control mouse IgG (sc-2025, Santa Cruz Biotechnology) at 4 °C. Subsequently, antibodies were collected using 25 μl of Protein A/G magnetic beads (88803, Fisher Scientific) for 2 h, followed by two washing steps with 1% NP-40 buffer. Proteins were eluted by addition of 1× SDS sample buffer under reducing conditions at 95 °C for 5 min. Quantitative analysis of the western blots was performed with protein levels normalized to VCL or ACTB expression. Uncropped immunoblots are presented in **Supplementary Figure 11**.

Chemicals. MG132 and cycloheximide (CHX) were purchased from Sigma and used at 10 μM and 100 μg/ml, respectively, in all experiments. (+)-JQ1 and OTX-015 were purchased from Selleckchem and used at the indicated concentrations.

***In vivo* ubiquitination assay.** 293T cells were transiently transfected with the indicated plasmids: pCW107-BRD3-WT or BRD3-degron-MT (2 μg), pCW107-SPOP-WT or SPOP-MT (2 μg), and CMV-8×His-Ub (2 μg). 42 h later, cells were treated with MG132 or DMSO for an additional 3 h. Cells were then washed with PBS and collected by centrifugation. A small amount of cells were lysed in RIPA buffer and the rest were lysed in Buffer C (6 M guanidine–HCl, 0.1 M Na_2HPO_4/NaH_2PO_4, 10 mM imidazole; pH 8). The WCE was sonicated and incubated with 60 μl of Ni-NTA agarose (Sigma) overnight at 4 °C. Next, Ni-NTA beads were washed once with Buffer C, twice with Buffer D (1 volume of Buffer C:3 volumes of Buffer E) and once with Buffer E (25 mM Tris-HCl, 20 mM imidazole; pH 6.8). Elution of bound proteins was processed through boiling in 1×SDS loading buffer contain- ing 300 mM imidazole. Samples were loaded, separated by SDS–PAGE and detected by immunoblotting.

***In vitro* ubiquitination and binding assays.** Wild-type and SPOP-binding- mutant (degron-MT) constructs of HA-tagged human BRD3 were purified from transiently transfected HEK-293T cells. Wild-type and mutant human SPOP species were cloned, expressed and purified as described previously, using a GST instead of an MBP affinity tag[7]. KLHL9, KLHL13, KLHL21 and Cdc34b were cloned, expressed and purified from *Escherichia coli* as described previously[39]. CUL3 and RBX1 were purified in a preassembled complex from insect cells and neddylated *in vitro* using purified components as described previously[40]. *In vitro* ubiquitination reactions with a total volume of 15 μl were assembled as follows: 10^7 HA-BRD3-expressing HEK-293T cells were harvested and lysed by sonica- tion in IP buffer (20 mM Tris-HCl, pH 7.4; 150 mM NaCl; 5% glycerol; 1 mM TCEP; 1× Roche protease inhibitor cocktail). Immunoprecipitates were prepared with 10 μl of anti-HA affinity gel (Sigma) and washed with IP buffer. For respec- tive samples, 2 μl of HA-BRD3 IP resin was used and supplemented with 0.3 μM SPOP, KLHL9, KLHL13 or KLHL21; 0.2 μM CUL3–Nedd8/RBX1; 0.7 μM Cdc34; 0.2 μM UbE1 (Boston Biochem); and 25 μM ubiquitin (Boston Biochem) in ubiquitination buffer (3 mM ATP, 10 mM $MgCl_2$, 50 mM Tris-HCl pH 7.6, and 0.5 mM DTT). Reactions were incubated at 37 °C for 45 min and stopped by addi- tion of SDS sample buffer. Samples were separated by SDS–PAGE and visualized through chemiluminescence using anti-HA (Sigma, A2095), HRP-coupled goat anti-mouse IgG (Bio-Rad, 170-6516), Clarity Western ECL Blotting Substrate (Bio-Rad, 1705061) and Fusion FX imaging platform (Vilber Lourmat).

For coimmunoprecipitation experiments *in vitro*, 1 μM recombinant SPOP-WT or SPOP mutants and 1 μl of HA-BRD3-WT IP resin were incubated in 200 μl of IP buffer (20 mM Tris-HCl pH 7.4, 150 mM NaCl, 5% glycerol) for 1 h at 4 °C. Thereafter, resin was washed twice in the same buffer and samples were separated by SDS–PAGE and visualized through chemiluminescence using anti-HA and anti-SPOP antibodies (see above).

qRT–PCR. RNA was extracted using the RNeasy kit (Qiagen) and processed by the Kapa SybrFAST One-Step qRT–PCR kit according to the manufacturer's instructions. qPCR was undertaken on an Applied Biosystems StepOnePlus System. Target mRNA expression was quantified using the comparative Ct method (ΔΔCt method) and normalized to cyclophilin expression. The following primers were used: *BRD2*, forward 5-CTACGTAAGAAACCCCGGAAG-3,

doi:10.1038/nm.4372

reverse 5-GCTTTTTCTCCAAAGCCAGTT-3; *BRD3*, forward 5-CCTCAGGG AGATGCTATCCA-3, reverse 5-ATGTCGTGGTAGTCGTGCAG-3; *BRD4*, forward 5-CTCCTCCTAAAAAGACGAAGA-3, reverse 5-GCCCCTTCTCTT TTTGACTTCGGA-3; *TRIM24*, forward 5-CAGCCACAAATGCCTAAGCAG-3, reverse 5-GTGTTGGGAACTTGGATAACTGG-3; *SPOP*, forward 5-GAAATGG TGTTTGCGAGTAAACC-3, reverse 5-GCCCGAACTTCACTCTTTGGA-3; *FOSL1*, forward 5-CTGCAGGCGGAGACTGACAA-3, reverse 5-TCCGGGATTTTGCAGATGGG-3; cyclophilin, (*PPIA*), forward 5-CAGG TCCTGGC ATCTTGTCC-3, reverse 5-TTGCTGGTCTTGCCATTCCT-3.

DNA and RNA sequencing of endometrial cell lines. Whole-exome sequencing was performed for all endometrial cancer cell lines profiled in the CCLE[41]. This data set was used to determine mutation status for SPOP cell lines included in this study. In addition, RNA sequencing was performed at the Broad Institute using the Illumina TruSeq protocol for 17 CCLE cell lines. Reads were aligned to the human reference genome build hg19 using TopHat version 1.4, and mRNA expression levels were determined using RNA-SeQC. Reads per kilobase of tran- script per million mapped reads (RPKM) values for each cell line were correlated with the median RPKM values of endometrial cancer tissues with recurrent *SPOP* point mutations identified in the TCGA portal[6]. A threshold of 10 RPKM was used to determine the overlay of robustly expressed genes in the cell lines with the genes expressed in human tumor tissues. For the analysis of transcriptional output changes in response to SPOP mutants, isogenic Ishikawa cells stably overexpressing either SPOP-WT or an SPOP mutant (endometrial, E50K, E47K; prostate, Y87C, W131G) were gen- erated. RNA-seq was performed on cells either untreated or treated with JQ1 (500 nM or 2 μM) for 4 h (**Supplementary Table 2**). Total RNA was extracted using the RNeasy kit (Qiagen), and sample quality was assessed using the Agilent Bioanalyzer. Library preparation (Illumina unstranded TruSeq Library includ- ing poly(A) enrichment) and RNA sequencing (Illumina NextSeq high output, v2,1 × 75 bp) was performed by Microsynth. Quality of sequencing was analyzed according to Phred score of Illumina and FastQC. Mapping to hg38 was done using STAR 2.52b. Genes with counts per million (c.p.m.) <0.5 mapped reads were considered not expressed and were filtered out. Subsequently, counts were normalized based on the number of reads acquired per sample, $\log_2$ transformed and subjected to the voom function of the limma package in Bioconductor. Signatures were derived by comparing samples in **Supplementary Table 2** and the following filters were used to define differentially expressed genes: c.p.m.> 45 in at least two samples; adjusted P value < 0.05 (according to the Benjamini–Hochberg test); IIogFCI > 0.9.

Human tumor samples. We used a previously characterized cohort of pri- mary prostate tumors with annotated *SPOP* mutations determined by high- resolution melt analysis assay that followed Sanger sequencing of exons 6 and 7 (ref. 3). Owing to tissue loss (a common problem encountered with tissue microarrays), only a subset of tumors was histologically analyzable. These tumors are a part of tissue microarrays composed of paraffin-embedded prostate tissue cores from two different institutes of pathology. As previously published, specimens were collected between 1993 and 2007 from the Institute of Surgical Pathology, University of Zurich, Switzerland, and the Institute of Pathology, University of Regensburg, Germany[42]. The local scientific ethics committees approved both cohorts (approval no. StV-Nr. 25/2007). Primary endometrial cancer tissues were retrieved from different sources. Tissue sections of 19 tumors identified from the literature with annotated recurrent *SPOP* mutations were collected as follows: TCGA-D1-A0ZO, TCGA-D1-A167, TCGA-D1-A168 and TCGA-D1-A17D from the Mayo Clinic[6]; TCGA-B5-A0JY, TCGA-B5-A0K0 and TCGA-NA-A5I1 from the Duke Cancer Center[6]; TCGA-BS-A0UT from the University of Hawaii Cancer Center[6]; TCGA-FI-A2EW from Washington University[6]; TCGA-N9-A4Q8 and TCGA-DI-A1NN from the MD Anderson Cancer Center[6]; 2001-02-G049T, 2005-08-G674T, MAD04-00646T, 1090095AT and 1090076AT from the Cooperative Human Tissue Network (CHTN)[4]; and 119, 127 and 136 from the Oregon Health & Science University (OHSU)[5]. We characterized an additional 84 primary endometrial cancer tis- sue samples by targeted DNA sequencing (36 endometrioid carcinomas, 26 serous carcinomas, 11 clear cell carcinomas and 11 carcinosarcomas) from two different cohorts from Basel and Zurich[43–45]. Therefore, two 0.6-mm-diameter tumor tissue cylinders were punched out of paraffin-embedded tissue blocks, and DNA was isolated using the Maxwell 16 FFPE Tissue LEV DNA Purification Kit (Promega) according to the manufacturer's instructions. DNA was quantified using the dsDNA HS Assay Kit with Qubit 2.0 (Thermo Fisher Scientific/Life Technologies), and 20 ng was used to prepare libraries using Ion AmpliSeq Library Kit 2.0 according to the manufacturer's instructions. A custom panel was applied for PCR-based amplification of the *SPOP* gene. Libraries were labeled with the Ion Xpress Barcode Adaptors 1-96 Kit (Thermo Fisher Scientific/Life Technologies) and quantified by qPCR with the Ion Library Quantitation Kit (Thermo Fisher Scientific/Life Technologies). Twenty to twenty-six libraries were multiplexed for template preparation and enrichment using the Ion PI Hi-Q OT2 200 Kit (Thermo Fisher Scientific/Life Technologies). Enriched samples were then loaded on an Ion PI Chip v3 (Thermo Fisher Scientific/Life Technologies) and sequenced on the Ion Proton System using the Ion PI Hi-Q Sequencing 200 Kit (Thermo Fisher Scientific/Life Technologies). Sequencing run quality metrics were taken from the Torrent Suite Software (Thermo Fisher Scientific/Life Technologies) for each run. Sequencing data were then analyzed with Ion Reporter Software (Thermo Fisher Scientific/Life Technologies). We identified another SPOP-D140Y-mutated serous cancer, while the remaining cases did not harbor any additional recurrent mutations nor any other type of mutation in *SPOP* at an allelic fraction higher than 0.2. The study was approved by the scientific ethics committee at the Institute of Surgical Pathology, University Hospital Zurich (approval no. KEK-ZH-NR: 2010-0358).

Immunohistochemistry. For the detection of BET and FOSL1 proteins, slides were first dehydrated. For antigen retrieval, slides were incubated in a water bath at 98 °C for 20 min using a citrate buffer at pH 6 (BETs) or pH 9 (FOSL1) (Diapath, T0050). For microarrays of prostate cancer tissue, the antigen retrieval for BRD2 and FOSL1 was extended to 40 min in total. Subsequently, slides were cooled to RT for 20 min and endogenous peroxidases were blocked for an additional 10 min with 3% H_2O_2 (VWR, 23615.248). After washing, slides were incubated for 10 min with a protein blocking solution (Dako, X0909). Then, slides were incu- bated with primary antibodies at the following concentrations for 1 h in antibody diluent reagent solution (Life Technologies, 003118): BRD2 (Abcam, ab13960; 1:500), BRD3 (Bethyl, A302-368A; 1:50), BRD4 (Abcam, ab128874; 1:400) and

FOSL1 (Sigma-Aldrich, AV31377; 1:2,000). For microarrays of prostate cancer tissue, the BRD2 antibody was used at a dilution of 1:200. Thereafter, slides were washed and incubated with biotinylated anti-rabbit IgG (Vector, BA-1000) in PBS for 30 min at RT and subsequently washed and incubated another 30 min with Vectastin ABC kit at a dilution of 1:150 in PBS. Detections were performed using the ImmPACT DAB system (Vector, SK-4105) for 4 min at RT followed by nuclear staining with Mayer hematoxylin (Diapath, C0303). Immunohistochemical staining was evaluated as follows for BET proteins: no detectable staining in more than 70% of tumor cell nuclei was referred to as negative, 30% or more tumor cell nuclei weakly stained (discernable nucleoli) as weak and more than 30% of nuclei strongly stained (invisible nucleoli) as strong.

Statistical analysis. GraphPad Prism version 7.00 (GraphPad Software) was used for analysis. Data are depicted as means ± s.e.m. unless otherwise speci- fied. An unpaired, two-tailed independent Student's t-test with unequal vari- ance assumption was performed to analyze cell culture experiments. Two-way ANOVA (Dunnett's post test) was used for multiple comparisons. Extra-sum-of- squares F-test was used to determine the statistical significance of dose-response curves. The Spearman correlation coefficient was used to compare RNA-seq expression data from *SPOP*-mutant human tumors and BET protein levels with endometrial cell line data. Kendall's tau-b was used to test correlation of immu- nohistochemical staining with *SPOP* mutation status.

Data availability. CCLE data are available online at http://www.broadin- stitute.org/ccle/home. The original mass spectrometry spectra have been deposited in the public proteomics repository MassIVE and are accessible at ftp://MSV000080401@massive.ucsd.edu when providing the data set password "ubiquitin." If requested, also provide the username "MSV000080401." Sequencing data have been deposited in the NCBI public database and are accessible under BioProject PRJNA357942.

37. Bendall, S.C. *et al*. Prevention of amino acid conversion in SILAC experiments with embryonic stem cells. *Mol. Cell. Proteomics* **7**, 1587–1597 (2008).
38. Mertins, P. *et al*. Integrated proteomic analysis of post-translational modifications by serial enrichment. *Nat. Methods* **10**, 634–637 (2013).
39. Enchev, R.I. *et al*. Structural basis for a reciprocal regulation between SCF and CSN. *Cell Rep*. **2**, 616–627 (2012).
40. Mosadeghi, R. *et al*. Structural and kinetic analysis of the COP9-signalosome activation and the cullin-RING ubiquitin ligase deneddylation cycle. *eLife* **5**, e12102 (2016).
41. Barretina, J. *et al*. The Cancer Cell Line Encyclopedia enables predictive modelling of anticancer drug sensitivity. *Nature* **483**, 603–607 (2012).
42. Mortezavi, A. *et al*. KPNA2 expression is an independent adverse predictor of biochemical recurrence after radical prostatectomy. *Clin. Cancer Res*. **17**, 1111–1121 (2011).
43. Lebeau, A. *et al*. Oestrogen receptor gene (*ESR1*) amplification is frequent in endometrial carcinoma and its precursor lesions. *J. Pathol*. **216**, 151–157 (2008).
44. Wild, P.J. *et al*. p53 suppresses type II endometrial carcinomas in mice and governs endometrial tumour aggressiveness in humans. *EMBO Mol. Med*. **4**, 808–824 (2012).
45. Dellas, A., Jundt, G., Sartorius, G., Schneider, M. & Moch, H. Combined PTEN and $p27^{kip1}$ protein expression patterns are associated with obesity and prognosis in endometrial carcinomas. *Clin. Cancer Res*. **15**, 2456–2462 (2009).

doi:10.1038/nm.4372

Supplementary Figure 1

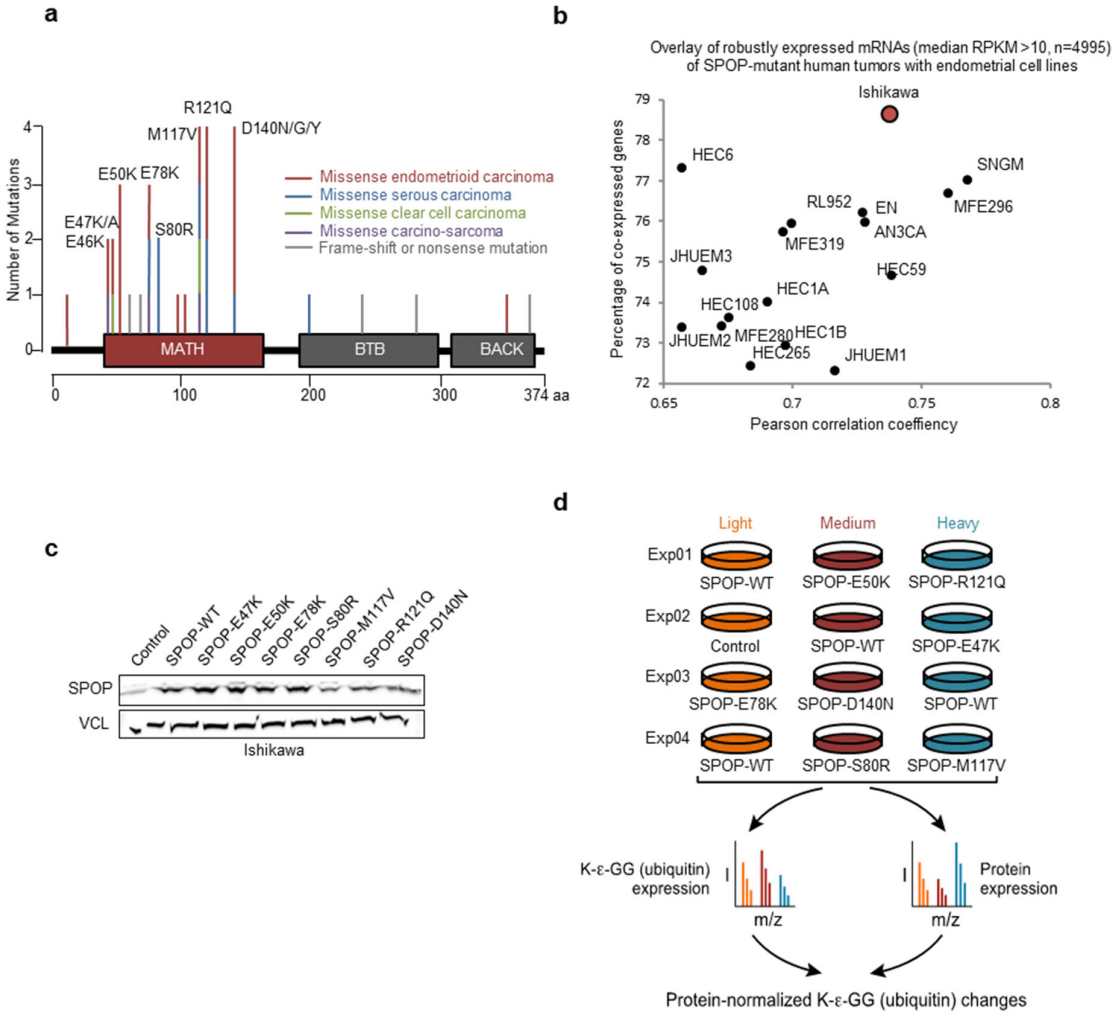

Supplementary Figure 1 Recurrent *SPOP* mutations in human endometrial cancer and schematic representation of proteomic approach. **(a)** Histogram of *SPOP* mutations as detected in three genomic studies of endometrial cancer and carcinosarcoma (mutation depicted with an allelic fraction of 0.1 or higher)[4-6]. **(b)** Overlay and correlation of robustly expressed mRNAs (genes with median RPKM > 10) in human endometrial cell lines with the median of pooled mRNAs expressed in *SPOP*-mutant endometrial cancer tissues (n=4995)[6]. **(c)** Western blot (WB) for indicated proteins of Ishikawa cells used for mass-spectrometry that express stably vector control, SPOP-WT, or seven different endometrial cancer SPOP mutants. (**d)** Schematic illustration showing the design of the proteomics experiments. Ishikawa isogenic cell line (c) were isotopically labeled and divided into four experiments, each of which contained a SPOP-WT cell line as a comparator within and across experiments. K-ε-GG ratios were normalized to protein level changes assessed in parallel.

Supplementary Figure 2

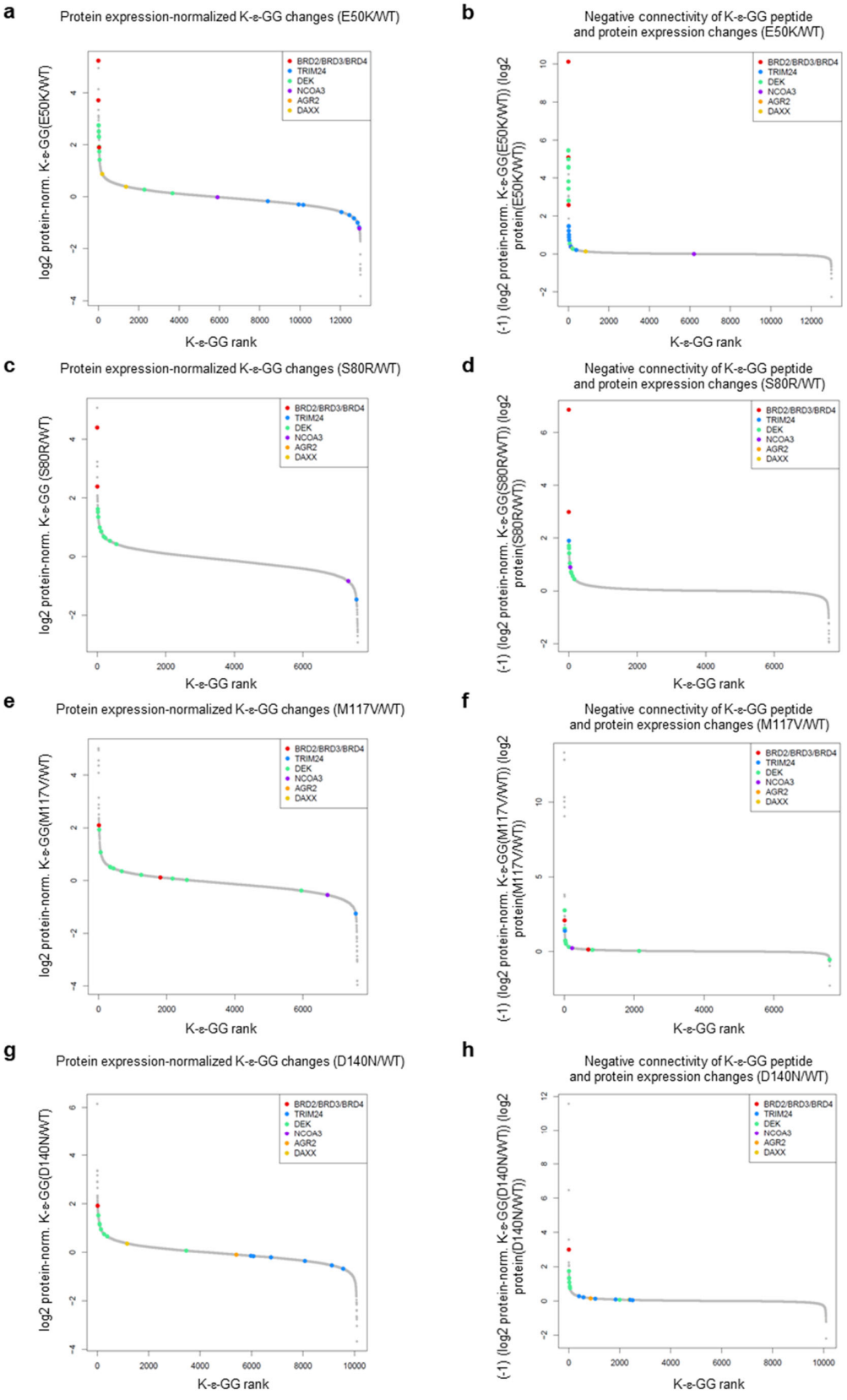

Supplementary Figure 2 Protein-normalized K-ε-GG changes of Ishikawa cells over-expressing wild-type SPOP compared to endometrial cancer SPOP mutants. **(a) (c) (e) (g)** Changes in the indicated peptides after overexpression of different representative SPOP mutants (E50K, S80R, M117V, D140N). (**b) (d) (f) (h)** Negative connectivity of K-ε-GG peptide and protein expression changes after overexpression of indicated SPOP mutants. To visualize K-ε-GG sites that undergo inverse changes at the protein level, normalized K-ε-GG data shown in panels a, c, e, g were inverted and multiplied by corresponding total protein expression changes of wild-type SPOP compared to endometrial cancer SPOP mutants.

Supplementary Figure 3

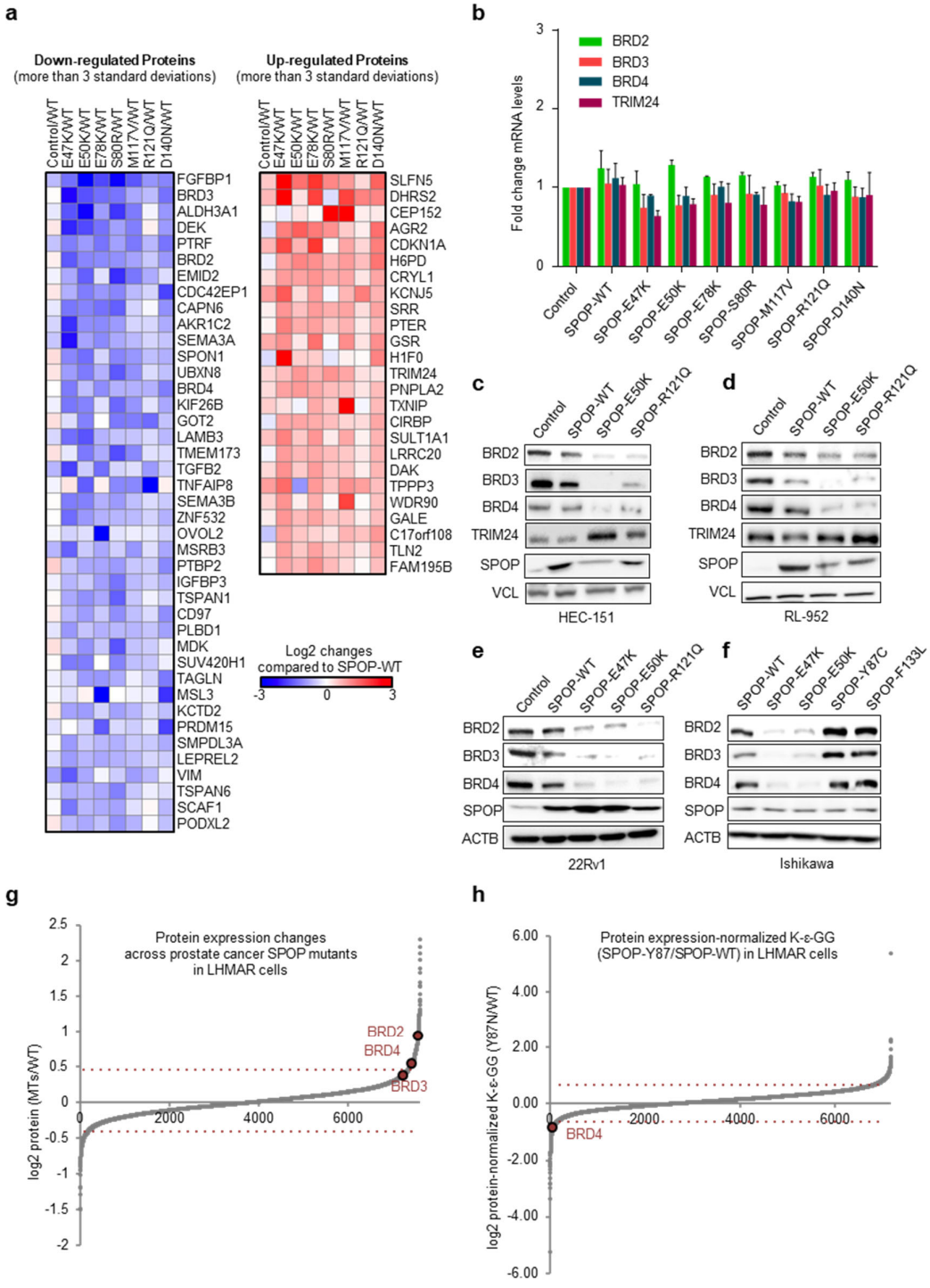

Supplementary Figure 3 Up- and down-regulated proteins in human endometrial cancer cell lines stably expressing SPOP mutants. **(a)** Expression changes by individual SPOP mutants in indicated proteins with more than 3 standard deviations depicted in a heatmap. **(b)** mRNA expression levels of indicated genes normalized to *Cyclophilin* and control in Ishikawa cells. All error bars, mean ± SEM (n=3). **(c) (d)** Representative WB for indicated proteins in HEC-151 (c) and RL-952 (d) endometrial cancer cells stably expressing two endometrial

cancer SPOP mutants. **(e)** Representative WB for indicated proteins in 22Rv1 prostate cancer cells expressing endometrial cancer SPOP mutants (n=3). **(f)** Representative WB for indicated proteins of Ishikawa cells stably expressing either SPOP-WT or SPOP mutants (two endometrial and two prostate mutants; n=3). N indicates the number of independent experiments performed. **(g)** Protein expression changes in human LHMAR cells over-expressing wild-type SPOP compared to prostate cancer SPOP mutants (average of SPOP-Y87N and -F133L)[8]. Dotted lines indicate 2 s.d. **(h)** Corresponding protein-normalized K-ε-GG changes for SPOP-Y87N.

Supplementary Figure 4

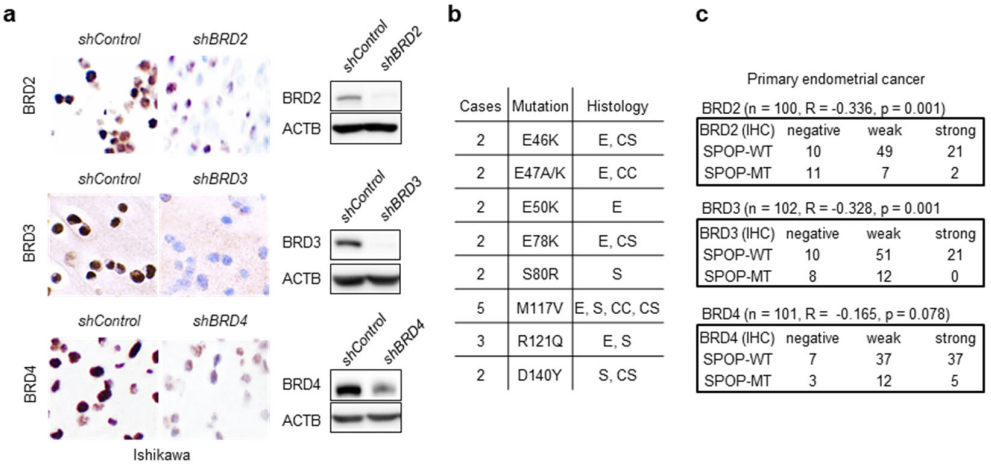

Supplementary Figure 4 BET protein immunohistochemistry (IHC) of primary human endometrial and prostate cancers. **(a)** Representative images IHC and corresponding WB for the indicated proteins of Ishikawa control and knockdown cells. **(b)** Table of SPOP-mutant endometrial tumors analyzed by IHC (E: endometrioid, S: serous, CC: clear cell, CS: carcino-sarcoma). **(c) (d)** Cross-tables and statistics using a 3-tiered IHC scoring system for BRD2, BRD3 and BRD4 of all human endometrial cancer samples, and stratified into histological subtypes (R- and p-values Kendall's tau-b). **(e)** Representative images of primary prostate cancer tissues stained for BRD2, BRD3 and BRD4 stratified accordingly *SPOP* mutation status (p-value Kendall beta-tau). **(f)** Table of *SPOP*-mutant prostate tumors analyzed by IHC. (**g)** Cross-tables and statistics using a 3-tiered IHC scoring system for BRD2, BRD3 and BRD4 of all human prostate cancer samples (R- and p-values Kendall beta-tau).

Supplementary Figure 5

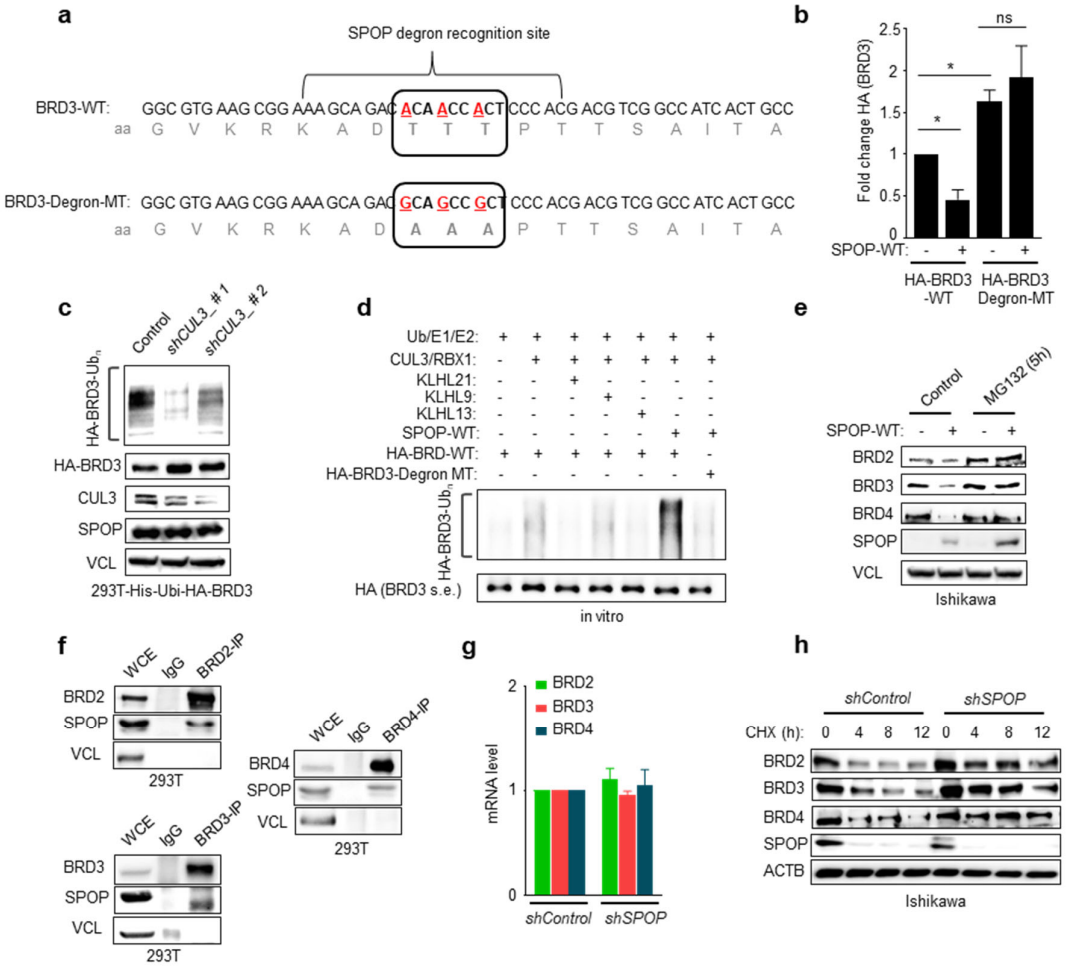

Supplementary Figure 5 Identification of SPOP degron recognition site within BET proteins. **(a)** Schema of the HA-BRD3-Degron-mutant (-MT) with indication of amino acid substitutions (T249A/T250A/T251A). **(b)** WB quantification of BRD3 protein levels shown in Fig. 2b (n=3). **(c)** *In vivo* ubiquitylation of HA-BRD3 in 293T cells transiently transfected with the indicated knockdown-constructs against *CUL3* followed by MG132 treatment. 8xHis-Ub pull down using nickel beads on lysed cells (n=3). **(d)** *In vitro* ubiquitylation of HA-BRD3. HA-BRD3-WT and Degron-MT was purified by anti-HA immunoprecipitation (IP) from 293T cells and incubated with the indicated proteins and subsequently probed for HA by WB (n=3). **(e)** Representative WB of transient over-expression of SPOP-WT in Ishikawa cells with or without MG132 treatment (n=3). **(f)** IP of individual BET proteins from 293T cells and subsequently probed for the indicated proteins (n=3). **(g)** mRNA expression changes induced by siRNA-mediated knockdown of *SPOP* normalized to *Cyclophilin* in Ishikawa cells (n=3). **(h)** Representative WB of BET protein levels after cycloheximide (CHX) treatment in control and shRNA *SPOP* Ishikawa cells (n=3). Representative WBs are shown. N indicates the number of independent experiments performed. All error bars, mean ± SEM. Statistical significance was determined by unpaired, two-tailed Student's t-test (n.s., non-significant, *P < 0.05, **P < 0.01, ***P < 0.001).

Supplementary Figure 6

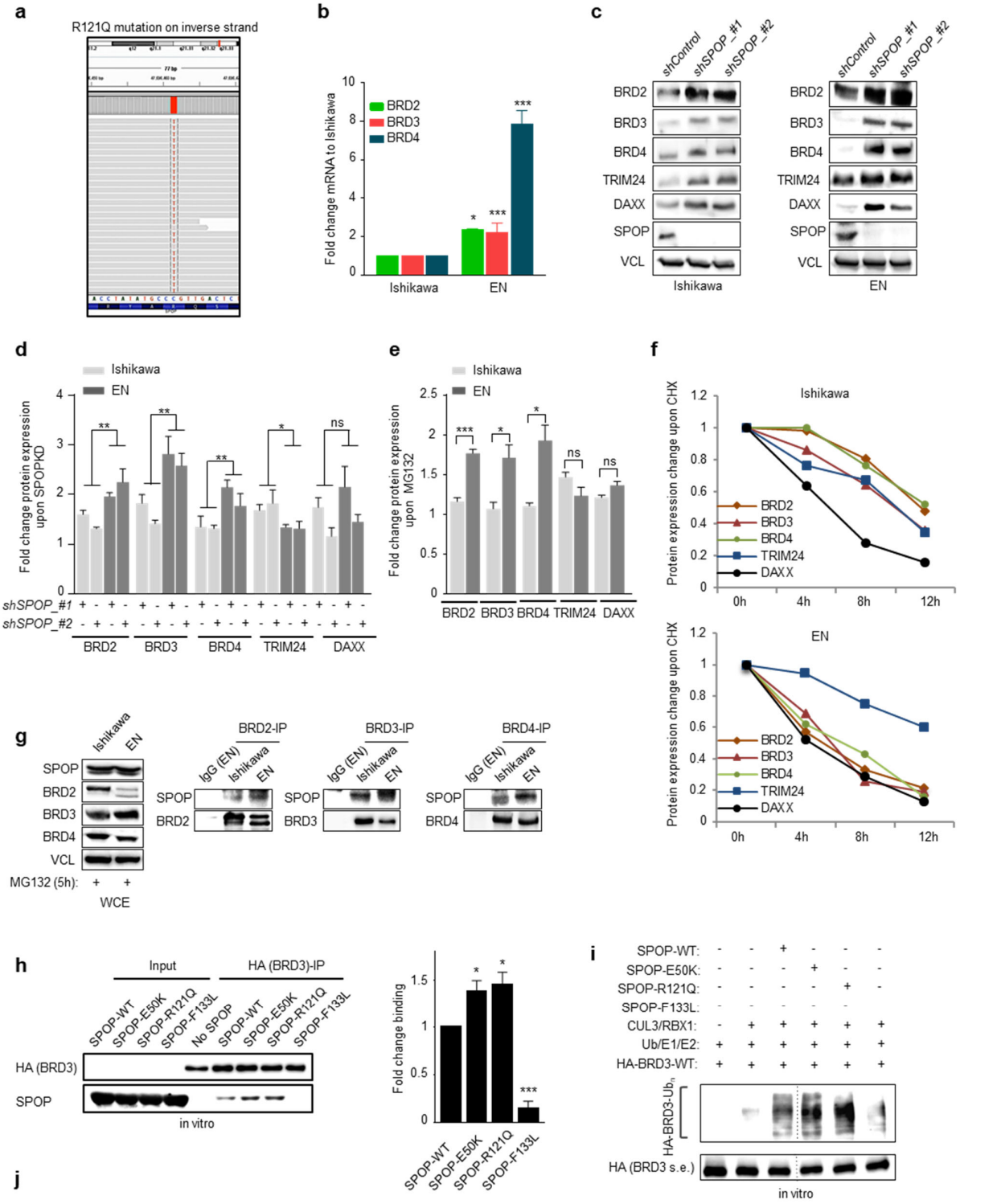

Supplementary Figure 6 Proteasomal degradation of BET proteins is enhanced in endometrial SPOP-R121Q mutant cancer cells. **(a)** IGV-screen shot of the inverse strand of the genomic *SPOP* locus of EN endometrial cells showing a C to T conversion corresponding to a R121Q substitution. **(b)** BRD2/3/4 mRNA levels in Ishikawa and EN (n=5). **(c), (d)** WB and quantification for indicated proteins upon knockdown of *SPOP* with shRNA in Ishikawa and EN cells (n=3). **(e)** WB quantification of indicated proteins in Ishikawa and EN cells with or without MG132 treatment shown in Fig. 3b (n=3). **(f)** WB analysis of indicated proteins after cycloheximide (CHX) treatment in Ishikawa and EN cells shown in Fig. 3c (n=3). **(g)** IP showing the interaction between SPOP-WT or SPOP-R121Q mutant with BRD2/3/4 in Ishikawa and EN cells (n=3). **(h)** *In vitro* binding of HA-BRD3-WT purified by anti-HA IP from 293T cells to indicated recombinant SPOP species (n=3). **(i)** *In vitro* ubiquitylation of HA-BRD3 (cropped immunoblot). HA-BRD3-WT was purified by anti-HA immunoprecipitation from 293T cells and incubated with the indicated proteins and subsequently probed for HA by WB. **(j)** Effect of transiently transfected SPOP-WT and SPOP-MTs on HA-BRD3-Degron-MT in 293T cells analyzed by WB (n=3). Representative WBs are shown. N indicates the number of independent experiments performed. All error bars, mean ± SEM. Statistical significance was determined by unpaired, two-tailed Student's t-test (n.s., non-significant, *P < 0.05, **P < 0.01, ***P < 0.001).

Supplementary Figure 7

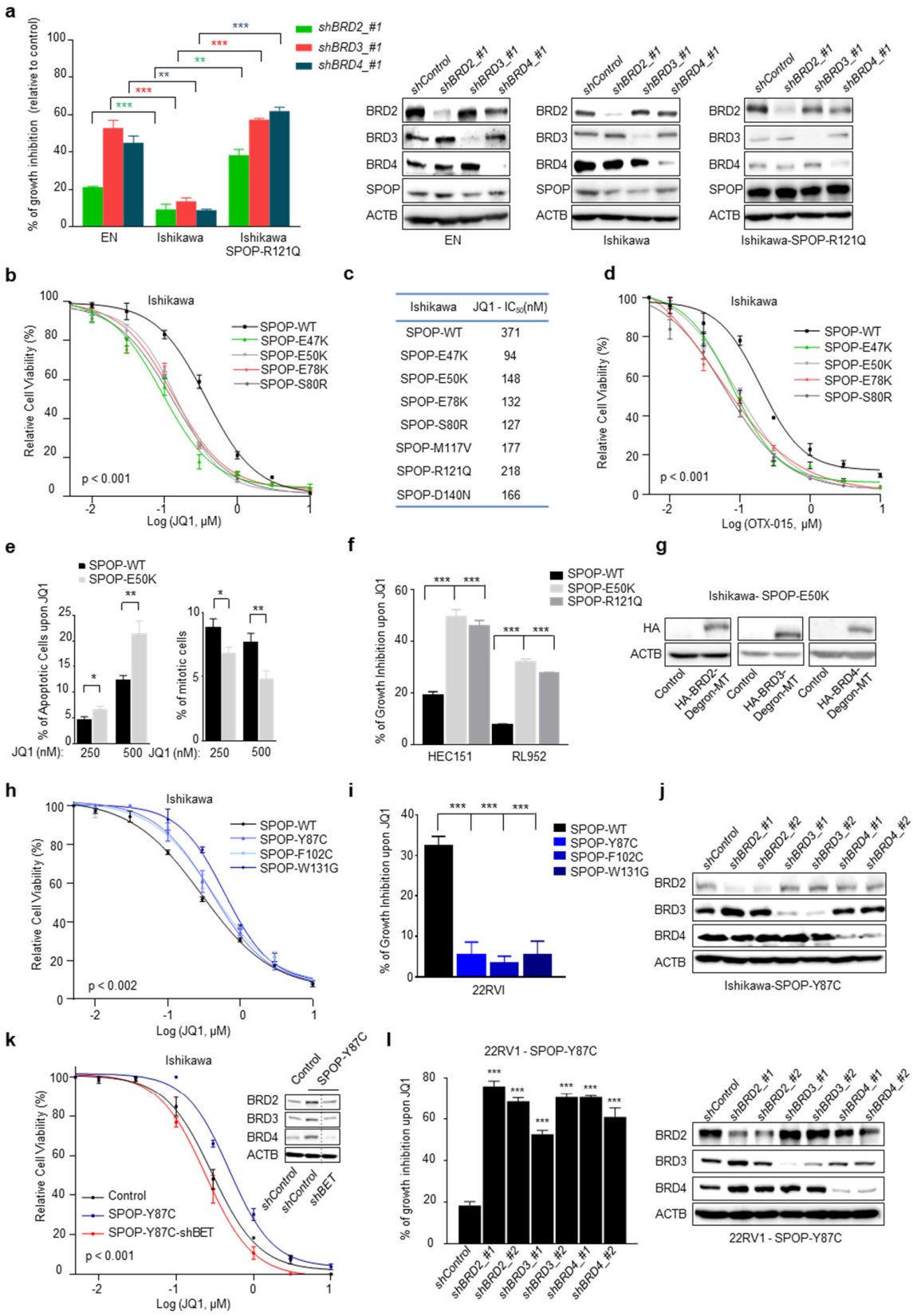

Supplementary Figure 7 Cancer associated SPOP mutations determine the response to BET inhibitors by altering BET protein levels. **(a)** Effect of *BRD2*, *BRD3* and *BRD4* shRNA-mediated depletion on cellular growth in EN, Ishikawa, and Ishikawa cells stably over-expressing SPOP-R121Q. Corresponding knockdown validation by WB for indicated proteins shown (n=3). **(b)** Dose-response curves to JQ1 in Ishikawa cells stably over-expressing SPOP-WT and four endometrial cancer SPOP-MTs (n=3, p-value is indicated below the dose-response curves by extra-sum of squares F test). **(c)** Table of the half maximal inhibitory concentration (IC_{50}) to JQ1 of Ishikawa cells stably expressing SPOP-WT and recurrent endometrial cancer mutants. **(d)** Dose response curve to OTX-015 in Ishikawa cells stably expressing SPOP-WT, and four recurrent endometrial SPOP-MTs (n=3, p-value is indicated below the dose-response curves by extra-sum of squares F test). **(e)** Quantification of apoptotic and mitotic figures in response to JQ1 in indicated stable Ishikawa cell lines (n=3; *P < 0.05, **P < 0.01, unpaired, two-tailed Student's t-test)**. (f)** Response to JQ1 in HEC-151 and RL-952 endometrial cancer cells stably expressing SPOP-WT and two endometrial cancer SPOP mutants in 3D culture (n=3; ***P < 0.001, unpaired, two-tailed Student's t-test). **(g)** Corresponding HA-BRD2/BRD3/BRD4 Degron-MTs overexpression validation by WB of experiment shown in Fig.4c. (**h)** Dose-response curves of Ishikawa cells expressing SPOP-WT and three prostate cancer SPOP mutants (n=3, p-value is indicated below the dose-response curves by extra-sum of squares F test). **(i)** Response to JQ1 of 22Rv1 prostate cancer cells stably expressing SPOP-WT and three prostate cancer SPOP mutants in 3D culture (n=6; ***P < 0.001, unpaired, two-tailed Student's t-test). **(j)** Corresponding knockdown validation by WB for BRD2/3/4 proteins of experiment shown in Fig.4d. **(k)** Cropped WB of combinatory BETs knockdown in Ishikawa-SPOP-Y87C cells showing restoration of JQ1 sensitivity to control level (n=3, p-value is indicated below the dose-response curves by extra-sum of squares F test). **(l)** Effect of single shRNA-mediated depletion of *BRD2*, *BRD3* and *BRD4* on JQ1 (200nM) sensitivity in 22RV1-SPOP-Y87C cells. Corresponding BETs knockdown validation by WB (n=3; ***P < 0.001, unpaired, two-tailed Student's t-test). Representative WBs are shown. N indicates the number of independent experiments performed. All error bars, mean ± SEM.

Supplementary Figure 8

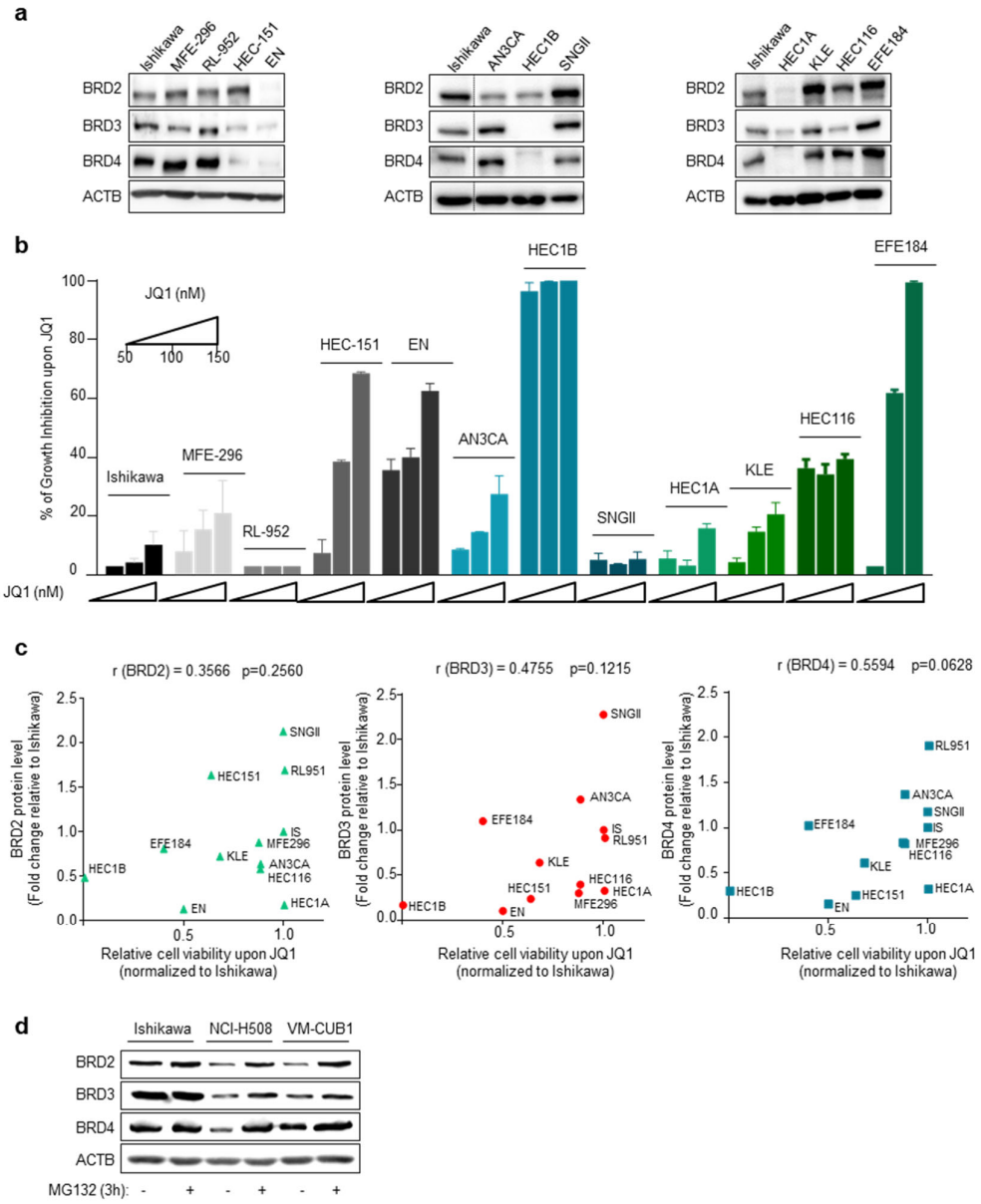

Supplementary Figure 8 Correlation of BET protein levels and JQ1 sensitivity in twelve endometrial cancer cell lines. **(a)** WB of BET protein levels across endometrial cancer cell lines with endogenous wild type SPOP (Ishikawa, MFE-296, RL-951, HEC-15, AN3CA, HEC-1B, SNG-II, HEC-1A, KLE, HEC-116, EFE-184) and SPOP-R121Q-mutant EN cancer cells. **(b)** Response to JQ1 in the same panel of endometrial cancer cell lines in 3D semi-solid culture conditions (n=3). **(c)** Correlation of JQ1 (150nM) response (b) with BET protein levels quantified by WB and normalized to β-Actin (a) in the same panel of endometrial cancer cell lines (n=3; r- and p-value Spearman rank correlation). **(d)** BRD2/3/4 protein levels by WB in Ishikawa, NCI-H508 and VM-CUB1 cells with or without MG132 treatment. Representative WBs are shown. N indicates the number of independent experiments performed. All error bars, mean ± SEM.

Supplementary Figure 9

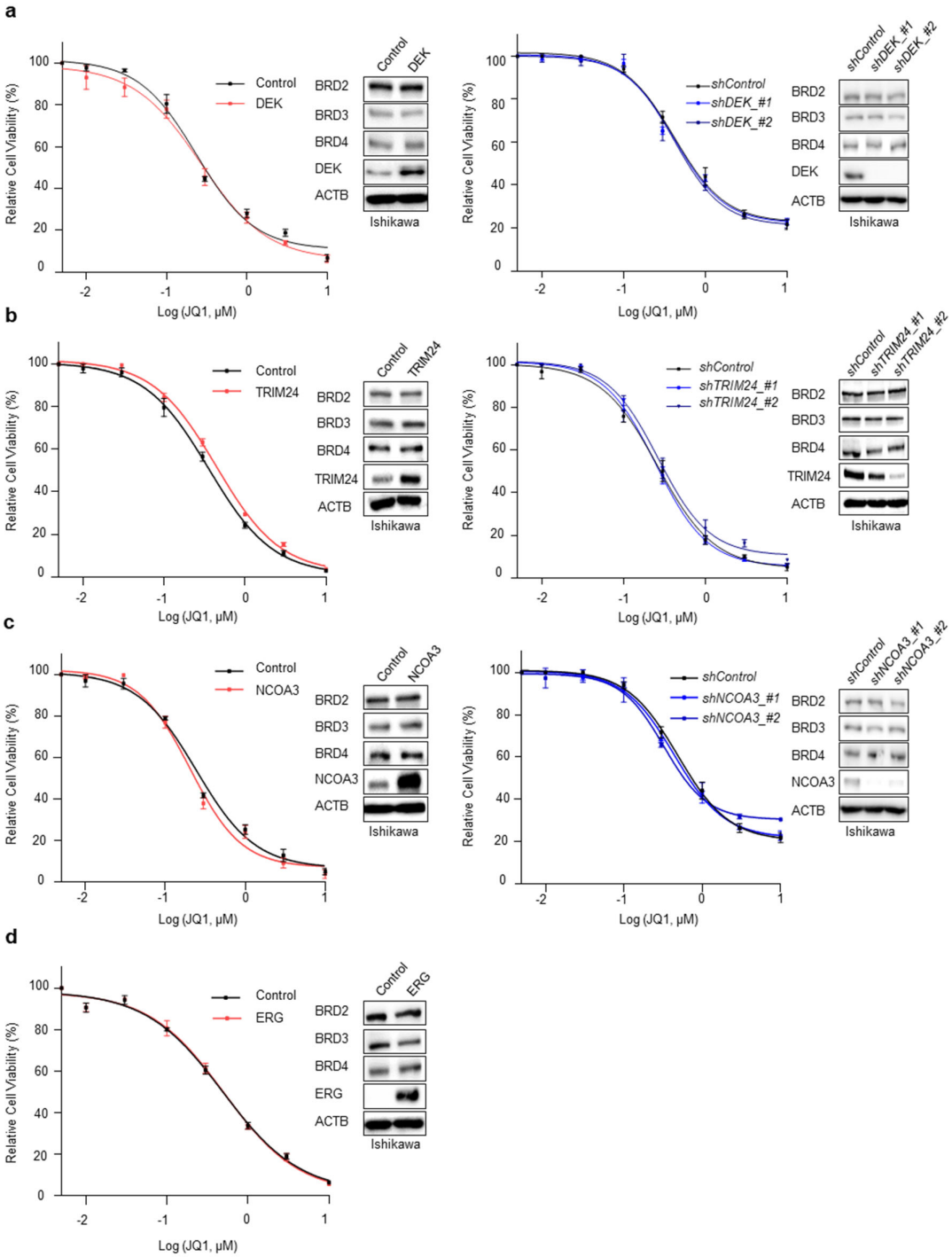

Supplementary Figure 9 Reported SPOP substrates do not affect BET protein levels and JQ1 sensitivity. **(a)** Effect of DEK overexpression and shRNA-mediated *DEK* knockdown on BET protein levels and JQ1 sensitivity in Ishikawa cells. **(b)** Effect of TRIM24 overexpression and shRNA-mediated *TRIM24* knockdown on BET protein levels and JQ1 sensitivity in Ishikawa cells. **(c)** Effect of NCOA3 overexpression and shRNA-mediated *NCOA3* knockdown on BET protein levels and JQ1 sensitivity in Ishikawa cells. **(d)** Effect of ERG overexpression on BET protein levels and JQ1 sensitivity in Ishikawa cells. Representative WBs are shown. All error bars, mean ± SEM (3 independent experiments)

Supplementary Figure 10

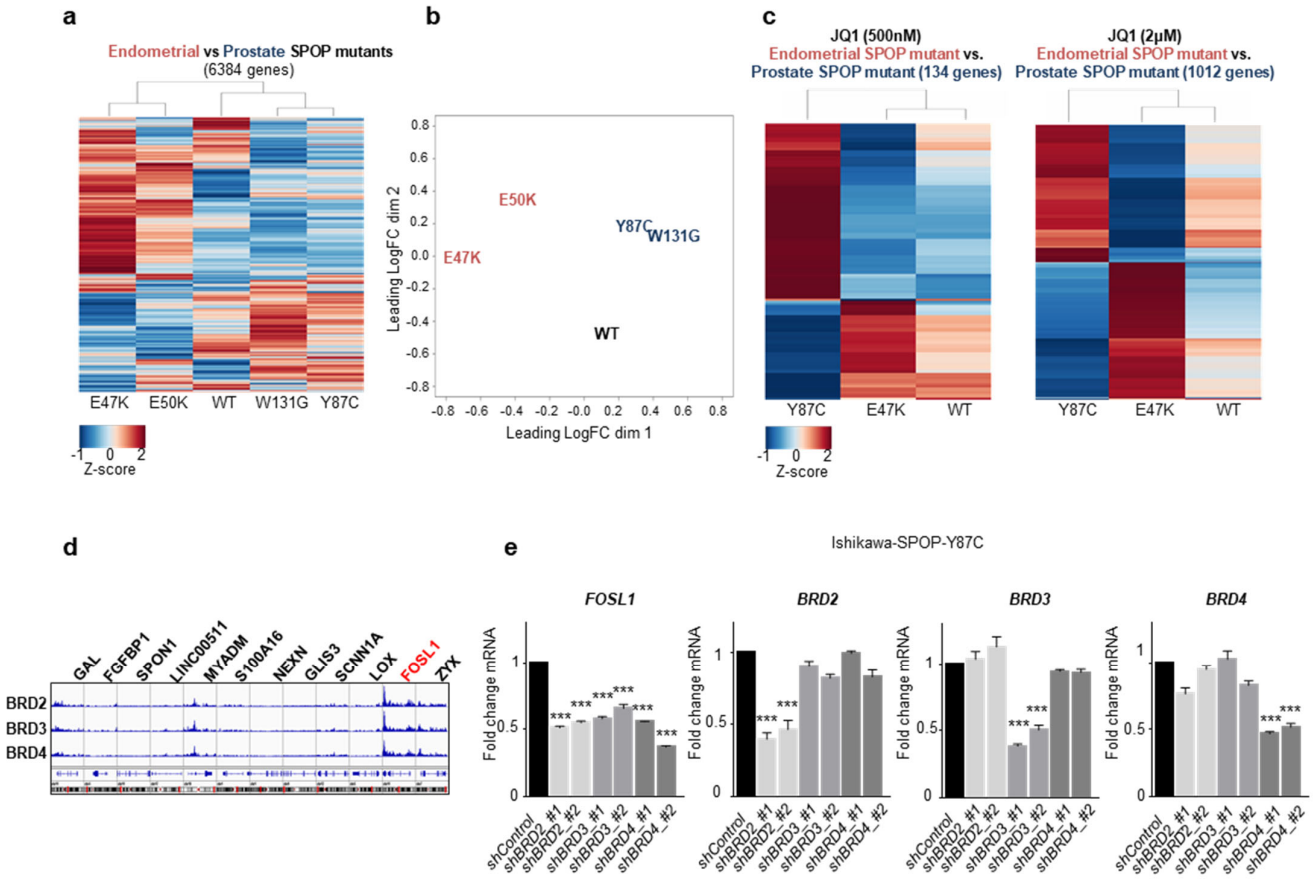

Supplementary Figure 10 Transcriptome analysis of Ishikawa cells overexpressing SPOP mutants. RNA-sequencing analysis of Ishikawa cells stably overexpressing either SPOP-WT or cancer SPOP mutants (two endometrial (ECa) E47K and E50K, two prostate (PCa) Y87C and W131G) shown as **(a)** hierarchical clustering or **(b)** Multiple dimensional scaling (MDS) plot. Genes with counts per million above 45 in at least 2 samples were considered (n= 6384 genes depicted in a-b). **(c)** Heat maps of differentially expressed genes in Ishikawa cells overexpressing endometrial (E47K) and prostate (Y87C) SPOP mutants in presence of JQ1 (500nM or 2µM). 134 genes were identified to be differentially expressed upon 500nM and 1012 genes upon 2µM JQ1 treatment. **(d)** Chip-seq profile of BRD2, BRD3, BRD4 on the depicted downregulated genes (n°= 12) shown in Fig.5a and b.[23] **(e)** Changes in *FOSL1* mRNA expression upon single shRNA-mediated knockdown of *BRD2*, *BRD3* and *BRD4* in Ishikawa-SPOP-Y87C cells. All error bars mean ± SEM. P values were derived from an unpaired, two-tailed Student's t-test (n=3¸*P < 0.05, **P < 0.01, ***P < 0.001).

ARTICLE 2

REPORT

De Novo Variants in SPOP Cause Two Clinically Distinct Neurodevelopmental Disorders

Maria J. Nabais Sá,[1] Geniver El Tekle,[2,3,4] Arjan P.M. de Brouwer,[1] Sarah L. Sawyer,[5] Daniela del Gaudio,[6] Michael J. Parker,[7] Farah Kanani,[7] Marie-José H. van den Boogaard,[8] ,Koen van Gassen,[8] Margot I. Van Allen,[9] Klaas Wierenga,[10] Gabriela Purcarin,[10] Ellen Roy Elias,[11,12] Amber Begtrup,[13] Jennifer Keller-Ramey,[13] Tiziano Bernasocchi,[2,3,4] Laurens van de Wiel,[14],Christian Gilissen,[15] Hanka Venselaar,[14] Rolph Pfundt,[1] Lisenka E.L.M. Vissers,[1] Jean-Philippe P. Theurillat,[2,3,16,*] and Bert B.A. de Vries[1,16,*]

Recurrent somatic variants in *SPOP* are cancer specific; endometrial and prostate cancers result from gain-of-function and dominant- negative effects toward BET proteins, respectively. By using clinical exome sequencing, we identified six *de novo* pathogenic missense variants in *SPOP* in seven individuals with developmental delay and/or intellectual disability, facial dysmorphisms, and congenital anomalies. Two individuals shared craniofacial dysmorphisms, including congenital microcephaly, that were strikingly different from those of the other five individuals, who had (relative) macrocephaly and hypertelorism. We measured the effect of *SPOP* variants on BET protein amounts in human Ishikawa endometrial cancer cells and patient-derived cell lines because we hypothesized that variants would lead to functional divergent effects on BET proteins. The *de novo* variants c.362G>A (p.Arg121Gln) and c. 430G>A (p.Asp144Asn), identified in the first two individuals, resulted in a gain of function, and conversely, the c.73A>G (p.Thr25Ala), c.248A>G (p.Tyr83Cys), c.395G>T (p.Gly132Val), and c.412C>T (p.Arg138Cys) variants resulted in a dominant-negative effect. Our findings suggest that these opposite functional effects caused by the variants in *SPOP* result in two distinct and clinically recognizable syndromic forms of intellec- tual disability with contrasting craniofacial dysmorphisms.

Pathogenic variants in a considerable number of highly mutable genes lead to cancer when they occur in somatic cells, and they can lead to neurodevelopmental disorders (NDD) if occur in the germline or early in the embryonic development.[1] They frequently disrupt normal cell prolif- eration and/or differentiation while evading cellular death. Moreover, mutational hotspots in both somatic cell lines and germlines point toward analogous functional effects of pathogenic variants. Examples include gain-of-function variants in genes of the RAS-MAP kinase pathway, such as *PTPN11*,[2,3] and loss-of-function variants in several genes of pathways that regulate chromatin remodeling, such as *ASXL1*.[4–6] Nevertheless, recognizing the clinical relevance and investigating the functional impact of *de novo* missense mutations in genes associated with NDD remains challenging. By using *in silico* and *in vitro* analyses, we examined the effect of *de novo* clustered missense *SPOP* var- iants identified in individuals with NDD on protein interactions.

SPOP (MIM: 602650) encodes the speckle-type POZ (pox virus and zinc finger protein; SPOP) protein in humans. SPOP homodimers function as a substrate adaptor of a larger cullin3-RING-based ubiquitin ligase complex that mediates the ubiquitination of target proteins; this ubiqui- tination usually leads to proteasomal degradation of the proteins.[7] SPOP contains an evolutionarily conserved *m*e- prin *a*nd tumor necrosis factor (TNF)-receptor associated factor (TRAF) *h*omology (MATH) domain; a bric-a-brac, tramtrack, and broad complex (BTB) domain (also known as a POZ domain); a three-box domain; and a C-terminal nuclear localization sequence.[8,9] The MATH domain medi- ates interaction with protein-ubiquitin ligase substrates, such as BRD2, BRD3, and BRD4 proteins, which are collec- tively referred to as BETs.[10]

Somatic missense *SPOP* variants restricted to the MATH domain are frequently identified in prostate cancer[11,12] and endometrial cancer.[10,13] Indeed, with up to 6–15% of localized prostate tumors harboring acquired heterozygous missense *SPOP* variants, *SPOP* is the most commonly point-mutated gene in prostate cancer.[12] These missense *SPOP* variants act in a dominant-negative fashion to repress ubiquitination and degradation of oncogenic

[1]Department of Human Genetics, Donders Institute for Brain, Cognition and Behavior, Radboud University Medical Center, 6525 GA Nijmegen, the Netherlands; [2]Functional Cancer Genomics, Institute of Oncology Research, 6500 Bellinzona, Switzerland; [3]Faculty of Biomedical Science, Università della Svizzera Italiana, 6900 Lugano, Switzerland; [4]University of Lausanne, 1015 Lausanne, Switzerland; [5]Department of Genetics, Children's Hospital of Eastern Ontario and Children's Hospital of Eastern Ontario Research Institute, University of Ottawa, Ottawa, ON K1H 8L1, Canada; [6]Molecular Diagnostic Lab- oratory, Department of Human Genetics, University of Chicago, Chicago, IL 60637, USA; [7]Department of Clinical Genetics, Sheffield Children's NHS Foundation Trust, Sheffield S10 2TH, UK; [8]Department of Genetics, UMC Utrecht, 3584 CX Utrecht, the Netherlands; [9]Department of Medical Ge- netics, University of British Columbia, Vancouver, BC V6H 3N1, Canada; [10]University of Oklahoma Health Sciences Center, Oklahoma City, OK 73104, USA; [11]Special Care Clinic, Children's Hospital Colorado, Aurora, CO 80011, USA; [12]University of Colorado School of Medicine, Aurora, CO 80045, USA; [13]GeneDx, Gaithersburg, MD 20877, USA; [14]Center for Molecular and Biomolecular Informatics, Radboud Institute for Molecular Life Sciences, Radboud University Medical Center, 6525 GA Nijmegen, the Netherlands; [15]Department of Human Genetics, Radboud Institute for Molecular Life Sciences, Radboud University Medical Center, 6525 GA Nijmegen, the Netherlands

[16]These authors contributed equally to this work

*Correspondence: jean-philippe.theurillat@ior.usi.ch (J.-P.P.T.), bert.devries@radboudumc.nl (B.B.A.d.V.)
https://doi.org/10.1016/j.ajhg.2020.02.001.

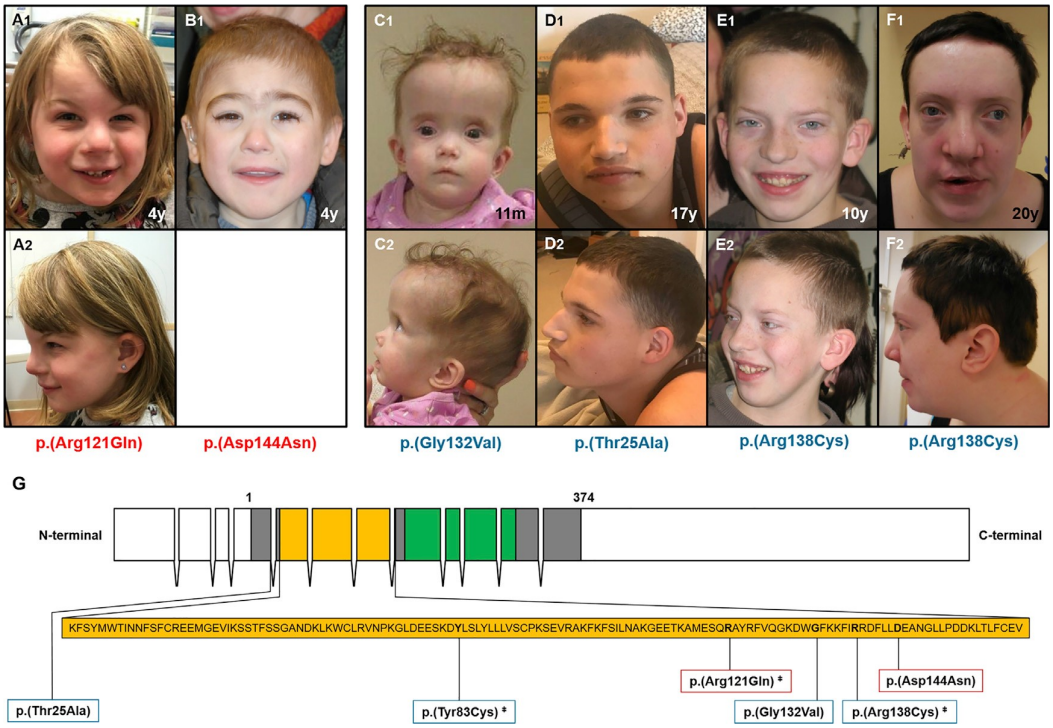

Figure 1. Craniofacial Dysmorphisms of Individuals and Their Respective *De Novo* Variants in *SPOP*

(A–F) Individuals 1 (A) and 2 (B) had microcephaly, a round face, prominent glabella, a depressed nasal bridge, narrow palpebral fissures, a short nose with anteverted nares, micrognathia, and/or a pointed chin. Individuals 3 (C), 4 (D), 5 (E), and 6 (F) had macrocephaly, a long face, a high anterior hairline, a high forehead, widely spaced eyes, a prominent and wide nasal bridge, a wide and bulbous nasal tip, underdeveloped nasal alae, and/or low-hanging columella. (G) *SPOP* mRNA with 12 exons (GenBank: NM_001007226.1; residues 1–374 correspond to the coding sequence, in grey), including the MATH domain, represented in yellow (residues 31–161) and the BTB domain (also called a POZ domain) represented in green (residues 173–297) (GenBank: NP_001007227.1; Uniprot: O43791). Affected amino acid residues are printed in bold. Variants eliciting a gain of function are noted in red; dominant-negative variants are noted in blue. *SPOP* variants marked with ǂ were identified in both germlines and somatic cell lines, as described in Table S2.

substrate proteins.[14–17] In contrast, recurrent missense *SPOP* variants in endometrial cancer result in a SPOP gain of function leading to enhanced degradation of distinct protein substrates, including the BET proteins.[10]

Two unrelated individuals with the same *de novo SPOP* variant were identified via trio-based clinical exome sequencing. One was in a cohort of 4,749 individuals with unexplained intellectual disability (ID) ascertained by the Department of Human Genetics of Radboud University Medical Center (Nijmegen, the Netherlands), and the other was ascertained at the Department of Genetics, University Medical Center Utrecht (Utrecht, the Netherlands). A third individual was identified in a cohort of 1,133 children with severe, undiagnosed devel- opmental disorders through the DDD research variant list on DECIPHER.[18] Additionally, four individuals with *SPOP* variants detected by clinical exome sequencing were identified via GeneMatcher.[19] One girl with ID was referred to the Molecular Diagnostic Laboratory at the University of Chicago for clinical exome sequencing (Chicago, Illinois, USA). The other individuals were selected from a cohort of 14,183 individuals who had neurodevelopmental disorders and who underwent trio-based clinical exome sequencing at GeneDx (Gaithersburg, Maryland, USA). All legal representatives signed consent to share medical infor- mation and clinical photographs, and this study was approved by the institutional review board Commissie Mensgebonden Onderzoek Regio Arnhem-Nijmegen un- der CMO approval number NL36191.091.11.

Six unique *de novo* missense variants in *SPOP* (GenBank: NM_001007226.1) were identified in peripheral blood of these seven individuals with intellectual disability: c.73A>G, p.Thr25Ala; c.248A>G, p.Tyr83Cys; c.362G>A, p.Arg121Gln; c.395G>T, p.Gly132Val; a recurrent c.412C>T, p.Arg138Cys; and c.430G>A, p.Asp144Asn (Figure 1; Tables 1 and 2; Table S1). All variants were confirmed by Sanger sequencing. With the exception of p.Thr25Ala, which is positioned six amino acids before the start of the MATH domain, all variants were located within the MATH domain. Three of these variants are iden- tical to those described in cancers of the prostate, endome- trium, lung, and large intestine (Table S2). *In silico* analyses, which we performed to assess evolutionary constraints on SPOP, showed that all affected amino acids are fully

Table 1. *De Novo* Likely Pathogenic Variants in *SPOP*

Location	cDNA Change [a,c]	Amino Acid Change [b,c]	Mutation Type	CADD	Domain	Predicted Effect on the Protein [28–30,d]	Affected Individuals
Exon 5	c.73A>G	p.Thr25Ala	missense	26.0	not in a domain	disease causing	individual 4
Exon 7	c.248A>G	p.Tyr83Cys	missense	25.6	MATH	disease causing	individual 7
Exon 8	c.362G>A	p.Arg121Gln	missense	32	MATH	disease causing	individual 1
Exon 8	c.395G>T	p.Gly132Val	missense	32	MATH	disease causing	individual 3
Exon 8	c.412C>T	p.Arg138Cys	missense	28.3	MATH	disease causing	individuals 5 and 6
Exon 8	c.430G>A	p.Asp144Asn	missense	28.9	MATH	disease causing	individual 2

[a]GenBank: NM_001007226.1.[b]GenBank: NP_001007227.1. [c]None of these SPOP variants were identified in the gnomAD.

[d]With the exception of p.Arg121Gln, which was predicted to be benign by PolyPhen-2, all variants were predicted to be disease causing by SIFT (v. 6.2.0), Mutation Taster (v2013), and PolyPhen-2.

conserved down to C. elegans (Figure S1). None of the variants were reported in the Genome Aggregation Database (gnomAD),20 and the CADD (combined annotation- dependent depletion) score21 was higher than 25 for all variants. In ExAC,20 SPOP contains fewer missense variants than expected (Z score ¼ 4.74), and no loss of function variant is described (pLi ¼ 0.99). In the DGV (Database of Genomic Variants; March 2019),[22] no CNVs, inversions, or indels were reported. We used MetaDome[23,24] to generate a tolerance landscape, which is a regional toler- ance plot for genetic variation and is based on the ratio of observed missense and synonymous ($d_N = d_S$) variants that are included in gnomAD r2.0[20] and are found in the protein-coding region of *SPOP*. All *de novo* SPOP variants are located in regions that are extremely intolerant to missense variants (Figure S2). We investigated the 3D loca- tion of the variants by using the experimentally solved 3D- conformation of the dimeric SPOP structure (PDB file 3hqi; Figure 2A).[25] The structure was analyzed with the YASARA and WHAT IF Twinset.[26,27] This analysis suggested that four of the six substitutions, p.Tyr83Cys, p.Arg121Gln, p.Gly132Val, and p.Arg138Cys, would directly affect the binding of substrates to SPOP. For the p.Asp144Asn and p.Thr25Ala variants, prediction of the binding conse- quences was non-informative. The p.Asp144Asn substitu- tion was not predicted to have a large effect on the local protein structure, and residue Thr 25 is too distant from the binding cleft.

Reverse deep phenotyping of the seven individuals revealed that all had intellectual disability, motor and speech delay, facial dysmorphisms, and congenital anomalies (Table 2; Table S3; Figure 1; Figure S3). Besides these com- mon features, individuals 1 and 2 shared craniofacial dysmorphisms that are strikingly different from those of individuals 3–7; in fact, when one considers the head circumference and forehead of individuals 1 and 2, their craniofacial dysmorphisms could even be said to be the opposite of the features of individuals 3–7. Individuals 1 and 2 both presented with specific features that include congenital microcephaly, hearing loss, and a recognizable facial gestalt, such as a small forehead, highly arched eye-brows, blepharophimosis, a full nasal tip, a flat philtrum, micrognathia, and a pointed chin. Between them, individ- uals 3–7 also shared specific facial dysmorphisms, in partic- ular (relative) macrocephaly, a high and broad forehead, and hypertelorism. Additional overlapping phenotypic abnormalities confined to the second group of five individ- uals were failure to thrive and short stature (2/5), cardio- vascular abnormalities (4/4), endocrine abnormalities (3/4), epilepsy (2/4), and sleep disturbance (4/5).

On the basis of the previously reported opposite func- tional effect of somatic *SPOP* variants in prostate and endometrial cancer (Table S2),[10] we hypothesized that the divergent phenotype of the two groups of individuals corre- sponds to differential functional effects. We envisaged that the *de novo* variants, including p.Arg121Gln, that were identified in the first group of individuals would result in a gain-of-function, and conversely, the variants, namely p.Tyr83Cys, that were detected in the second group would have a dominant-negative effect. To investigate this, we measured BET protein amounts in human Ishikawa endometrial cancer cells, an isogenic model system, in which we introduced all *de novo SPOP* variants. Variants p.Arg121Gln and p.Asp144Asn resulted in reduced amounts of the BET proteins BRD2, BRD3, and BRD4, sug- gesting that these are gain-of-function variants comparable to those seen in endometrial cancer (Figures 2B, S4A, and S5). In contrast, the variants p.Thr25Ala, p.Tyr83Cys, p.Gly132Val, and p.Arg138Cys resulted in an upregulation of BRD2, BRD3, and BRD4 protein amounts and are hence *SPOP* variants such as those seen in prostate cancer and are acting in a dominant-negative manner. Importantly, and in conjunction with the notion of altered protein stability, we did not observe relevant transcriptional changes in BET proteins in response to these mutants (Figure S4B). We confirmed the nature of the variants by measuring the kinetics of protein degradation by using two variants that represent either gain-of-function or domi- nant-negative effects. Indeed, after inhibition of protein synthesis with cycloheximide, BET amounts remained

Table 2. Genotype and Phenotype of Individuals with *De Novo* Pathogenic Mutations in *SPOP*

	Individuals		Individuals				
	1	**2**	**3**	**4**	**5**	**6**	**7**
Gender/ Current age	F; 4 years 7 months	M; 10 years	F; 10 months	M; 17 years 11 months	M; 17 years 9 months	F; 20 years	F; 15 years
Genotype							
cDNA change [a]	c.362G>A	c.430G>A	c.395G>T	c.73A>G	c.412C>T	c.412C>T	c.248A>G
Protein change [b]	p.Arg121Gln	p.Asp144Asn	p.Gly132Val	p.Thr25Ala	p.Arg138Cys	p.Arg138Cys	p.Tyr83Cys
Inheritance	*de novo*	*de novo*	*de novo*	*de novo*	*de novo*	*de novo*	*de novo*
Effect on BET proteins	gain-of-function	gain-of-function	loss-of-function	loss-of-function	loss-of-function	loss-of-function	loss-of-function
Phenotype[d]							
Age at measurements	4 years 7 months	16 months	10 months	17 years 11 months	17 years 9 months	20 years	15 years
Height in cm (centile range)[c]	104.5 cm (~50th)	77 cm (10th–25th)	65.1 cm (−2.5SD)	151.8 cm (−3.1SD)	178.5 cm (50th–75th)	172 cm (90th–97th)	158.8 cm (25th–50th)
Weight in kg (centile range)[c]	15.3 kg (10th–25th)	8.8 kg (−2.3 SD)	5.6 kg (−4 SD)	49.7 kg (3rd)	73 kg (50th–75th)	89 kg (97th)	90.7 kg (+2.5 SD)
HC in cm (centile range)[c]	44 cm (−4 SD)	40.5 cm (−5 SD)	49 cm (+3.5 SD)	NA (25th)	56.4 cm (75th–90th)	57 cm (+2.5 SD)	56 cm at 5 years (+4 SD)
Intellectual disability/ developmental delay[d]	+ (mild)	+ (severe)	+	+ (IQ − 46)	+ (IQ − 45)	+ (IQ − 53)	+ (mild)
Epilepsy	−	NA	−	+	+	NA	−
Behavioral abnormalities[d]	+	+	NA	+	+	+	+
Craniofacial dysmorphims[d]	++	++	+	+	+	+	+
Hearing impairment[d]	+	+	−	−	−	−	−
Cardiovascular abnormality[d]	−	−	+	+	NA	+	+
Endocrine abnormality[d]	−	−	−	+	+	NA	+
Sleep disturbance[d]	−	NA	−	+	+	+	+

Abbreviations are as follows: +, present; −, absent; F, female; M, male; SD, standard deviation; HC, head circumference; IQ, intelligence quotient score; and NA, not available.
[a]GenBank:NM_001007226.1.
[b]GenBank: NP_001007227.1.
[c]Percentile range; if the percentile is <3rd or >97th, standard deviation (SD) is indicated.
[d]Further specified in Table S2

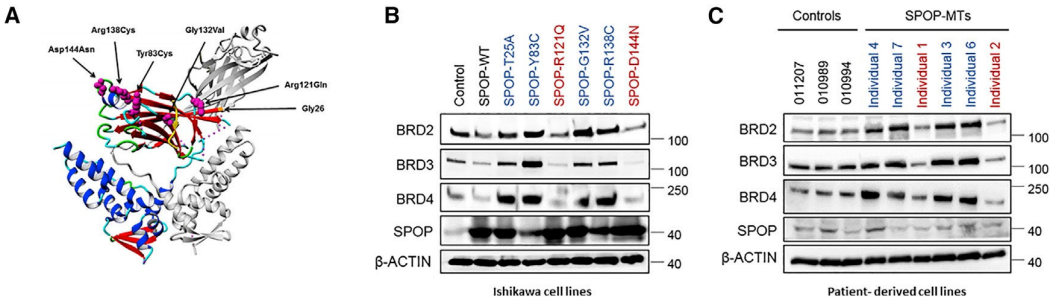

Figure 2. *De Novo SPOP* Variants Produce Opposing Effects on BET Amounts

(A) 3D structure of an asymmetric homodimer SPOP (one monomer is shown in grey), including the MATH domain (most beta strands are in the upper part of the protein and are shown as red arrows) and the BTB domain (blue helices and three beta strands on the lower part). Except for variant p.Thr25Ala, tered residues (magenta spheres) occurred in the MATH domain. The p.Thr25Ala residue is not shown because the protein structure starts with residue 26 (orange extremity of a red beta strand). The displayed mutated residues are closely located to the binding cleft, where the MATH domain interacts with its substrates (yellow peptide). The structure shows that Gly 132 is located at the bottom of the binding cleft, where the introduction of a larger valine affects the conformation and modifies substrate interaction. Tyr 83, Arg 138, and Asp 144 can be found clustered together on the surface of the protein. The alteration of both Tyr 83 and Arg 138 into a cysteine is very likely to affect the local structure surrounding the binding cleft and, hence, disturb SPOP sub- strate interaction. The substitution of an Asp for an Asn at position 144 is not large enough to affect the structure in a similar way, so we cannot predict the effect of this substitution for now. Amino acid residue Arg 121 is located on the protein surface on the opposite side of the binding cleft, where its side chain supports Tyr 123. Changing this residue to a slightly smaller Gln could affect the position of Tyr 123 and change the interaction of SPOP with its substrate. Lastly, Thr 25 is even more distant from the binding cleft. This residue is not present in the PDB file, but because Gly 26 is present as the first residue of the solved protein chain, we could still infer the effect of this change. The change of a Thr into a smaller Ala is not expected to cause strong structural changes or to affect the binding site directly. (B) Representative immunoblot showing that the p.Asp144Asn and p.Arg121Gln SPOP substitutions downregulate, whereas p.Thr25Ala, p.Tyr83Cys, p.Gly132Val, and p.Arg138Cys upregulate, BRD2, BRD3, and BRD4 protein amounts when compared with wild-type SPOP (SPOP-WT) in Ishikawa endometrial cancer cells. (C) When proband-derived Epstein-Barr Virus (EBV)-immortalized PBMC lines from individuals 1, 2, 3, 4, 6, and 7 were compared to cell lines from three healthy individuals (controls), the same effect as for the isogenic cells (in B) was observed. b-ACTIN was used as loading control. Molecular weights are indicated (kDa).

stable upon expression of SPOP-p.Arg138Cys. In contrast, protein half-life was more dramatically reduced upon expression of SPOP-p.Asp144Asn as compared to that of wild-type SPOP (Figure S6). Consistent with the notion that BETs are degraded through the proteasome, treatment with MG132 restored BET amounts in both contexts. Pro- band-derived EBV-immortalized peripheral blood mononuclear cell (PBMC) lines from individuals 1, 2, 3, 4, 6, and 7 were additionally obtained and cultured as previously described.[31] Notably, measurements of BET amounts in pro- band-derived cell lines matched those found in healthy individuals in terms of the deregulation found in the isogenic system generated in Ishikawa endometrial cancer cells (Figures 2B, 2C, and S4C), suggesting that the *de novo* variants are causally linked to the functional effects observed.

We identified seven individuals with NDD and *de novo SPOP* missense variants that caused either reduced (individuals 1 and 2) or increased (individuals 3–7) BET amounts. Furthermore, variants resulted in growth abnormalities, including a head size spectrum ranging from microcephaly to macrocephaly and distinct recognizable facial dysmorphisms. Whereas individuals with gain-of-function variants presented with microcephaly, individuals with variants leading to BET's functional loss had absolute macrocephaly or a head circumference (HC) in the normal centile range, though exceeding the centile for height (relative macrocephaly). Of note, individuals 5 and 6, who had the same *de novo* p.Arg138Cys variant, had absolute macrocephaly and a normal HC, respectively, suggesting interfamilial variability. So far, no true congenital macrocephaly has been observed, although birth HC measurements of in- dividuals 5, 6, and 7 were unknown. Specifically, individuals 3 and 4, who were born with below average HC, showed postnatal ventriculomegaly, which also contrib- uted to absolute or relative macrocephaly, respectively. Additional investigation is needed if we are to understand the intricate mechanisms involved in head growth in individuals with pathogenic *SPOP* variants; such mechanisms might be determined by cell signaling pathways that govern cell proliferation and overlap with cancer pathways.[32] Functionally, BET proteins are involved in cell-cycle progression.[33] In mice, BRD2, BRD3, and BRD4 were found to be downregulated in differentiating neural progenitor cells, whereas their amounts remained unaltered in proliferating neural progenitor cells.[34] In addition, in *Brd2*-deficient neuroepithelial cells, cell-cycle progression was accelerated, whereas neuronal differentiation as well as cell-cycle exit were impaired.[35] These results correlate well with the congenital microcephaly found in two individuals with a STOP gain of function resulting in fewer BET proteins and, hence, supposedly less neuronal differentiation. Conversely, more BET proteins would stimulate the latter process, which might result in macrocephaly. Lastly, a c.910C>T (p.His304Tyr; GenBank: NM_058243.2) hetero- zygous missense variant in *BRD4* has been described as resulting in macrocephaly and short stature, resembling

features in individuals with dominant-negative variants in *SPOP*.[36] Interestingly, this *BRD4* variant might result in increased protein stability because it is in close proximity to the SPOP degron (AA292–299).

Diverse and eventually mirror phenotypes caused by ge- netic variation in the same gene are increasingly recognized (e.g. *CDKN1C*[37] and *RAC1*[38]). Different explanations that have been proposed for the resultant excess or inhibition of cell proliferation and differentiation include disruption of a single neurodevelopmental step that is sensitive to gene dosage[39] and the possibility of a gene's influencing several biologic pathways resulting in different consequences depending on temporal and cellular contexts within a genetic background.[1] In particular, the (re)occurrence of specific genetic variants in the substrate-binding MATH domain of SPOP, which results in opposite functional effects, emphasizes the key role of this domain in cell biology.

In summary, *SPOP* variants have been identified in individuals with intellectual disability and in tumor samples, which suggests that *SPOP* variants occurring at different times of development, specifically in germline versus somatic tissue, result in different consequences, i.e., neurodevelopmental delay or cancer, respectively. Individuals with NDD and *de novo SPOP* variants could be differentiated on the basis of distinct craniofacial dysmorphisms and congenital anomalies, indicating the presence of diverse clinically recognizable intellectual-disability syndromes. The opposing effects of variants impairing SPOP function provide a molecular basis for the contrasting phenotypic differences.

Supplemental Data

Supplemental Data can be found online at https://doi.org/10.1016/j.ajhg.2020.02.001.

Acknowledgements

We are grateful to all the families for participating in this study.

We thank the Care 4 Rare Canadian Consortium for logistical help and scientific expertise for individual 1. We are thankful to Erin Torti (GeneDx, Inc) for bringing us in contact with the clinicians of families 3, 4, and 5. We would like to acknowledge the work of Julian A. Martinez-Agosto and Rebecca H. Signer, who evaluated individual 4 within the Undiagnosed Diseases Network research study at UCLA (Los Angeles, CA, USA). We also thank S.D. van der Velde-Visser for the technical assistance with cell culturing at the Cell Culturing Facility of Genome Research Nijmegen (Nijmegen, the Netherlands). This work was financially supported by grants from the Dutch Organization for Health Research and Development (ZON-MW grants 917–86– 319 and 912–12–109 to B.B.A.d.V.), the Krebsliga Schweiz (KLS- 4248-08-2017 to J.P.T), the Swiss National Science Foundation (PP00P3_179072 to J.P.T),

Declaration of Interests

Amber Begtrup and Jennifer Keller-Ramey are employees of GeneDx,

Received: July 14, 2019

Accepted: February 5, 2020

Web Resources

Genome Aggregation Database, https://gnomad.broadinstitute.org/gene/ENSG00000121067

OMIM, https://www.omim.org/

References

1. Hoischen, A., Krumm, N., and Eichler, E.E. (2014). Prioritization of neurodevelopmental disease genes by discovery of new mutations. Nat. Neurosci. *17*, 764–772.
2. Tartaglia, M., Kalidas, K., Shaw, A., Song, X., Musat, D.L., van der Burgt, I., Brunner, H.G., Bertola, D.R., Crosby, A., Ion, A., et al. (2002). PTPN11 mutations in Noonan syndrome: molecular spectrum, genotype-phenotype correlation, and phenotypic heterogeneity. Am. J. Hum. Genet. *70*, 1555–1563.
3. Tartaglia, M., Niemeyer, C.M., Fragale, A., Song, X., Buechner, J., Jung, A., Hä hlen, K., Hasle, H., Licht, J.D., and Gelb, B.D. (2003). Somatic mutations in PTPN11 in juvenile myelomo- nocytic leukemia, myelodysplastic syndromes and acute myeloid leukemia. Nat. Genet. *34*, 148–150.
4. Gelsi-Boyer, V., Trouplin, V., Adélaïde, J., Bonansea, J., Cervera, N., Carbuccia, N., Lagarde, A., Prebet, T., Nezri, M., Sainty, D., et al. (2009). Mutations of polycomb-associated gene ASXL1 in myelodysplastic syndromes and chronic myelomonocytic leukaemia. Br. J. Haematol. *145*, 788–800.
5. Hoischen, A., van Bon, B.W., Rodr´ıguez-Santiago, B., Gilissen, C., Vissers, L.E., de Vries, P., Janssen, I., van Lier, B., Hastings, R., Smithson, S.F., et al. (2011). De novo nonsense mutations in ASXL1 cause Bohring-Opitz syndrome. Nat. Genet. *43*, 729–731.
6. Carbuccia, N., Murati, A., Trouplin, V., Brecqueville, M., Adélaïde, J., Rey, J., Vainchenker, W., Bernard, O.A., Chaffanet, M., Vey, N., et al. (2009). Mutations of ASXL1 gene in myeloproliferative neoplasms. Leukemia *23*, 2183–2186.
7. Cheng, J., Guo, J., Wang, Z., North, B.J., Tao, K., Dai, X., and Wei, W. (2018). Functional analysis of Cullin 3 E3 ligases in tumorigenesis. Biochim Biophys Acta Rev Cancer *1869*, 11–28.
8. Nagai, Y., Kojima, T., Muro, Y., Hachiya, T., Nishizawa, Y., Wakabayashi, T., and Hagiwara, M. (1997). Identification of a novel nuclear speckle-type protein, SPOP. FEBS Lett. *418*, 23–26.
9. Zapata, J.M., Pawlowski, K., Haas, E., Ware, C.F., Godzik, A., and Reed, J.C. (2001). A diverse family of proteins containing tumor necrosis factor receptor-associated factor domains. J. Biol. Chem. *276*, 24242–24252.
10. Janouskova, H., El Tekle, G., Bellini, E., Udeshi, N.D., Rinaldi, A., Ulbricht, A., Bernasocchi, T., Civenni, G., Losa, M., Svinkina, T., et al. (2017). Opposing effects of cancer-type-specific SPOP mutants on BET protein degradation and sensitivity to BET inhibitors. Nat. Med. *23*, 1046–1054.
11. Baca, S.C., Prandi, D., Lawrence, M.S., Mosquera, J.M., Roma- nel, A., Drier, Y., Park, K., Kitabayashi, N., MacDonald, T.Y., Ghandi, M., et al. (2013). Punctuated

Stransky, N., et al. (2012). Exome sequencing identifies recurrent SPOP, FOXA1 and MED12 mutations in prostate cancer. Nat. Genet. *44*, 685–689.

13. Le Gallo, M., O'Hara, A.J., Rudd, M.L., Urick, M.E., Hansen, N.F., O'Neil, N.J., Price, J.C., Zhang, S., England, B.M., God- win, A.K., et al.; NIH Intramural Sequencing Center (NISC) Comparative Sequencing Program (2012). Exome sequencing of serous endometrial tumors identifies recurrent somatic mu- tations in chromatin-remodeling and ubiquitin ligase com- plex genes. Nat. Genet. *44*, 1310–1315.
14. Geng, C., He, B., Xu, L., Barbieri, C.E., Eedunuri, V.K., Chew, S.A., Zimmermann, M., Bond, R., Shou, J., Li, C., et al. (2013). Prostate cancer-associated mutations in speckle-type POZ protein (SPOP) regulate steroid receptor coactivator 3 pro- tein turnover. Proc. Natl. Acad. Sci. USA *110*, 6997–7002.
15. Theurillat, J.P., Udeshi, N.D., Errington, W.J., Svinkina, T., Baca, S.C., Pop, M., Wild, P.J., Blattner, M., Groner, A.C., Ru- bin, M.A., et al. (2014). Prostate cancer. Ubiquitylome analysis identifies dysregulation of effector substrates in SPOP-mutant prostate cancer. Science *346*, 85–89.
16. An, J., Ren, S., Murphy, S.J., Dalangood, S., Chang, C., Pang, X., Cui, Y., Wang, L., Pan, Y., Zhang, X., et al. (2015). Trun- cated ERG Oncoproteins from TMPRSS2-ERG Fusions Are Resistant to SPOP-Mediated Proteasome Degradation. Mol. Cell *59*, 904–916.
17. Marzahn, M.R., Marada, S., Lee, J., Nourse, A., Kenrick, S., Zhao, H., Ben-Nissan, G., Kolaitis, R.M., Peters, J.L., Pounds, S., et al. (2016). Higher-order oligomerization promotes localization of SPOP to liquid nuclear speckles. EMBO J. *35*, 1254–1275.
18. Deciphering Developmental Disorders, S.; and Deciphering Developmental Disorders Study (2015). Large-scale discovery of novel genetic causes of developmental disorders. Nature *519*, 223–228.
19. Sobreira, N., Schiettecatte, F., Valle, D., and Hamosh, A. (2015). GeneMatcher: a matching tool for connecting investi- gators with an interest in the same gene. Hum. Mutat. *36*, 928–930.
20. Lek, M., Karczewski, K.J., Minikel, E.V., Samocha, K.E., Banks, E., Fennell, T., O'Donnell-Luria, A.H., Ware, J.S., Hill, A.J., Cummings, B.B., et al.; Exome Aggregation Consortium (2016). Analysis of protein-coding genetic variation in 60,706 humans. Nature *536*, 285–291.
21. Kircher, M., Witten, D.M., Jain, P., O'Roak, B.J., Cooper, G.M., and Shendure, J. (2014). A general framework for estimating the relative pathogenicity of human genetic variants. Nat. Genet. *46*, 310–315.
22. MacDonald, J.R., Ziman, R., Yuen, R.K., Feuk, L., and Scherer, S.W. (2014). The Database of Genomic Variants: a curated collection of structural variation in the human genome. Nu- cleic Acids Res. *42*, D986–D992.
23. Wiel, L., Baakman, C., Gilissen, D., Veltman, J.A., Vriend, G., and Gilissen, C. (2019). MetaDome: Pathogenicity analysis of genetic variants through aggregation of homologous hu- man protein domains. Hum. Mutat. *40*, 1030–1038.
24. Wiel, L., Venselaar, H., Veltman, J.A., Vriend, G., and Gilissen, C. (2017). Aggregation of population-based geneticvariation over protein domain homologues and its potential use in ge- netic diagnostics. Hum. Mutat. *38*, 1454–1463.
25. Zhuang, M., Calabrese, M.F., Liu, J., Waddell, M.B., Nourse, A., Hammel, M., Miller, D.J., Walden, H., Duda, D.M., Seyedin, S.N., et al. (2009). Structures of SPOP-substrate complexes: insights into molecular architectures of BTB-Cul3 ubiquitin ligases. Mol. Cell *36*, 39–50.
26. Krieger, E., Koraimann, G., and Vriend, G. (2002). Increasing the precision of comparative models with YASARA NOVA–a self-parameterizing force field. Proteins *47*, 393–402.
27. Vriend, G. (1990). WHAT IF: a molecular modeling and drug design program. J. Mol. Graph *8*, 52–56.
28. Sim, N.L., Kumar, P., Hu, J., Henikoff, S., Schneider, G., and Ng, P.C. (2012). SIFT web server: predicting effects of amino acid substitutions on proteins. Nucleic Acids Res. *40*, W452– W457.
29. Adzhubei, I.A., Schmidt, S., Peshkin, L., Ramensky, V.E., Gera- simova, A., Bork, P., Kondrashov, A.S., and Sunyaev, S.R. (2010). A method and server for predicting damaging missense mutations. Nat. Methods *7*, 248–249.
30. Schwarz, J.M., Cooper, D.N., Schuelke, M., and Seelow, D. (2014). MutationTaster2: mutation prediction for the deep- sequencing age. Nat. Methods *11*, 361–362.
31. de Brouwer, A.P., van Bokhoven, H., and Kremer, H. (2006). Comparison of 12 reference genes for normalization of gene expression levels in Epstein-Barr virus-transformed lympho- blastoid cell lines and fibroblasts. Mol. Diagn. Ther. *10*, 197–204.
32. Pirozzi, F., Nelson, B., and Mirzaa, G. (2018). From micro- cephaly to megalencephaly: determinants of brain size. Dia- logues Clin. Neurosci. *20*, 267–282.
33. Doroshow, D.B., Eder, J.P., and LoRusso, P.M. (2017). BET inhibitors: a novel epigenetic approach. Ann. Oncol. *28*, 1776–1787.
34. Li, J., Ma, J., Meng, G., Lin, H., Wu, S., Wang, J., Luo, J., Xu, X., Tough, D., Lindon, M., et al. (2016). BET bromodomain inhi- bition promotes neurogenesis while inhibiting gliogenesis in neural progenitor cells. Stem Cell Res. (Amst.) *17*, 212–221.
35. Tsume, M., Kimura-Yoshida, C., Mochida, K., Shibukawa, Y., Amazaki, S., Wada, Y., Hiramatsu, R., Shimokawa, K., and Matsuo, I. (2012). Brd2 is required for cell cycle exit and neuronal differentiation through the E2F1 pathway in mouse neuroepithelial cells. Biochem. Biophys. Res. Commun. *425*, 762–768.
36. Jin, H.S., Kim, J., Kwak, W., Jeong, H., Lim, G.B., and Lee, C.G. (2017). Identification of a Novel Mutation in BRD4 that Causes Autosomal Dominant Syndromic Congenital Cata- racts Associated with Other Neuro-Skeletal Anomalies. PLoS ONE *12*, e0169226.
37. Milani, D., Pezzani, L., Tabano, S., and Miozzo, M. (2014). Beckwith-Wiedemann and IMAGe syndromes: two very different diseases caused by mutations on the same gene. Appl. Clin. Genet. *7*, 169–175.
38. Reijnders, M.R.F., Ansor, N.M., Kousi, M., Yue, W.W., Tan, P.L., Clarkson, K., Clayton-Smith, J., Corning, K., Jones, J.R., Lam, W.W.K., et al.; Deciphering Developmental Disorders Study (2017). RAC1 Missense Mutations in Developmental Disor- ders with Diverse Phenotypes. Am. J. Hum. Genet. *101*, 466–477.
39. Jacquemont, S., Reymond, A., Zufferey, F., Harewood, L., Wal- ters, R.G., Kutalik, Z., Martinet, D., Shen, Y., Valsesia, A., Beck- mann, N.D., et al. (2011). Mirror extreme BMI phenotypes associated with gene dosage at the chromosome 16p11.2 locus. Nature *478*, 97–102.

The American Journal of Human Genetics, Volume *106*

Supplemental Data

De Novo Variants in *SPOP* Cause Two Clinically Distinct Neurodevelopmental Disorders

Maria J. Nabais Sá, Geniver El Tekle, Arjan P.M. de Brouwer, Sarah L. Sawyer, Daniela del Gaudio, Michael J. Parker, Farah Kanani, Marie-José H. van den Boogaard, Koen van Gassen, Margot I. Van Allen, Klaas Wierenga, Gabriela Purcarin, Ellen Roy Elias, Amber Begtrup, Jennifer Keller-Ramey, Tiziano Bernasocchi, Laurens van de Wiel, Christian Gilissen, Hanka Venselaar, Rolph Pfundt, Lisenka E.L.M. Vissers, Jean-Philippe P. Theurillat, and Bert B.A. de Vries

Supplemental Data

Supplemental Material and Methods

Cell culture and Infection. Ishikawa cells were purchased from Sigma and grown in F12/DMEM (Dulbecco's Modified Eagle Medium; Gibco, Invitrogen Corporation, Carlsbad, CA, USA) supplemented with 10% fetal bovine serum (FBS; Gibco) and 1% Penicilin/Streptomycin/L-Glutamate. Patient-derived Epstein-Barr Virus (EBV)-immortalized B cell lines were grown in RPMI (Gibco) supplemented with 15% FBS (Gibco), 20 mM HEPES (Gibco) and 1% Penicilin/Streptomycin/L-Glutamate. All cells were incubated at 37°C and 5% CO_2. Cells were routinely tested for mycoplasma contamination. For SPOP over-expression, cells were infected with a derivate of the pLX304 vector in which the cytomegalovirus (CMV) promoter has been exchanged to a PGK promoter and the blasticidin exchanged by a puromycin resistance cassette (pLX_TRC_307, available at Addgene as Plasmid 41392, pCW107). All ORFs were cloned into pLX_TRC_307 using *Nhe*1 and *Mlu*1 (New England BioLabs, Beverly, MA, USA). After infection, cells were selected in the presence of puromycin (2 μg/ml).

Chemicals. MG-132 and Cycloheximide (CHX) were purchased from Sigma and used at 10 μM and 100 μg/ml in all experiments, respectively.

Antibodies and Immunoblotting. Antibodies used in immunoblotting were: anti-BRD2 (A302-583A, Bethyl Labs), anti-BRD3 (Sc-81202, Santa Cruz), anti-BRD4 (Sc-48772, Santa Cruz), anti-SPOP (ab81163, Abcam), and anti-ß- ACTIN (Sc-47778, Santa Cruz). All antibodies were employed at dilutions suggested by the manufacturers. For immunoblotting, cells were washed with PBS and subsequently lysed in radioimmunoprecipitation assay (RIPA) buffer (Sigma) and sonicated. Protein concentration was determined using the bicinchoninic acid assay (BCA) reagent (ThermoFisher),

same amounts of protein were separated by SDS-PAGE (Biorad) and transferred onto polyvinylidene difluoride (PVDF) membrane (ThermoScientific). The membrane was incubated for one hour in 5% nonfat dry milk/TBS-T (Tris-buffered saline-Tween 20) blocking buffer followed by incubation with the primary antibody overnight at 4°C. The membrane was washed with TBS-T followed by incubation with horseradish peroxidase-conjugated secondary antibody (Promega).

Gene Expression Studies. RNA was extracted using the Rnasy kit (Qiagen) and processed by Kapa SybrFAST one-Step qRT-PCR kit according to manufacturer`s instructions. Quantitative PCR (q-PCR) was undertaken on an Applied Biosystems StepOnePlus System. The target mRNA expression was quantified using ΔΔCt method and normalized to *β-Actin* expression. The following primers were used: *BRD2*, forward 5`-CTACGTAAGAAACCCCGGAAG-3', reverse 5`-GCTTTTTCTCCAAAGCCAGTT-3'; *BRD3*, forward 5`-CCTCAGGGAGATGCTATC-CA-3', reverse 5`-ATGTCGTGGTAGTCGTGCAG-3'; *BRD4*, forward 5`-CTCCTC-CTAAAAAGACGAAGA-3', reverse 5`-GCCCCTTCTCTTTTTGACTTCGGA-3'; *SPOP*, forward 5`- GAAATGGTGTTTGCGAGTAAACC-3', reverse 5`-GCCCGAA-CTTCACTCTTTGGA-3'; *β-ACTIN,* forward 5'-AAGGAGCCCCACGAAAAAT-3', reverse 5'-ACCGAACTTGCATTGATTCCAG-3'.

Supplemental References:

[1] Sievers F *et al. Mol. Syst. Biol.* **7,** 539 (2011).

[2] Altschul SF, Gish W, Miller W, Myers EW, Lipman DJ. *J. Mol. Biol.* **215,** 403–410 (1990).

[3] Altschul SF *et al. Nucleic Acids Res.* **25,** 3389–3402 (1997).

[4] Wiel L, Baakman C, Gilissen D, Veltman JA, Vriend G, Gilissen C. *Hum Mutat.* **40,** 1030–1038 (2019).

[5] Wiel L, Venselaar H, Veltman JA, Vriend G, Gilissen C. *Hum Mutat.* **38,** 1454–1463 (2017).

Supplemental Figures

```
O43791_Homo_sapiens                CYTQIKVVKF SYMWTINNFS FCREEMGEVI KSSTFSSGAN DKLKWCLRVN 72
Q6ZWS8_Mus_musculus                CYTQIKVVKF SYMWTINNFS FCREEMGEVI KSSTFSSGAN DKLKWCLRVN 72
Q7T330_Danio_rerio                 CYTQIKVVKF SYMWTINNFS FCREEMGEVI KSSTFSSGAN DKLKWCLRVN 72
NP_650325.1_Drosophila_melanogaster CYTQVKVVKF SYMWTINNFS FCREEMGEVL KSSTFSAGAN DKLKWCLRVN 101
P34568_Caenorhabditis_elegans      CHTQVKVVKF NYMWTINNFS FCREEMGEVL KSSTFSAGCN DKLKWCLRIN 136

O43791_Homo_sapiens                PKGLDEESKD YLSLYLLLVS CPKSEVRAKF KFSILNAKGE ETKAMESQRA 122
Q6ZWS8_Mus_musculus                PKGLDEESKD YLSLYLLLVS CPKSEVRAKF KFSILNAKGE ETKAMESQRA 122
Q7T330_Danio_rerio                 PKGLDEESKD YLSLYLLLVS CPKSEVRAKF KFSILNAKGE ETKAMESQRA 122
NP_650325.1_Drosophila_melanogaster PKGLDEESKD YLSLYLLLVS CNKSEVRAKF KFSILNAKRE ETKAMESQRA 151
P34568_Caenorhabditis_elegans      PKGLDEESRD YLSLYLLLVQ CNKSEVRAKF KFSILNAKRE ETKAMESQRA 186

O43791_Homo_sapiens                YRFVQGKDWG FKKFIRRDFL LDEANGLLPD DKLTLFCEVS VVQDSVNISG 172
Q6ZWS8_Mus_musculus                YRFVQGKDWG FKKFIRRDFL LDEANGLLPD DKLTLFCEVS VVQDSVNISG 172
Q7T330_Danio_rerio                 YRFVQGKDWG FKKFIRRDFL LDEANGLLPD DKLTLFCEVS VVQDSVNISG 172
NP_650325.1_Drosophila_melanogaster YRFVQGKDWG FKKFIRRDFL LDEANGLLPE DKLTIFCEVS VVADSVNISG 201
P34568_Caenorhabditis_elegans      YRFVQGKDWG FKKFIRRDFL LDEANGLLPG DRLSIFCEVS VVAETVNVTG 236
```

Figure S1. Cross-species Alignment by Clustal Omega[1] of the Protein Sequences of the MATH Domain of SPOP, Including the Eight Amino Acid Residues Just Before this Domain. All six mutated amino acids are conserved down to the worm *Caenorhabditis elegans*. Protein accession numbers used for alignment are given before the sequences. The position of the last amino acid residue in each row is given right after the respective sequences. A blastp[2] and (PSI)-BLAST[3] search did not indicate that there is a SPOP orthologue in *Saccharomyces cerevisiae*.

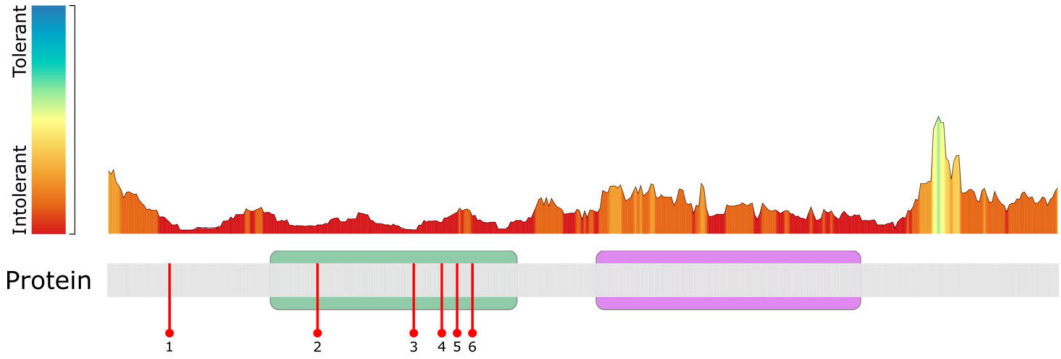

Figure S2. Tolerance Landscape of the Speckle-type POZ Protein (NM_001007226.1, ENST00000393328.2). The tolerance landscape is obtained via MetaDome[4,5] and calculated as a missense over synonymous ratio (based on SNVs present in gnomAD r2.0) computed over the protein-coding part of the *SPOP* gene. The tolerance score is corrected for the sequence composition of the protein coding region based on the total possible missense and synonymous variants and computed as a sliding window of 21 residues over the entirety of the gene's protein. The green/blue peaks correspond to regions more tolerant to missense variation and the red valleys indicate intolerant regions. The protein is schematically represented containing Pfam protein domains annotated as colored boxes. The green box corresponds to the MATH domain (PF00917), and the purple box corresponds to the BTB/POZ domain (PF00651). The found missense variants are annotated as red pins in the following manner: (1) p.(Thr25Ala), (2) p.(Tyr83Cys), (3) p.(Arg121Gln), (4) p.(Gly132Val), (5) p.(Arg138Cys), (6) p.(Asp144Asn). All of these variants are located in very intolerant (dark red) regions to missense variants.

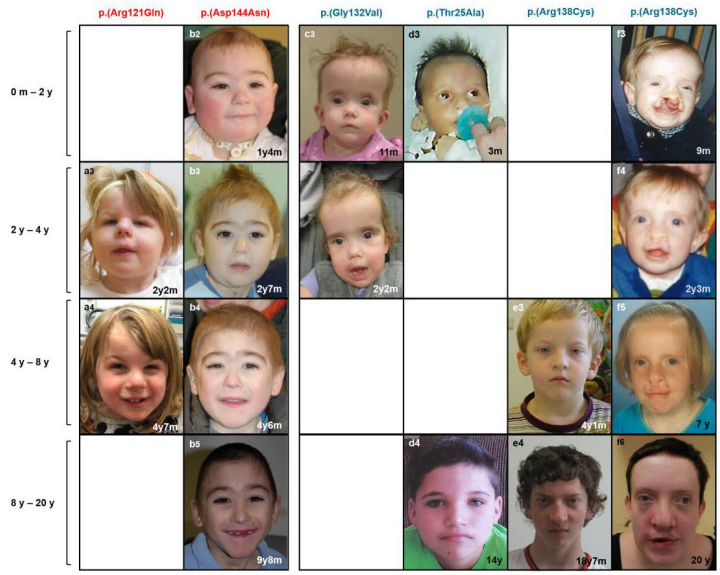

Figure S3. Craniofacial Dysmorphisms of Individuals 1-6 (A-F) with Pathogenic *De Novo SPOP* Variants (gain-of-function in red or dominant-negative in blue) at Different Ages. m: months. y: years. Individuals 1 (**A**) and 2 (**B**) had microcephaly, round face, prominent glabella, depressed nasal bridge, narrow palpebral fissures, short nose with anteverted nares, micrognathia or a pointed chin. Individuals 3 (**C**), 4 (**D**), 5 (**E**) and 6 (**F**) had macrocephaly, a long face, high anterior hairline, high forehead, widely spaced eyes, prominent and wide nasal bridge, wide and bulbous nasal tip, underdeveloped nasal alae, low hanging columella

5

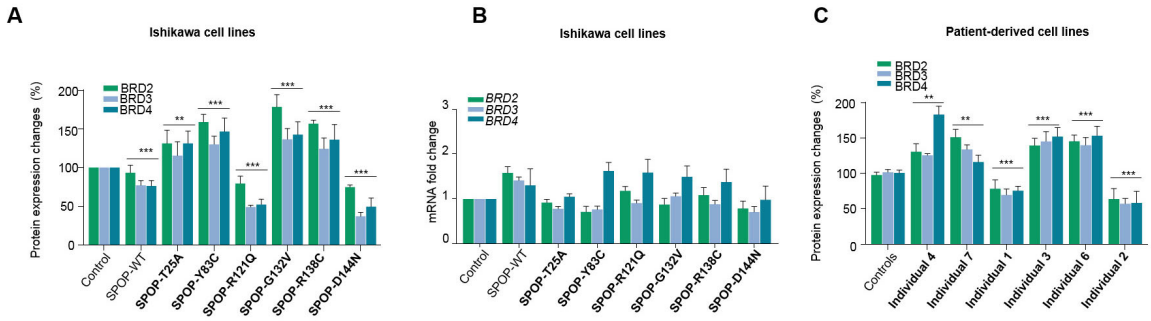

Figure S4. Quantification of BET mRNA and protein expression. A, WB quantification of BRD2, BRD3 and BRD4 proteins normalized to β-ACTIN, shown in Figure 2B, in Ishikawa cells. Protein levels are normalized to the control cell line. **B,** mRNA expression levels of the *BRD2*, *BRD3* and *BRD4* genes normalized to *β-Actin* and Control in Ishikawa cells. All error bars, mean ± s.e.m (n=3, independent experiment). **C,** WB quantification of BRD2, BRD3 and BRD4 proteins normalized to β-ACTIN, shown in Figure 2C, in patient-derived cell lines. Protein levels are normalized to the average levels measured in the three healthy individual cell lines (Controls). All error bars, mean + s.e.m (n=3, independent experiment). P-values were derived from an unpaired, two-tailed Student's t-test (*P < 0.05, **P < 0.01, ***P < 0.001) when comparing BET protein levels to control cell lines.

6

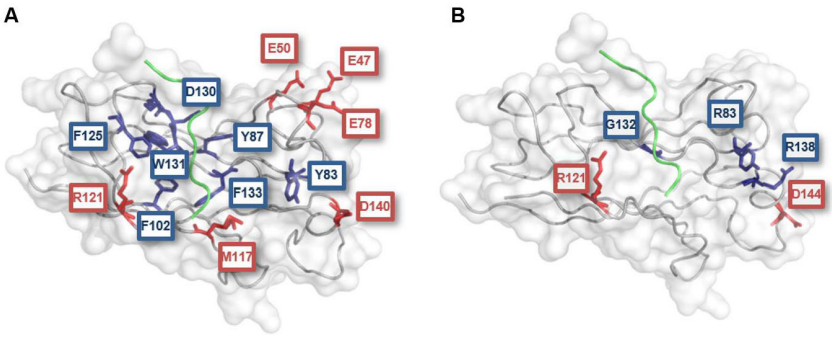

Figure S5. Comparison of the Distribution of Cancer-Associated (Somatic) and NDD-Associated (Germline) *SPOP* Variants within the MATH Domain. A, Recurrently mutated (n≥6) amino acid residues in endometrial cancer and prostate cancer are highlighted in red and blue, respectively (https://cancer.sanger.ac.uk/cosmic/gene/analysis?ln=SPOP#distribution, accessed November 4th 2019). **B,** Mutated amino acid residues in individuals with neurodevelopmental disorders (NDD). Residues with *de novo* gain-of-function and dominant-negative variants are depicted in red and blue, respectively. Please note that all mutated residues shown in B have also been found to be mutated in tumor cell lines (see Table S2), although not all residues were as frequently mutated as those shown in A. This figure was made using PDB file 3IVV.

Reference: Zhuang M *et al*. *Mol Cell*. **36,** 39-50 (2009).

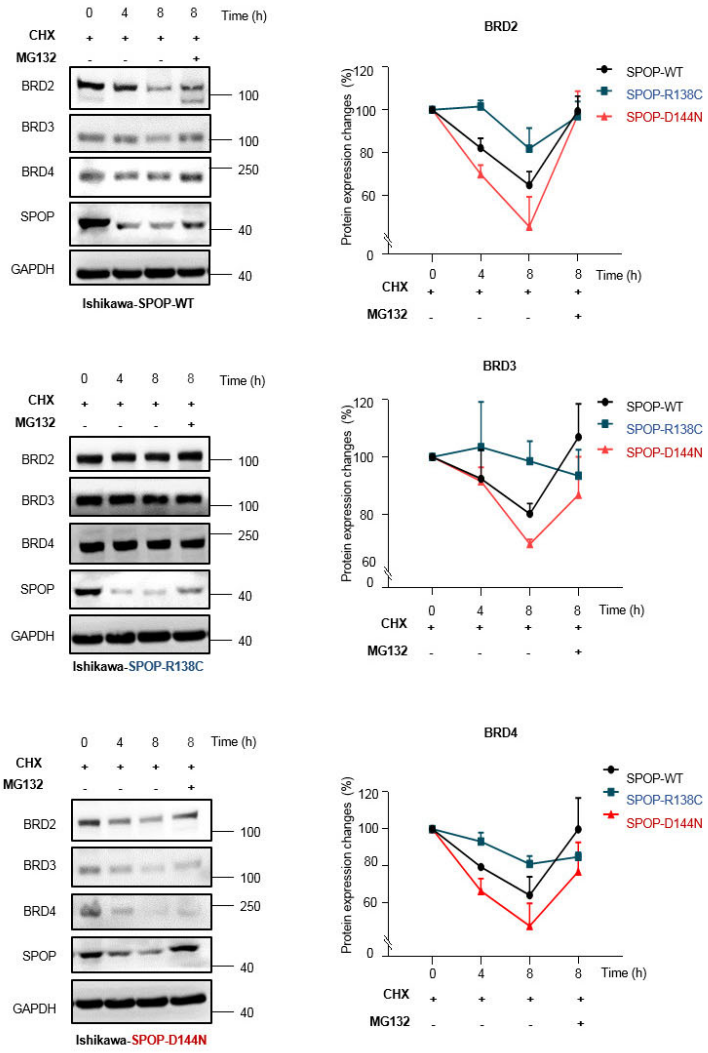

Figure S6. Characterization of BET proteins degradation. Representative immunoblots and quantification of indicated proteins after treatment with cycloheximide (CHX, 100 µg/mL) alone, or in combination with MG132 (10 µM) in Ishikawa cells. All error bars, mean + s.e.m (n=3, independent experiment). Time is indicated in hours (h). Molecular weights are indicated in kilodaltons (kDa).

Table S2. *SPOP* Variants Identified in Both Germline and Somatic Cell Lines.

Location	cDNA change [a]	Amino acid change [b]	Mutation ID in Cosmic [c]	Primary tumor tissue (number of samples) [c]	References (PMID = PubMed IDentifier) [c]	Predicted effect on the protein	References (PMID = PubMed IDentifier)
Variants detected in both germline and somatic cell lines							
Exon 7	c.248A>G	p.(Tyr83Cys)	COSM5414799	Prostate (n=6)	26928463, 24998678	Dominant-negative	25278611, 28805821
Exon 8	c.362G>A	p.(Arg121Gln)	COSM980811	Endometrium (n=8) and lung (n=1)	23104009, 28481359, 25308272, 28485815, 28940304	Gain-of-function	28805821
Exon 8	c.412C>T	p.(Arg138Cys)	COSM4729697	Large intestine (n=2)	27149842, 25344691	NA	n/a
Somatic variants occurring in the same amino acid position as in the germline							
Exon 8	c.395G>A	p.(Gly132Glu)	COSM5414952	Haematopoietic and lymphoid tissue (n=1)	23654205	NA	n/a
Exon 8	c.413G>A	p.(Arg138His)	COSM6938938	Large intestine (n=1)	28481359	NA	n/a
Exon 8	c.413G>C	p.(Arg138Pro)	COSM3728329	Haematopoietic and lymphoid (n=1)	24241536	NA	n/a
Exon 8	c.431A>G	p.(Asp144Gly)	COSM2698398	Large intestine (n=3)	24755471	NA	n/a
Germline variants not observed in somatic cell lines							
Exon 5	c.73A>G	p.(Thr25Ala)	not in Cosmic	n/a	n/a	n/a	n/a
Exon 8	c.395G>T	p.(Gly132Val)	not in Cosmic	n/a	n/a	n/a	n/a
Exon 8	c.430G>A	p.(Asp144Asn)	not in Cosmic	n/a	n/a	n/a	n/a

[a] RefSeq NM_001007226.1.
[b] RefSeq NP_001007227.1
[c] https://cancer.sanger.ac.uk/cosmic/gene/analysis?ln=SPOP#distribution, accessed November 4th 2019.
Abbreviations are as follows: NA, not available; n/a, not applicable.

Table S3. Genotype and Phenotype of Individuals with *De Novo* Pathogenic Mutations in *SPOP*

	Individuals		Individuals				
	1	2	3	4	5	6	7
Gender	F	M	F	M	M	F	F
Current age	4y 7m	10y	10m	17y 11m	17y 9m	20y	15y
Genotype							
cDNA change [a]	c.362G>A	c.430G>A	c.395G>T	c.73A>G	c.412C>T	c.412C>T	c.248A>G
Protein change [b]	p.(Arg121Gln)	p.(Asp144Asn)	p.(Gly132Val)	p.(Thr25Ala)	p.(Arg138Cys)	p.(Arg138Cys)	p.(Tyr83Cys)
Inheritance	*de novo*	*de novo*	*de novo*	*de novo*	*de novo*	*de novo*	*de novo*
Effect on BET proteins	gain-of-function	gain-of-function	loss-of-function	loss-of-function	loss-of-function	loss-of-function	loss-of-function
Phenotype							
Growth [c]							
Gestational age at birth	40w 3d	39w	33w 5d	39w	38w	37w	40w
Length at birth in cm (centile range)	47 cm (10th-25th)	NA	46.4 cm (3rd-10th)	47 cm (10th-25th)	NA	47 cm (10th-25th)	54.6 cm (97th)
Weight at birth in g (centile range)	3.033 kg (10th-25th)	2.409 kg (3rd)	2.575 kg (3rd-10th)	2.700 kg (3rd-10th)	3.070 kg (10th-25th)	3.000 kg (10th-25th)	3.800 kg (75th-90th)
HC at birth in cm (centile range; SD)	32 cm (-3SD) at 16d	NA (microcephaly)	33.5 cm (10th-25th)	35 cm (25th-50th)	NA	NA	NA (macrocephalic)
Age at measurements	4y 7m	16m	10m	17y 11m	17y 9m	20y	15y
Height in cm (centile range)	104.5 cm (~50th)	77 cm (10th-25th)	65.1 cm (-2.5SD)	151.8 cm (-3.1SD)	178.5 cm (50th-75th)	172 cm (90th-97th)	158.8 cm (25th-50th)
Weight in kg (centile range)	15.3 kg (10th-25th)	8.8 kg (-2.3SD)	5.6 kg (-4SD)	49.7 kg (3rd)	73 kg (50th-75th)	89 kg (97th)	90.7 kg (+2.5SD)
HC in cm (centile range)	44 cm (-4SD)	40.5 cm (-5SD)	49 cm (+3.5SD)	NA (25th)	56.4 cm (75th-90th)	57 cm (+2.5SD)	56 cm at 5y (+4SD)
Prenatal and Neonatal History							
Prenatal structural anomalies	+ (long bones < -3 SD)	-	+ (polyhydramnios; breech presentation)	+ (hypoplastic left heart)	-	-	NA
Congenital abnormalities	+ (congenital microcephaly)	+ (congenital microcephaly)	+ (congenital heart disease)	+ (congenital heart disease)	NA	+ (congenital heart disease, bilateral CLP)	+ (multicystic kidney dysplasia)
Other neonatal problems	+ (jaundice requiring phototherapy)	+ (jaundice that self-resolved, respiratory	+ (hypotonia, swallowing dysfunction and feeding	+ (bradycardia, dysrhytmia,	NA	-	+ (hypotonia, respiratory and feeding difficulties)

		difficulties requiring tracheostomy)	difficulties)	thrombocytopenia)			
Psychomotor Development							
Motor delay	+	+	+	+	+	+	+
Age at walking (months)	19m	~ 36m	NA	36m	17m	24m	24m
Speech delay	+	+	+	+	+	+	NA
Age at first words (years)	60 words at 2y 10m	vocalising at ~ 6y	NA	4y	NA	~ 5y	NA
Intellectual disability	n/a	+ (severe)	n/a	+ (IQ=46)	+ (IQ=45)	+ (IQ=53)	+ (mild)
Neuropsychiatric Abnormalities							
Epilepsy	-	NA	-	+	+	NA	-
Other neurological abnormalities	+ (hypertonia)	-	+ (central hypotonia)	+ (left hemiparesis, intractable migraines, dystonia, chorea)	NA	NA	-
Brain MRI abnormalities (years)	+ (5 y: simplified gyri)	NA	+ (4 m: enlargement of all ventricles, prominent subarachnoid spaces and bifrontal extra-axial fluid spaces; 17 m: mildly increased ventriculomegaly; symmetrically dysmorphic hippocampi)	+ (16y: borderline enlarged ventricles and slightly small corpus callosum splenium)	- (5y)	NA	-
Behavioral abnormalities	+ (decreased stranger anxiety)	+ (autoagression)	NA	+ (overfriendliness, ADHD, agitation)	+ (autism)	+ (severe temper tantrums)	+ (anxiety)
Craniofacial dysmorphims							
Cranium/Forehead	brachycephaly, prominent glabella	narrow forehead, low anterior hairline	frontal bossing, triangular face	-	large forehead	large forehead	large forehead
Ear	dysplastic simple ears with thickened helix	-	low-set small ears	low-set small ears	protruding ears	low-set posteriorly rotated ears	-
Eye	highly arched eyebrows, underdeveloped supraorbital ridges, downslanted narrow palpebral fissures, deeply set eyes	highly arched eyebrows, synophrys, long eyelashes, epicanthus, telecanthus, narrow palpebral fissures	hypertelorism, deep set eyes	hypertelorism	hypertelorism, long palpebral fissures, sparse and thin eyebrows	hypertelorism, sparse and thin eyebrows	asymmetric palpebral fissures
Nose	prominent nasal bridge, wide and bulbous nasal	low and wide nasal bridge, wide and	short, low nasal bridge, upturned nares	-	prominent nasal bridge, bulbous nasal tip	prominent and wide nasal bridge, wide and	prominent nose

	tip, underdeveloped nasal alae	bulbous nasal tip, short nose				bulbous nasal tip	
Mouth	flat philtrum	flat philtrum	wide gums	high-arched palate	-	bilateral CLP	thin lips
Chin	pointed chin	pointed chin	micrognathia	pointed chin	pointed chin	-	-
Hands	clinodactyly of the 5th digits bilaterally	-	-	-	NA	distally tapered, long fingers; clinodactyly of the 5th fingers	-
Feet	-	-	-	-	NA	short wide feet, pes cavus, short broad halluces	-
Other phenotypic abnormalities							
Hearing impairment	+ (sensorineural hearing loss)	+ (bilateral hearing loss)	-	-	-	-	-
Ophthalmologic abnormality	-	+ (bilateral optic nerve hypoplasia)	+ (small optic discs)	+ (abnormality of refraction)	-	+ (strabismus)	+ (abnormality of refraction)
Cardiovascular abnormality	-	-	+ (small VSD, PS and supravalvular PS, mild right ventricular outflow obstruction)	+ (variant of hypoplastic left heart syndrome [ASD, small LV, MV and Ao] with left ventricular outflow tract obstruction [subaortic membrane, bicuspid aortic valve, coartation of the descending Ao])	NA	+ (ASD)	+ (PDA and small VSD)
Respiratory abnormality	-	+ (tracheostomy at 3 m)	-	+ (episode of hemoptysis)	NA	-	-
Gastrointestinal abnormality	-	+ (gastrostomy at 3 m)	+ (choking episodes, GERD, Sandifer syndrome, gastrostomy at 6 m)	-	NA	-	+ (chronic constipation, GERD)
Urogenital abnormality	-	+ (bilateral vesicoureteric reflux)	-	+ (hypogonadism)	+	NA	+ (left multicystic kidney disease)
Skin abnormality	-	-	-	-	NA	-	+ (eczema)
Endocrine abnormality	-	-	-	+ (testosterone treatment)	+ (hypothyroidism)	NA	+ (hypothyroidism)
Sleep disturbance	-	NA	-	+ (sleep apnea)	+	+ (sleep apnea)	+ (sleep apnea)
Other	+ (sacral dimple)	-	+ (failure to thrive)	+ (failure to thrive in infancy, bleeding disorder with platelet	NA	NA	+ (unusual fat distribution)

		dysfunction, chronic jaundice, mild scoliosis, osteoporosis and vitamin D deficiency)

[a] NM_001007226.1.
[b] NP_001007227.1.
[c] percentile range; if percentile <3rd or >97th, standard deviation (SD) is indicated.
Abbreviations are as follows: +, present; -, absent; F, female; M, male; y, years; m, months; w, weeks; d, days; SD, standard deviation; HC, head circumference; CSF, cerebrospinal fluid; Ao, aorta; MV, mitral valve; LV, left ventricule; ASD, atrial septal defect; VSD, ventricular septal defect; PDA, patent ductus arteriosus; PS, pulmonary stenosis; ADHD, attention deficit hyperactivity disorder; IQ, intelligence quotient score; CLP, cleft lip and palate; GERD, gastroesophageal reflux disease; NA, not available; n/a, not applicable.

ARTICLE 3

(Under Review)

Dual Functions of SPOP and ERG Dictate Differential Therapy Responses in Prostate Cancer

Tiziano Bernasocchi[1,2*], Geniver El Tekle[1,2*], Marco Bolis[1*], Azzurra Mutti[1], Arianna Vallerga[1], Laura P. Brandt[3], Filippo Spriano[1,2], Tanya Svinkina[4], Marita Zoma[1,2], Valentina Ceserani[1], Anna Rinaldi[1], Hana Janouskova[1], Daniela Bossi[1], Manuela Cavalli[1], Simone Mosole[1], Roger Geiger[5], Ze Dong[6], Cai-Guang Yang[6], Domenico Albino[1], Andrea Rinaldi[1], Peter Schraml[7], Simon Linder[8], Giuseppina M. Carbone[1], Andrea Alimonti[1], Francesco Bertoni[1], Holger Moch[7], Steven A. Carr[4], Wilbert Zwart[8], Marianna Kruithof-de Julio[3], Mark A. Rubin[3], Namrata D. Udeshi[4], Jean-Philippe P. Theurillat[1+]

[*] These authors contributed equally to this work.

[+]Correspondence to: JeanP_Theurillat@ior.iosi.ch

[1]Institute of Oncology Research, Faculty of Biomedical Sciences, USI, Bellinzona, TI 6500, Switzerland. [2]University of Lausanne, Lausanne, VD 1011, Switzerland. [3]Department of Biomedical Research, University of Bern, 3008 Bern, Switzerland. [4]The Broad Institute of MIT & Harvard, Cambridge, MA 02142, USA. [5]Institute for Research in Biomedicine, Bellinzona, TI 6500, Switzerland. [6]State Key Laboratory of Drug Research, Shanghai Institute of Materia Medica, Chinese Academy of Sciences, Shanghai 201203, China. [7]Department of Pathology and Molecular Pathology, University Hospital Zurich, Zurich, ZH 8091, Switzerland. [8]The Netherlands Cancer Institute, Oncode Institute, 1066CX Amsterdam, Netherlands.

Driver genes with a mutually exclusive mutation pattern across tumor genomes are thought to have overlapping roles in tumorigenesis. In contrast, we show here that mutually-exclusive prostate cancer driver alterations involving the *ERG* transcription factor and the ubiquitin ligase adaptor *SPOP* are synthetic sick. At the molecular level, the incompatible cancer pathways are driven by opposing functions in SPOP. ERG up-regulates wild type SPOP to dampen androgen receptor (AR) signaling and sustain ERG activity through degradation of the bromodomain histone reader ZMYND11. Conversely, SPOP-mutant tumors stabilize ZMYND11 to repress ERG-function and enable oncogenic androgen receptor signaling. This dichotomy regulates the response to therapeutic interventions in the AR pathway. While mutant SPOP renders tumor cells susceptible to androgen deprivation therapies, ERG promotes sensitivity to high-dose androgen therapy and pharmacological inhibition of wild type SPOP. More generally, these results define a distinct class of antagonistic cancer drivers and a blueprint toward their therapeutic exploitation.

Normal cells transform into cancer cells by the acquisition of genetic aberrations in so-called driver genes. In some instances, the functional redundancy of mutations in different genes result in a mutually-exclusive mutation pattern across tumor genomes because one alteration is sufficient to activate the specific oncogenic pathway. Based on this assumption, bioinformatic tools have been generated to search for functional redundancy of mutated genes in larger cancer genome data sets [247, 248].

In prostate cancer, recurrent gene fusions involving the *ERG* transcription factor and point mutations in the ubiquitin ligase adaptor *SPOP* are two truncal mutations that are mutually exclusively distributed across tumor genomes (Fig. 1a and Extended Data Fig. 1a)[47-51]. The underlying cause for this exquisite pattern remains controversial. While earlier reports suggested a functional redundancy between mutant SPOP and ERG based on the finding that mutant SPOP stabilizes the ERG oncoprotein[147, 249], more recent studies challenge this view by showing descriptive evidence for divergence in tumorigenesis[51, 250].

RESULTS

Activation of the ERG oncogene and missense mutation in SPOP are synthetic sick

To shed light into the functional relationship of these recurrent driver genes, we assessed the impact of

SPOP mutations and ERG activation on the cellular growth of mouse prostate epithelial organoids. In agreement with recent reports, lentiviral-transduced point mutants of SPOP (SPOP-Y87C, SPOP-W131G) or a truncated version of ERG, which typically results from gene fusion with androgen-regulated genes in prostate cancer (ΔERG, amino acids 33-486), promoted cell growth (Fig. 1b, Extended Data Fig. 1b)[57, 139, 251, 252]. While SPOP mutant organoids displayed a round shape, the over-expression of ΔERG gave rise to characteristic finger-like protrusions. Surprisingly, the joint expression of both drivers considerably diminished cell growth and reduced finger-like protrusions, implying a synthetic sick relationship between the two genetic alterations. Cytological follow up analysis revealed reduced proliferation (evidenced by reduced Ki-67 and increased p16 positivity) rather than cell death as underlying cause (Extended Data Fig. 1c).

We wondered if the observed synthetic sick relationship also applied to established cancer cells from advanced, castration-resistant metastatic disease. Forced expression of mutant SPOP (SPOP-Y87C, SPOP-W131G) promoted 3D growth of *ERG* fusion-negative LAPC-4 human prostate cancer cells. The oncogenic effect was paralleled by an increase in the expression of the oncogenic transcription factors MYC and HOXB13 and a decrease in the cell cycle inhibitor p21 as seen also in an organoid line derived from $Spop^{F133V}$-mutant transgenic mice (Extended Data Fig. 1d, e)[139]. In contrast, we observed the opposite phenotypic and molecular changes in VCaP human prostate cancer cells harboring the recurrent *TMPRSS2-ERG* fusion (Fig. 1c, d & Extended Data Fig. 1f-h). In this setting, mutant SPOP (SPOP-Y87C, -F102C, -W131G, -F133S) dramatically decreased the proliferation of cancer cells in culture and the growth of xenograft tumor models *in vivo*. Conversely, forced expression of ΔERG significantly reduced the growth of SPOP-Y83C mutant LuCaP-147 patient-derived xenograft (PDX) cancer cells *in vivo* and in culture (Fig. 1e, Extended Data Fig. 2a, b)[253], adding orthogonal support for a synthetic sick relationship between mutant SPOP and ΔERG in advanced prostate cancer. In addition, over-expression of MYC promoted cancer cell growth in both VCaP and LuCaP-147 cells (Extended Data Fig. 2c, d). The latter finding largely excludes that the over-expression system *per se* is the underlying cause of the synthetic sick relationship mentioned above.

Next, we wondered if genetic or pharmacologic suppression of ERG signaling may revert the growth suppressing function of mutant SPOP in VCaP cells. Indeed, knockdown of ERG by short-hairpin RNA interference decreased the growth of VCaP control cells and of cells over-expressing wild-type SPOP, while

it promoted the growth of cells over-expressing SPOP-W131G (Extended Data Fig. 2e). In addition, low doses of the ETS inhibitor YK-4-279 promoted specifically the growth of VCaP cells over-expressing mutant SPOP (Fig. 1f). We noted a similar effect when VCaP cells were co-treated with a small molecule inhibitor of SPOP (Extended Data Fig. 2f)[225]. In aggregate, the data support an antagonistic relationship between oncogenic activation of ERG and a loss of SPOP function in prostate cancer cells.

Mutant SPOP induced androgen receptor signaling antagonizes ERG activity

In *SPOP* mutant prostate cancer, several dysregulated SPOP substrates (e.g. NCOA3, TRIM24, BET proteins) have been shown to boost the AR pathway [51, 127, 131, 139-141, 228, 254-256], leading ultimately to high levels of AR target genes and increased AR binding affinity in human tumor tissues (Extended Data Fig. 2g,h)[51, 257]. In contrast, *ERG*-fused cancer cells express typically lower levels of AR target genes (Extended Data Fig. 2h)[51]. In line with this, the principle component analysis (PCA) of primary cancers also shows a marked difference in the transcriptional output of both tumor subtypes that remains detectable in advanced metastatic disease tissues and derived xenograft models (Extended Data Fig. 2i,j).

We posited that differential levels of androgen receptor (AR) signaling in *SPOP* mutant versus *ERG*-fused cancers may be at the root of the incompatibility between these driver events. Thus, we analyzed the effect of mutant SPOP (SPOP-MTs; SPOP-Y87C, -F102C, -F133S) on AR- and ERG-related transcription in VCaP cells, and generated custom signatures using ChIP-seq data and matched RNA seq samples (Supplementary Table 1)[258]. As expected, SPOP-MTs increased the transcription of genes bound by AR and induced by its ligand dihydrotestosterone (DHT), whereas genes bound by AR and repressed by DHT were further reduced (Fig. 2a, Extended Data Fig. 3a, b, and Supplementary Data Table 1). Remarkably, we observed the opposite effect on genes bound only by ERG. Mutant SPOP downregulated ERG-induced genes (e.g. MYC) and upregulated ERG-repressed genes, respectively (Fig. 1d). In line with these findings, we found the most striking transcriptional changes in co-bound genes linked to cellular differentiation and cell cycle arrest that are directly induced by DHT and repressed by ERG (e.g. HOXA genes, CDKN1A/p21, Fig. 1d, Fig. 2b, Extended Data Fig. 3b, c).

The dramatic upregulation of this geneset was paralleled by a downregulation of cell cycle genes (e.g. E2F and MYC targets), implying a direct link between the induction AR/ERG co-bound genes, the repression of

ERG targets, cell differentiation and the synthetic sick relationship of ERG and mutant SPOP (Fig. 1d, Fig. 2c, Extended Data Fig. 3d-e).

Conversely, we assessed the consequence of ERG over-expression in LNCaP cells under low DHT levels where mutant SPOP triggers AR signaling and tumor growth (Extended Data Fig. 3f,g)[140, 141]. Over-expression of ΔERG in this setting robustly reverted the induction of signatures related to cell proliferation (e.g. E2F and MYC targets) and AR signaling. Taken together, the data implies a reciprocal incompatibility of mutant SPOP induced AR signaling and the function of the ERG oncogene.

Next, we verified if corresponding transcriptional changes were found in clinical tissue samples. Indeed, ERG-regulated genes culled from VCaP cells were up-regulated in *ERG*-fused and down-regulated in *SPOP*-mutant primary tumors (Fig. 2d, Extended Data Fig. 4a)[51]. Importantly, the most striking changes between the two groups were found again in the AR/ERG co-bound gene set in primary prostate cancers (Extended Data Fig. 4b)[49, 51]. The results underscore both the relevance of our cell culture-based data and highlight the transcriptional differences among *ERG*- and *SPOP*-driven tumors.

ZMYND11 is a SPOP substrate that induces AR and represses ERG transcription

Using tandem mass tag (TMT)-based quantitative mass-spectrometry, we set out to search for SPOP substrates that may influence the activity of AR and ERG and thereby may cause to the synthetic sick relationship between mutant SPOP and ERG in VCaP cells overexpressing mutant SPOP (SPOP-MTs; SPOP-Y87C, -F102C, -W131G, Extended Data Fig. 4c). Because recurrent loss-of-function SPOP mutants impair substrate ubiquitylation and proteasomal degradation, we searched for proteins which expression levels increase without concomitant increase in mRNA levels (Fig. 3a, Extended Data Fig. 4c, d). Overall, we noted a strong correlation of protein with mRNA expression changes with consistent changes of our AR and ERG custom signatures at the protein level (Fig. 3a., Extended Data Fig. 4e). In addition, we found a marked upregulation of the known SPOP substrate and AR activator TRIM24 at the protein level (Fig. 1c & 3a, Supplementary Table 2)[141, 255] and subsequently assessed if TRIM24 and more generally AR is implicated in the synthetic sick relationship between mutant SPOP and ERG. Indeed, knockdown of TRIM24 by two short hairpin RNAs partially reverted the growth inhibition mediated by mutant-SPOP in VCaP cells and reduced AR signaling (Extended Data Fig. 4f, g), while over-expression of AR was sufficient to decrease

cellular growth (Extended Data Fig. 4h, i).

The most striking upregulation was noted for the bromodomain histone reader ZMYND11 (Fig. 3a, Extended Data Fig. 4d). In line with a SPOP substrate, wild type SPOP bound, ubiquitylated and decreased the expression of HA-ZYMND11 in a proteasome-dependent manner (Extended Data Fig. 5a, b). We found two degron sequences that were required for efficient SPOP-mediated ubiquitylation and protein degradation (Extended Data Fig. 5c-f). As expected, SPOP mutants failed to bind and adequately ubiquitylate HA-ZMNYD11-WT (Extended Data Fig. 5g-i)[127, 131, 147, 228, 249, 254-256]. Finally, we confirmed that expression of mutant SPOP prolonged the half-life of endogenous ZMYND11 in VCaP cells and upregulated ZMYND11 expression in other prostate cancer cells (Extended Data Fig. 5j, k).

Next, we assessed if ZMYND11 protein upregulation also contributed to the synthetic sick relationship. In support, forced expression of the degron-deficient variants of ZMYND11 (HA-ZMYND11-DMT1/DMT2) was sufficient to diminish the growth of VCaP cells (Fig. 3b, Extended Data Fig. 6a, b), while knockdown of ZMYND11 partially reverted the growth inhibition mediated by mutant SPOP (Fig. 3c).

We postulated that ZMYND11 up-regulation could contribute to the synthetic sick relationship by repressing the transcriptional activity of the ERG oncogene or enhancing AR signaling. To this end, expression changes induced by HA-ZMYND11-DMT2 largely overlapped with genes perturbed by mutant SPOP while the opposite was noted when ZMYND11 expression was reduced by RNA interference (Fig. 3c, d, Extended Data Fig. 6c). In comparison to mutant SPOP, AR and ERG target genes were similarly dysregulated by HA-ZMYND11-DMT2 (Fig. 3e). Because the PWWP domain of ZMYND11 has been involved in the regulation of transcription through its ability to bind H3K36me3 histone marks [259], we tested the contribution of this domain to the overall transcriptional output. Indeed, the PCA of VCaP cells over-expressing either HA-ZMYND11-DMT2 or a PWWP domain deficient mutant (W294A) revealed a major contribution of this domain to the ZMYND11 induced transcriptional changes (Extended Data Fig. 6d). We subsequently mapped the genomic occupancy of ZMYND11 in VCaP cells expressing the SPOP-Y87C mutant by chromatin immunoprecipitation sequencing (ChIP-seq) and found an enrichment of ZMYND11 binding sites at promoter regions controlling ERG-induced genes (e.g. MYC,) and AR/ERG co-bound genes (e.g. p21/CDKN1A) (Fig. 3b, f, g, Extended Data Fig. 6e-i). The data imply a critical enhancer function of ZMYND11 in boosting AR

signaling and repressing ERG signaling downstream of mutant SPOP.

Wild type SPOP is required for ERG oncogenic function

We reasoned that ERG-driven tumors might require wild type SPOP to degrade ZMYND11 and thereby unlock the oncogenic function of ERG. In support, over-expression of wild type SPOP increased the 3D growth of mouse prostate epithelial organoids and VCaP cells only when ERG was over-expressed (Fig. 1b, Extended Data Fig. 2e, 7a, b). Remarkably, ERG-fused human tumor tissues displayed also the highest SPOP mRNAs levels (Fig. 4a). Thus, we wondered if ERG itself may directly upregulate SPOP transcription to support its own oncogenic activity. Indeed, mining ERG ChIP-seq data in VCaP cells revealed ERG bindings sites in the promoter region of SPOP (Extended Data Fig. 7c). Moreover, knockdown of ERG reduced SPOP protein levels in VCaP cells, while forced expression of a ΔERG led to the upregulation of SPOP mRNA and protein levels in PC3 cells (Fig. 4b, Extended Data Fig. 2e, 7d).

We then asked if the elevated SPOP levels in the context of forced ΔERG expression have a functional impact on the oncogenic activity of ΔERG in the androgen-independent PC3 cells, in which ERG promotes tumor cell invasion [260]. Indeed, the reduction of SPOP levels by RNA interference reduced the ability of ΔERG to invade into matrigel (Fig. 4c). Similarly, knockdown of SPOP in VCaP cells reduced cell growth in 3D cell culture and impaired ERG-mediated gene transcription (Extended Data Fig. 7e, f). In accordance with the ability of mutant SPOP to repress the function of endogenous wild type SPOP in a dominant-negative manner, the over-expression of mutant SPOP (SPOP-Y87C, -F102C, -W131G, -F133S) phenocopied the effect of SPOP knockdown on ERG-mediated invasion in PC3 cells (Extended Data Fig. 7g, h). In agreement with the established repressive function of ZMYND11 on ERG, we found that over-expression of HA-ZMNYD11-DM2 was sufficient to repress ERG-induced invasion and established target genes in PC3 cells (Fig. 4d, e). Taken together, the data imply the existence of a positive feed-forward loop, in which ΔERG promotes the expression of SPOP to sustain its oncogenic activity.

ERG and mutant SPOP trigger different responses to therapeutic interventions

Based on the above-mentioned differences in tumorigenesis, we speculated that ERG or mutant SPOP could also trigger different therapeutic responses. In light of the dependency of ERG-driven tumors on wild

type SPOP function, we hypothesized that *ERG*-fusion positive cells may be particularly sensitive to pharmacological inhibition of SPOP. We analyzed the response of the SPOP small molecule inhibitor compound 6b (SPOP-i) in *ERG*-fused, *SPOP* mutant and other prostate cancer cell lines and patient-derived xenograft models (PDX) [225]. The SPOP inhibitor increased the protein but not the mRNA levels of established SPOP substrates and ZMNYD11 while the related inactive analog compound 6c did not (Extended Data Fig. 8a-c). The latter did also not exert any activity in 3D culture models (Extended Data Fig. 8d). In agreement with our previous results, we found that *ERG*-fused cells (VCaP, LuCaP-23.1, -35) were more sensitive to SPOP-i than *ERG*-negative cells (22Rv1, LNCaP, PC3), while *SPOP* mutant cells (LuCaP-78, -147) were particularly insensitive in 3D culture models and in xenograft tumor models *in vivo* (Fig. 5a and Extended Data Fig. 8e-j). Strikingly, the sensitivity to SPOP-i *in vivo* correlated well with ERG protein expression levels in the respective *ERG*-fusion positive cell line and PDX model (Fig. 5b). We further validated our results in the mouse prostate epithelial organoids and confirmed the increased sensitivity of ΔERG-expressing cells to SPOP inhibition in this isogenic system (Fig. 5c).

Given the notion that wild type SPOP dampens AR function in the context of ERG to sustain tumor growth, we asked if VCaP cells are particularly susceptible to increased DHT levels. Indeed, exposure to high-dose of testosterone *in vivo* or DHT *in vitro* induced similar molecular changes as for the over-expression of mutant SPOP and greatly suppressed the growth of *ERG*-fusion positive cells but not of *SPOP* mutant cells *in vitro* and *in vivo* (Fig. 1c, 5a, d and Extended Data Fig. 9a-i). In analogy to SPOP inhibition, the sensitivity to high testosterone *in vivo* correlated very well with ERG protein expression levels in the respective *ERG*-fusion positive cell line and PDX models (Fig. 5b). The data suggests a therapeutic opportunity for SPOP inhibition or high-dose androgen therapy in prostate cancers that express high levels of ERG.

Conversely, and because *SPOP* mutant cancers are driven predominantly by androgen signaling and consequently display high-level activation of AR-related transcripts in human tumor tissues, we speculated that these tumors may be particular susceptible to androgen deprivation or anti-androgen therapies (ADT) (Extended Data Fig. 2h). Indeed, the prevalence of *SPOP* mutations in primary tumors -and tumors that had progressed after initial surgery or radiotherapy- is consistently higher as compared to tumors that had become resistant to subsequent ADT (also referred as castration-resistant prostate cancer, CRPC, Extended Data Fig.

9j). In line with the notion that this difference may be related to a better response of SPOP mutant tumors to ADT, SPOP mutant tumor display a trend towards better overall survival despite progressing faster after initial therapy (Extended Data Fig. 9k, l). To functionally analyze the response of androgen deprivation or the anti-androgen enzalutamide, we chose to ectopically expressed different SPOP variants and ΔERG in the androgen-dependent human LAPC4 prostate cancer cells that are wild-type for both driver genes. In accordance with the clinical observation, the presence of mutant SPOP (SPOP-Y87C, SPOP-W131G) rendered LAPC4 cells more susceptible to either ADT or enzalutamide in comparison to cells expressing control vector (Fig. 5e, Extended Data Fig. 9m). In contrast, ΔERG rendered the same cells more resistant to enzalutamide. In line with the previous findings in VCaP and LuCaP-147 cells, ΔERG expression rendered LAPC4 cells susceptible to high levels of DHT, while mutant SPOP had the opposite effect (Extended Data Fig. 9m). Taken together, the different responses to established and experimental therapeutic modalities observed between mutant SPOP and ERG add further credence to their divergent roles of the AR pathway related to tumorigenesis.

DISCUSSION

Although multiple studies over recent years have uncovered different genetically-defined subtypes of primary prostate cancer, their biological understanding and therapeutic implications remain largely unexplored territory. Here, we report two diametrically different paths toward tumorigenesis triggered by either highly recurrent missense mutation in *SPOP* or gene fusion involving the *ERG* oncogene. Importantly, wild type SPOP emerges as a critical component that enforces oncogenic ERG signaling in part through dampening AR activity, while mutant SPOP drives tumorigenesis through activation of AR signaling. In addition, we show that the bromodomain histone reader ZMYND11 is a SPOP substrate implicated downstream of SPOP in the opposing regulation of the ERG and AR pathway in the two tumor subtypes (Extended Data Fig. 10a). The AR and ERG pathways have been previously reported to have a partially antagonistic relationship [261, 262], further corroborating our findings.

Because activation of the androgen receptor by androgens represents a key lineage specific oncogenic pathway in prostate cancer, androgen deprivation/antagonization therapies (ADT) remain the uniform treatment modality up to this very day. That said, the responses to ADT are highly variable and may last from a few weeks up to many years. Here, we provide functional evidence that pre-existing prostate cancer founder

mutations influence the treatment response. Most notably, *SPOP* mutations promote susceptibility to androgen deprivations therapies. In agreement with our findings, earlier reports have shown underrepresentation of *SPOP* mutant tumors in cohorts of castration-resistant disease and a more favorable response to the abiraterone and enzalutamide[102, 263].

Conversely, we show that the presence of the ERG oncogene increases the susceptibility of tumor cells to high-dose androgen therapy, while cells expressing mutant SPOP remain largely unaffected. This is of clinical interest because testosterone treatment of patients with advanced castration-resistant disease has recently shown to trigger anti-tumor responses in around one third of the patients[264]. It is tempting to speculate that these insights may help to discern responders from non-responders.

In addition, we provide evidence that the antagonistic relationship between mutant SPOP and ERG may be used towards the development of new therapeutic avenues. More specifically, we show that ERG-driven cancer cells are particularly sensitive to the inhibition of wild-type SPOP using recently developed small molecule inhibitors[225]. Our preclinical data suggests that SPOP inhibition may be effective in clinical settings where ERG is robustly expressed (e.g. neo-adjuvant setting or early metastatic disease).

More generally, our results identify another paradigm for antagonistic driver genes in prostate cancer that has recently emerged also for other cancer types [265-267]. In analogy to prostate cancer, truncal point mutations in *DNMT3A* and gene fusions in *PML-RARA* are mutually exclusive drivers in acute myeloid leukemia (AML). Similarly to SPOP, intact DNMT3A has been found to be critical for PML-RARA-driven leukemia (Extended Data Fig. 10b, c) [268, 269]. Importantly, we demonstrate here for prostate cancer that the concept of antagonistic driver genes can be exploited to identify therapeutic opportunities.

Acknowledgements

We thank the University of Washington and Eva Corey and Donna M. Peehl for providing the Patient-Derived Xenografts (PDX) models. We thank Martina Storz, Susanne Dettwiler, Carmen Gavrisan, and Christiane Mittmann for histology assistance. We thank Enrica-Mira Catò and all members of the IOR/IRB animal core facility for technical assistance and the animal work. In addition, we thank all member of the laboratory for scientific discussions. The results shown here are in whole or part based upon data generated by

the TCGA Research Network: https://www.cancer.gov/tcga. J.P.T is funded by a Swiss National Science Foundation Professorship (PP00P3_150645 & PP00P3_179072) grant, and grants by the Swiss Cancer League, the Lega Ticinese contro il cancro, and the Fidinam Foundation. This work was also supported in part by grants from the National Cancer Institute (NCI) Clinical Proteomic Tumor Analysis Consortium grants NIH/NCI U24-CA210986 and NIH/NCI U01 CA214125 (to S.A.C.).

Author Contributions

T.B. and J.P.T. originally developed the concept, further elaborated on it and designed the experiments together with G.E.T. and M.B. ; T.B. and G.E.T. performed experiments and analyzed the data together with N.D.U., S.A.C., A.M., T.S., L.P.B., F.S., M.Z., V.C., Anna R., H.J., D.B., M.C., D.A. and R.G.. T.B. and G.E.T. performed xenograft tumor experiments in immunodeficient mice. Z.D. and C.G.Y. provided SPOP 6b and SPOP 6c compounds. M.S. , S.D. and S.M. performed immunohistochemical experiments and J.P.T the subsequent analysis. H.M. and P.S. provided prostate cancer samples. M.B., A.V. and Andrea R. analyzed genomic and RNA-Seq data. J.P.T, H.M., S.A.C., M. A. R., M.K.J., A.A., F.B., W.Z. and G.M.C provided funding and resources. J.P.T., T.B., G.E.T. and M.B. interpreted the data and wrote the paper. T.B., G.E.T. and M.B. contributed equally to this work.

Author Information

MAR is listed as a co-inventor on US and International patents in the diagnostic and therapeutic fields of ETS gene fusion prostate cancers (Harvard and University of Michigan) and SPOP mutations (Weill Cornell Medicine). JPT has received funding for the venue of scientific conferences from Astellas, MSD, and Janssen/Cilag. The remaining authors declare no competing financial interests. Correspondence and requests for materials should be addressed to J.P.T. (JeanP_Theurillat@ior.iosi.ch)

Methods

Cell culture, Transfection and Infection

VCaP, LNCaP, PC3, 22Rv1, HEK293 cells were purchased from ATCC. LAPC-4 were a gift from Prof. Helmut Klocker. VCaP and HEK293 were grown in DMEM with Glutamax (Gibco); LNCaP, PC3, 22Rv1, LAPC-4 in RPMI medium (Gibco); all were supplemented with 10% full bovine serium (FBS; Invitrogen), or

10% charcoal-stripped serum (CSS; One Shot Fetal Bovine Serum, Charcoal Strippped, Gibco) for androgen deprivation therapy response, and 1% Penicilin/Streptomycin. LuCaP-147 were grown in StemPro medium (hESC SFM StemPro, Gibco) with regular supplements. All cells were incubated at 37°C and 5% CO_2 and routinely tested for mycoplasma contamination.

For stable knockdown experiments, cells were infected with pLKO-1 vectors (Sigma) and the following clones were used; *SPOP*: TRCN0000140431 (shSPOP_1) and TRCN000013911 (shSPOP_2); *TRIM24*: TRCN000021262 (shTRIM24_1) and TRCN0000195528 (shTRIM24_2); *ERG*: TRCN0000429354 (shERG_1) and TRCN0000432394 (shERG_2); *ZMYND11*: TRCN0000275479 (shZMYND11_1) and TRCN0000275542 (shZMYND11_2). After infection, cells were selected in the presence of puromycin (2 μg/ml).

For SPOP, ΔERG, HA-ZMYND11-WT, HA-ZMYND11-DMT1, HA-ZMYND11-DMT2, MYC and AR over-expression a derivate of the pLX304 vector was used throughout in which the CMV promoter has been exchanged to a PGK promoter and the blasticidin cassette left unchanged (ΔERG constructs) or exchanged by a puromycin resistance cassette (SPOP constructs) (pLX_TRC_307, available at Addgene as Plasmid 41392, pCW107). All ORFs were cloned into pLX_TRC_307 using Nhe1 and Mlu1. Tumors from PDX LuCaP-78, -147, -35,-23.1 were collected, dissociated and cultured as previosly described[270].

Chemicals

MG-132 (M7449) and Cycloheximide (CHX, C4859) were purchased from Sigma and used at 20 μM and 100 μg/ml in all experiments, respectively. SPOP inhibitor (SPOP-i, compound 6b) and its inactive analog (compound 6c), were provided by the laboratory of C. Yang (State Key Laboratory of Drug Research, Shanghai Institute of Materia Medica). DHT (5α-Dihydrotestosterone) was purchased from Sigma (D-073), MDV3100 (Enzalutamide) was purchased from APExBIO (A3003). YK-4-279 (ETS inhibitor) was purchased from Selleckchem. All chemicals were used at the indicated concentration.

Dose-response curves and cell-growth assays

Cells were seeded (between $1x10^3$ and $1x10^4$ per well) in a 96-well plate. Cells were subsequently treated with serial dilutions of DHT (in 10% CSS medium), or enzalutamide; SPOP inhibitor, ETS inhibitor to determine

dose-response curves or were left untreated for cell-growth assays. Proliferation at corresponding time points was assessed by MTT (Methylthiazolyldiphenyl-tetrazolium bromide) assay according to the manufacturer's recommendations (Sigma). For each time point, absorbance (OD, 590 nm) was measured in a microplate reader.

Matrigel Invasion assay

Invasion assay was performed as previously described[271]. Briefly, equal number of PC3 cells were seeded into 10cm dishes and starved with a medium without fetal bovine serum for 24 hr.; subsequently $1x10^5$ cells were resuspended in 100 µl of starved medium and seeded onto the basement of a Boyden chamber (CLS3422; Sigma) coated with Matrigel. RPMI with 10% fetal bovine serum was added to the lower chamber. After 48hr, invaded cells were fixed with 10% of formalin and stained with crystal violet. Absorbance was measured at 560 nm**.**

Clonogenic assay in methylcellulose

Cells were seeded (between $5x10^3$ and $1x10^4$) in methylcellulose (Methocult H4100, StemCell Technologies) in triplicate. Cells were left untreated for cell-growth assay. For SPOP inhibitor assay, cells were treated with vehicle (0.1% DMSO) or drug (SPOP-i) at corresponding concentration. For androgen therapy, cells were treated with vehicle (0.01% Methanol) or DHT at corresponding concentration. Cells were incubated at 37°C and 5% CO_2 for 7-28 days and colonies were stained with MTT solution at 37°C overnight and absorbance (OD, 590 nm) was measured in a microplate reader.

Mouse Prostate Organoid Generation and Experiments

Prostate tissue was extracted from euthanized mice, digested and seeded in Matrigel as previously described[272]. To overexpress *SPOP* species and *ΔERG* genes, mouse prostate cells were virally infected by spinoculation for 1hr at 600g at 32 °C and selected with puromycin. For the ‘‘organoid formation assay’’ $1.5x10^4$ single cells were plated per well onto 40µl of Matrigel on day 1 and organoids were grown in Revised human prostate organoids medium as previously described[270]. The number of formed organoids that reached 100 µM of diameter was counted on days 14 post plating with cellSens software (Olympus). For the Dose-Response experiment $1x10^4$ mouse prostate cells were plated in 40µl of Matrigel and treated with vehicle

(0.1% DMSO) or drug (SPOP-i) at indicated concentration for 7 days. Live/dead staining was purchased from Promega (G9711) and performed according to the manufacturer's protocol. The genetically engineered Mouse Prostate Organoids, derived from PbCre;$R26^{F133V}$, were generated as previosly described[139]

Immunohistochemistry

Cytoblocks were prepared from the pellets of organoids by adding plasma and thrombin in order to obtain a solid matrix. Once solidified, the organoids were fixed in 10% formalin (Thermo Scientific, 5701) and embedded in paraffin as a normal tissue. Sections of 4 µm were used for IHC analyses and hematoxylin and eosin (H&E) staining (Diapath, C0303) and (Diapath, C0363) respectively. Once dried the sections were treated with OTTIX plus solution (Diapath, X0076) and OTTIX shaper solution (Diapath, X0096) to dewax and rehydrate the sections. Antigen retrieval was performed using pH 6 solutions at 98°C for 20 min. Successively the endogenous peroxidases and non-specific binding sites were blocked using 3% H2O2 (VWR chemicals, 23615.248) and Protein-Block solution (DAKO Agilent technologies, X0909) respectively, for 10 min. Sections were then stained for anti-p16 (ab211542, Abcam, 1:1200), anti-Ki67 (Clone SP6; Lab Vision Corporation #RT-9106-R7, RTU). IHC analyses were performed using Imagescope software.

***In vivo* experiments**

All animal experiments were carried out in male athymic nude mice (Balb/c nu/nu, 6-8 weeks old), NSG mice (NOD Scid Gamma, 6-8 weeks old), and NRG (NOD Rag gamma, 6-8 weeks old) accordingly to protocol approved by the Swiss Veterinary Authority (No. TI-14-2014, TI-38-2018, TI-39-2018 and TI-42-2018). Patient-derived xenografts (PDX) LuCaP-147, -78, -35, -23 were provided by Eva Corey (University of Washington) and maintained as previously described[273]. $2x10^6$ VCaP cells, $5x10^6$ LuCaP-147, LuCaP-23.1, LuCaP-35 and LuCaP-78 were resuspended in 100 µl of PBS and Matrigel 1/1 and subcutaneously injected into both of the dorsal flanks of the mice. Tumor growth was recorded using digital caliper and tumor volumes were calculated using the formula $(L \times W^2)/2$, where L=length and W=width of tumor. For the testosterone propionate (25mg/kg) and SPOP inhibitor (SPOP-i, 50mg/kg) treatment, the mice were grouped randomly and the treatment started when the mean tumor volume reached $100m^3$. Tumor volume and weight were measured 2 times per week. Testosterone propionate was resuspended first in ethanol (150mg/kg) and then in Corn oil (Sigma) at a final concentration of 25mg/kg. SPOP inhibitor was resuspended in Dulbecco's phosphate

buffered saline (PBS) at a final concentration of 50 mg/kg. At the end of the experiment, mice were euthanized, tumors extracted and weighted. Testosterone level was measured using the Human Testosterone ELISA Kit from Abcam (ab174569). In order to recapitulate the levels of supraphysiological testosterone administrated in clinical trials[264], mice reaching at least 3 times the testosterone levels measured before the treatment initiated were included in the depicted data.

Antibodies, Immunoblotting, and Immunoprecipiation

Antibodies used in immunoblotting and immunoprecipitation assays were: anti-SPOP (ab81163, Abcam), anti-TRIM24 (Sc-271266, Santa Cruz), anti-ß-ACTIN (4967, Cell Signaling), anti-AR (Sc-7305, Santa Cruz), anti-GADPH (Sc-47724, Santa Cruz), anti-ERG (Sc-271048, Santa Cruz), anti-VCL (SAB1404522, Sigma), anti-ZMYND11 (NBP2-20960, Novus Biologicals), anti-HA (H3663, Sigma), anti-BRD2 (A302-583A, Bethyl Labs), anti-NCOA3 (2126, Cell Signaling), anti-DEK (610948, BDBioscience), anti-p21 (2947S, Cell Signaling) , anti-c-MYC (5605S, Cell Signaling), anti-HOXB13 (Sc-28333, Santa Cruz), anti-PTEN (9559, cell signaling), anti-p21 (ab188224, Abcam), anti-HOXB13 (NBP2-43655, Novus biologicals). All antibodies were employed at dilutions suggested by the manufacturers.

For immunoblotting, cells were washed with PBS and subsequently lysed in RIPA buffer (Sigma) and sonicated. Protein concentration was determined using the BCA reagent (ThermoFisher), same amounts of protein were separated by SDS-PAGE (Biorad) and transferred onto PVDF membrane (ThermoScientific). The membrane was incubated for one hour in 5% nonfat dry milk/TBS-T blocking buffer followed by incubation with the primary antibody overnight at 4°C. The membrane was washed with TBS-T followed by incubation with horseradish peroxidase-conjugated secondary antibody (Promega).

To detect interactions of SPOP and ZMYND11, cells were lysed in 1 % NP40 buffer (50mM Tris-HCl pH 7.4, 150 mM NaCl, 1 % NP40) with 2x protease inhibitor cocktail (Complete, Roche), sonicated, and 3 mg of lysate were incubated overnight with 2 µg of anti-HA-tag or control mouse IgG antibody (sc-2025, Santa Cruz Biotechnology) at 4 °C. Subsequently, antibodies were collected by 25 µl protein A/G magnetic beads (88803, Fisher Scientific) for 2h, followed by 2 washing steps with 1 % NP40 buffer. Proteins were eluted by addition of 1x SDS-sample buffer under reducing conditions at 95 °C for 5 min.

***In Vivo* Ubiquitylation Assay**

293T cells were transiently transfected with indicated plasmids: pCW107-HA-ZMYND11-WT or HA-ZYMND11-DMT1/DMT2 (2 μg), pCW107-SPOP-WT or SPOP-MT (2 μg), CMV-8x Ubi-His (2 μg). 42 hours later, cells were treated with MG-132 (20μM) or DMSO for additional 7 hours. Cells were then washed with PBS and collected by centrifugation. Small amount of cells was lysed in RIPA buffer and the rest in Buffer C (6M guanidine –HCL, 0.1 M Na2HPO4/NaH2PO4, 10mM Imidazole, pH=8). The whole cells extract was sonicated and incubated with 60 μl of Ni-NTA agarose (Sigma) overnight at 4°C. Next, Ni-NTA beads were washed once with Buffer C, twice with Buffer D (1 volume of Buffer C: 3 volumes of Buffer E) and once with Buffer E (25 mMTris-HCL, 20 mM Imidazole, pH=6.8). Elution of bound proteins was processed by boiling in 1x SDS loading buffer containing 300 mM Imidazole. Samples were loaded, separated by SDS-PAGE, and detected by immunoblotting.

Gene Expression Studies

RNA was extracted using the RNeasy kit (Qiagen) and processed by Kapa SybrFAST one-Step qRT-PCR kit according to manufacturer`s instructions. qRT-PCR was undertaken on an Applied Biosystems StepOnePlus System. The target mRNA expression was quantified using ΔΔCt method and normalized to Actin expression. The following primers were used: *SPOP*, forward 5'-GAAATGGTGTTTGCGAGTAAACC-3', reverse 5`-TACCTACGCTTCCAGTCTCTG-3'; *ERG*, forward 5'-TGTATGCCAGCATTTGTTTCTT-3', reverse 5'- TTGCTGGTCTTGCCATTCCT-3'; *β-ACTIN,* forward 5'-AAGGAGCCCCACGAAAAAT-3', reverse 5'-ACCGAACTTGCATTGATTCCAG-3'; *PLAU,* forward 5'- TACGGCTCTGAAGTCACCACCAAAAT-3', reverse 5'-CCCCAGCTCACAATTCCAGTCAA-3'; *PLAT,* forward 5'-CACTGGGCCTGGGCAAACATA-3', reverse 5'-CACGTCAGCCTGCGGTTCTTC-3'; *TMPRSS2,* forward 5'-CAGGAGTGTACGGGAATGTGATGGT-3', reverse 5'-GATTAGCCGTCTGCCCTCATTTGT-3'; *KLK2*, forward 5'- CTGCCCATTGCCTAA AGAAG-3', reverse 5'- GTAGAGCGGGTGTGGGAAG-3'; *PSA* forward 5'-GAGCACCCCTATCAACCCCCTATT -3' , reverse 5'- AGCAACCCTGGACCTCACACCTAA-3'; *ZMYND11,* forward 5'-ATGGCACGTTTAACAAAAAGACG-3', reverse 5'-CGGTCAATGTTGGCAATCTGC-3'; *BRD2*, forward 5'-CTACGTAAGAAACCCCGGAAG-3', reverse 5'-GCTTTTTCTCCAAAGCCAGTT-3; *TRIM24*, forward 5`-CAGCCACAAATGCCTAAGCAG-3', reverse

5’-GTGTTGGGAACTTGGATAACTGG-3; *NCOA3*, forward 5’-AGACGGGAGCAGGAAAGTAAA-3’, reverse 5’-GTAAAAGCGGTCCTAAGGAGTC-3’; *DEK*, forward 5’-AACTGCTTTACAACAGGCCAG-3’ , reverse 5’-ATGGTTTGCCAGAAGGCTTTG-3’.

RNA-Seq of VCaP, LNCaP and LuCaP cells

RNA sequencing for all experiments involving LuCaP xenografts, VCaP and LNCaP cells was performed at the Institute of Oncology Research using Next Ultra II Directional RNA Library Prep Kit for Illumina and sequenced on the Illumina NextSeq500 with single-end, 75 base pair long reads. The overall quality of sequencing reads was evaluated using a variety of tools, namely FastQC (Andrews S., 2010), RSeQC[274], AfterQC[275] and Qualimap[276]. Sequence alignments to the reference human genome (GRCh38) was performed using STAR [277] (v.2.5.2a). Gene-expression was quantified at gene level by using the comprehensive annotations made available by Gencode[278]. Specifically, we used *v27* release of the Gene Transfer File (GTF). Raw-counts were further processed in the *R* Statistical environment and downstream differential expression analysis was performed using the DESeq2[279] pipeline.

Genes being expressed at very low levels were automatically filtered out through the *Independent Filtering* feature embedded in DESeq2 (alpha = 0.05). Differential-expression results were ranked according to the computed Wald-statistics values. Subsequently, gene-set enrichment testing was performed using Camera[280] pre-ranked (inter-gene correlation equal to 0.1, parametric test procedure). Statistical enrichments were assessed for gene-sets belonging to the Hallmark collection, which is curated by the Molecular Signature DataBase[281, 282] (*MSigDB*), and for custom ERG and DHT-specific gene-signatures. All enrichments were corrected for multiple testing using Benjamini and Hochberg FDR adjusted p-value.

Identification of ERG and AR related gene signatures

We retrieved RNA-seq data from GEO Dataset *GSE83652*[252] to identify transcriptional perturbations in VCaP cells following treatment with DHT or following silencing of ERG. To this purpose we completely reprocessed samples SRR3713255-57, SRR3713267-72 using *STAR* and *DESeq2* as previously described for VCaP cells. In addition, to identify direct targets, we integrated information relative to AR and ERG chromatin binding sites, which we derived from GEO Dataset *GSE28950*[258]. To maximize the number of peaks and to

reduce false negatives, we merged results of experiments performed at different time points, namely 2h and 18h after DHT exposure. De-multiplexed reads were aligned to *hg38* release of the human reference genome using bwa-mem[283] (0.7.15). MACS[284] (v.2.1.0) was used to perform peak calling procedure using a cutoff FDR q-value of 0.01 and a mappable genome size optimized for *hg38* equal to 2.9 gigabases. Downstream analysis was performed in R statistical environment. We identified binding sites overlapping promoters by using bedtools[285].

Promoters were defined as DNA regions ranging from 1500 *bp* upstream to 500 *bp* downstream of Transcription Start Sites (TSSs).

To discriminate between ERG- and AR- specific transcriptional responses we stratified genes into three main classes: genes whose promoter regions are bound by *AR* but not by *ERG*, genes whose promoters are bound by ERG but not by *AR*, and finally, genes whose promoters are co-bound by both AR and ERG. AR bound only genes were further subdivided into two sets, those being significantly (FDR<0.05) induced following DHT treatment and those being significantly repressed. A similar approach was applied to ERG bound only genes, where genes were subdivided into ERG-induced and ERG-repressed gene-sets, if they were respectively down or up-regulated following *ERG* silencing. To be more stringent in the definition of AR-specific and ERG-specific signatures, we excluded genes from the ERG-induced set that were also significantly up-regulated following DHT treatment, *vice-versa* we excluded ERG-repressed genes that were significantly down-regulated following DHT-treatment. The same criteria were applied for DHT-specific gene-sets. Finally, defined an additional gene-set (DHT-induced/ERG-repressed) consisting of genes being co-bound by AR and ERG in their promoter region, which were significantly up-regulated following DHT treatment but also significantly upregulated following ERG-silencing. All gene-sets are detailed in Supplementary Table 1. Overlap between custom derived gene-signatures and the most represented Hallmark's gene-sets was assessed using GeneOverlap R package (Shen L, Sinai M, 2013). Two-dimensional network visualization was generated with Cytoscape. [286]

Gene-set testing and RNA-Seq data processing of clinical samples

Publicly available RNA-Seq data for primary prostate cancer were obtained from The Caner Genome Atlas[51] (TCGA) database and retrieved from Genomics Data Commons (GDC) in form of gene-centric raw

counts, using *TCGAbiolinks* package[287]. We selected individuals characterized by either SPOP or ERG fusion, and a third group defined as "others", which includes all remaining samples, excluding those patients exhibiting any other ETS-rearrangement. Differential expression and gene-set enrichment between samples harboring ERG fusions and SPOP-mutations were performed using *DESeq2* and *Camera* (pre-ranked) as previously described for prostate cancer cells. Single-sample gene-set enrichment analysis (GSVA[288] package) was applied to measure, for each individual patient, the overall activity of the custom gene-sets that were previously generated in VCaP cells. Following differential expression analysis between ERG-rearranged and SPOP mutant primary tumors, we defined two gene-sets consisting of SPOP-upregulated (n = 443, log_2FC >1, FDR<0.05) and ERG-upregulated (n = 359, log_2FC >1, FDR<0.05) genes.

PolyA+ RNASeq data for metastatic prostate cancer were obtained from SU2C cohort[56]. Normalized *RPKM* values, retrieved through *cBioportal*, were log transformed and patient's categorization (SPOP/ERG/OTHER) was performed in the same manner as for primary tumors. To evaluate whether transcriptional differences occurring between ERG-rearranged and SPOP-mutant individuals were also conserved in CRPC setting, we quantified the above mentioned SPOP-upregulated/ERG-upregulated signatures in the SU2C 2019 cohort, using single-sample gene-set enrichment analysis. The obtained ssGSEA scores were scaled in a range between -1 and 1 (SPOP-Upregulated) and between 1 and -1 (ERG-upregulated, inverted). Subsequently we averaged these rescaled values in order to obtain an aggregate score.

Circular representation of interactions between gene-sets

Chord diagrams were generated using circlize[289] package in R statistical environment.

Strings, whose thickness is proportional to the number of shared elements, represent common genes between sets.

ZMYND11 ChIP-seq in VCaP cells

ChIP-seq using anti-ZMYND11 antibody (NBP2-20960, Novus Biologicals) was performed in VCaP cells, overexpressing either wild-type SPOP or mutant SPOP harboring Y87C point mutation. Briefly, to isolate chromatin, cells (120.000.000 per IP) were cross-linked using 1% Formaldehyde cross-link protein-DNA complexes and crosslinking was terminated by the addition of 1/10 volume 1.25 M glycine for 5 min at

room temperature followed by cell lysis and sonication, resulting in an average chromatin fragment size of 200 bp. Samples lysis was performed as previously described using MNase enzyme 1000 gel units=1 uL[290]. After adding the MNase sonication buffer, the samples were sonicated for 30 cycles, 30 sec ON and 30 sec OFF at high voltage. ChIP and input DNA (50 ng) were used for indexed library preparation using NEBNext Ultra II DNA Library Prep kit and subjected to 75 *bp* single-end sequencing on the Illumina NextSeq500. All procedures were performed at the Institute of Oncology Research. De-multiplexed reads were aligned to *hg38* release of the human reference genome using bwa-mem[283] (0.7.15). MACS[284] (v.2.1.0) was used to perform peak calling procedure using a cutoff FDR q-value of 0.01 and a mappable genome size optimized for *hg38* equal to 2.9 gigabases. Downstream analysis was performed in R statistical environment. ChIPseeker[291] was used to annotate peaks and to represent the distribution of ZMYND11 binding sites relative to Transcription Start Sites (TSSs). The R package chipenrich[292] was subsequently used to determine enrichment or depletion of ZMYND11 peaks in regions surrounding *TSSs* of genes that are included in Hallmarks or custom gene-set collections. Surrounding regions were defined as ranging from 5kb upstream to 5kb downstream of their *TSSs* (locusdef = 5kb), which is in line with the overall behavior of ZMYND11 binding sites around *TSSs* (Extended Data Fig. 6f-g).

Identification of AR-binding sites in primary prostate cancer specimen

Publicly available ChIP-Seq data were retrieved from GSE120738[3]. ChIP-seq data were reprocessed as described for ZMYND11 samples. Differential binding affinity of AR between ERG-rearranged and SPOP-mutant tumors was performed using DiffBind (Stark R and Brown G, 2011).

Frequency of SPOP mutations across patients' cohorts

We defined the percentage of SPOP-mutant and TMPRSS2-ERG positive tumors across different patients' cohorts originating from multiple sources. Patients with primary/loco-regional prostate tumors were derived from TCGA and MSK-IMPACT Clinical Sequencing cohorts[102]. Patients with tumor-progression (non-castrate) were derived from MSK-IMPACT and TCGA cohorts, by including from the latter only individuals that showed tumor-progression based on survival information. Castration resistant prostate cancer patients were retrieved from MSK-IMPACT, Beltran et. al[58] and from the SU2C[56] .datasets. Neuroendocrine prostate cancer samples were retrieved from the SU2C cohort (samples annotated with

neuroendocrine features) and from Beltran et al[58]. Total number of *SPOP*-mutant and *TMPRSS2-ERG* tumors were determined based on the clinical annotations of the individual studies and integrated with fusion information from TCGA Fusion Gene Database (www.tumorfusions.org). Survival analysis was performed in R statistical environment using the TCGA and MSK-IMPACT clinical sequencing cohort.

Quantitative liquid-chromatography-mass spectrometry (LC-MS/MS)

In solution digestion VCaP cell pellets were lysed at 4 ºC in 8 M urea, 50 mM Tris-HCl pH 8.0, 150 mM NaCl, 1 mM EDTA, 2 µg/µl aprotinin (Sigma-Aldrich), 10 µg/µl leupeptin (Roche), and 1 mM phenylmethylsulfonyl fluoride (PMSF) (Sigma). Protein concentration was determined using a bicinchoninic acid (BCA) protein assay (Pierce). Proteins were reduced with 5 mM (DTT) for 45 min at room temperature (RT), followed by alkylation with 10 mM iodoacetamide for 30 min at room temperature in the dark. The urea concentration was reduced to 2 M using 50 mM Tris-HCl, pH 8. Samples were digested for 2 h at 25 ºC with endoproteinase Lys-C (Wako Laboratories) at an enzyme-to-substrate ratio of 1:50. Samples were subsequently digested overnight at 25 ºC with sequencing grade trypsin (Promega) at an enzyme-to-substrate ratio of 1:50. Following overnight digestion, samples were acidified to a final concentration of 1% formic acid.

Peptide samples were desalted on a 100 mg tC18 Sep-Pak SPE cartridge (Waters). Cartridges were conditioned with 1 mL of 100% MeCN, 1 mL of 50% MeCN/0.1% FA, and 4x with 1 mL of 0.1% TFA. The sample was loaded, and washed 3x with 1 mL of 0.1% TFA, 1x with 1 mL of 1% FA, and eluted 2x with 600 µl of 50% MeCN/0.1% FA.

TMT labeling of peptides

Peptides were labeled with TMT 10-plex isobaric mass tagging reagents (Thermo Fisher Scientific). Each TMT reagent was resuspended in 41 µL of MeCN. Peptides were resuspended in 100 µL of 50 mM HEPES and combined with TMT reagent. Samples were incubated at RT for 1 h while shaking. The TMT reaction was quenched with 8 µL of 5% hydroxylamine at RT for 15 min with shaking. TMT labeled samples were combined, dried to completion, reconstituted in 100 µL of 0.1% FA, and desalted on StageTips or 100 mg SepPak columns as described above.

Basic Reverse Phase (bRP) Fractionation

The TMT labeled samples were fractionated using offline high pH reversed-phase chromatography (bRP) as previously described [Mertins et al Nat Prot]. Samples were fractionated using Zorbax 300 Extend C18 column (4.6 × 250 mm, 300 Å, 5 µm, Agilent) on an Agilent 1100 series high-pressure liquid chromatography (HPLC) system. Samples were reconstituted in 900 µL of 4.5 mM ammonium formate (pH 10) in 2% (vol/vol) acetonitrile (MeCN) (bRP solvent A). Samples were injected with Solvent A at a flow rate of 1 mL/min and separated using a 96 min gradient. The gradient consisted of an initial increase to 16% solvent B (90% MeCN, 5 mM ammonium formate, pH 10), followed by 60 min linear gradient from 16% solvent B to 40% B and successive ramps to 44% and 60% at a flow rate of 1 mL/min. Fractions were collected in a 96-deep well plate (GE Healthcare) and pooled in a non-contiguous manner into final 24 proteome fractions. Pooled fractions were dried to completeness using a SpeedVac concentrator.

Liquid chromatography and mass spectrometry

Desalted peptides were resuspended in 3% MeCN/0.1% FA and analyzed by online nanoflow liquid chromatography tandem mass spectrometry (LC-MS/MS) using Q-Exactive plus mass spectrometer (Thermo Fisher Scientific) coupled on-line to a Proxeon Easy-nLC 1200 as previously described [Mertins et al Nature Protocols]. Briefly, 1 ug of each sample was loaded onto a microcapillary column (360 µm outer diameter × 75 µm inner diameter) containing an integrated electrospray emitter tip (10 µm), packed to approximately 22 cm with ReproSil-Pur C18-AQ 1.9 µm beads (Dr. Maisch GmbH) and heated to 50 ºC. Samples were analyzed with 110 min LC-MS method. The 110 min method contained a mobile phase with a flow rate of 200 nL/min, comprised of 3% acetonitrile/0.1% formic acid (Solvent A) and 90% acetonitrile/0.1% formic acid (Solvent B), with the following gradient profile: (min:%B) 0:2; 1:6; 85:30; 94:60; 95:90; 100:90; 101:50; 110:50 (the last two steps at 500 nL/min flow rate). The Q-Exactive plus MS was operated in the data-dependent mode acquiring HCD MS/MS scans (r =35,000) after each MS1 scan (r = 70,000) on the 12 most abundant precursor ions using an MS1 target of 3 × 10^6 and an MS2 target of 5 × 10^4 . The maximum ion time utilized for MS/MS scans was 120 ms; the HCD-normalized collision energy was set to 30; the dynamic exclusion time was set to 20 s, isotope exclusion function was enabled, and peptide match function was set to preferred. Charge exclusion was enabled for charge states that were unassigned, 1 and >6.

MS Data Analysis

All data were analyzed using Spectrum Mill software package v 6.1 pre-release (Agilent Technologies). Similar MS/MS spectra acquired on the same precursor m/z within +/- 60 s were merged. MS/MS spectra were excluded from searching if they were not within the precursor MH+ range of 750-4000 Da or if they failed the quality filter by not having a sequence tag length >0. MS/MS spectra were searched against UniProt human database. All spectra were allowed +/- 20 ppm mass tolerance for precursor and product ions, 30% minimum matched peak intensity, and "trypsin allow P" enzyme specificity with up to 4 missed cleavages. The fixed modifications were carbamidomethylation at cysteine, and TMT at N-termini and internal lysine residues. Variable modifications included oxidized methionine and N-terminal protein acetylation. Individual spectra were automatically designated as confidently assigned using the Spectrum Mill autovalidation module. Specifically, a target-decoy based false-discovery rate (FDR) scoring threshold criteria via a two-step auto threshold strategy at the spectral and protein levels was used. First, peptide mode was set to allow automatic variable range precursor mass filtering with score thresholds optimized to yield a spectral level FDR of 1 %. A protein polishing autovalidation was applied to further filter the peptide spectrum matches using a target protein-level FDR threshold of 0. Following autovalidation, a protein-protein comparison table was generated, which contained experimental ratios. For all experiments, non-human contaminants and reversed hits were removed. Furthermore, data were filtered to only consider proteins with 2 or more unique peptides and was median normalized.

Statistical analysis

GraphPad Prism version 8.3 (GraphPad Software) was used for statistical analysis. Data are depicted as mean + s.e.m. unless otherwise specified. The number of independent experiments or mice used is indicated in each figure legends. Unpaired Student's t-test was used for comparisons between two groups, one-way analysis of variance (ANOVA) with multiple comparisons for two groups or more, and two-way ANOVA with multiple comparisons for repeated measurements. Multiple comparisons tests were corrected by controlling the False Discovery Rate (FDR) using Benjamini and Hochberg's method. . Correlation analyses were performed using Pearson correlation coefficients.

Data Availability

The original mass spectra have been deposited in the public proteomics repository MassIVE and are accessible at ftp://MSV000082915@massive.ucsd.edu when providing the dataset password: prostate. If requested, also provide the username: MSV000082915. This data will be made public upon acceptance of the manuscript.

RNA-Seq data generated have been deposited in the *ArrayExpress* database at EMBL-EBI and were assigned the accessions *E-MTAB-7165, E-MTAB-7170, E-MTAB-7173*. These data are accessible when providing the datasets username and password as follow:

Username: *Reviewer_E-MTAB-7165* Password: *4sJqpicv*

Username: *Reviewer_E-MTAB-7170* Password: *AAA65MMy*

Username: *Reviewer_E-MTAB-7173* Password*: sIpcob0o*.

CHiP-Seq data generated have been deposited in the *ArrayExpress* database at EMBL-EBI and were assigned the accessions *E-MTAB-7174*. These data are accessible when providing the dataset username and password as follow:

Username: *Reviewer_E-MTAB-7174* Password: *onwwwwni*

All these data will be made public upon acceptance of the manuscript.

Figure 1

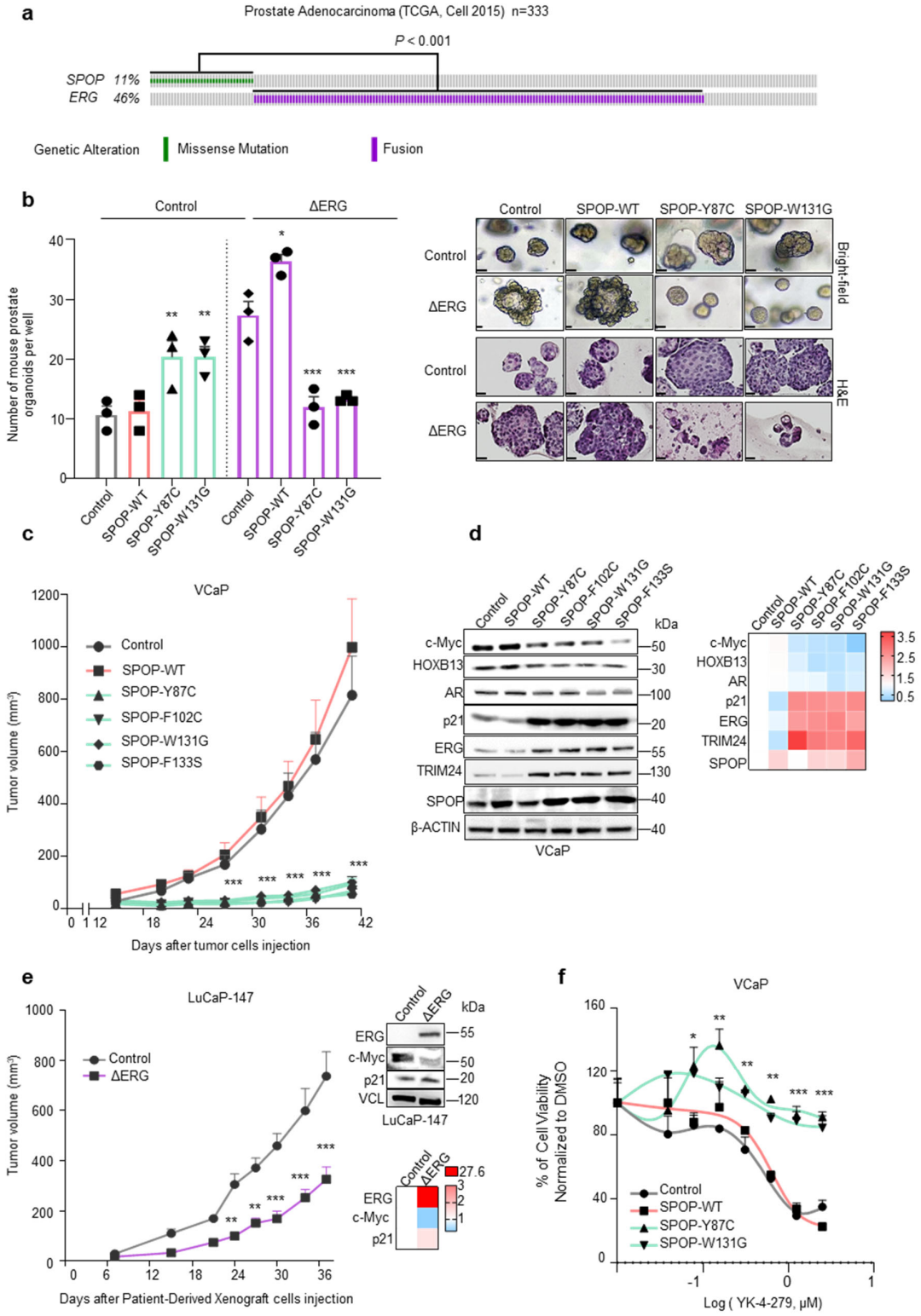

Figure 1. Genetic alterations in *SPOP* and *ERG* are synthetic sick. a, Distribution of genetic alterations in *SPOP* and *ERG* across 333 primary prostate cancers in TCGA database[51]. **b,** 3D growth of mouse prostate epithelial organoids derived from C57BL/6 mice over-expressing the indicated SPOP and ERG species (bar represents 20 μm) (n=3). Representative bright field pictures and haematoxylin and eosin (H&E) stained

sections are shown. **c,** *In vivo* growth of VCaP xenografts over-expressing the indicated SPOP species in immune-compromised mice (each group, n=10). **d,** Immunoblot of VCaP cells over-expressing the indicated SPOP species and corresponding quantification of the indicated protein levels depicted as heatmap. Protein expression changes were normalized to β-ACTIN and Control cell line. **e**, Tumor growth kinetics of xenografts established from LuCaP-147 PDX (SPOP-Y83C) stably overexpressing ΔERG or Control vector (each group, n=10). Corresponding immunoblot and quantification depicted as heatmap. Protein expression changes were normalized to Vinculin (VCL) and Control cell line. **f,** Dose-response curve of VCaP cells overexpressing the indicated SPOP species and treated with the ETS-inhibitor YK-4-279. All error bars, mean + s.e.m. P values were determined by one-way ANOVA (b) or two-way ANOVA (c,e,f) with multiple comparisons and adjusted using Benjamini-Hochberg post-test $*P < 0.05$, $**P < 0.01$, $***P < 0.001$. Molecular weights are indicated in kilodaltons (kDa).

Figure 2

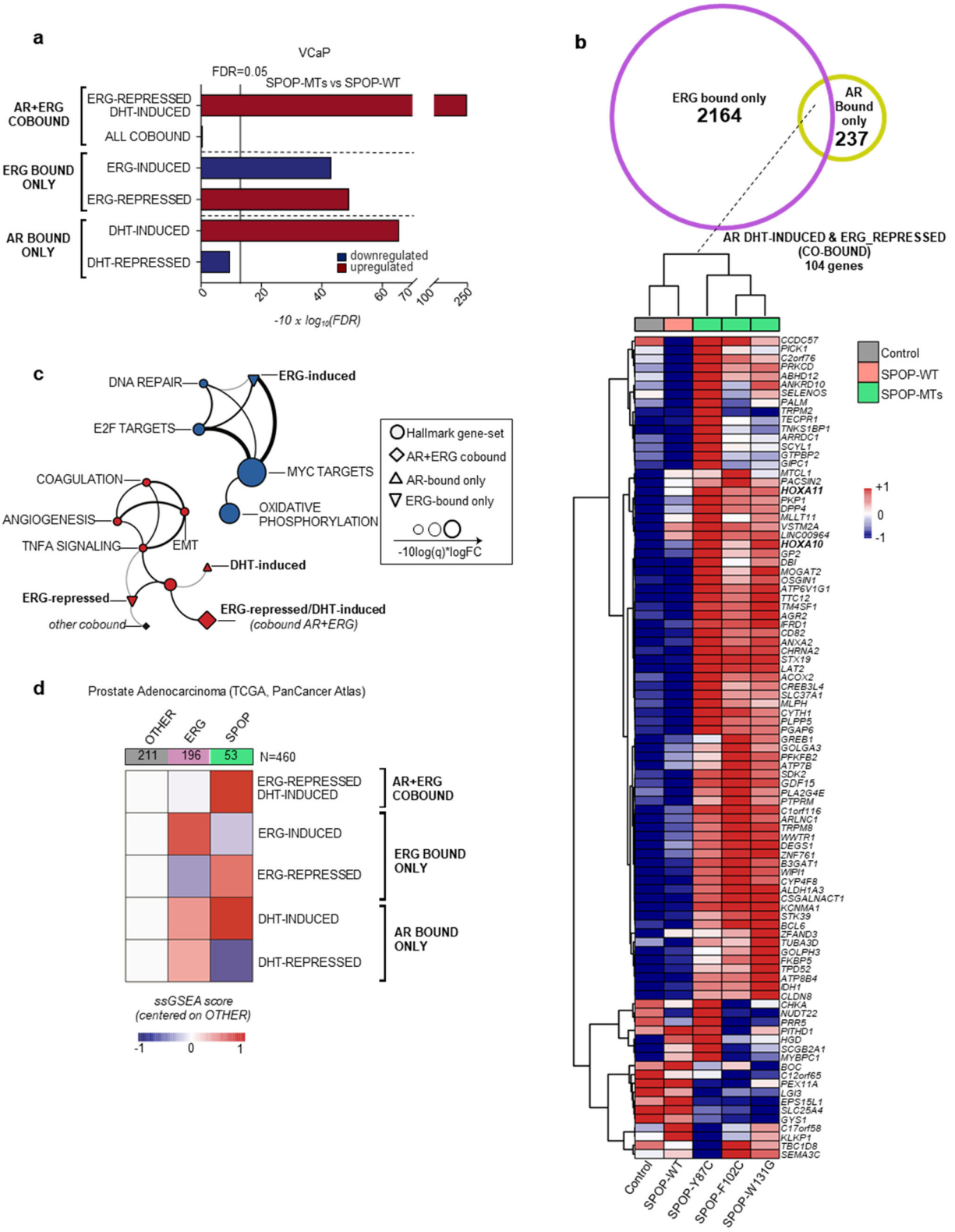

Figure 2. Mutant SPOP-induced androgen receptor signaling antagonizes ERG activity. a, Gene-set enrichment analysis of VCaP cells overexpressing SPOP mutant (SPOP-MTs; SPOP-Y87C, -F102C, -W131G) versus SPOP-wild type (-WT), based on RNA-seq data. Experiments were performed using three replicates

for each condition. Enrichments are determined on custom gene-sets of direct androgen receptor (AR) and ERG target genes (Supplemental Table 1). Enrichments and FDR-adjusted p-values are computed with *Camera* (pre-ranked) **b,** Venn Diagram and heatmap depicting the expression of genes included in the custom gene-set of AR/ERG co-bound genes that are repressed by ERG and induced by DHT in VCaP cells overexpressing SPOP-MTs (SPOP-Y87C, F102C, W131G), SPOP-WT and vector Control. Genes (rows) and samples (columns) were clustered using Euclidean distance. Gene expression values, normalized using variance stabilizing transformation (vst) were scaled and centered by row prior of clustering. Columns represent average expression of three replicates for each condition. **c,** Two-dimensional network representing overlaps between the 10 most significantly enriched Hallmark and custom gene-sets, identified when comparing SPOP-MTs (SPOP-Y87C, F102C, W131G) to SPOP-wild type (-WT) overexpressing VCaP cells. Thickness of edges is proportional to the significance of the overlap of the connected nodes measured by Fisher test. Only edges with FDR value <0.05 are shown. Size of nodes is proportional to gene-set enrichment significance and equals to -10 x $\log_{10}$ (FDR). **d**, Heatmap representing gene-set activity stratified according to tumor subtype, derived from TCGA cohort. For each tumor group, the average value of single sample GSEA scores was considered. Values were scaled and referenced to samples that did not harbor any ETS-fusion (*ERG*, *ETV1*, and *ETV4)* or point mutations in *SPOP*[51].

Figure 3

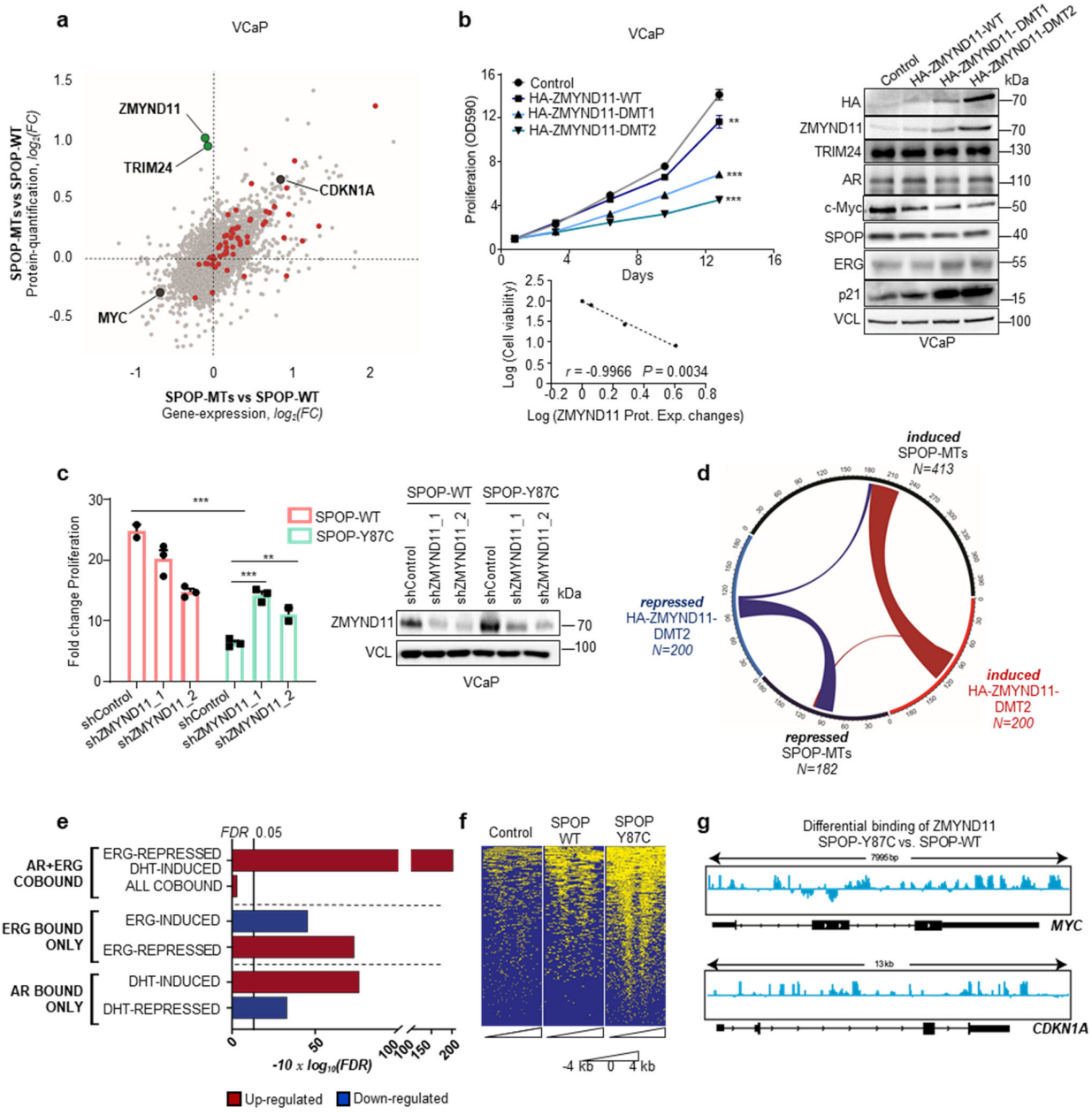

Figure 3. ZMYND11 is a SPOP substrate and influences AR- and ERG-dependent gene transcription. **a,** Scatter plot of SPOP-MTs (average across SPOP-Y87C, -F102C, -W131G) versus SPOP-WT transcriptome (n=3, biological replicates) and proteome expression changes in VCaP cells (n=2, biological replicates). Genes from custom signature DHT-Induced/ERG-Repressed genes (AR+ERG co-bound) are highlighted in red. TRIM24 and ZMYND11 are the most upregulated proteins without changes at mRNA levels and are highlighted in green. CDKN1A (p21) upregulated at both mRNA and protein levels, and MYC downregulated at both mRNA and protein levels, are highlighted in black. **b,** 2D proliferation assay of VCaP cancer cells overexpressing HA-ZMNYD11-WT and derived degron-deficient mutants (DMT1/2) (n=3). Corresponding immunoblot of indicated proteins. Correlation between cell viability and ZMYND11 protein expression changes (Prot. Exp. Changes), as quantified by immunoblot in the same cell lines. *P* values were calculated using Pearson rank correlation. **c,** Fold-change cell viability of VCaP cancer cells over-expressing the

indicated SPOP species with and without *ZMYND11* knockdown using two different short hairpin RNAs, at day 16 (n=3). Protein expression of the indicated proteins was analyzed by immunoblotting. **d,** Chord-diagram of transcriptionally regulated genes by either SPOP-MTs or HA-ZMYND11-DMT2 in VCaP cells (FDR<0.05). Strings, whose thickness is proportional to the number of shared elements, represent common genes between sets. **e,** Gene-set enrichment analysis of VCaP cell overexpressing HA-ZMYND11-DMT2 compared to Control, based on RNA-seq data. Enrichments are performed on custom gene-sets of direct androgen receptor (AR) and ERG target genes. FDR-adjusted p-values are computed with *Camera* (pre-ranked). **f**, Heatmap of ChIP-seq signals around TSS regions (+/- 4kb) at which ZMYND11 bindings were identified by peak calling procedure (Macs2). **g**, IGV-derived screenshots representing loglikelihood ratio of ZMYND11 bindings in mutant SPOP (SPOP-Y87C) vs wild-type SPOP over-expressing VCaP cells. Reported are *MYC* (up) and *CDKN1A* (bottom). All error bars, mean ± s.e.m. *P* values were determined by two-way ANOVA (**b**) or one-way ANOVA with multiple comparisons and adjusted using Benjamini-Hochberg post-test (**c**). $^{**}P < 0.01$, $^{***}P < 0.001$. Molecular weights are indicated in kilodaltons (kDa).

Figure 4

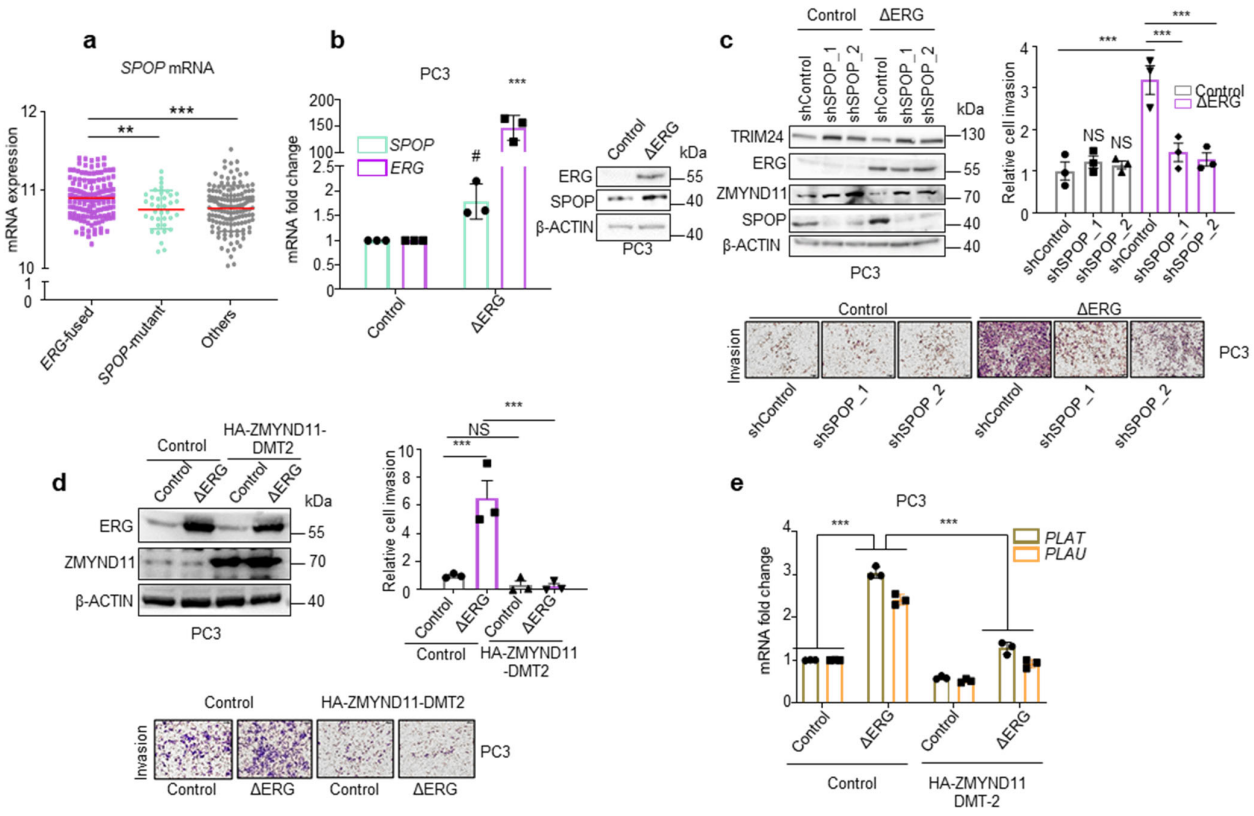

Figure 4. SPOP-WT is an ERG target gene and required for ERG-mediated cell invasion. a, *SPOP* mRNA expression levels in 333 primary prostate cancer tissues stratified according to the indicated driver mutations[51]. Error bars, mean ± s.d. **b,** SPOP mRNA and protein levels in response to forced expression of ΔERG in PC3 prostate cancer cells by qPCR and immunoblotting, respectively. Error bars, mean + s.e.m. (n=3). *P* values were determined by unpaired, two-tailed Student's t-test. $^{\#}P < 0.05$; Control versus ΔERG for *SPOP* expression levels. $^{***}P < 0.001$; Control versus ΔERG for *ERG* expression levels. **c,** Transwell Matrigel invasion assay of PC3 cells with forced expression of ΔERG and knockdown of SPOP using two different short hairpin RNAs. Protein expression of the indicated proteins was assessed in parallel by immunoblotting. Error bars, mean ± s.e.m. (n=3). **d,** Transwell Matrigel invasion assay of PC3 cells with forced expression of ΔERG and HA-ZMYND11-DMT2 and corresponding immunoblot analysis. Error bars, mean ± s.e.m. (n=3). **e,** Analysis of the ΔERG- and HA-ZMYND11-DMT2-induced transcriptional changes in the ERG target genes *PLAU* and *PLAT*. All error bars, mean ± s.e.m. *P* values were determined by one-way ANOVA with multiple comparisons and adjusted using Benjamini-Hochberg post-test (**a,c,d,e**). NS, not significant. $^{**}P < 0.01$, $^{***}P < 0.001$. Molecular weights are indicated in kilodaltons (kDa).

Figure 5

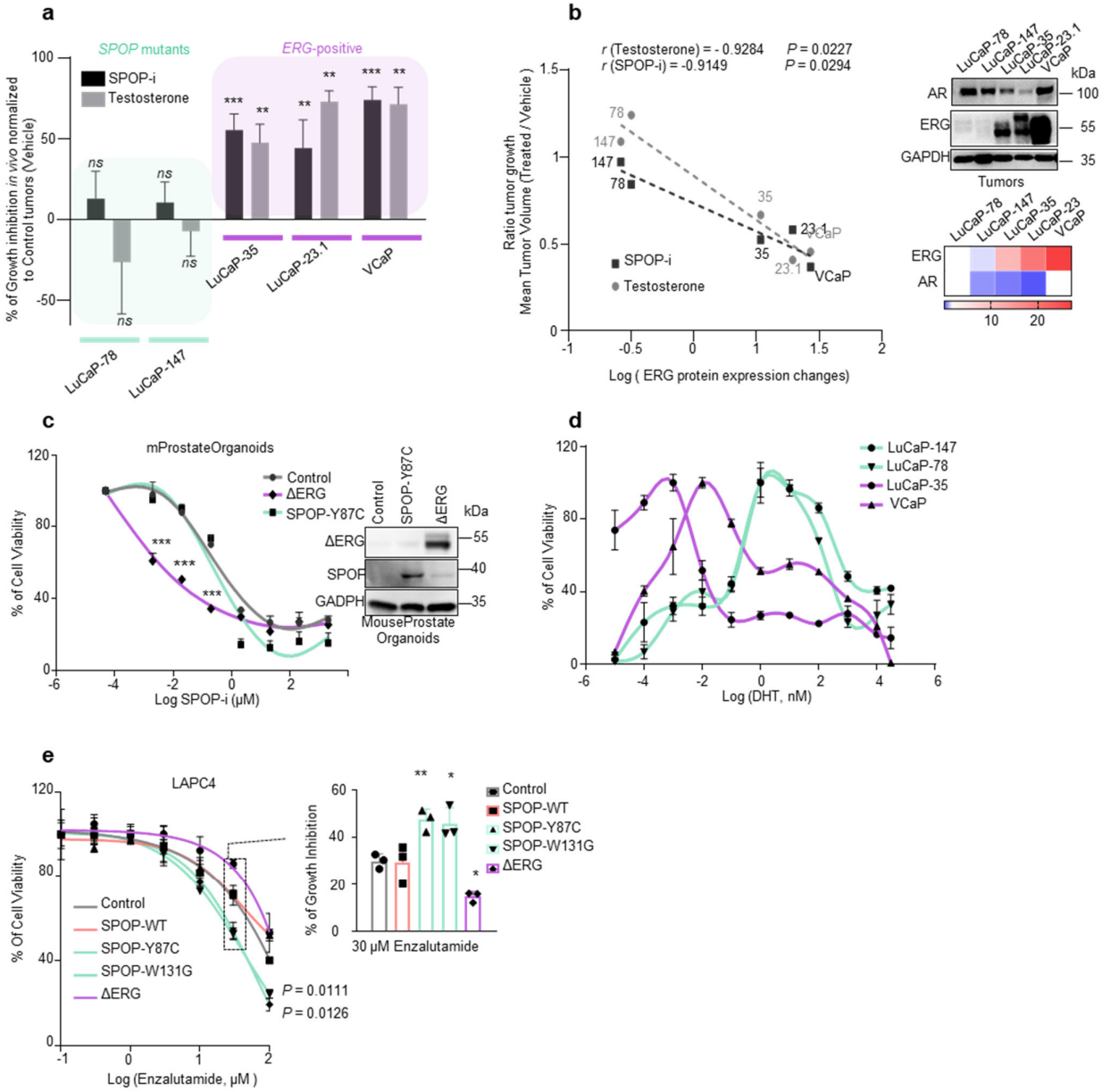

Figure 5. ERG and mutant SPOP trigger different responses to therapeutic interventions. a, Sensitivity to Testosterone and SPOP-i treatment in xenograft and PDX models. LuCaP-23.1, LuCaP-35 and VCaP are *ERG*-positive cancer cells. LuCaP-147 and LuCaP-78 are *SPOP* mutant cancer cells (respectively SPOP-Y83C and SPOP-W131G). Growth inhibition is calculated using the last tumor measurements as shown in Extended Data Fig. 8f-j and 9e-i. **b**, Correlation of sensitivity to SPOP-i or testosterone treatment shown in Extended Data Fig. 8f-j and 9e-i, with ERG protein levels, as quantified by immunoblot, in PDX models and xenografts. *P* values were calculated using Pearson rank correlation. Corresponding immunoblot and quantification of AR and ERG protein levels depicted as a heatmap. Protein expression changes were normalized to GAPDH and LuCaP-78. **c,** Dose-response curves to SPOP-i treatment of Mouse Prostate Organoids overexpressing ΔERG, SPOP-Y87C and Control vector**. d,** Dose-response curves to DHT treatment of VCaP, LuCaP-35, LuCaP-78 and

LuCaP-147 PDX cancer cells. Prior to DHT treatment, PDX were grown in standard media without DHT. VCaP were starved for 24h in CSS medium (RPMI + 10% charcoal-stripped serum). **e,** Enzalutamide sensitivity of LAPC4 cells overexpressing ΔERG or SPOP mutant species (Y87C, W131G). All error bars, mean + s.e.m. *P* values were determined by unpaired, two-tailed Student's t-test (a), **P* < 0.05, ***P* < 0.01, ****P* < 0.001. Molecular weights are indicated in kilodaltons (kDa).

Extended Data Figure 1

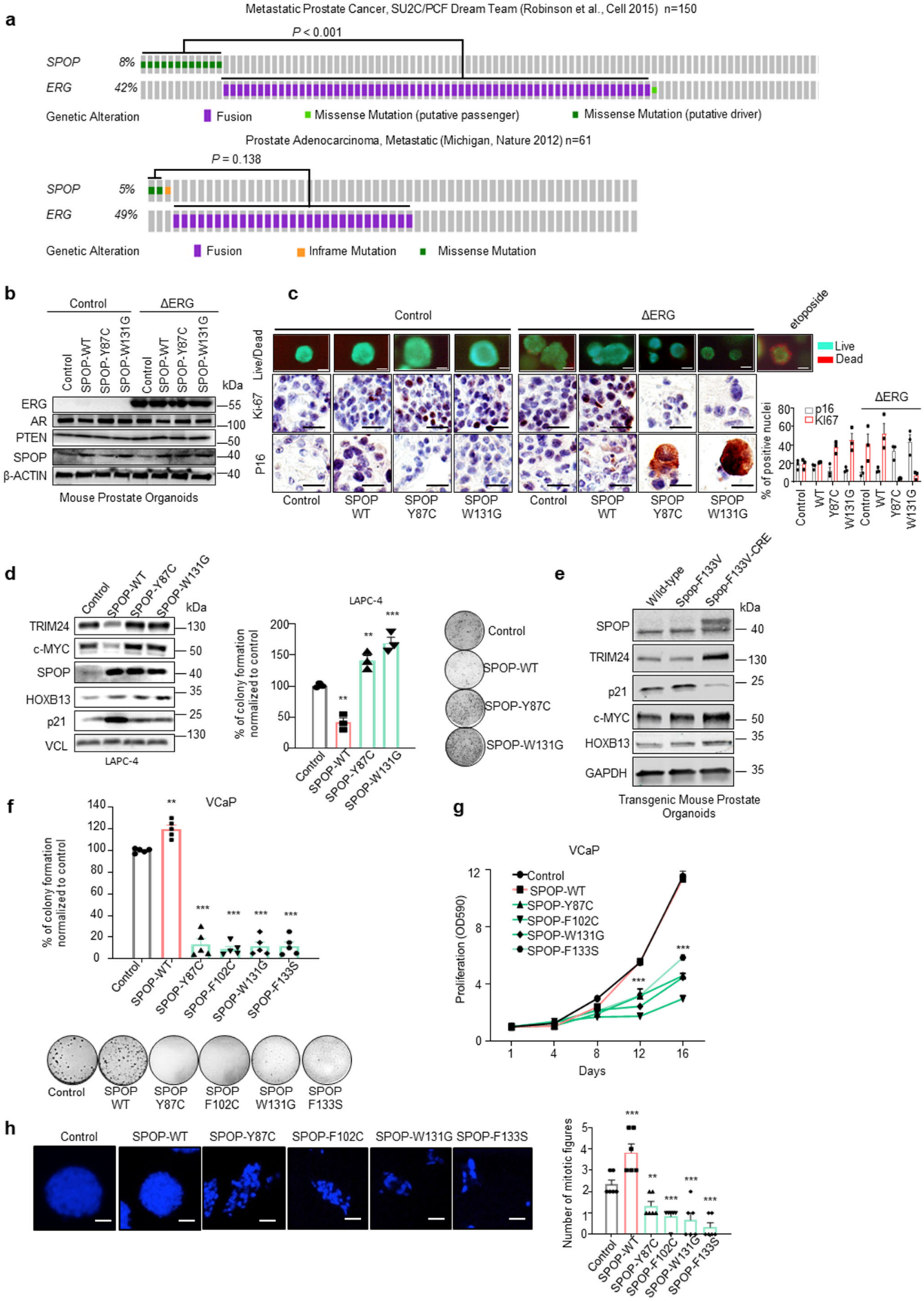

Extended Data Figure 1. Genetic alterations in *SPOP* and *ERG* are mutually exclusive across metastatic prostate cancers and synthetic sick. a, Distribution of genetic alterations in *SPOP* and *ERG* transcription factor across 150 and 61 metastatic prostate cancer, respectively[49, 50]. **b,c,** Immunoblot expression analysis of indicated proteins in mouse prostate organoids over expressing indicated SPOP mutants (MTs) and ΔERG and corresponding live and dead staining (bar 20 μm). Ki67 and p16 immunohistochemistry and corresponding quantification. **d,** 3D colony formation assay in methylcellulose of LAPC4 human prostate cancer cells over-expressing the indicated SPOP MTs and corresponding immunoblot (n=3). **e,** Immunoblot of indicated proteins in Wild-type, SPOP-F133V-CRE negative and SPOP F133V-CRE positive organoids line derived from *SPOP* ^{F133V} transgenic mouse model. **f,g,** 3D growth in methylcellulose (n=5) and 2D proliferation assay of *TMPRSS2-ERG* positive VCaP human prostate cancer cells over-expressing the indicated SPOP MTs. **h**, Corresponding mitotic count by DAPI (bar represents 100 μm). All error bars, mean + s.e.m. *P* values were determined by one-way ANOVA (**d,f,h**) or two-way ANOVA (**g**) with multiple comparisons and adjusted using Benjamini-Hochberg post-test. $^{**}P < 0.01$, $^{***}P < 0.001$. Molecular weights are indicated in kilodaltons (kDa).

Extended Data Figure 2

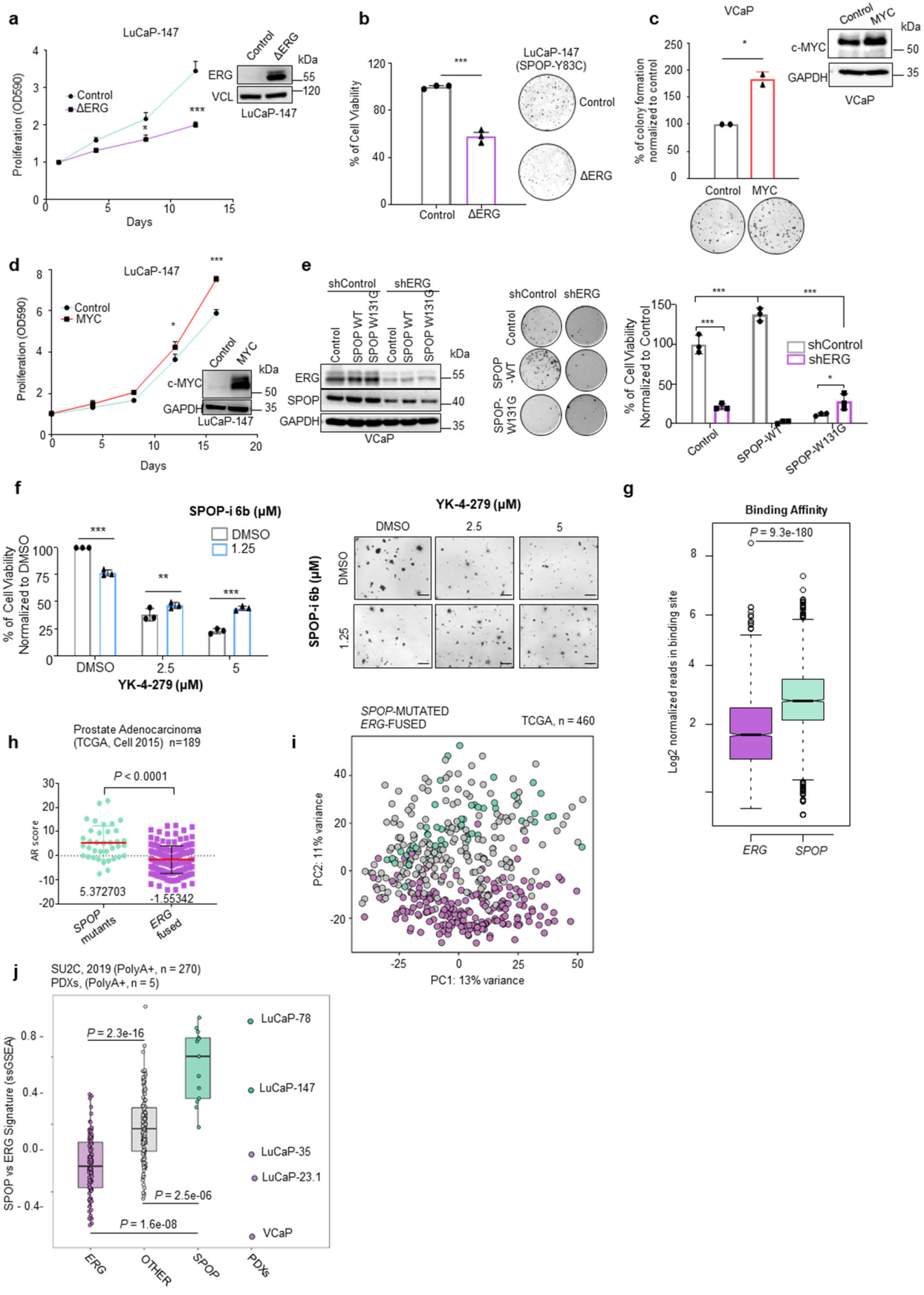

Extended Data Figure 2. Antagonistic relationship between oncogenic activation of ERG and loss of SPOP function in prostate cancer cells. a,b, 2D (**a**) and 3D (**b**) proliferation assay of LuCAP-147 (SPOP-Y83C) PDX cells overexpressing ΔERG and corresponding immunoblot (n=3). **c,** 3D proliferation assay of VCaP cells overexpressing MYC (n=2). **d**, 2D proliferation assay of LuCaP-147 overexpressing MYC (n=3) and corresponding immunoblot. **e,** 3D proliferation assay of VCaP cells overexpressing SPOP-WT and SPOP-131G , with or without knockdown of ERG with a short hairpin RNA (shERG_1) and corresponding quantification and immunoblot (n=3). **f,** 2D proliferation assay of VCaP cells treated with SPOP-i (compound 6b) and ETS inhibitor (compound YK-4-279). Cell viability was assessed 4 days after treatment. Pictures are representative and have been taken after incubation with MTT reagent (bar 200 μm). **g,** The Box plots show distribution of normalized reads in binding sites over all the identified differentially bound (DB) regions (FDR = 0.0)5 in ERG-fused (violet) vs SPOP-mutant (green) samples. *P*-values were determined using Wilcoxon-test. **h**, AR score of primary prostate tumors ERG or SPOP mutant's positive (TCGA)[51, 293]. **i,** PCA-analysis based on RNA-Seq derived mRNA expression levels (TCGA cohort). ERG-fused (violet) and SPOP-mutant (green). Individuals were annotated into subtypes as described in Material and Methods. **j**, The boxplots represent transcriptional activity of SPOP integrated-signature (see Materials and Methods) in CRPC samples (SU2C-2019 cohort, left) and PDX-models. Scores are determined using integrated signatures derived from primary prostate tumors (TCGA-cohort). ERG-fused samples are depicted in violet, SPOP-mutants samples are depicted in green. Samples not harboring SPOP mutations or ERG rearrangements are represented in grey. *P* values were determined using Wilcoxon-test, and adjusted for multiple comparisons (FDR). All error bars, mean + s.e.m. *P* values were determined by an unpaired, two-tailed Student's t-test (**b,c**) or two-way ANOVA (**a, c, d, e, f**) with multiple comparisons and adjusted using Benjamini-Hochberg post-test. **P* < 0.05, ****P* < 0.001. Molecular weights are indicated in kilodaltons (kDa).

Extended Data Figure 3

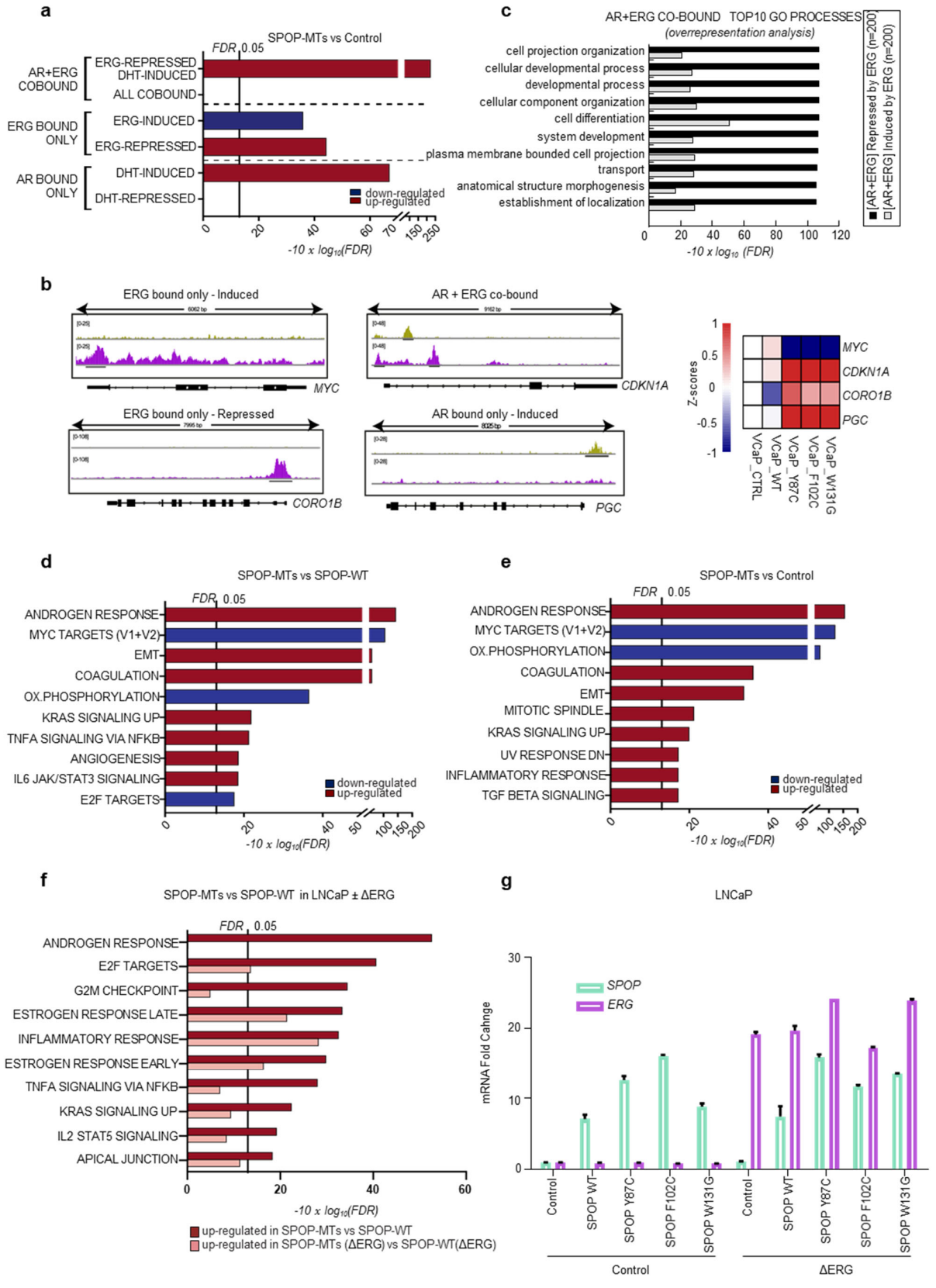

Extended Data Figure 3. Gene expression and pathway analysis related to the synthetic sick relationship between mutant SPOP and ERG in VCaP cells. a, Gene-set enrichment analysis of SPOP mutants (-MTs) overexpressing VCaP cells compared to control, based on RNASeq data. Enrichments are performed on custom gene-sets of direct androgen receptor (AR) and ERG target genes. FDR-adjusted p-values are computed with *Camera* (pre-ranked) **b,** Left: Exemplified tracks of genes bound by AR (green) and/or ERG (violet) derived from custom ERG and AR signatures determined in VCaP cells (see Materials and Methods). Right: Heatmap showing mRNA expression of *MYC, CDKN1A, CORO1B* and *PGC* in control, wild-type and SPOP-mutant VCaP cells. Columns represent average expression across replicates. **c,** Enrichment analysis of gene ontology (GO) biological processes in the AR/ERG co-bound gene set, induced or repressed by ERG. **d**, Gene-set enrichment analysis of SPOP-mutants (-MTs) compared to SPOP-wild type (-WT) overexpressing VCaP cells, based on RNASeq data. Enrichments are performed on Hallmark gene-sets and FDR-adjusted p-values are determined with *Camera* (pre-ranked). **e**, Gene-set enrichment analysis of SPOP-mutants (-MTs) compared to Control VCaP cells, based on RNASeq data. Enrichments are performed on Hallmark gene-sets and FDR-adjusted p-values are determined with *Camera* (pre-ranked). **f,** Gene set enrichment analysis of LNCaP cells overexpressing either mutant (SPOP-MTs, SPOP-Y87C, or wild-type SPOP, in presence or absence of concomitant ΔERG expression. FDR-adjusted p-values were computed with Camera (pre-ranked). **g**, Corresponding relative mRNA expression level of *SPOP* and *ERG* measured by qPCR (**f**). Cells were hormone-starved for 48h.

Extended Data Figure 4

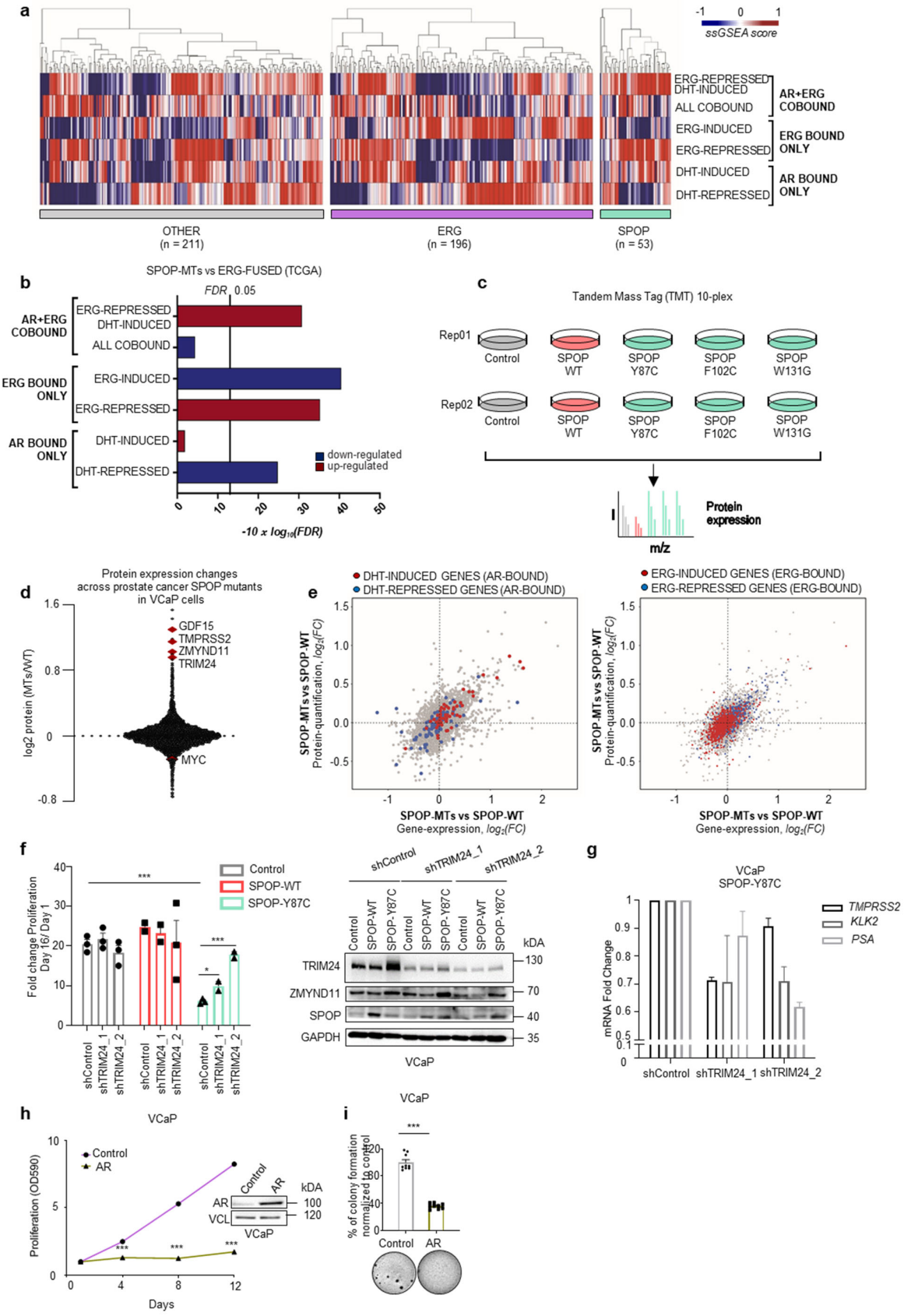

Extended Data Figure 4. Direct AR and ERG target gene expression changes in human tumor tissues. **a,** Heatmap of individual tumors based on single sample GSEA scores as shown in Fig. 2d. Values were scaled and centered by row. Association of individuals to subtypes was performed as described in Materials and Methods. **b,** Enrichment analysis of direct AR and ERG target genes in primary prostate cancers[49]. FDR-adjusted p-values are determined with Camera (pre-ranked). Association of individuals to subtypes was performed as described in Materials and Methods. **c,** Schematic illustration showing the design of the proteomics experiments. Tandem Mass Tag (TMT)-based quantitative mass-spectrometry (n=2, biological replicates) was used in VCaP cells overexpressing Control vector (Control), SPOP-WT, or three different SPOP mutants (SPOP-Y87C, SPOP-F102C and SPOP-W131G). **d**, Protein expression changes in VCaP cells over-expressing SPOP-WT compared to SPOP mutants (average of SPOP-Y87C, -F102C, W-131G). Top proteins being upregulated are highlighted in red (GDF15, TMPRSS2, ZMYND11, TRIM24). **e,** Scatter plot of SPOP-MTs (average across SPOP-Y87C, -F102C, -W131G) versus SPOP-WT transcriptome and proteome expression changes in VCaP cells (n=2 biological replicates). Custom gene signatures changes are highlighted. AR bound only genes being DHT induced (red) or DHT repressed (blue) in left panel; ERG bound only genes being ERG induced (red), or ERG repressed (blue) in right panel **f,**, 2D proliferation assay of VCaP cancer cells over-expressing the indicated SPOP mutants with and without TRIM24 knockdown using two different short hairpin RNAs. Expression of the indicated proteins was analyzed by immunoblotting (n=3). **g**, AR target genes expression changes in VCaP cells overexpressing SPOP-Y87C with and without TRIM24 knockdown using two different short hairpin RNAs. **h,i** , 2D (**f**) and 3D (**g**) proliferation assay of VCaP cancer cells over-expressing AR (n=3). All error bars, mean + s.e.m. *P* values were determined by unpaired, two-tailed Student's t-test (**i**) or two-way ANOVA (**f**,**h**) with multiple comparisons and adjusted using Benjamini-Hochberg post-test. *$P < 0.05$, ***$P < 0.001$. Molecular weights are indicated in kilodaltons (kDa).

Extended Data Figure 5

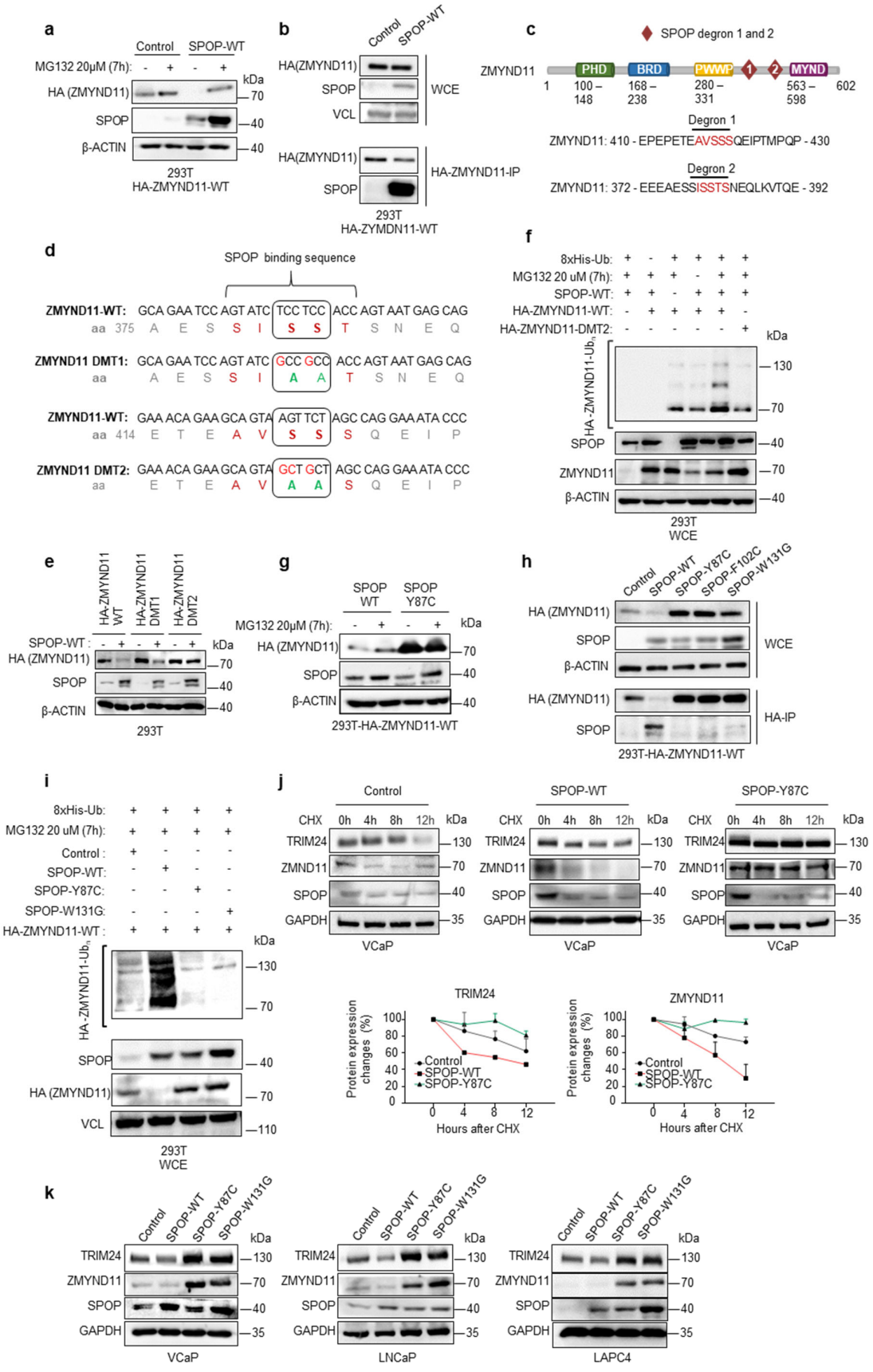

Extended Data Figure 5. ZMYND11 is a SPOP substrate. a, Over-expression of HA-ZMYND11 and SPOP-WT in 293T cells and subsequent expression analysis of the indicated proteins by immunoblotting. **b,** Whole cell extracts (WCE) of 293T cells over-expressing HA-ZMYND11-WT and different SPOP species and corresponding anti-HA-immunoprecipitation (HA-IP). Expression of the indicated proteins was analyzed by immunoblotting. **c,** Domain structure of ZMYND11 with indicated SPOP-degron and ubiquitin sites. **d,** Schematic illustration of the SPOP degron sequences on ZMYND11. The degron-deficient mutants (DMT) were generated by two serine-to-alanine substitutions. **e**, Forced expression of SPOP-WT together with HA-ZMYND11-WT or two degron deficient mutants (DMT1 & DMT2) in 293T cells. **f**, *In vivo* ubiquitylation assay of HA-ZMYND11 in 293T cells. Cell were transiently transfected with the indicated constructs and histidine-tagged (his-tag), ubiquitylated proteins were pulled down using nickel beads. Ubiquitylated HA-tagged ZMYND11 was detected by immunoblotting. **g,** Over-expression of HA-ZMYND11 and SPOP-Y87C in 293T cells and subsequent expression analysis of the indicated proteins by immunoblotting after proteasomal inhibition with MG132. **h**, Whole cell extracts (WCE) and corresponding anti-HA-immunoprecipitation (HA-IP) of 293T cells over-expressing HA-ZMYND11-WT and different SPOP-MTs species as indicated. Expression of the indicated proteins was analyzed by immunoblotting. **i**, *In vivo* ubiquitylation assay of HA-ZMYND11 in 293T cells. Cell were transiently transfected with the indicated constructs and histidine-tagged (his-tag), ubiquitylated proteins were pulled down using nickel beads. Ubiquitylated HA-tagged ZMYND11 was detected by immunoblotting. **j**, Immunoblots and quantification of indicated protein expression changes after treatment with cycloheximide (CHX, 100 µg/mL) in VCaP cells overexpressing the indicated SPOP species (n=2). All error bars, mean + s.e.m . Time is indicated in hours (h). **k,** Immunoblots of indicated proteins in VCaP, LNCaP and LAPC4 human prostate cancer cells overexpressing the indicated SPOP species. Molecular weights are indicated in kilodaltons (kDa).

Extended Data Figure 6

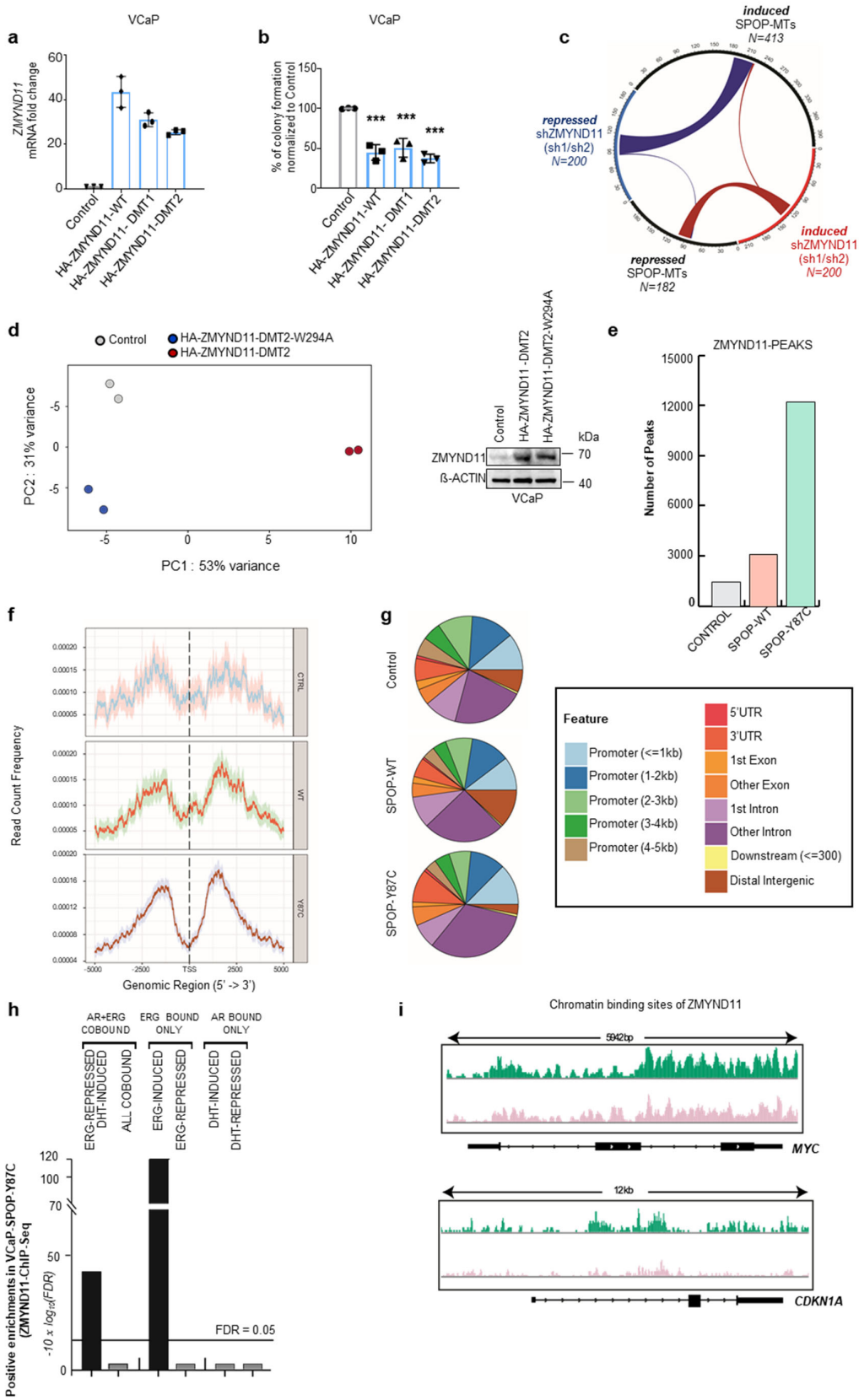

Extended Data Figure 6. ZMYND11 influences ERG target genes transcription. a, mRNA expression levels of VCaP cancer cells over-expressing HA-ZMNYD11-WT and derived degron-deficient mutants (DMT1/2) measured by qPCR. **b,** Corresponding 3D colony formation assay in methylcellulose (n=3). Error bars, mean ± s.e.m *P* values were determined by one-way ANOVA with multiple comparisons and adjusted using Benjamini-Hochberg post-test . ***$P < 0.001$. **c,** Chord diagram of genes transcriptionally regulated by either mutant SPOP (SPOP-MTs, SPOP-Y87C, -F102C, -W131G) or knockdown of ZMYND11 by two different short hairpin RNAs (shZMYND11 sh1/sh2 ; shZMYND11_1 and shZMYND11_2) in VCaP cells (FDR<0.05). Strings, whose thickness is proportional to the number of shared elements, represent common genes between sets. **d,** PCA-analysis based on RNA-Seq derived mRNA expression levels of the differentially expressed genes identified from the comparison between SPOP-mutant and SPOP-wild type overexpressing VCaP cells (FDR<0.05). Samples from the same experiment are shown: Controls (grey), HA-ZMYND11-DMT2 (red) HA-ZMYND11-DMT2-W294A (blue). Right: corresponding immunoblot. Molecular weights are indicated in kilodaltons (kDa). **e,** Number of genomic ZMYND11 peaks measured by ChIP sequencing in VCaP cells overexpressing SPOP-mutant (SPOP-Y87C), SPOP-wild type (-WT) and control vector (Control). **f,** Density plots representing ZMYND11 read count frequency respective to TSSs (+/- 5kb) as determined from ChIP-Sequencing experiments. Top: Control VCaP cells; Center: VCaP cells overexpressing SPOP-WT; Bottom: VCaP cells overexpressing Y87C SPOP mutation. **g,** Localization of ZMYND11 binding sites, stratified according to genomic regions. **h,** Enrichment analysis, performed using chipenrich[292], of genes identified by ChIP-Seq to contain ZMYND11 peaks (within 5 kb flanking each of their TSSs), performed on AR- and ERG-derived gene sets in VCaP cells overexpressing SPOP-Y87C. **i,** IGV-derived screenshots representing chromatin binding sites of ZMYND11 on *MYC* (UP) and *CDKN1A* (bottom) as determined from ChIP-Seq experiments in VCaP cells overexpressing either wildtype (light pink) or mutant-SPOP (Y87C, dark green). Tracks are rescaled for their respective sequencing depth in order to be comparable.

Extended Data Figure 7

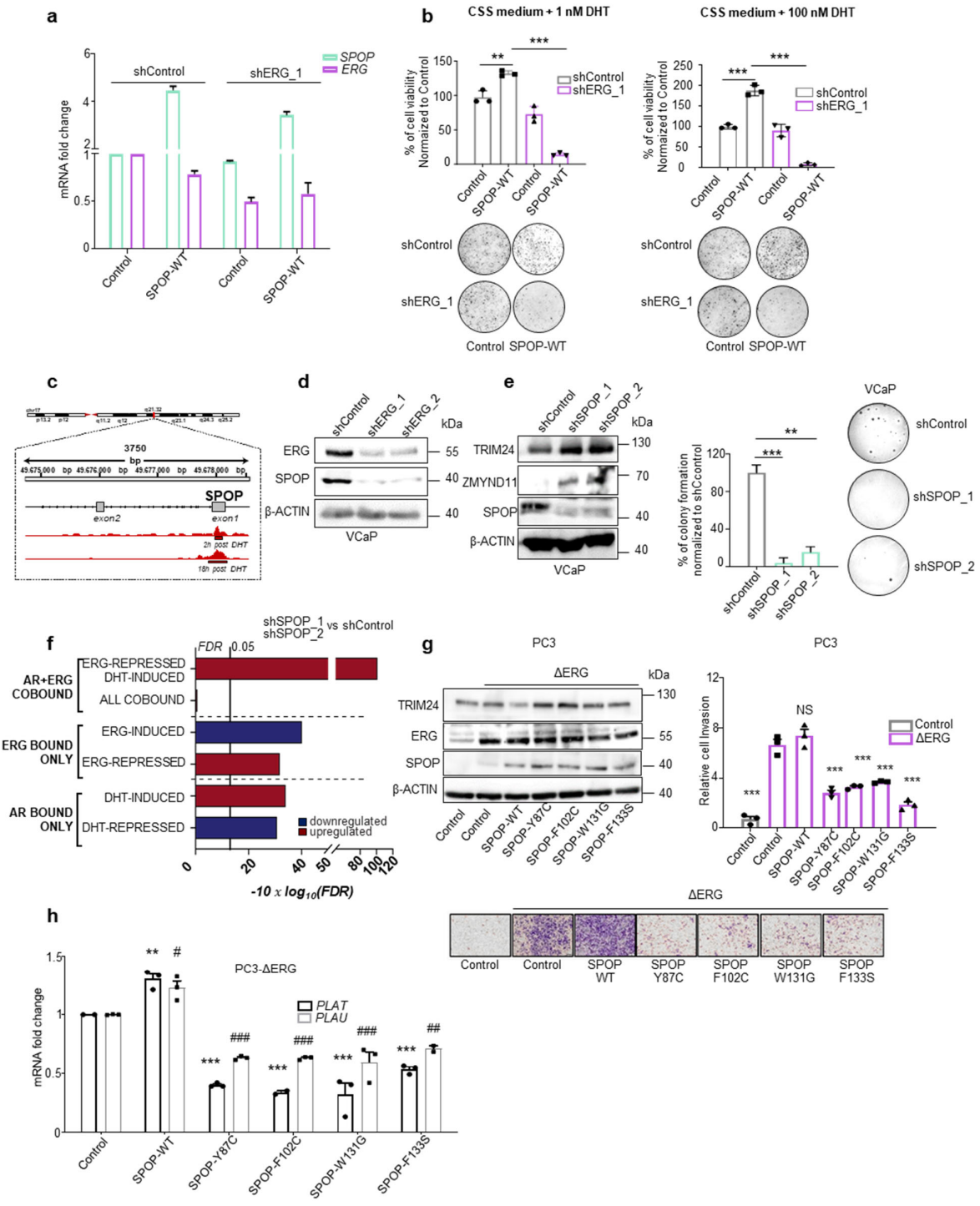

Extended Data Figure 7. SPOP is transcriptionally up-regulated by ERG and wild type SPOP is required for ERG-mediated oncogenic phenotypes. a,b, mRNA expression of VCaP cancer cells over-expressing SPOP-WT in the context of ERG knockdown with one short hairpin RNA (**a**) and corresponding 3D proliferation assay in response to DHT treatment (**b**). Cells were plated in medium supplemented with 10% charcoal-stripped serum (CSS medium). **c**, IGV screenshot of the SPOP promoter showing ERG binding sites around exon 1[258]. **d,** Knockdown of ERG with two different short hairpin RNAs in VCaP cells followed by

immunoblot expression analysis of the indicated proteins. **e,** Knockdown of SPOP with two different short hairpin RNAs in VCaP cells followed by immunoblot expression analysis of the indicated proteins and corresponding 3D growth in methylcellulose. **f,** Gene-set enrichment analysis of SPOP knockdown compared to shControl VCaP cells, based on RNA-Seq data. Enrichments are performed on custom gene-sets of direct androgen receptor (AR) and ERG target genes. FDR-adjusted p-values are computed with *Camera* (pre-ranked). **g,** Transwell invasion assay of PC3 cells over-expressing ΔERG and indicated SPOP mutants. Corresponding protein expression changes assessed by immunoblotting (n=3). **h**, Corresponding mRNA analysis of the ERG target genes *PLAU* and *PLAT* measured by qPCR. All error bars, mean + s.e.m. *P* values were determined by unpaired, two-tailed Student's t-test (**b**) , one-way ANOVA (**e, g**) or two-way ANOVA (**h**) with multiple comparisons and adjusted using Benjamini-Hochberg post-test. NS, not significant. $*P < 0.05$, $**P < 0.01$, $***P < 0.001$; *PLAT* expression levels in Control versus each cell line ., $^{\#}P < 0.05$, $^{\#\#}P < 0.01$, $^{\#\#\#}P < 0.001$; *PLAU* expression levels in Control versus each cell line.

Extended Data Figure 8

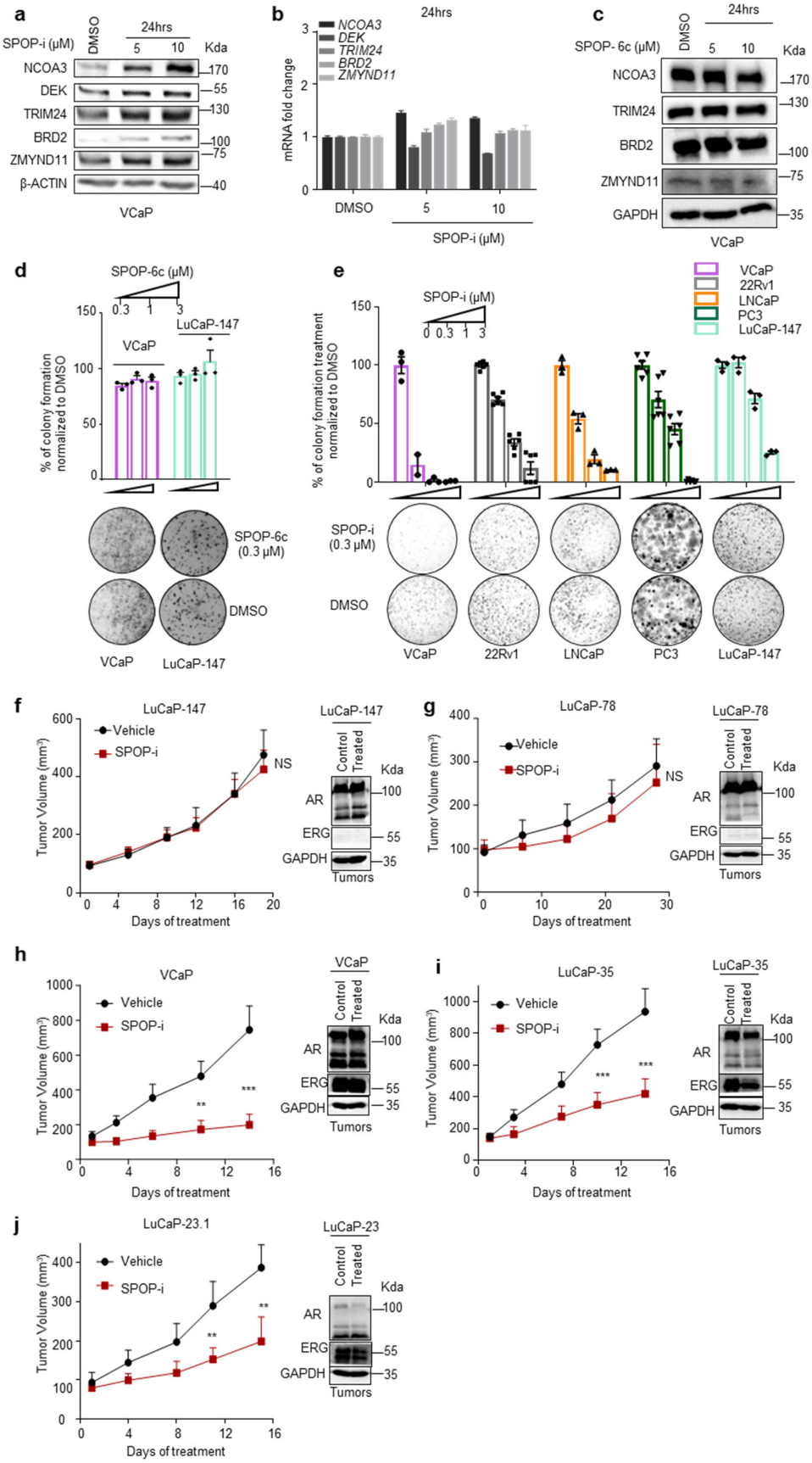

Extended Data Figure 8. ERG-positive tumor cells are particularly sensitive to SPOP inhibition. a, Immunoblot expression analysis of indicated SPOP substrates upon treatment with SPOP inhibitor (SPOP-i, compound 6b) in VCaP cells. **b,** Corresponding mRNA expression analysis of SPOP substrates by qPCR. **c**, Immunoblot expression analysis of indicated SPOP substrates upon treatment with SPOP-6c (inactive analog of compound 6b) in VCaP cells. **d**, 3D colony formation assay in methylcellulose of VCaP and LuCaP-147 cells upon SPOP-6c treatment. **e,** SPOP-i-mediated 3D growth inhibition in methylcellulose in the indicated prostate cancer cell lines. Error bars, mean ± s.e.m. **f,** Tumor growth kinetics with (n =10) or without (vehicle; n = 10) SPOP-i treatment in xenografts established from LuCaP-147 (SPOP-Y83C) PDX cells and corresponding immunoblot. **g,** Tumor growth kinetics with (n = 4) or without (vehicle; n = 4) SPOP-i treatment in xenografts established from LuCaP-78 (SPOP-W131G) PDX cells and corresponding immunoblot. **h,** Tumor growth kinetics with (n = 11) or without (vehicle; n = 11) SPOP-i treatment in xenografts established from VCaP cells and corresponding immunoblot. **i,** Tumor growth kinetics with (n = 8) or without (vehicle; n = 10) SPOP-i treatment in LuCaP-35 (ERG-positive) PDX and corresponding Immunoblot. **j,** Tumor growth kinetics with (n = 6) or without (vehicle; n = 8) SPOP-i treatment in LuCaP-23.1 (ERG-positive) PDX and corresponding immunoblot. All SPOP-i treatment initiated when tumors reached an average of 100mm^3. All error bars, mean + s.e.m. *P* values were determined by two-way ANOVA (**f, g, h, i, j,**) with multiple comparisons and adjusted using Benjamini-Hochberg post-test. NS, not significant. ***P* < 0.01, ****P* < 0.001.

Extended Data Figure 9

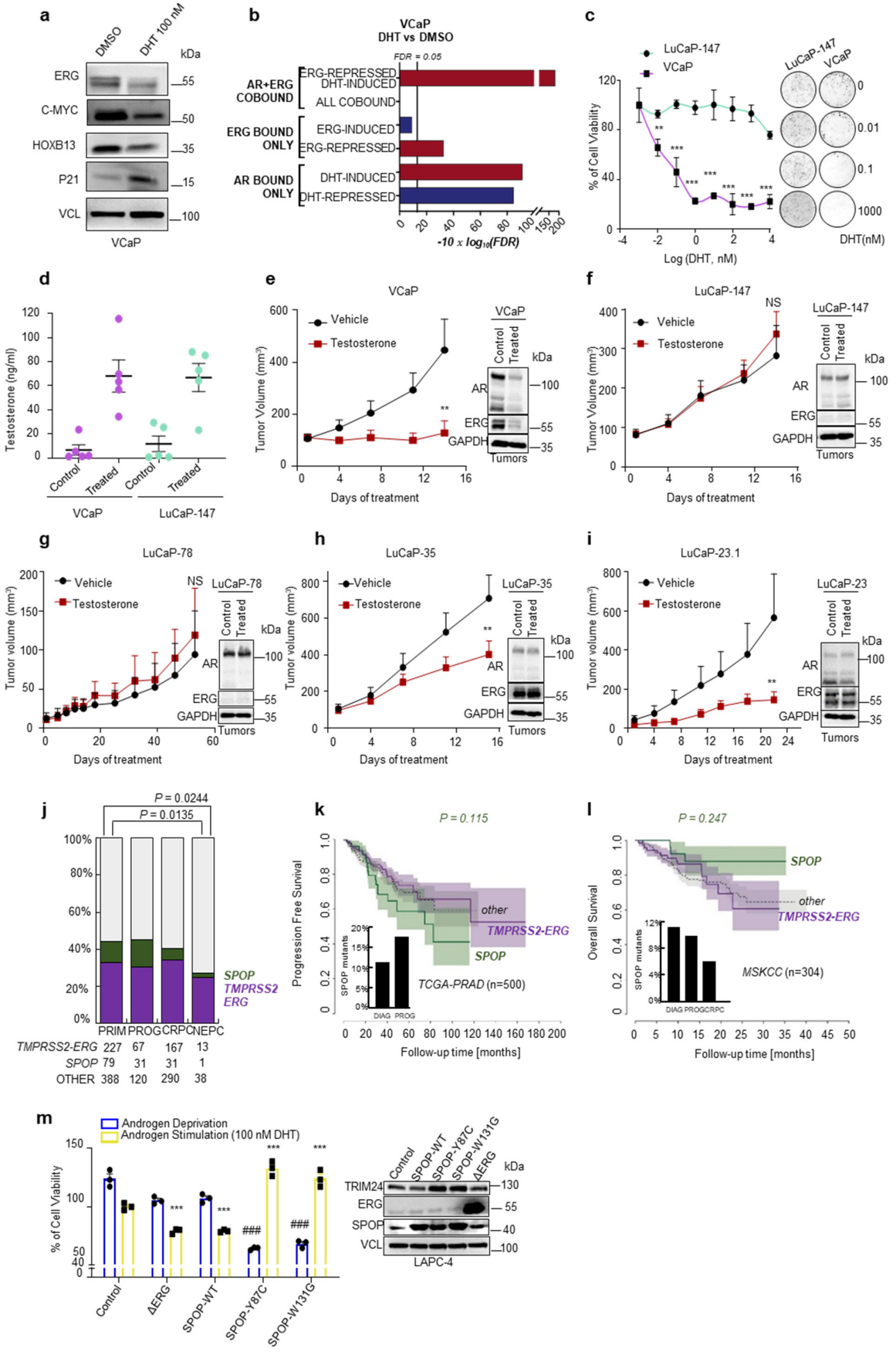

Extended Data Figure 9. ERG and mutant SPOP trigger opposite responses to High-Dose Androgen Therapy. a, Immunoblot expression analysis of VCaP cell line treated for 7 days with DMSO or DHT (100nM). Cells were cultured in normal growth culture medium (DMEM Glutamax + 10% FBS). **b,** Gene-set enrichment analysis of DHT-treated (100 nM) VCaP cells compared to control (DMSO), based on RNASeq data. Enrichments are performed on custom gene-sets of direct androgen receptor (AR) and ERG target genes. FDR-adjusted p-values are computed with Camera (pre-ranked). **c,** 3D proliferation assay of VCaP (ERG positive) and LuCaP-147 (SPOP-Y83C) PDX cells in response to high doses of dihydrostestosterone (DHT). Cells were seeded in normal medium (DMEM Glutamax + 10% FBS and StemPro respectively) and treated once with corresponding DHT concentration. Error bars, mean ± s.e.m. **d,** Testosterone levels measured in mice before and after 7 days of daily treatment**.** Error bars, mean ± s.e.m. **e,** Tumor growth kinetics with (n = 6) or without (vehicle; n = 6) testosterone treatment in xenografts established from VCaP (ERG positive) cells and corresponding immunoblot. Treatment initiated when tumors reached 100mm^3. **f,** Tumor growth kinetics with (n = 10) or without (vehicle; n = 10) testosterone treatment in xenografts established from LuCaP-147 (SPOP-Y83C) cells and corresponding immunoblot. Treatment initiated when tumors reached 100mm^3. **g,** Tumor growth kinetics with (n = 4) or without (vehicle; n = 4) testosterone treatment in xenografts established from LuCaP-78 (SPOP-W131G) cells and corresponding immunoblot. Treatment initiated when tumors reached 100mm^3. **h,** Tumor growth kinetics with (n = 10) or without (vehicle; n = 10) testosterone treatment in xenografts established from LuCaP-35 cells and corresponding immunoblot. Treatment initiated when tumors reached 100mm^3. **i,** Tumor growth kinetics with (n =12) or without (vehicle; n = 12) testosterone treatment in xenografts established from LuCaP-23.1 cells and corresponding immunoblot. **j,** Bar plots indicate the relative frequency of *SPOP*-mutant and *TMPRSS2-ERG* positive tumors across composite primary, progressed, castration-resistant and neuroendocrine patients' cohorts (PRIM = primary; PROG = progressed; CRPC = castration resistant; NEPC = neuroendocrine)[56, 58, 102]. Statistical significance between the expected frequencies observed within primary tumors and those observed in castration resistant prostate cancer was determined by chi-squared **k,** Progression-free survival of prostate cancer patients derived from the TCGA-cohort. Curves representing TMPRSS2-ERG rearranged and SPOP-mutant patients are indicated in violet and green, respectively. The area around the curves represents 80% confidence interval. The bar plot in the lower left corner indicates the percentage of SPOP-mutant tumors within all patients who were diagnosed with prostate cancer (DIAG) and within the individuals who developed a progression of the disease (PROG). **l**. Overall survival of prostate cancer patients derived from the MSK-IMPACT cohort. Curves representing *TMPRSS2-ERG* rearranged and *SPOP*-mutant patients are indicated in violet and green, respectively. The area around the curves represents 80% confidence interval. The bar plot in the lower left corner indicates the percentage of SPOP-mutant tumors within all patients who were diagnosed with prostate cancer (DIAG), within individuals who developed a metastatic progression of the disease (PROG), and within individuals who developed castration-resistant prostate cancer (CRPC). **m,** Response to androgen deprivation or high androgen treatment (100nm DHT) of LAPC4 cells overexpressing ΔERG or indicated SPOP mutants species (Y87C, W131G) in 2D cell culture and corresponding immunoblot. Cells were cultured in CSS (charcoal-stripped serum) medium and DHT was added at the corresponding concentration. Viability was assessed after 7 days. ***$P < 0.001$.; Control versus each cell line under androgen stimulation. $^{###}P < 0.001$; Control versus each cell line under androgen deprivation. All error bars, mean + s.e.m unless otherwise specified. *P* values were determined by two-way ANOVA (**c**, **e**, **f, g, h, i, m**) with multiple comparisons and adjusted using Benjamini-Hochberg post-test. NS, not significant. **$P < 0.01$, ***$P < 0.001$.

Extended Data Figure 10

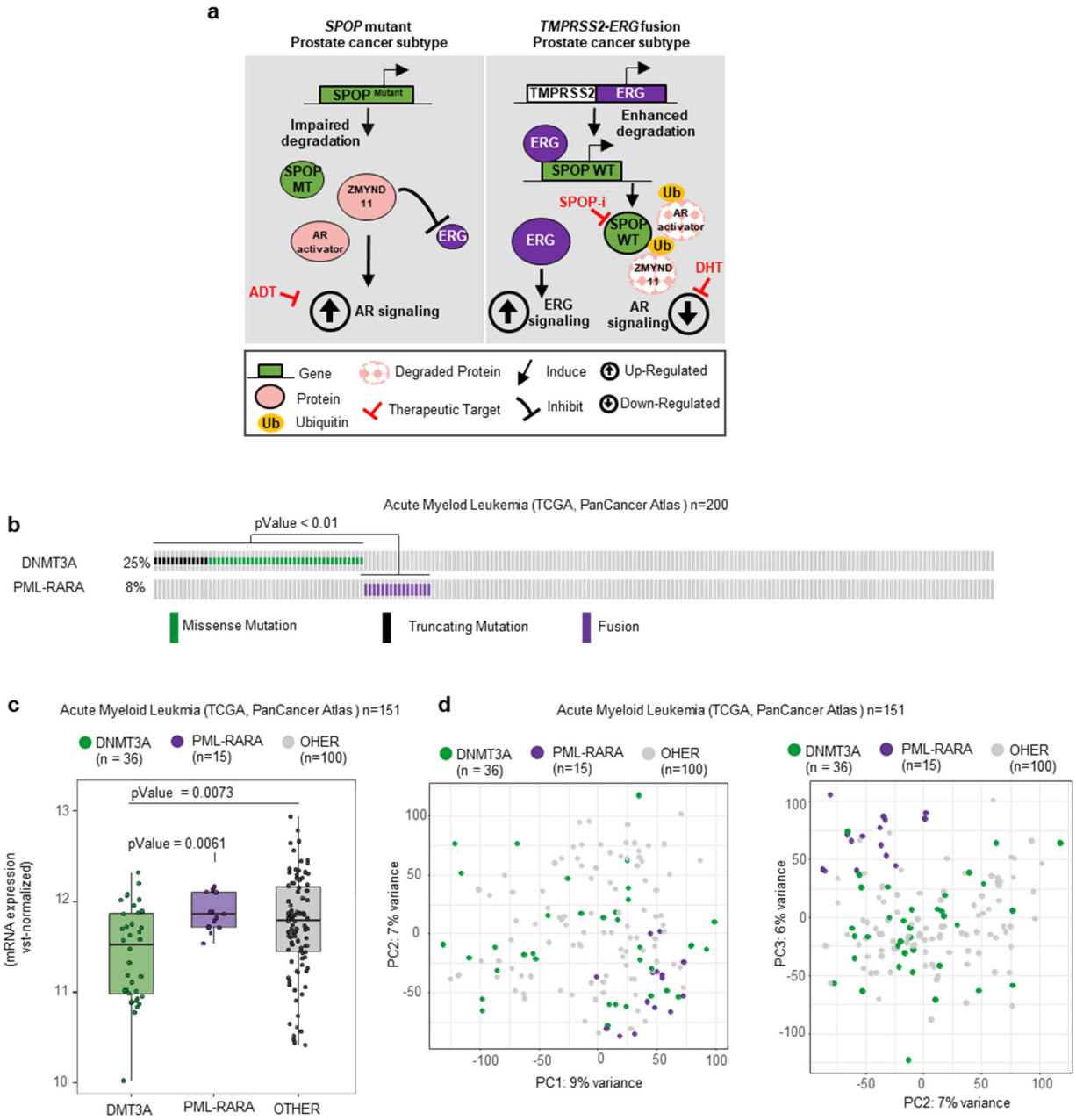

Extended Data Figure 10. ***SPOP*** **and** ***ERG*** **are part of a distinct class of antagonistic driver genes. a,** Schematic representation of the proposed model for the aversive relationship between mutant *SPOP* and *ERG* in prostate cancer**. b,** Distribution of genetic alterations in *RARA* and *DNMT3* across 151 acute myeloid leukemia patients in TCGA database[269]. **c,** Boxplots showing RNA-Seq based mRNA expression levels of DNMT3A among acute myeloid leukemia patients, stratified according to presence/absence of PML-RARA fusion and DNMT3A mutation status. **d,** PCA-analysis based on RNA-Seq derived mRNA expression levels of the top 1000 most variable genes of the TCGA-AML cohort. RARA-fused (violet) and DNMT3A-mutant (green).